THESIS
2
2009

LIBRARY
Michigan State
University

This is to certify that the
dissertation entitled

Characterization of Retention Behavior
of Hybrid Stationary Phases

presented by

Amber Michelle Hupp

has been accepted towards fulfillment
of the requirements for the

Doctoral degree in Chemistry

Victoria McGuffin
Major Professor's Signature

5/6/2009
Date

MSU is an Affirmative Action/Equal Opportunity Employer

PLACE IN RETURN BOX to remove this checkout from your record.
TO AVOID FINES return on or before date due.
MAY BE RECALLED with earlier due date if requested.

DATE DUE	DATE DUE	DATE DUE

5/08 K:/Proj/Acc&Pres/CIRC/DateDue.indd

CHARAC
C

CHARACTERIZATION OF RETENTION BEHAVIOR OF HYBRID STATIONARY PHASES

By

Amber Michelle Hupp

A DISSERTATION

Submitted to
Michigan State University
in partial fulfillment of the requirements
for the degree of

DOCTOR OF PHILOSOPHY

Chemistry

2009

CHARACTERIZ
OF HYE

Reversed-phase liquid c

ization of complex sam

terization is necessary in o

ize the experimental contr

ation mechanism of

nvestigated using a series

ogen-containing PAHs (A

First, a comparison a

thermodynamic and kinet

ained (Chapter 3),

ntially modified Gau

ention factors and k

ver-length linear veloc

ictable among the mo

hapes with the stat

chromatograms. Based on

determined appropriate m

ther, the effect of

ecomputation concern

ABSTRACT

CHARACTERIZATION OF RETENTION BEHAVIOR
OF HYBRID STATIONARY PHASES

By

Amber Michelle Hupp

Reversed-phase liquid chromatography (RPLC) is the leading method for separation of complex samples. A deep understanding of the retention mechanism is necessary in order to maximize the beneficial contributions and minimize the detrimental contributions to the separation. In this dissertation, the retention mechanism of inorganic – organic hybrid stationary phases is investigated using a series of polycyclic aromatic hydrocarbons (PAHs) and nitrogen-containing PAHs (NPAHs).

First, a comparison and validation of theoretical methods that extract thermodynamic and kinetic information from liquid chromatographic data is performed (Chapter 3). Three theoretical models (statistical moment, exponentially modified Gaussian (EMG), and Thomas models) are evaluated. Retention factors and kinetic rate constants are compared as a function of column length, linear velocity, and solute carbon number. Retention factors are comparable among the models. Kinetic rate constants differ considerably among the models, with the statistical moment and EMG models showing the most similar trends. Based on these results, the statistical moment and EMG models are deemed appropriate methods to use in experimental liquid chromatography.

Next, the effect of temperature on a hybrid C_{18} phase is evaluated to afford information concerning the retention mechanism (Chapter 4). In methanol

...ase the retention ...
...tor with ring number a...
...tion mechanism. The or...
...utes. The kinetic rate cons...
...ble for NPAHs. In ac...
...ar than those in methano...
...re similar to those f...
...anism is predominant for...
...ly more negative and a...
...tor factor. The k...
...ction in acetonitrile mob...

Finally, the effect of ...
...lated (Chapter 5). Mo...
...ethylamine and pyrid...
...dehyde, acetone, are m...
...ase dependent. Ma...
...several solutes on the...
...rement to peak sha...
...oes the most overa...
...oes the next most ...
...obably removes the ta...

mobile phase, the retention factors for the NPAHs, along with the trends of retention with ring number and annelation structure, are consistent with the partition mechanism. The changes in molar enthalpy are very similar for all solutes. The kinetic rate constants indicate that adsorption at silanol sites could play a role for NPAHs. In acetonitrile, the retention factors for the NPAHs are larger than those in methanol. In addition, the retention factors for the NPAHs are more similar to those for their parent PAHs, indicating the adsorption mechanism is predominant for these solutes. The changes in molar enthalpy are slightly more negative and are sufficient to account for the small changes in retention factor. The kinetic behavior also reflects the increased role of adsorption in acetonitrile mobile phase.

Finally, the effect of mobile phase additives on several hybrid phases is evaluated (Chapter 5). Mobile phase modifiers used for silanol blockage, such as triethylamine and pyridine, and those for metal chelation, such as acetic acid and acetyl acetone, are investigated. The effect of each modifier is both solute and phase dependent. Many of the mobile phase modifiers improve peak shape for several solutes on the hybrid C_{18} phases, but do not cause a universal improvement to peak shape. The combination of triethylamine and acetic acid provides the most overall peak shape improvement, while triethylamine alone provides the next most improvement. However, no modifier or pair of modifiers completely removes the tailing from all peaks.

To my wonderful parents, Tom and Jille

A

As I begin to write this

ly important and influential

their unending support. F

mazing advisor, Vicki Mc

ould have ever hoped for

in ways that I can

he and energy you have s

I've learned more about w

I'll never be able to succe

grateful I am for you

Next, I would like to a

Dr. Buening, and my tho

Dr. Kathy Hunt. In addi

being in me from the v

During my time here

years yet I am most

being your teaching stra

become a better educato

for welcoming us to

Incredibly, your fr

I want to give a

hours with whom I

ACKNOWLEDGMENTS

As I begin to write this section of my thesis, I realize that there have been many important and influential people in my life who I would like to acknowledge for their unending support. First, I would like to thank my inspiring and always encouraging advisor, Vicki McGuffin. Vicki, you are the most fantastic role-model I could have ever hoped for in an advisor. I have learned an incredible amount from you, in ways that I continue to understand each day. I appreciate all the time and energy you have spent on me over these years. And, even though I have learned more about writing and public speaking than I ever thought I could, I will never be able to successfully write or speak words that could acknowledge how grateful I am for you.

Next, I would like to acknowledge my meticulous second reader, Professor Merlin Bruening, and my thoughtful committee members, Professors Greg Swain and Kathy Hunt. In addition, I would like to thank Professor Gary Blanchard for believing in me from the very beginning and allowing me to start a tab at your "bar". During my time here at MSU I discovered a number of wonderful teaching mentors, yet I am most indebted to Dr. Kathy Severin. Kathy, thank you for sharing your teaching strategies and for always helping me learn how and why to become a better educator and leader. Finally, thank you Lisa Dillingham for warmly welcoming us to the department, your thoughtful and caring attitude, and most importantly, your friendship.

I want to give a big shout-out to the present and past McGuffin group members with whom I have shared this experience. I will never forget the

...ecial memories we hav...

...ring Rashad, Yuen-ng, a...

...ssay, Melissa, John, an...

...raduate school. A special th...

...ost very memorable ones

...y best friends. And to those

...ha bod and good g-dly mo...

...sco - Beth, Lagoo, Alli, Sa...

And last but very muc...

...thing I say here cannot e...

...r and dad. Julie and Tom

...e ups and the downs) an...

...issue. I love you guys - ...

...ool, maybe I can pick up t...

...e years, I gained an addi...

...ike Amy and their extende...

...t even begin to acknowle...

...ess is no way I would be ...

...e from making me laugh

...ness about nonlinear iso...

...ly. But most of all, I than...

...best friend.

incredible memories we have made in and out of the lab. Thank you to Carl, Xiaoping, Rashad, Yuening, and Mel for kindly welcoming me into the group and to Kahsay, Melissa, John, and Lucas for keeping me sane during my last years in graduate school. A special thanks to my friend Mel for making these grad school years very memorable ones and teaching me that it's okay to talk science with my best friends. And to those friends who've made me laugh, shared bubble tea, Thai food, and good girly movies, and reminded me that there IS life outside of school – Beth, Lagoo, Alli, Sam, Thu, Jill – a great big thank you to you!

And last but very much not least, I want to thank my wonderful family. Anything I say here cannot express the love and appreciation that I feel for my mom and dad, Jille and Tom. You have been by my side since day one (through all the ups and the downs) and continue to inspire me to better myself in any way possible. I love you guys - thanks for being you! Now that I'm *finally* out of school, maybe I can pick up the tab for dinner every now and then! In the last few years, I gained an additional family and feel very blessed to have Sandy, Dave, Amy, and their extended family as a very loving part of my life. And, how do I even begin to acknowledge my wonderful husband? Chris, without you, there is no way I would be where I am today. I appreciate everything you do for me – from making me laugh in the way only you know how, to listening to me talk endlessly about nonlinear isotherms, to bringing me dinner when I'm doing a "big study". But most of all, I thank you for being the most wonderful husband and my very best friend.

T

ST OF TABLES .....

ST OF FIGURES .....

APTER 1. INTRODUCTIO

troduction .....

hermodynamic and k

1.2.1. Thermodynamic

1.2.2. Kinetic theory

Methods for thermodyn

1.3.1. Perturbation me

1.3.2. Shallow bed me

1.3.3. Chromatograph

Previous investigations

1.4.1. Fundamental stu

1.4.2. Effect of alkyl on

1.4.3. Effect of support

1.4.4. Effect of mobile

1.4.5. Effect of solute s

Conclusions .....

References .....

APTER 2. EXPERIMENT

troduction .....

Column preparation a

Stationary phases

Chromatographic syst

2.4.1. One detector s

2.4.2. Four detector

Conclusions .....

References .....

APTER 3. EXPERIM

TRACTING RETENTIO

QUID CHROMATOG

troduction .....

heory .....

3.2.1. Plate height

3.2.2. Exponential

3.2.3. Thomas mo

Methods .....

3.3.1. Reagents

3.3.2. Experiments

TABLE OF CONTENTS

LIST OF TABLES x

LIST OF FIGURES xiii

CHAPTER 1. INTRODUCTION AND BACKGROUND 1
1.1. Introduction 1
1.2. Thermodynamic and kinetic theory 7
1.2.1. Thermodynamic theory 11
1.2.2. Kinetic theory 13
1.3. Methods for thermodynamic and kinetic studies 16
1.3.1. Perturbation methods 17
1.3.2. Shallow bed method 19
1.3.3. Chromatographic methods 21
1.4. Previous investigations 31
1.4.1. Fundamental studies of the retention mechanism 31
1.4.2. Effect of alkyl chain length and bonding density 35
1.4.3. Effect of support 45
1.4.4. Effect of mobile phase composition 49
1.4.5. Effect of solute structure and concentration 54
1.5. Conclusions 63
1.6. References 65

CHAPTER 2. EXPERIMENTAL METHODS 70
2.1. Introduction 70
2.2. Column preparation and packing 70
2.3. Stationary phases 73
2.4. Chromatographic systems 75
2.4.1. One detector system for mobile phase modifier study 75
2.4.2. Four detector system for temperature and pressure study 77
2.5. Conclusions 79
2.6. References 80

CHAPTER 3. EXPERIMENTAL EVALUATION OF METHODS FOR EXTRACTING RETENTION FACTORS AND KINETIC RATE CONSTANTS IN LIQUID CHROMATOGRAPHY 81
3.1. Introduction 81
3.2. Theory 83
3.2.1. Plate height model 83
3.2.2. Exponentially modified Gaussian model 86
3.2.3. Thomas nonlinear chromatography model 88
3.3. Methods 89
3.3.1. Reagents 89
3.3.2. Experimental system 89

3.3.3. Data analysis ..
3.4 Results and discussion
3.4.1. Retention factor
3.4.2. Kinetic rate con
3.5 Conclusions .....
3.6 References .....

APPENDIX 3A.1. COMPAR
PLATE HEIGHT MODEL US
3A.1 Introduction .....
3A.2 Classical kinetic approa
3A.3 Modern kinetic approach
3A.4 Comparison of plate he
3A.5 Discussion .....
3A.6 References .....

CHAPTER 4. THERMODYN
BRIDGED-ETHYLENE HY
4.1 Introduction .....
4.2 Theory .....
4.3 Methods .....
4.3.1. Reagents .....
4.3.2. Experimental s
4.3.3. Data analysis ..
4.4 Results and discuss on
4.4.1. Methanol mob
4.4.2. Acetonitrile mo
4.5 Conclusions .....
4.6 References .....

CHAPTER 5. EFFECT
SHAPE USING BR
PHASES.....
5.1 Introduction .....
5.2 Methods .....
5.2.1. Reagents ...
5.2.2. Experimental s
5.2.3. Data analysis
5.3 Results .....
5.3.1. Methanol mob
5.3.2. Acetonitrile mo
5.4 Discussion .....
5.4.1. Effect of bridge
5.4.2. Effect of polar
5.4.3. Effect of mob
5.4.4. Effect of mob

3.3.3. Data analysis 89
3.4. Results and discussion 91
3.4.1. Retention factor 91
3.4.2. Kinetic rate constants 101
3.5. Conclusions 116
3.6. References 117

APPENDIX 3A.1. COMPARISON OF VARIOUS APPROACHES TO THE PLATE HEIGHT MODEL USING STATISTICAL MOMENTS 118
3A.1. Introduction 118
3A.2. Classical kinetic approaches 118
3A.3. Modern kinetic approaches 120
3A.4. Comparison of plate height models 122
3A.5. Discussion 132
3A.6. References 133

CHAPTER 4. THERMODYNAMIC AND KINETIC CHARACTERIZATION OF A BRIDGED-ETHYLENE HYBRID C_{18} STATIONARY PHASE 134
4.1. Introduction 134
4.2. Theory 136
4.3. Methods 136
4.3.1. Reagents 136
4.3.2. Experimental system 136
4.3.3. Data analysis 138
4.4. Results and discussion 138
4.4.1. Methanol mobile phase 139
4.4.2. Acetonitrile mobile phase 153
4.5. Conclusions 162
4.6. References 166

CHAPTER 5. EFFECT OF MOBILE PHASE MODIFIERS ON PEAK SHAPE USING BRIDGED-ETHYLENE HYBRID STATIONARY PHASES 168
5.1. Introduction 168
5.2. Methods 170
5.2.1. Reagents 170
5.2.2. Experimental system 171
5.2.3. Data analysis 171
5.3. Results 173
5.3.1. Methanol mobile phase 173
5.3.2. Acetonitrile mobile phase 188
5.4. Discussion 203
5.4.1. Effect of bridged-ethylene hybrid (BEH) particle 203
5.4.2. Effect of polar embedded group 203
5.4.3. Effect of mobile phase 205
5.4.4. Effect of mobile phase modifiers 206

5.4.5. Additional argu
5.5 Conclusions
5.6 References

APPENDIX 5A.1. DETAIL
MODIFIERS
5A.1 Introduction
5A.2 Methanol mobile phase
5A.2.1 XBridge C
5A.2.2 XBridge Shield
5A.2.3 Bridged-ethylen
5A.3 Acetonitrile mobile phas
5A.3.1 XBridge C
5A.3.2 XBridge Shield
5A.3.3 Bridged-ethylen
5A.4 Conclusions

CHAPTER 6. CONCLUSION
6.1 Introduction
6.2 Study of theoretical and
6.3 Study of hybrid stationar
6.4 Conclusions
6.5 References

5.4.5. Additional arguments 211
5.5. Conclusions 212
5.6. References 214

APPENDIX 5A.1. DETAILED AFFECTS OF THE MOBILE PHASE MODIFIERS 216
5A.1. Introduction 216
5A.2. Methanol mobile phase with modifiers 216
5A.2.1. XBridge C_{18} 216
5A.2.2. XBridge Shield RP_{18} 218
5A.2.3. Bridged-ethylene hybrid (BEH) particle 220
5A.3. Acetonitrile mobile phase with modifiers 222
5A.3.1. XBridge C_{18} 222
5A.3.2. XBridge Shield RP_{18} 225
5A.3.3. Bridged-ethylene hybrid (BEH) particle 227
5A.4. Conclusions 231

CHAPTER 6. CONCLUSIONS AND FUTURE DIRECTIONS 232
6.1. Introduction 232
6.2. Study of theoretical analysis methods 232
6.3. Study of hybrid stationary phases 234
6.4. Conclusions 238
6.5. References 239

Table 3.1 Retention factor
are calculated
0.088 cm/s .....

Table 3.2 Retention factor
linear velocity
the statistical
4 and 1 .....

Table 3.3: Retention factor
linear velocity
EMG model by

Table 3.4: Retention factor
linear velocity
Thomas model

Table 3.5: Rate constants
constants are c
data collected a

Table 3.6: Rate constants
linear velocity
moment model

Table 3.7: Rate constants
linear velocity
EMG model by c

Table 3.8: Rate constants
linear velocity
Thomas model b

Table 3A.1: Mass transfer
Deemter and P
respectively .....

Table 3A.2: Corrected plate
Equations 3A.1 a

Table 3A.3: Mass transfer
calculated us ng

LIST OF TABLES

Table 3.1 Retention factors as a function of length (L). The retention factors are calculated with the EMG difference model at a linear velocity of 0.088 cm/s **97**

Table 3.2 Retention factors for coumarin-labeled fatty acids as a function of linear velocity (u). The retention factors are calculated with the statistical moment model by difference between detectors 4 and 1 ..... **98**

Table 3.3: Retention factors for coumarin-labeled fatty acids as a function of linear velocity (u). The retention factors are calculated with the EMG model by difference between detectors 4 and 1 ..... **99**

Table 3.4: Retention factors for coumarin-labeled fatty acids as a function of linear velocity (u). The retention factors are calculated with the Thomas model by difference at detector 4 ..... **100**

Table 3.5: Rate constants calculated as a function of length (L). The constants are determined with the EMG difference method using data collected at a linear velocity of 0.088 cm/s **107**

Table 3.6: Rate constants for coumarin-labeled fatty acids as a function of linear velocity (u). The rate constants are calculated using the moment model by difference between detectors 4 and 1 ..... **108**

Table 3.7: Rate constants for coumarin-labeled fatty acids as a function of linear velocity (u). The rate constants are calculated using the EMG model by difference between detectors 4 and 1 ..... **109**

Table 3.8: Rate constants for coumarin-labeled fatty acids as a function of linear velocity (u). The rate constants are calculated using the Thomas model by difference at detector 4 ..... **110**

Table 3A.1: Mass transfer contributions to plate height according to van Deemter and Purnell calculated using Equations 3A.1 and 3A.2, respectively **123**

Table 3A.2: Corrected plate height (dH_L) using van Deemter and Purnell Equations 3A.1 and 3A.2, respectively **125**

Table 3A.3: Mass transfer contributions to plate height according to Giddings calculated using Equation 3A.3 ..... **126**

Table 3A.4: Corrected plate

Table 3A.5: Mass transfer c
coupling calcula

Table 3A.6: Corrected plate
3A.4 .....

Table 3A.7: Corrected plate

Table 4.1: Retention facto
solutes in met
are given for
aminopyrene
benz[a]anthrac
dibenz[a,j]acr

Table 4.2: Rate constan
defined in Tab

Table 4.3: Activation ene
defined in Ta

Table 4.4: Retention fac
acetonitrile.

Table 4.5: Rate consta
defined in Ta

Table 4.6: Activation e
Solutes def

Table 5.1: Retention f
methanol m
aminopyren
benz[a]anth
dibenz[a,j]a

Table 5.2: Retention
acetonitrile
5.1 .....

Table 5A.1 Effect of
plate he g
phase. S

Table 3A.4: Corrected plate height (dH_L) using Giddings Equation 3A.3 ..... **127**

Table 3A.5: Mass transfer contributions to plate height according to Giddings coupling calculated using Equation 3A.4 ..... **129**

Table 3A.6: Corrected plate height (dH_L) using Giddings coupling Equation 3A.4 ..... **130**

Table 3A.7: Corrected plate height (dH_L) for modern kinetic method **131**

Table 4.1: Retention factor and change in molar enthalpy for PAH and NPAH solutes in methanol. Values in parentheses have large errors and are given for illustrative purposes only. Solutes: pyrene (P), 1-aminopyrene (1AmP), 1-azapyrene (1AzaP), 4-azapyrene (4AzaP), benz[a]anthracene (B[a]A), benz[a]acridine (B[a]Ac), dibenz[a,j]acridine (D[aj]Ac), dibenz[c,h]acridine (D[ch]Ac)..... **142**

Table 4.2: Rate constants for PAH and NPAH solutes in methanol. Solutes defined in Table 4.1..... **148**

Table 4.3: Activation energy for PAH and NPAH solutes in methanol. Solutes defined in Table 4.1..... **152**

Table 4.4: Retention factors and molar enthalpy for PAH and NPAH solutes in acetonitrile. Solutes defined in Table 4.1..... **154**

Table 4.5: Rate constants for PAH and NPAH solutes in acetonitrile. Solutes defined in Table 4.1..... **159**

Table 4.6: Activation energy for PAH and NPAH solutes in acetonitrile. Solutes defined in Table 4.1..... **163**

Table 5.1: Retention factor (k), reduced plate height (h), and skew (s) for methanol mobile phase without modifier. Solutes: pyrene (P), 1-aminopyrene (1AmP), 1-azapyrene (1AzaP), 4-azapyrene (4AzaP), benz[a]anthracene (B[a]A), benz[a]acridine (B[a]Ac), dibenz[a,j]acridine (D[aj]Ac), dibenz[c,h]acridine (D[ch]Ac)..... **174**

Table 5.2: Retention factor (k), reduced plate height (h), and skew (s) for acetonitrile mobile phase without modifier. Solutes defined in Table 5.1 ..... **189**

Table 5A.1 Effect of mobile phase modifier on retention factor (k), reduced plate height (h), and skew (s) for XBridge C_{18} with methanol mobile phase. Solutes defined in Table 5.1 ..... **217**

Table 5A.2: Effect of mob
plate he ght (
methanol mob

Table 5A.3: Effect of mob
plate he ght (h
phase. Solutes

Table 5A.4: Effect of mob
plate he ght (h
mob le phase.

Table 5A.5: Effect of mob
plate he ght (h
mob le phase

Table 5A.6: Effect of mob
plate he ght
aceton tr.e m

Table 5A.7: Effect of mo
plate he ght
mob le phase

Table 5A.8: Effect of mo
plate he ght
mob.le phase

Table 5A.2: Effect of mobile phase modifier on retention factor (k), reduced plate height (h), and skew (s) for XBridge Shield RP_{18} with methanol mobile phase. Solutes defined in Table 5.1 ..... **219**

Table 5A.3: Effect of mobile phase modifier on retention factor (k), reduced plate height (h), and skew (s) for BEH support with methanol mobile phase. Solutes defined in Table 5.1 ..... **221**

Table 5A.4: Effect of mobile phase modifier on retention factor (k), reduced plate height (h), and skew (s) for XBridge C_{18} with acetonitrile mobile phase. Solutes defined in Table 5.1..... **223**

Table 5A.5: Effect of mobile phase modifier on retention factor (k), reduced plate height (h), and skew (s) for XBridge C_{18} with acetonitrile mobile phase. Solutes defined in Table 5.1..... **224**

Table 5A.6: Effect of mobile phase modifier on retention factor (k), reduced plate height (h), and skew (s) for XBridge Shield RP_{18} with acetonitrile mobile phase. Solutes defined in Table 5.1 ..... **226**

Table 5A.7: Effect of mobile phase modifier on retention factor (k), reduced plate height (h), and skew (s) for BEH support with acetonitrile mobile phase. Solutes defined in Table 5.1..... **228**

Table 5A.8: Effect of mobile phase modifier on retention factor (k), reduced plate height (h), and skew (s) for BEH support with acetonitrile mobile phase. Solutes defined in Table 5.1..... **229**

Figure 1.1 Synthesis schem
polymeric sy
synthesis surfa

Figure 1.2 Bridged-ethyle

Figure 1.3 Energy coordin
the mobile ph
thermodynamic

Figure 2.1 C18 coumarin-la

Figure 2.2 Chemical struct
showing deriva
XBridge C18 (E

Figure 2.3 Schematic diag
chromatograph
detector for m
splitting tee. S
AMP: current to

Figure 2.4 Schematic diag
chromatograph
detectors for te
splitting tee. S
optic post ampl
voltage amplifi

Figure 3.1 Regression ana
linear velocity
NLC (— —). A

Figure 3.2 Retention fact
calculated w
at a linear ve
C_{18} (■) C_{22}

Figure 3.3: Retention fa
factors were
Thomas (▲)

LIST OF FIGURES

Figure 1.1 Synthesis schemes for stationary phases. monomeric synthesis (A), polymeric synthesis: solution polymerization (B), polymeric synthesis: surface polymerization (C)..... **2**

Figure 1.2 Bridged-ethylene hybrid support with C_{18} derivatization..... **6**

Figure 1.3 Energy coordinate diagram depicting the transfer of solute X from the mobile phase (m) to the stationary phase (s). Associated thermodynamic and kinetic parameters described in the text..... **10**

Figure 2.1 C_{10} coumarin-labeled fatty acid **72**

Figure 2.2 Chemical structure of the bridged-ethylene hybrid (BEH) phases showing derivatization of each C_{18} phase on the BEH support. (A) XBridge C_{18} (B) XBridge Shield RP_{18}..... **74**

Figure 2.3 Schematic diagram of the experimental system for capillary liquid chromatography with one on-column laser-induced fluorescence detector for mobile phase modifier study. I: injection valve, T: splitting tee, S: splitting capillary, F: filter, PMT: photomultiplier tube, AMP; current to voltage amplifier **76**

Figure 2.4 Schematic diagram of the experimental system for capillary liquid chromatography with four on-column laser-induced fluorescence detectors for temperature and pressure study. I: injection valve, T: splitting tee, S: splitting capillary, R: restricting capillary, FOP: fiber-optic positioner, F: filter, PMT: photomultiplier tube, AMP; current to voltage amplifier **78**

Figure 3.1 Regression analysis of the C_{18} coumarin-labeled fatty acid at a linear velocity of 0.062 cm/s. Peak ( ), EMG (------), NLC (— —), ADS (——)..... **92**

Figure 3.2 Retention factor plotted versus distance. The retention factors were calculated with the moment (A), EMG (B), and Thomas (C) models at a linear velocity of 0.088 cm/s. C_{10} (◆) C_{12} (□) C_{14} (▲) C_{16} (◇) C_{18} (■) C_{20} (○)..... **93**

Figure 3.3: Retention factor plotted versus carbon number. The retention factors were calculated with the moment (○), EMG (□), and Thomas (▲) models at a linear velocity of 0.088 cm/s..... **102**

Figure 3.4: Rate constant
determined w
using data co
C_{-4} (▲) C_{-8} (

Figure 3.5: Rate constant
(B_i phase plot:
calculated us
at a linear velo

Figure 4.1: Structures of
nitrogen-subst
exam ned in th

Figure 4.2: Representat ve
in methanol (3
void time
represented by

Figure 4.3: Representat ve
for methanol
benz[a]anthrace
dibenz[c,h]acr

Figure 4.4: Representat ve
for aceton trile
benz[a]acr d ne
dibenz[c,h]acr

Figure 4.5: Representat ve
for aceton trile
benz[a]anthrac
dibenz[c,h]acr

Figure 4.6: Representat
for aceton trile
benz[a]acr d
dibenz[c,h]ac

Figure 5.1 Retention fac
RP_{-8} (B), br
mobile phas
acetic acid
Negat ve ret

Figure 3.4: Rate constant plotted versus distance. The rate constants were determined with the moment (A), EMG (B), and Thomas (C) models using data collected at a linear velocity of 0.088 cm/s. C_{12} (□) C_{14} (▲) C_{16} (◇) C_{18} (■) C_{20} (○) **104**

Figure 3.5: Rate constant from stationary to mobile (A) and mobile to stationary (B) phase plotted versus carbon number. The rate constants were calculated using moment (○), EMG (□), and Thomas (▲) models at a linear velocity of 0.088 cm/s **114**

Figure 4.1: Structures of the polycyclic aromatic hydrocarbons (PAHs) and nitrogen-substituted polycyclic aromatic hydrocarbons (NPAHs) examined in this study **137**

Figure 4.2: Representative chromatograms of pyrene (A) and 4-azapyrene (B) in methanol (303 K) and acetonitrile (303 K) mobile phases. The void time marker (4-bromomethyl-7-methoxy coumarin) is represented by * **140**

Figure 4.3: Representative graph of retention factor versus inverse temperature for methanol mobile phase. A: pyrene (○), 1-aminopyrene (●), benz[a]anthracene (□), benz[a]acridine (■), dibenz[a,j]acridine (◆), dibenz[c,h]acridine (◇), B: 1-azapyrene (△), 4-azapyrene (▲).. **144**

Figure 4.4: Representative graph of rate constant versus inverse temperature for acetonitrile mobile phase. pyrene (○), benz[a]anthracene (□), benz[a]acridine (■), dibenz[a,j]acridine (◆), dibenz[c,h]acridine (◇) **151**

Figure 4.5: Representative graph of retention factor versus inverse temperature for acetonitrile mobile phase. A: pyrene (○), 1-aminopyrene (●), benz[a]anthracene (□), benz[a]acridine (■), dibenz[a,j]acridine (◆), dibenz[c,h]acridine (◇), B: 1-azapyrene (△), 4-azapyrene (▲).. **156**

Figure 4.6: Representative graph of rate constant versus inverse temperature for acetonitrile mobile phase. pyrene (○), benz[a]anthracene (□), benz[a]acridine (■), dibenz[a,j]acridine (◆), dibenz[c,h]acridine (◇) **161**

Figure 5.1 Retention factor for each solute on XBridge C_{18} (A), XBridge Shield RP_{18} (B), bridged-ethylene hybrid (C) in methanol as a function of mobile phase modifier. pure methanol (▩), triethylamine (▨), acetic acid (▩), acetyl acetone (▨). Solutes defined in Table 5.1. Negative retention factors are indicated by * **179**

Figure 5.2 Reduced plate
Shelc RP-g (B
function of moc
( ), acetic ac
5.1 .....

Figure 5.3 Skew for each
and bridged-et
phase modifie
%), acetyl ac
skews are plo

Figure 5.4 Retention facto
RP-g (B), and
function of m
triethylamine (
acetic acid
Table 5.1 .....

Figure 5.5 Reduced plate
Shelc RP-g (B
function of m
triethylamine (
acetic acid
Table 5.1 .....

Figure 5.6 Skew for each
and bridged-e
mobile phase
acetic acid
acetic acid
Table 5.1 .....

Figure 5.2 Reduced plate height for each solute on XBridge C_{18} (A), XBridge Shield RP_{18} (B), and bridged-ethylene hybrid (C) in methanol as a function of mobile phase modifier. pure methanol (■), triethylamine (▒), acetic acid (▓), acetyl acetone (▒). Solutes defined in Table 5.1 ..... **182**

Figure 5.3 Skew for each solute on XBridge C_{18} (A), XBridge Shield RP_{18} (B), and bridged-ethylene hybrid (C) in methanol as a function of mobile phase modifier. pure methanol (■), triethylamine (▒), acetic acid (▓), acetyl acetone (▒). Solutes defined in Table 5.1 Negative skews are indicated by * **185**

Figure 5.4 Retention factor for each solute on XBridge C_{18} (A), XBridge Shield RP_{18} (B), and bridged-ethylene hybrid (C) in acetonitrile as a function of mobile phase modifier. pure acetonitrile (■), triethylamine (▒), acetic acid (▓), acetyl acetone (▒), pyridine (▒), acetic acid with triethylamine (▒). Solutes defined in Table 5.1 ..... **194**

Figure 5.5 Reduced plate height for each solute on XBridge C_{18} (A), XBridge Shield RP_{18} (B), and bridged-ethylene hybrid (C) in acetonitrile as a function of mobile phase modifier. pure acetonitrile (■), triethylamine (▒), acetic acid (▓), acetyl acetone (▒), pyridine (▒), acetic acid with triethylamine (▒). Solutes defined in Table 5.1 ..... **197**

Figure 5.6 Skew for each solute on XBridge C_{18} (A), XBridge Shield RP_{18} (B), and bridged-ethylene hybrid (C) in acetonitrile as a function of mobile phase modifier. pure acetonitrile (■), triethylamine (▒), acetic acid (▓), acetyl acetone (▒), pyridine (▒), acetic acid with triethylamine (▒). Solutes defined in Table 5.1 ..... **200**

INTROD

1.1. Introduction

Reversed-phase chr

atographic methods

PLC the stationary phas

tively more polar solvent

the retention mechanism

tention mechanism is

ctions and minimize

derstanding is also help

tionary phases with bette

Understanding and

derstanding and deter

tionary phase is synthes

meric or polymeric

meric synthesis involv

the silica surface

only half of the ava

in chain. Polymeric s

ces with silica in the p

the synthesis is

erally, if water is a

CHAPTER 1

INTRODUCTION AND BACKGROUND

1.1. Introduction

Reversed-phase chromatography is the most widely used of all liquid chromatographic methods [1,2]. In reversed-phase liquid chromatography (RPLC), the stationary phase is a nonpolar material while the mobile phase is a relatively more polar solvent. The separation of a series of solutes is governed by the retention mechanism of the phase. Thus, a deep understanding of the retention mechanism is necessary in order to maximize the beneficial contributions and minimize the detrimental contributions to the separation. This understanding is also helpful to guide the development of commercially available stationary phases with better performance.

Understanding and controlling the stationary phase synthesis is essential to understanding and determining the retention mechanism for a separation. The stationary phase is synthesized onto a solid support particle, commonly silica, by monomeric or polymeric surface modification [3,4], as shown in Figure 1.1. Monomeric synthesis involves the reaction of monofunctional silanes with silanol sites on the silica surface (Figure 1.1A). Monomeric phases are sterically limited with only half of the available silanol groups being covalently modified by the alkyl chain. Polymeric synthesis involves the reaction of di- or trifunctional silanes with silica in the presence of water. If water is included in the reaction slurry, the synthesis is referred to as solution polymerization (Figure 1.1B). Alternatively, if water is added to the silica surface prior to the introduction of the

Figure 1.1. Synthesis s
Convergent synthesis s
polymerization. Adapte

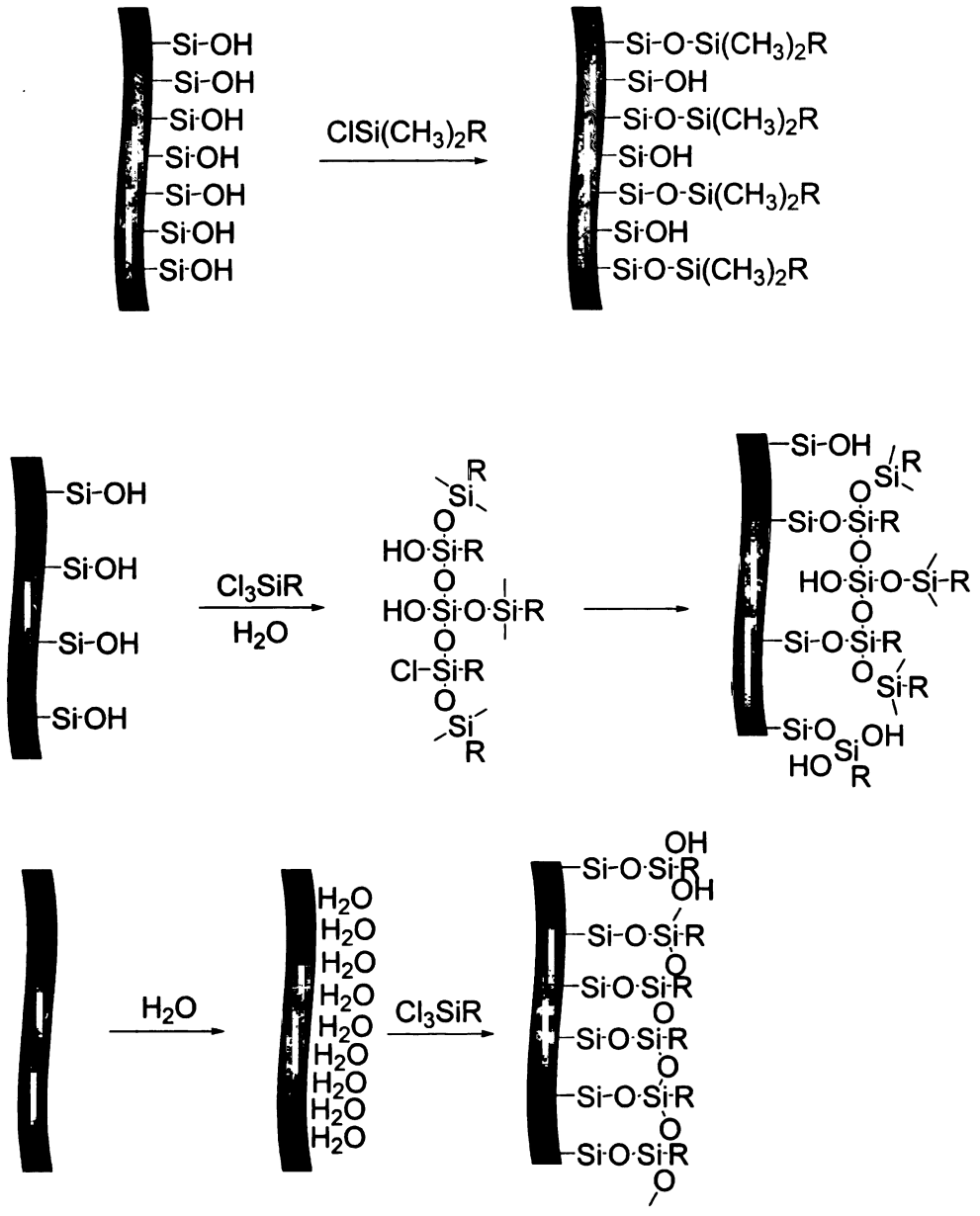

Figure 1.1. Synthesis schemes for stationary phases. A) monomeric synthesis B) polymeric synthesis: solution polymerization C) polymeric synthesis: surface polymerization. Adapted from Sander, Pursch, and Wise [3].

ere the synthesis is re

Pyrenc synthesis results

surface with more silanol g

ost common RPLC stat on

ecoteryl.

The bulk retent on m

ocess of a permeable sur

e noble and the stat on

mechanically results from c

ace reduction and orienta

ell. The comb nat on of

ules in the stat onary pha

ethylation, res dual silano

ecule. Solutes may intera

eakly basic siloxane gro

teractions are primarily res

entional RPLC phase that s

ay have some contr but on

The adsorpt on mec

retention mechanism. F

ica surface. Common s

ica and alumina, as

chlorobenzene) and porou

silane, the synthesis is referred to as surface polymerization (Figure 1.1C). Polymeric synthesis results in higher bonding densities of the alkyl chain at the surface, with more silanol groups being covalently linked to alkyl chains. The most common RPLC stationary phases are derivatized with C_{18}, followed by C_8, and phenyl.

The bulk retention mechanism is partition because the stationary phase consists of a permeable surface where the solute can completely dissolve in both the mobile and the stationary phases. Interaction with the stationary phase predominantly results from dispersion forces, however other interactions, such as dipole induction and orientation, ion-dipole, and hydrogen-bonding can occur as well. The combination of these interactions will influence the solubility of the solute in the stationary phase and thus, influence its retention. However, after derivatization, residual silanol groups may remain at the surface of the underlying particle. Solutes may interact with the weakly acidic silanol groups (Si-OH) and weakly basic siloxane groups (Si-O-Si) of the underlying silica. These interactions are primarily responsible for the adsorption mechanism [5-8]. Thus, a typical RPLC phase that should have a bulk partition-like retention mechanism may have some contribution from solute adsorption at residual silanols.

The adsorption mechanism has several features that distinguish it from the partition mechanism. First, the stationary phase consists of an impermeable, solid surface. Common stationary phases include inorganic materials such as silica and alumina, as well as organic materials such as poly(styrene-divinylbenzene) and porous graphitic carbon. Most of these adsorbents are

...terogeneous, having su...

...tional groups general...

...ron donor-acceptor (Bro...

...ecause) interactions, an...

...ractions, there is often ...

...tional groups of the sta...

...longer. Also, becaus...

...se there are a limited n...

...ecules are in competition...

...ongly interacting species ...

...ostly different from the...

The partition and ad...

...ation mechanisms in R...

...of one another. When a...

...eferable design, it is gen...

...for a combination occ...

...ssential to the separa...

...ractions that occur by a...

Silica is by far ...

...matography. A numb...

...ntiophases, have b...

...ems of efficiency, rig...

...the number of improve...

heterogeneous, having surface sites with different functional groups. These functional groups generally exhibit strong and selective interactions, including proton donor-acceptor (Brönsted acid-base) and electron donor-acceptor (Lewis acid-base) interactions, among others [9]. As a consequence of these strong interactions, there is often a fixed stoichiometry between the solute and the functional groups of the stationary phase, most frequently 1:1, but occasionally 2:1 or higher. Also, because the stationary phase is a solid with a fixed surface area, there are a limited number of surface sites. Consequently, the solute molecules are in competition for the surface sites and may be displaced by more strongly interacting species. These features of the adsorption mechanism make it distinctly different from the partition mechanism.

The partition and adsorption mechanisms are the most widely observed retention mechanisms in RPLC [9], and may occur individually or in combination with one another. When a combination of mechanisms occurs by specific and deliberate design, it is generally beneficial to the resulting separation. However, when a combination occurs unintentionally or by accident, it is generally detrimental to the separation. Thus, in RPLC, efforts to reduce solute-silanol interactions that occur by an adsorption mechanism are important.

Silica is by far the most widely used solid support for liquid chromatography. A number of other solid supports, such as zirconia, titania, and polymeric phases, have been used. However, silica is superior to other supports in terms of efficiency, rigidity, and general performance. Thus, in recent years, a large number of improvements to silica-based phases have been made that

...ntly reduce the deter...

...ssure high purity s...

...metallic impurities that a...

...[7-9] In addition, enco...

...erically-hindered mono...

...creased interaction of...

...hases incorporating a p...

...ered the underlying ...

...selectivity of the sep...

The improvemen...

...types of separat...

...ilicas with silica-b...

...ngle temperature, a...

...ethyl groups. For this...

...hybrid inorganic pa...

...secondary phase. Th...

...minimized by the...

...methoxysilylethan...

...layer of silica yet...

...ction the ethylene...

...ethanols available t...

...ifications for this ...

...characterize its retent...

directly reduce the detrimental interaction of solutes with residual silanols. For instance, high purity silica, introduced in the 1980's, reduces peak tailing from metallic impurities that are known to affect of the acidity of the silanol sites [10,11]. In addition, endcapping with trimethylsiloxane and using trifunctional and sterically-hindered monofunctional silanes in the derivatization steps provide decreased interaction of solutes with the underlying support [12,13]. Likewise, phases incorporating a polar embedded group in the alkyl chain have been used to shield the underlying support in an effort to reduce peak tailing while modifying the selectivity of the separation [14-16].

The improvements made on silica supports have significantly influenced the types of separations that can currently be performed. Nevertheless, problems with silica-based materials continue to exist at high and low pH, extreme temperature, and for solutes that are more likely to adsorb to residual silanol groups. For this reason, a new type of support material based on a hybrid organic – inorganic particle has been developed and widely used as an RPLC stationary phase. This bridged-ethylene hybrid (BEH) particle (Figure 1.2) is synthesized by the co-condensation of tetraethyoxysilane with 1,2-bis(triethoxysilyl)ethane [17]. These support particles have the mechanical strength of silica yet the high pH stability of polymeric particles [17,18]. In addition, the ethylene bridge in the backbone is thought to decrease the number of silanols available to bind to basic solutes. Despite the wide number of useful applications for this phase, only a small number of studies have attempted to characterize its retention behavior.

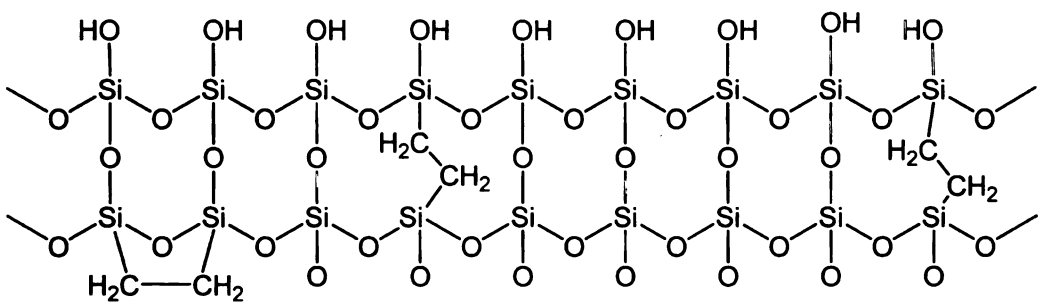

Figure 1.2. Bridged-ethylene hybrid (BEH) support

This dissertation

ssociation in RPLC. St

escribed. The retent

ntal theory. In ad

hermodynamic and k

In this chapter, t

is briefly summariz

hermodynamic and k

ethods to the part

romatography is rev

2.1 Thermodynam

Thermodynam

teraction between t

ormation is intrins

rocesses and understa

rocesses. This inf

ept. Both thermo

olution [9,20].

The thermod

e stationary phase

ost commonly, the

ecial reaction.

The first-order rea

This dissertation examines the fundamental properties that govern a separation in RPLC. Stationary phases built on both silica and hybrid supports are studied. The retention processes are quantitated using thermodynamic and kinetic theory. In addition, various experimental methods for extracting thermodynamic and kinetic parameters from solute zone profiles are evaluated.

In this chapter, the fundamental theories of thermodynamics and kinetics are briefly summarized and the experimental methods of determining thermodynamic and kinetic parameters are described. The application of these methods to the partition and adsorption retention mechanisms in liquid chromatography is reviewed [19].

1.2. Thermodynamic and kinetic theory

Thermodynamic information provides an understanding of the energies of interaction between the solute and the mobile and stationary phases. This information is intrinsically related to retention and selectivity. Kinetic information provides an understanding of the rates of mass transport and surface interaction processes. This information is intrinsically related to the efficiency or plate height. Both thermodynamic and kinetic information are necessary to optimize resolution [9,20].

The thermodynamics and kinetics of solute transfer between the mobile and stationary phases in liquid chromatography can be treated in several ways. Most commonly, the retention process is treated as if it were analogous to a chemical reaction. For a partition mechanism, this may be represented as a simple first-order reaction

$X_m \rightleftharpoons X_s$

a solute (X) distributed

four adsorption mechan

ves a second-order rea

$X_m + S \rightleftharpoons XS$

y

$X_m + DS \rightleftharpoons XS + D_m$

ere D is a displacing

ncentrations of stationa

ese mechanisms

The treatment of th

ese simplistic view. F

the reactants have

ween them. The chro

roscopic level, as it

ceives are also hel

ck mobile phase c

e surface of the stat

ion. The stationary p

ves different retent

ion of the solute in the

mical reaction. S

$$X_m \rightleftharpoons X_s \tag{1.1}$$

for a solute (X) distributed between the mobile (m) and stationary (s) phases. For an adsorption mechanism, where the number of stationary phase sites (S) is limited, a second-order reaction is more appropriate

$$X_m + S \rightleftharpoons XS \tag{1.2}$$

or

$$X_m + DS \rightleftharpoons XS + D_m \tag{1.3}$$

where D is a displacing agent that is added to the mobile phase. If the concentrations of stationary phase sites and the displacing agent are sufficiently large, these mechanisms may be treated as pseudo-first-order reactions.

The treatment of the retention process as a chemical reaction involves a rather simplistic view. First, chemical reactions occur in homogeneous solution and the reactants have relatively well defined energies and diffusion distances between them. The chromatographic system is intrinsically heterogeneous at the macroscopic level, as it involves two immiscible phases. Moreover, the phases themselves are also heterogeneous at the microscopic and molecular levels. The bulk mobile phase composition may be substantially different from that near the surface of the stationary phase or in the pores of the stationary phase support. The stationary phase may have several different types of retention sites or even different retention mechanisms. Because of these heterogeneities, the energy of the solute in the mobile and stationary phases is not as well defined as *in* a chemical reaction. Second, given sufficient time, the chemical reaction can

ıbıe a state of equ

ıctions are equal and

ıctants remain consta

ıy can never acn eve

ıtable conditions, acn e

ıs simplistic view, th

ıction is prevalent a

ıgnitude of the var ous

If the retention p

ıeir coordinate diag

ıermodynamic and k

ıe mobile phase

ıction state (X_2). T

ıalpy (ΔH) and m

ıween the final and

ıeighted average

ıonary and mobile

The kinetic asp

ıction-state theor

ıracterized by a fas

ıe pseudo-equilibrium c

ıction state and t

ıcesses, e.g. the

achieve a state of equilibrium in which the rates of the forward and reverse reactions are equal and the activities (or concentrations) of the products and reactants remain constant. The chromatographic system, by virtue of dynamic flow, can never achieve this macroscopic state of equilibrium but may, under suitable conditions, achieve a microscopic condition of steady state [20]. Despite this simplistic view, the treatment of liquid chromatography as a chemical reaction is prevalent as it provides considerable insight to the rank and magnitude of the various contributions to the retention mechanism.

If the retention process is considered as a chemical reaction, then an energy coordinate diagram (Figure 1.3) can be used to explain the analogous thermodynamic and kinetic contributions. In this diagram, the solute transfers from the mobile phase (X_m) to the stationary phase (X_s) through a high-energy transition state ($X_{\ddagger}$). The thermodynamic parameters, e.g. the change in molar enthalpy (ΔH) and molar volume (ΔV), are characterized by the difference between the final and initial states. These thermodynamic quantities represent the weighted average value in all of the available states in the heterogeneous stationary and mobile phases, respectively.

The kinetic aspects of the retention event can be described by using transition-state theory. The transfer from mobile to stationary phase is characterized by a fast equilibrium between the mobile phase and transition state with pre-equilibrium constant $K_{m\ddagger}$, followed by a rate-limiting step between the transition state and the stationary phase with rate constant k_{sm}. The kinetic parameters, e.g. the activation enthalpy ($\Delta H_{\ddagger m}$) and activation volume ($\Delta V_{\ddagger m}$),

Figure 1.3. Energy co
mobile phase (m)
parameters

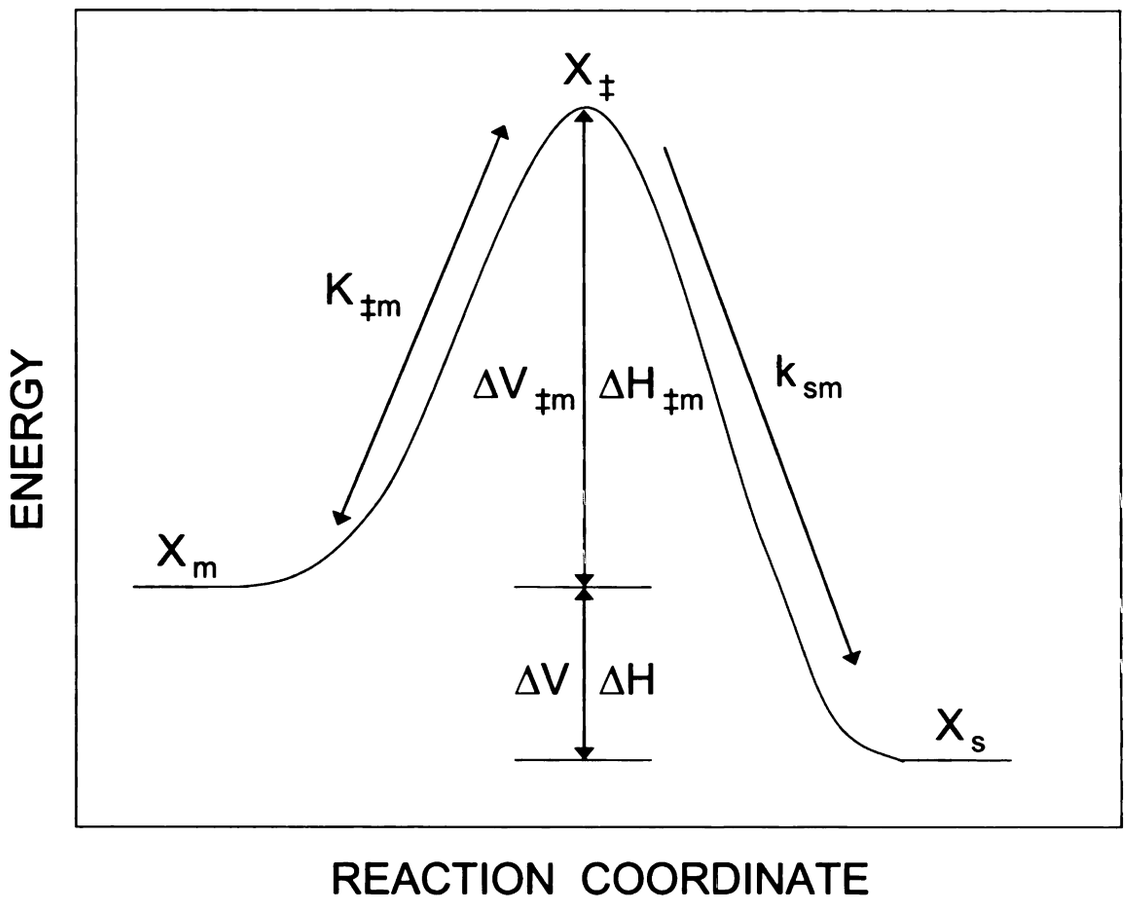

Figure 1.3. Energy coordinate diagram depicting the transfer of solute X from the mobile phase (m) to the stationary phase (s). Associated thermodynamic and kinetic parameters are described in the text.

an be used to eluc dat

ister from stationary

ze constant k_{ms} are

ation volume (ΔV_{s}

ia available paths be

ermodynamic and k

'21. Thermodynamic

As noted above

ie chromatographic s

actions may be acc

ecular phases (a

$$K = \frac{a_s}{a_m} = K_D$$

where K is the equil b

ere The phase rat o

e volume of the mob

The equilibrium

ated ΔG_i by

$$K = e^{-\Delta G / RT}$$

where R is the gas c

ated to the chang

adsorption equ

can be used to elucidate the kinetic description of the retention event. For the transfer from stationary to mobile phase, the pre-equilibrium constant $K_{s\ddagger}$ and rate constant k_{ms} are used to determine the activation enthalpy ($\Delta H_{s\ddagger}$) and activation volume ($\Delta V_{s\ddagger}$). These kinetic quantities represent a weighted average of all available paths between the final and initial states. The derivation of these thermodynamic and kinetic quantities is described in the following sections.

1.2.1. Thermodynamic theory

As noted above, equilibrium is not attained due to the dynamic nature of the chromatographic system. However, at the microscopic level, steady-state conditions may be achieved in which the activity of the solute in the mobile and stationary phases (a_m and a_s, respectively) achieves a constant value

$$K = \frac{a_s}{a_m} = k\beta \tag{1.4}$$

where K is the equilibrium constant, k is the retention factor, and β is the phase ratio. The phase ratio is defined as the volume of the stationary phase divided by the volume of the mobile phase.

The equilibrium constant is related to the change in molar Gibbs free energy (ΔG) by

$$\ln K = \frac{-\Delta G}{RT} \tag{1.5}$$

where R is the gas constant and T is the temperature. The Gibbs free energy is related to the changes in molar enthalpy (ΔH) and molar entropy (ΔS) by the Gibbs-Helmholtz equation [21]

$\Delta G = \Delta H - T\Delta S$

Substitution of Equat

ation to the molar entr

$\ln K = \ln\beta = \frac{-\Delta H}{RT} + \frac{\Delta}{R}$

The change in molar

ogram of the retent

This will yield a slope

ntact that contains

hase ratio. When

ained from the

ccurate determination

The molar entropy

ermination of the

ocess for an endot

the solute from mob

ractions, most su

hermodynamically favorab

ocess when there

number or distr

hange in volume

ntropy as the solut

The change i

$\Delta E = P\Delta V$

$$\Delta G = \Delta H - T\,\Delta S \tag{1.6}$$

By substitution of Equation 1.6 into Equation 1.5, the retention factor can be related to the molar enthalpy and molar entropy as

$$\ln k = \ln K - \ln\beta = \frac{-\Delta H}{RT} + \frac{\Delta S}{R} - \ln\beta \tag{1.7}$$

The change in molar enthalpy can be determined by graphing the natural logarithm of the retention factor versus inverse temperature at constant pressure. This will yield a slope that is related to the change in molar enthalpy, and an intercept that contains information about the change in molar entropy and the phase ratio. When the phase ratio is known, the molar entropy can be determined from the intercept. However, the phase ratio is often not known and accurate determination of the molar entropy is not possible. The phase ratio and the molar entropy must be independent of temperature for accurate determination of the molar enthalpy. The change in molar enthalpy will be positive for an endothermic transfer and negative for an exothermic transfer of the solute from mobile to stationary phase. Although there are some noteworthy exceptions, most successful separations in liquid chromatography involve an energetically favorable exothermic process. The change in molar entropy will be positive when there is a favorable dissipation of energy through an increase in the number or distribution of microstates. This most commonly occurs through a change in volume or concentration, leading to a change in configurational entropy, as the solute is transferred from the mobile to stationary phase.

The change in molar enthalpy is defined as [21]

$$\Delta H = \Delta E + P\Delta V \tag{1.8}$$

ere ΔE is the cha

ure and P is th

ves

$$\ln K = \frac{-\Delta E}{RT} - \frac{P\Delta V}{RT} +$$

he change in ma

gram of the rea

ed a slope th

ta contains info

ase ratio. Thes

termination of th

ference in volu

ases, the possi

ation of the so

22 Kinetic the

Kinetic info

hanism than

proaches to de

hermodynam

ction. The G

he second a

haracterize the

ch of these a

reaction pro

where ΔE is the change in molar internal energy, ΔV is the change in molar volume, and P is the pressure. Substitution of Equation 1.8 into Equation 1.7 yields

$$\ln k = \frac{-\Delta E}{RT} - \frac{P\,\Delta V}{RT} + \frac{\Delta S}{R} - \ln\beta \qquad (1.9)$$

The change in molar volume can be determined by graphing the natural logarithm of the retention factor versus pressure at constant temperature. This will yield a slope that is related to the change in molar volume, and an intercept that contains information about the molar internal energy, molar entropy, and phase ratio. These parameters must be independent of pressure for accurate determination of the molar volume. The change in molar volume includes the difference in volume that the solute occupies in the mobile and stationary phases, the possible change in volume of the phases, and the difference in solvation of the solute between phases.

1.2.2. Kinetic theory

Kinetic information provides a deeper understanding of the retention mechanism than does thermodynamics alone. There are two common approaches to describe the kinetic behavior. The first approach, consistent with the thermodynamic treatment, is to consider the retention process as a chemical reaction. The general principles of chemical kinetics are then applicable [21]. The second approach, commonly used in chemical engineering, is to characterize the rates at which the individual mass transfer processes occur. Each of these approaches provides a valuable and complementary description of the retention process and will be described herein.

If the retention p

action according to Eq

$$X_m \underset{k_{ms}}{\overset{k_{sm}}{\rightleftharpoons}} X_s$$

ere k_{sm} and k_{ms} are t

ate to stationary p

ese designations f

ssertion, regardless

ese are "lumped" ra

ress behavior includ

ed stationary phase

stance to mass tr

ehavior are related

ehavior by

$$\frac{k_{sm}}{k_{ms}}$$

The detailed

pendence of therm

is expressed by t

$$k_{sm} = A_{sm} \exp \frac{-\Delta E}{RT}$$

ere A_{sm} is the pre

ecule from mobile

If the retention process is treated as a first-order or pseudo-first-order reaction according to Equation 1.1,

$$X_m \underset{k_{ms}}{\overset{k_{sm}}{\rightleftharpoons}} X_s \tag{1.10}$$

then k_{sm} and k_{ms} are the corresponding rate constants for solute transfer from mobile to stationary phase and from stationary to mobile phase, respectively. These designations for the rate constants will be used throughout this dissertation, regardless of the retention mechanism (partition, adsorption, etc.). These are "lumped" rate constants, i.e. they comprise all contributions to the kinetic behavior including the sorption/desorption event, diffusion in the mobile and stationary phases, diffusion in pores and stagnant layers, interfacial resistance to mass transfer, etc. The rate constants, which reflect the kinetic behavior, are related to the retention factor, which reflects the thermodynamic behavior, by

$$k = \frac{k_{sm}}{k_{ms}} \tag{1.11}$$

The detailed kinetic parameters can be elucidated by applying a combination of thermodynamic and transition-state theories. The rate constant k_{sm} is expressed by the Arrhenius equation [21] as

$$k_{sm} = A_{\ddagger m} \exp\left(\frac{-\Delta E_{\ddagger m}}{RT}\right) \tag{1.12}$$

where $A_{\ddagger m}$ is the pre-exponential factor and $\Delta E_{\ddagger m}$ is the activation energy for the transfer from mobile to stationary phase. By rearrangement,

$$\ln k_{sm} = \ln A_{\ddagger m} - \frac{\Delta E_{\ddagger m}}{RT}$$

The activation energy ca

the constant versus in

pose that is related to

rmation about the p

the energetic barrier tha

stationary phase.

Using classical

ypes by

$$E_{\ddagger m} = \Delta H_{\ddagger m} - RT - p$$

Substitution of Equa

$$\ln k_{sm} = \ln A_{\ddagger m} - \frac{\Delta H_{\ddagger}}{}$$

The activation volume

the constant versus

that is related to the a

and the activation e

the pre-exponential f

ivation volume. T

to be overcome fo

ivation enthalpy

ivation volume v a

can be used to dete-

$$\ln k_{sm} = \ln A_{\ddagger m} - \frac{\Delta E_{\ddagger m}}{RT} \tag{1.13}$$

The activation energy can be determined by graphing the natural logarithm of the rate constant versus inverse temperature at constant pressure. This will yield a slope that is related to the activation energy, and an intercept that contains information about the pre-exponential factor. The activation energy represents the energetic barrier that must be overcome for the solute transfer from mobile to stationary phase.

Using classical thermodynamic relationships, the activation energy is given by

$$\Delta E_{\ddagger m} = \Delta H_{\ddagger m} + RT - P\Delta V_{\ddagger m} \tag{1.14}$$

By substitution of Equation 1.14 into Equation 1.13

$$\ln k_{sm} = \ln A_{\ddagger m} - \frac{\Delta H_{\ddagger m} + RT - P\Delta V_{\ddagger m}}{RT} \tag{1.15}$$

The activation volume can be determined by graphing the natural logarithm of the rate constant versus pressure at constant temperature. This will yield a slope that is related to the activation volume, and an intercept that contains information about the activation enthalpy and pre-exponential factor. The activation enthalpy and pre-exponential factor must be independent of pressure for determination of activation volume. The activation volume represents the volumetric barrier that must be overcome for the solute transfer from mobile to stationary phase. The activation enthalpy can then be calculated from the activation energy and activation volume via Equation 1.14. In a similar manner, the rate constant k_{ms} can be used to determine the activation energy ($\Delta E_{s\ddagger}$), activation volume ($\Delta V_{s\ddagger}$),

activation enthalpy

ase. These kinetic

olumetric requ re

ermodynamic descr p

Another approa

aluate the ind v

ocessing. M yate

ster processes:

fusion and sorpt on

ccurs in the bulk m

ough the packed b

the bulk mobile p

ase. Intrapart cle

ace. This proces

ase n the pore, bu

the solute sorbs to

ction desorpt on e

ical and sepa

ocess. The math

ation 1.3.3.2.1.

3. Methods for t

This section

ication of thermo

and activation enthalpy ($\Delta H_{s\ddagger}$) for the solute transfer from stationary to mobile phase. These kinetic quantities provide a detailed description of the energetic and volumetric requirements of the retention process that complement the thermodynamic description.

Another approach, which is more common in the engineering literature, is to evaluate the individual mass transfer processes that contribute to band broadening. Miyabe and Guiochon [22] have identified four primary mass transfer processes: axial dispersion, external mass transfer, intraparticle diffusion, and sorption/desorption kinetics. Axial dispersion is broadening that occurs in the bulk mobile phase, including axial diffusion and multiple paths through the packed bed. External mass transfer occurs as the solute moves from the bulk mobile phase through the thin stagnant film at or near the particle surface. Intraparticle diffusion occurs as the solute diffuses into the pore of the particle. This process consists not only of solute diffusion through the mobile phase in the pore, but also surface diffusion on the wall of the particle. Finally, as the solute sorbs to and from the surface, slow mass transfer arises from the sorption/desorption event. These mass transfer processes are considered as individual and separable contributions to the overall broadening and rate constant. The mathematical treatment of this approach will be described in Chapter 1.3.3.2.1.

1.3. Methods for thermodynamic and kinetic studies

This section reviews the traditional methods for characterization and evaluation of thermodynamic and kinetic parameters for a separation [19].

1.3.1. Perturbatio

Among the a

rameters, pertu

rtions represen

tionary phase

rturbation is a

mentation of t

n be achieved

ouble momen

ew conditions

ectrum and

ter simplicity.

without interfere

ists of the so

ifter. One of

ning which th

ained. Hence

ether those of

der to minimiz

ose to unity a

mentation fo

n be applied

does not contra

1.3.1. Perturbation methods

Among the available methods for evaluation of thermodynamic and kinetic parameters, perturbation methods play an important role [23,24]. Perturbation methods represent the simplest approach, wherein the solute, mobile phase, and stationary phase of interest are contained in a small, static cell. A fast perturbation is applied to the equilibrium in order to alter the activity or concentration of the solute in the mobile and stationary phases. The perturbation may be achieved by rapidly changing conditions such as temperature, pressure, or dipole moment. After perturbation, the rate of relaxation of the system to the new conditions is monitored, followed by mathematical extraction of the equilibrium and rate constants. The advantage of the perturbation methods is their simplicity, where thermodynamic and kinetic behavior can be measured without interference from flow contributions. The measured rate constants consist of the sorption/desorption process and diffusional contributions to mass transfer. One of the limitations of these methods is that they require perturbation, during which the actual thermodynamic and kinetic behavior of the system is altered. Hence, the determined values of equilibrium and rate constants are neither those of the initial state nor those of the final state after perturbation. In order to minimize the required perturbation, the equilibrium constant should be as close to unity as possible. This ensures the greatest change in activity or concentration for a given perturbation of the system. In addition, the perturbation must be applied uniformly to the entire system and with sufficient speed that it does not contribute to the observed kinetic behavior. Although these methods

ze very promising. th

eatively limited.

1.3.1.1. Temperature j

The temperatu

erturbation methods

ic data including re

ermodynamic change and

ilibrium constant

Equation 1.16

$$\frac{\partial \ln K}{\partial T}_p = \frac{\Delta H}{RT^2}$$

The temperature pu

ering [29], or opt

structure and the s

rganic and biochem

1.3.1.2. Pressure ju

The pressure

ic data, including

pendence on pre

hange in molar vo

$$\frac{\partial \ln K}{\partial P}_T = \frac{-\Delta V}{RT}$$

The pressure pulse

lease of pressure

are very promising, their application to chromatographic systems has been relatively limited.

1.3.1.1. Temperature jump method

The temperature jump method is the most versatile and useful of the perturbation methods. This method is based on the concept that chemical equilibria, including retention processes, are usually associated with a non-zero enthalpy change and, thus, are temperature dependent. The shift in the equilibrium constant depends on the change in molar enthalpy according to Equation 1.16

$$\left(\frac{\partial \ln K}{\partial T}\right)_P = \frac{\Delta H}{RT^2} \tag{1.16}$$

The temperature pulse can be induced by Joule heating [25-28], dielectric heating [29], or optical heating [30]. The instrument is relatively simple to construct and the speed of heating is sufficient for a wide range of inorganic, organic and biochemical equilibrium reactions.

1.3.1.2. Pressure jump method

The pressure jump method is based on the concept that chemical equilibria, including retention processes, display a more or less marked dependence on pressure. The shift in the equilibrium constant depends on the change in molar volume according to Equation 1.17.

$$\left(\frac{\partial \ln K}{\partial P}\right)_T = \frac{-\Delta V}{RT} \tag{1.17}$$

The pressure pulse can be produced either by a sudden application or a sudden release of pressure in the system. The pressure jump method does not have as

wide a range of appl

ited number of react

owever, this method

ranged species, due t

3.1.3. Dipole jump r

The dipole jum

uced by photoexc

ments in the grou

estruction after pho

e relative affinity of

he change in solub

ment as well as th

ited state. Beca

estruction cross sec

ction, excited-stat

ese effects, the s

ole activity (or co

3.2. Shallow bed

The shallow

estruction metho

ecovery phase p

ction. The expe

estruction (release

wide a range of application as the temperature jump method because of the limited number of reactions that exhibit a sufficiently large pressure dependence. However, this method has been beneficial for the study of sorption/desorption of charged species, due to their relatively large changes in molar volume [31].

1.3.1.3. Dipole jump method

The dipole jump method is based on the change in dipole moment induced by photoexcitation. Many chromophores exhibit different dipole moments in the ground and excited states as a consequence of electronic redistribution after photoexcitation. This change in dipole moment can influence the relative affinity of the solute for the mobile and stationary phases [32]. The net change in solubility is dependent upon the magnitude of the change in dipole moment as well as the absorption cross section and fraction of molecules in the excited state. Because high photon flux may be required to ensure large absorption cross sections, due care must be taken to avoid thermal heating. In addition, excited-state reactions of the solute must be avoided. In the absence of these effects, the shift in the equilibrium constant depends on the change in solute activity (or concentration) according to Equation 1.4.

1.3.2. Shallow bed method

The shallow bed method can be considered as an intermediate between perturbation methods and chromatographic methods. In this method, the stationary phase particles are packed in an extremely short ("zero length") column. The experiments may be performed in two ways: sorption (uptake) or desorption (release) methods. In the sorption method, a mobile phase solution

ıtaining the solute flo

ıncentration of the sol

ident solution. If the

ayer surrounding the p

rough this layer w

reversible processes

ssumed sorption rate

ıbstrate that has bee

his measurement p

easurement is then re

sorption rate curve.

An alternative a

he desorption metho

low of a mobile phas

hen is abruptly s

be described from

unction of time, t

easurement. Specif

ıltaneous molec

be F, as follows

$$\frac{[dn/(t_2)/dt_1]}{F}$$

By integration, the

containing the solute flows through the shallow bed at a high linear velocity. The concentration of the solute in the effluent solution is nearly identical to that in the influent solution. If the linear velocity is sufficiently high, the stagnant diffusion layer surrounding the particle will be thin. Hence, the time required for diffusion through this layer will be small compared to the time required for the slow intraparticle processes. As a result, the intraparticle processes will determine the observed sorption rate. After a certain time, the flow is stopped and the amount of solute that has been sorbed is measured by eluting it out of the shallow bed. This measurement provides a single point on the sorption curve. This experiment is then repeated for varied sorption times to construct the complete sorption rate curve.

An alternative approach that is less time-consuming and labor-intensive is the desorption method. In this method, the shallow bed is pre-equilibrated by flow of a mobile phase solution containing the solute. To initiate the experiment, the flow is abruptly shifted to a solute-free mobile phase, which causes the solute to be desorbed from the bed. By detecting the eluted solute concentration as a function of time, the desorption curve can be constructed from a single experiment. Specifically speaking, the concentration C(t) is a function of the instantaneous molecular desorption rate of the solute ($dn_i(t) / dt$) and of the flow rate (F) as follows

$$C(t) = \frac{(dn_i(t)/dt)}{F} \tag{1.18}$$

After integration, the desorption rate curve is constructed as

$$n = F\int_0^t C(t)\,dt$$

he desorption rate

retical models, su

ble to extract the ra

3.3. Chromatograp

Chromatograph

ining thermody

ulation methods

king through the c

henomena to the zo

matographic met

3.3.1. Frontal meth

In frontal analy

lution containing a

roduced continuou

lumn becomes sa

lumn gradually inc

ter position of the

lumn constant

e amount of solut

lange point of t

easing concentra

$$n_i(t) = F\int_0^t C(t)\,dt \qquad (1.19)$$

The desorption rate curve is then fit by nonlinear regression to different theoretical models, such as the linear driving force model and spherical diffusion model, to extract the rate constants [33-36].

1.3.3. Chromatographic methods

Chromatographic methods are the most widely used methods for determining thermodynamic and kinetic behavior of the system. In contrast to perturbation methods, chromatographic methods are dynamic with mobile phase flowing though the column at all times. In this way, the contribution of flow phenomena to the zone profile cannot be neglected. The two most common chromatographic methods are frontal and impulse methods.

1.3.3.1. Frontal method

In frontal analysis, the column is pre-equilibrated with the mobile phase. A solution containing a known concentration of solute in the mobile phase is introduced continuously. As the solute sorbs onto the stationary phase, the column becomes saturated and the concentration of solute eluting from the column gradually increases, forming a characteristic breakthrough curve. The mean position of the breakthrough curve can be related to the concentration and equilibrium constant of the solute as well as the sorption capacity of the column. The amount of solute sorbed is calculated from the breakthrough curve providing a single point of the isotherm. This process is repeated for progressively increasing concentrations of the solute to construct the complete isotherm.

To obtain k

retically calculate

ifferent values of th

ium isotherm

breakthrough curves

efficient is determ

between the theoret

is assumed that th

ect to the frontal ar

the average conce

3.3.2. Impulse me

The impulse

ple solute onto the

lumn or post-colu

affected by any of

3.3.2.1. Plate hei

In this mode

by the mean ar

thickening or plate

accurate method u

the shape of the zo

respectively) ar

To obtain kinetic information, theoretical breakthrough curves are numerically calculated for each concentration step. These theoretical curves use different values of the rate constant in the transport model, together with the equilibrium isotherm determined from the breakthrough data. The theoretical breakthrough curves are then compared to the experimental ones. The rate coefficient is determined in such a way that the best agreement is observed between the theoretical and experimental breakthrough curves. In this approach, it is assumed that the rate constant remains constant during each concentration step in the frontal analysis measurement and that this rate constant corresponds to the average concentration of each step [22].

1.3.3.2. Impulse method

The impulse method is generally performed by injecting a small volume of the solute onto the column. The elution of the solute zone is monitored by on-column or post-column detection. The retention factor and rate constants can be extracted by any of the following models.

1.3.3.2.1. Plate height model

In this model, the thermodynamic and kinetic parameters are determined from the mean and the broadening of the zone profile, respectively. The broadening or plate height may be determined in a variety of ways, but the most accurate method uses statistical moments as they make no assumptions about the shape of the zone profile. The first and second statistical moments (M_1 and M_2, respectively) are calculated from the zone profile as

$$M_1 = \frac{\int C(t)\,t\,dt}{\int C(t)\,dt}$$

$$M_2 = \frac{\int C(t)(t - M_1)^2 dt}{\int C(t)\,dt}$$

where C(t) is the co

represents the mean r

$$k = \frac{M_1 - t_0}{t_0}$$

where t_0 is the elution

The method

application of Gauss

can be related to the p

$$N = \frac{\sigma^2}{L} = \frac{M_2 L}{M_1^2}$$

where σ^2 is the varian

Mass kinetics (C_s) is

Equations [20] and is g

$$C_{ss} = \frac{2k}{(1-k)^2 k_{ms}}$$

$$k_{ms}$$

$$C_{ss} = \frac{2ku}{(1-k)^2 dH_L}$$ an

$$M_1 = \frac{\int C(t)\, t\, dt}{\int C(t)\, dt} \tag{1.20}$$

$$M_2 = \frac{\int C(t)(t - M_1)^2 dt}{\int C(t)\, dt} \tag{1.21}$$

where C(t) is the concentration as a function of time. The first moment represents the mean retention time and is related to the retention factor by

$$k = \frac{M_1 - t_0}{t_0} \tag{1.22}$$

where t_0 is the elution time for a non-retained compound.

The method of calculating kinetic rate constants is derived by extrapolation of Giddings' work [20]. The plate height in the length domain (H_L) can be related to the peak variance or second moment in the time domain by

$$H_L = \frac{\sigma_L^2}{L} = \frac{M_2\, L}{M_1^2} \tag{1.23}$$

where σ^2 is the variance and L is the column length. The mass transfer term for slow kinetics (C_s) is derived from the generalized nonequilibirum theory of Giddings [20] and is given by

$$C_s = \frac{2k}{(1+k)^2 k_{ms}} \tag{1.24}$$

Thus,

$$k_{ms} = \frac{2\, k\, u}{(1+k)^2 dH_L} \quad \text{and} \quad k_{sm} = \frac{2\, k^2\, u}{(1+k)^2 dH_L} \tag{1.25}$$

where u is the linear

arising from slow mass

As discussed n

rate height contribut

approach the stat st ca

$$W_{ac} = \frac{L}{u}\delta_g$$

$$W_{pc} = \frac{2L}{u}(\delta_{ax} - \delta_f - \delta_g$$

where δ_g is a dimens

$$\delta_{ax} = \varepsilon_b(1-\varepsilon_b)(\alpha - \beta$$

The contributions to

for macroparticle diffus

$$\delta_g = \frac{D_i}{u^2}\delta_g^2$$

$$\delta_f = (1-\varepsilon_b)\frac{R_p}{3k_f}(\alpha -$$

$$\delta_{ax} = (1-\varepsilon_b)\frac{R_p^2}{15D_e}$$

where ε_b and ε are

boring material, R_p

the external mass

where **u** is the linear velocity and dH_L is the contribution to the plate height arising from slow mass transfer, and is described in more detail in Chapter 3.2.1.

As discussed in Chapter 1.2.2, Miyabe and Guiochon have evaluated the plate height contributions to various mass transfer processes [22]. In their approach, the statistical moments can be further elucidated as

$$M_1 = \frac{L}{u}\delta_0 \tag{1.26}$$

$$M_2 = \frac{2L}{u}(\delta_{ax} + \delta_f + \delta_d) \tag{1.27}$$

where δ_0 is a dimensionless retention parameter given by

$$\delta_0 = \varepsilon_u + (1-\varepsilon_u)(\varepsilon + \rho K) \tag{1.28}$$

The contributions to M_2 from axial dispersion (δ_{ax}), external mass transfer (δ_f), and intraparticle diffusion (δ_d), respectively, are given by

$$\delta_{ax} = \left(\frac{D_L}{u^2}\right)\delta_0^2 \tag{1.29}$$

$$\delta_f = (1-\varepsilon_u)\left(\frac{R_p}{3k_f}\right)(\varepsilon + \rho K)^2 \tag{1.30}$$

$$\delta_d = (1-\varepsilon_u)\left(\frac{R_p^2}{15\,D_e}\right)(\varepsilon + \rho K)^2 \tag{1.31}$$

where ε_u and ε are the inter and intraparticle porosities, ρ_p is the density of the packing material, R_p is the particle radius, D_L is the axial dispersion coefficient, k_f is the external mass transfer coefficient, D_e is the intraparticle diffusivity, and K is

he equilibrium co

negligibly sma

$$H = \frac{W_z}{W_x^2} \frac{L}{2u} =$$

The different par

imated or cal

ternal mass tra

ore diffusion coe

tationary phase

The plate

mmetric and a

ut as axial d

ources of error

nservation be

ntribute to th

culation and s

ked columns

rameters will

rance, includ

curately calcu

the calculat

the equilibrium constant. Under conditions where the rate of sorption/desorption is negligibly small, the plate height can be written as

$$H = \left(\frac{M_2}{M_1^2}\right)\left(\frac{L}{2u}\right) = \frac{D_L}{u^2} + \frac{\delta_f}{\delta_0^2} + \frac{\delta_d}{\delta_0^2} \tag{1.32}$$

The different parameters that are related to mass transfer processes can be estimated or calculated based on the above equations. For example, the external mass transfer coefficient, diffusion coefficient in the mobile phase, and pore diffusion coefficient can all be estimated, and the diffusion coefficient in the stationary phase can thus be calculated.

The plate height model assumes that all contributions to variance, both symmetric and asymmetric, that are not directly attributable to fast processes such as axial dispersion arise from slow kinetics. There are several potential sources of error in this method. First, this method requires that the solute concentration be within the linear region of the isotherm, such that it does not contribute to the variance. Second, this method relies on the accurate calculation and subtraction of all fast mass transfer terms, which is difficult for packed columns in liquid chromatography. Empirical estimations of these parameters will introduce errors. Moreover, any extra-column contributions to variance, including those from the injector, detector, connectors, etc., must be accurately calculated and subtracted. Again, there are no theoretical methods for the calculation of these parameters, so empirical estimations are necessary.

1.3.3.2.2. Expone

If an incre

ner zone broade

rocesses that a

These processes

a Gaussian funct

$$C(t) = \frac{A}{\sqrt{2\pi}\sigma_g} \exp$$

where A is the ar

e standard dev

In addition

es slow relative

ntribute to the

echanism that c

is contribution is

$$C(t) = A \exp \frac{-(t$$

where t is the sta

The zone p

nolution of the

The functions ar

given by the exp

1.3.3.2.2. Exponentially modified Gaussian (EMG) model

If an incremental length of the chromatographic column is considered, then zone broadening can arise from multiple paths, diffusion, and mass transfer processes that are fast relative to the time spent in the incremental length. These processes contribute to the symmetric broadening, which is described by a Gaussian function

$$C(t) = \frac{A}{\sqrt{2\pi}\sigma_g} \exp\left(-0.5 \left(\frac{t - t_g}{\sigma_g} \right)^2 \right) \tag{1.33}$$

where A is the area, t_g is the retention time of the Gaussian component, and σ_g is the standard deviation of the Gaussian component.

In addition, zone broadening can arise from mass transfer processes that are slow relative to the time spent in the incremental length. These processes contribute to the asymmetric broadening. For a partition or adsorption mechanism that can be considered as a first-order or pseudo-first-order reaction, this contribution is given by an exponential function

$$C(t) = A \exp\left(\frac{-(t - t_g)}{\tau} \right) \tag{1.34}$$

where τ is the standard deviation of the exponential component.

The zone profile observed at the end of the total column length is the convolution of the Gaussian and exponential contributions, i.e. the multiplication of the functions and integration within each incremental length. This convolution is given by the exponentially modified Gaussian (EMG) equation

$$C(t) = \frac{A}{2\pi} \exp \frac{\sigma_g^2}{2\pi^2} -$$

The zone profile is

egression parame

s calculated as

$$t_c = t_g -$$

and the correspond

$$\alpha = \frac{t_c - t_0}{t_0}$$

The metho

ained by extrac

slow kinetics in the

ly rearrangement

$$t_g = \frac{2\pi t_c}{\sigma^2}$$ and

The EMG m

arise from slow

method. First, th

ear region of the

Second, any extra

minated. In pra

omatographic d

detector [37]. It

$$C(t) = \frac{A}{2\tau} \exp\left(\frac{\sigma_g^2}{2\tau^2} + \frac{t_g - t}{\tau}\right)\left(\operatorname{erf}\left(\frac{t - t_g}{\sqrt{2}\sigma_g} - \frac{\sigma_g}{\sqrt{2}\tau}\right) + 1\right) \tag{1.35}$$

The zone profile is fit to the EMG equation by nonlinear regression to extract the regression parameters (A, t_g, σ_g, τ). From these parameters, the retention time t_r is calculated as

$$t_r = t_g + \tau \tag{1.36}$$

and the corresponding retention factor is calculated as

$$k = \frac{t_r - t_0}{t_0} \tag{1.37}$$

The method of calculating kinetic rate constants from the EMG model is derived by extrapolation of Giddings' work [20,37]. The mass transfer term for slow kinetics in the partition or adsorption mechanism is given by Equation 1.24. By rearrangement, the rate constants are given by

$$k_{ms} = \frac{2kt_0}{\tau^2} \quad \text{and} \quad k_{sm} = \frac{2k^2 t_0}{\tau^2} \tag{1.38}$$

The EMG model assumes that all contributions to asymmetric broadening (τ) arise from slow kinetics. There are several potential sources of error in this method. First, this method requires that the solute concentration be within the linear region of the isotherm, such that it does not contribute to the asymmetry. Second, any extra-column contributions to asymmetry must be minimized or eliminated. In practice, this is achieved by detection at several points along the chromatographic column and subtraction of the parameters determined at each detector [37]. It is noteworthy that the EMG method does not require *a priori*

estimation. Whe

extra-column co

13.3.2.3. Gidd

By mean

retetical trea

first-order cond

$C_{out} = A_0 \sqrt{\frac{K'}{x}}$

where k is a m

onstant, equa

ution time of

onsidering to th

pression to E

orresponding r

The G

ymmetric bro

ources of erro

oncentration be

ontribute to th

ontributions fro

asses be negl

n the injection

estimation, whether by theoretical or empirical means, of symmetric column or extra-column contributions to broadening.

1.3.3.2.3. Giddings model

By means of stochastic theory [20], Giddings derived a model suitable for theoretical treatment of the adsorption mechanism under first-order or pseudo-first-order conditions

$$C(x) = A\gamma \sqrt{k/x}\, I_1\left(2\gamma\sqrt{kx}\right) \exp\left(-\gamma x - \gamma k\right) \qquad (1.39)$$

where I_1 is a modified Bessel function of the first kind, and γ is a dimensionless constant, equal to the product of the desorption rate constant (k_{ms}) and the elution time of a non-retained compound (t_0). After conversion from the time domain (t) to the retention factor domain (x), the zone profile is fit by nonlinear regression to Equation 1.39. From the regression parameters (A, k, γ), the corresponding retention factor and rate constants are calculated.

The Giddings model assumes that all contributions to symmetric and asymmetric broadening arise from slow kinetics. There are several potential sources of error in this method. First, this method requires that the solute concentration be within the linear region of the isotherm, such that it does not contribute to the broadening. Second, this method requires that column contributions from multiple paths and diffusion in the mobile and stationary phases be negligible. Moreover, any extra-column contributions, including those from the injector, detector, connectors, etc., must also be negligible. Unlike the

ate height and

rase contribution

1.3.3.2.4. Nonlin

All of t

ermodynamic

stream. How

hases with a l

esirable to be a

A conve

ar frontal pro

ime profiles by

an be considere

Equation 1.2j

ven by

$$C_x = \frac{A_x}{KC_g}$$

where

$$\ldots = e^{-\ldots} \int_0^{\ldots} e$$

C_g and I_0 a

oncentration.

Then $(x_1$ th

plate height and EMG methods, there is no *a posteriori* method to correct for these contributions.

1.3.3.2.4. Nonlinear chromatography models

All of the impulse methods described above are suitable for thermodynamic and kinetic measurements within the linear region of the isotherm. However, some mechanisms such as adsorption have stationary phases with a limited number of sites that may be easily overloaded. Hence, it is desirable to be able to evaluate their behavior under nonlinear conditions.

A convenient method to extract thermodynamic and kinetic information from frontal profiles was reported by Thomas [38] and later modified for elution zone profiles by Wade et al. [39]. This model was derived for mechanisms that can be considered as second-order sorption and first-order desorption reactions (Equation 1.2) under linear and nonlinear conditions. This theoretical model is given by

$$C(x) = \left(\frac{A\gamma}{KC_0}\right)\left(1-\exp\left(-\gamma KC_0\right)\right)\left(\frac{\left(\sqrt{k/x}\, I_1\left(2\gamma\sqrt{kx}\right)\right)\exp\left(-\gamma x-\gamma k\right)}{1-T\left(\gamma k,\gamma x\right)\left(1-\exp\left(-\gamma KC_0\right)\right)}\right) \tag{1.40}$$

where

$$T(u,v) = e^{-v}\int_0^u e^{-t} I_0\left(\sqrt{2vt}\right) dt \tag{1.41}$$

and I_0 and I_1 are modified Bessel functions of the first kind and C_0 is the initial concentration. After conversion from the time domain (t) to the retention factor domain (x), the zone profile is fit by nonlinear regression to Equation 1.40. From

ne regression pa

ze constants are

The Thom

ajmetric broad

sa combination o

everal potential s

rfaces and the s

sum contribut

ationary phase

luding those

ngle Un

ssion method

Other non

Braz and Gu

ed kinetic info

odes. The

rfaces are slow

ctensive mode

ss kinetics of

ution of the ga

the profiles.

the regression parameters (A, k, γ, KC_0), the corresponding retention factor and rate constants are obtained.

The Thomas model assumes that all contributions to symmetric and asymmetric broadening arise from nonlinear isotherms and slow kinetics, which is a combination of mass transfer and sorption/desorption processes. There are several potential sources of error in this method. First, this method assumes the kinetics and the isotherm to be Langmuirian. Second, this method requires that column contributions from multiple paths and diffusion in the mobile and stationary phases be negligible. Moreover, any extra-column contributions, including those from the injector, detector, connectors, etc., must also be negligible. Unlike the statistical moment and EMG methods, there is no *a posteriori* method to correct for these contributions.

Other nonlinear chromatography models have been reviewed by Golshan-Shirazi and Guiochon [40,41]. Among those that provide both thermodynamic and kinetic information are the reaction-dispersive and transport-dispersive models. The reaction-dispersive model presumes that sorption/desorption kinetics are slow relative to the fast kinetics of mass transfer. The transport-dispersive model presumes that mass transfer kinetics are slow relative to the fast kinetics of sorption/desorption. These simplifications allow numerical solution of the general rate model for comparison of theoretical and experimental zone profiles.

1.4. Previous in

Although a

reversed-phase

hese phases are

nteractions, an

ecessight and

ny questions ar

ew the thermo

derstanding of

operties of the

ase and solute s

1.4.1. Fundamenta

For many ye

hanism in reve

escribed to descr

ies indirectly ba

ased on thermocy

ost reviewed by

hart et al. [43,4

ude the lattice m

Classification

he most importan

ho deve

1.4. Previous investigations

Although a wide range of stationary phases are available, the vast majority of reversed-phase separations are performed with alkyl-bonded silica phases. These phases are based on dispersion (London) forces [9], the most universal of all interactions, and hence are broadly applicable. Although many studies have added insight and attempted to definitively characterize the retention mechanism, many questions and controversies still remain. The following section serves to review the thermodynamic and kinetic studies that have provided a better understanding of the underlying processes of retention in regards to the properties of the alkyl-bonded phase and support, properties of the mobile phase, and solute structure and concentration [19].

1.4.1. Fundamental studies of the retention mechanism

For many years, there has been a lively debate concerning the retention mechanism in reversed-phase liquid chromatography. Many models have been developed to describe the retention mechanism, some of which are directly and others indirectly based on thermodynamic concepts. Models that are directly based on thermodynamics include the general solution or solubility parameter model reviewed by Tijssen et al. [42] and the solvophobic model developed by Horvath et al. [43,44]. Models that are indirectly based on thermodynamics include the lattice models developed by Martire and Boehm [45] and by Dill [46].

Classification of the retention mechanism as partition or adsorption is one of the most important issues in RPLC. A theoretical perspective was provided by Dill [46], who developed lattice models for both the partition and adsorption

echanisms. In

nd the underly

redicted using s

ring of the solu

ntact interactions

redicted that the

ain length. Solu

ound end and

ain. As the b

becomes more res

predicted to dec

ximately 8.1

dominant mech

s) to be partition

Experimenta

traction mechan

and Carr [47].

stem and compa

heptylbenzenes

ree energy of a

hange in free ener

hexadecane to

ree was calcula

mechanisms. In both mechanisms, the surface consisted only of alkyl chains and the underlying silica support was not considered. Solute retention was predicted using simple, thermodynamically related parameters: the entropy of mixing of the solute, the configurational entropy of the bonded chain, and the contact interactions of the solute with the solvent and bonded chain. This model predicted that the extent of partitioning becomes more important with increasing chain length. Solute molecules have the lowest concentration near the proximal or bound end and the highest concentration near the distal or free end of the chain. As the bonding density increases and space between the chains becomes more restricted, adsorption becomes more important. In fact, partition is predicted to decrease to zero as the chains reach their maximum density of approximately 8.1 $\mu mol/m^2$. However under most typical conditions, the predominant mechanism for long-chain alkylsilicas, particularly octadecylsilica, is likely to be partition or partition-like in nature.

Experimental studies have also been used to examine the partition and adsorption mechanisms in reversed-phase liquid chromatography. In a study by Tan and Carr [47], liquid-liquid extraction was used as a model of a true partition system and compared with monomeric octylsilica and octadecylsilica phases. The alkylbenzenes were used as model solutes in order to determine the change in free energy of a methylene group ($\Delta\Delta G$) in each system. The ratio of the change in free energy of a methylene group for transfer from the mobile phase to bulk hexadecane to that for transfer from the mobile phase to the stationary phase was calculated. Values of this ratio that are close to unity denote a

pation mechan s

orded phase cha

was close to un ty

ess than 70 %. .n

emonstrated tha

rous silica to h

However, phases

gher ΔG rat os

ed 23 μmol m^{-2}

ults confirmed

ark et al. [46]

ocrystalline silica.

orresponding m

s bulk hexade

romeric phas

G ratios were

ase was grea

ecessarily impl

stead that the

ay be more s

ults demonst

ic polymeric a

ular adsorpt

partition mechanism, where the methylene group can be fully embedded in the bonded phase chain. For both octylsilica and octadecylsilica, the observed ratio was close to unity when the concentration of methanol in the mobile phase was less than 70 %, indicating a partition-like mechanism. Tan and Carr [47] further demonstrated that shorter chains have larger ratios ranging from 2.2 to 1.5 for methylsilica to hexylsilica, indicative of a more adsorption-like mechanism. Moreover, phases with a low bonding density of 0.6 $\mu mol/m^2$ have significantly higher $\Delta\Delta G$ ratios of 1.8 to 2.0, while those with higher bonding densities of 1.4 and 2.3 $\mu mol/m^2$ have smaller and approximately equal ratios of 1.3. These results confirmed the predictions of the lattice model of Dill [46]. Later studies by Park et al. [48] examined polymeric phases ranging from methylsilica to octadecylsilica. The ratios were closer to unity for polymeric phases than for the corresponding monomeric phases. This implies that polymeric phases act more like bulk hexadecane and exhibit a more partition-like mechanism than do monomeric phases. For all stationary phases examined in these studies, larger $\Delta\Delta G$ ratios were observed when the concentration of methanol in the mobile phase was greater than 70 %. The authors suggested that this did not necessarily imply that adsorption was dominant under these conditions but, instead, that the structure of the bonded phase may be different or that methanol may be more soluble in the stationary phase at higher concentrations. These studies demonstrate that the retention of a nonpolar solute with both monomeric and polymeric alkylsilica phases is more similar to a partition-like mechanism than an adsorption-like mechanism.

The driving

an arse from inte

stationary phase.

ased on the gen

range in free en

mobile phase. Th

rmation of a cav

e van der Waals

[9]. This mocel

ticularly those

structure. Howeve

[3], which demon

ore greatly to the

separate the mo

solute transfer

bile phase), and

e stationary pha

decreased w t

action coefficient

reasing chain

culated from Eq

transfer of a me

ion from Gas

The driving force for the separation is an important issue in RPLC, as it can arise from interactions of the solute with the mobile phase and/or with the stationary phase. The solvophobic model developed by Horvath et al. [43,44] is based on the general concept that the predominant contribution to the net change in free energy of retention arises from processes taking place in the mobile phase. The model includes changes in free energy arising from the formation of a cavity in the solvent, the reduction in free volume of the solute, and the van der Waals and electrostatic interactions between the solute and solvent [49]. This model has been very successful in predicting trends in retention, particularly those upon a change in mobile phase composition and solute structure. However, this view was challenged in a critical study by Carr et al. [50], which demonstrated that interactions with the stationary phase contribute more greatly to the free energy of retention than was previously thought. In order to separate the mobile and stationary phase contributions, partition coefficients for solute transfer were measured from the gas phase to water (as a model of the mobile phase), and from the gas phase to hexadecane (as a partition model of the stationary phase). The partition coefficients to water were relatively small and decreased with increasing chain length of the alkylbenzene. In contrast, the partition coefficients to hexadecane were substantially larger and increased with increasing chain length. The corresponding changes in molar free energy, calculated from Equation 1.5, exhibited similar trends. The average free energy for transfer of a methylene group was 0.67 kJ/mol from gas phase to water, -2.53 kJ/mol from gas phase to hexadecane, and -3.20 kJ/mol from water to

exadecane.

hase are s

hase and, h

This s

hange in fr

obile phas

ethanol-wa

ositive In

hase to t

ontributio

vorable c

ontributio

hese stud

hase in th

4.2. Effe

Man

hase in

ibbering

ave exam

Kirs

her enga

nteraction

ffes of a

hexadecane. Thus, the attractive interactions of the solute with the stationary phase are significantly greater than the repulsive interactions with the mobile phase and, hence, constitute the predominant contribution to their retention.

This work was extended by Ranatunga and Carr [51], who determined the change in free energy for transfer of a methylene group as a function of the mobile phase composition. For all mobile phases examined (40 to 100 % methanol-water and acetonitrile-water), the changes in molar free energy were positive. In other words, the transfer of alkylbenzenes from the organic mobile phase to the gas phase was an energetically unfavorable event. The contributions of molar enthalpy were unfavorable and slightly greater than the favorable changes in molar entropy. In all cases, however, the mobile phase contributions were significantly less than the stationary phase contributions. These studies conclusively demonstrate the predominant role of the stationary phase in the retention mechanism of reversed-phase liquid chromatography.

1.4.2. Effect of alkyl chain length and bonding density

Many studies have been performed to elucidate the role of the bonded phase in the retention process. Some of these studies have focused on discerning the effect of alkyl chain length and bonding density, whereas others have examined the effect of the synthetic method.

Krstulovic et al. [52] examined a series of silica bonded phases with alkyl chain lengths varying from 1 to 18. With increasing chain length, a small but systematic increase in the logarithm of selectivity ($\alpha = k_2/k_1$) for a homologous series of alkylbenzenes was observed in both methanol-water and acetonitrile-

water mobile phases

quid-liquid extract

he alkyl chain after

ased more deta

ction of the alky

several homologous

f carbon number

bserved between

bserved between

ted that this decr

f the solute was

ected to suggest

he solute into the

ase of the stationa

ectly with the co

ver the solute ca

ver the stationa

ese solutes w

tionary phase a

or further exam

hase/aqueous ph

logous series

orrelation of th

water mobile phases. This effect, which was not observed in similar studies of liquid-liquid extraction (partition), was attributed to the more ordered structure of the alkyl chain after it was immobilized on the silica support. Tchapla et al. [53] provided more detailed measurements of retention factor and selectivity as a function of the alkyl chain length. They found that the methylene selectivity for several homologous series decreased in a stepwise manner near a critical value of carbon number for each particular stationary phase. The decrease was observed between solutes with 4 and 8 carbons for a hexylsilica phase, yet was observed between 12 and 18 carbons for an octadecylsilica phase. The authors noted that this decrease in selectivity occurred when the length of the alkyl chain of the solute was equal to or exceeded that of the stationary phase. This seemed to suggest that the partition mechanism involves a vertical penetration of the solute into the stationary phase. When the solute carbon number is less than that of the stationary phase, all carbon atoms are able to intercalate and interact directly with the corresponding carbon atoms of the stationary phase. However, when the solute carbon number is greater, the remaining carbon atoms cannot enter the stationary phase and, thus, undergo weaker dispersive interactions. Hence, solutes with carbon number greater than the chain length of the stationary phase are less retained and exhibit lower selectivity. Tchapla et al. [54] further examined the temperature dependence of butadecylsilica and octadecylsilica phases. The van't Hoff plots showed linear behavior for all homologous series under all conditions in the temperature range of 298 to 338 K. Extrapolation of the data from the van't Hoff plot showed two convergent points

where the

number 12 -

oxaacetyls

decreased

arbon num

bserved n

hese trend

etica nse

ermacy and

uggest a

hases

My

hases with

ight mode

omponents

ydrazine

by calculat

arbon conte

ermined est

ractions w

e kinetic b

ferias with

where the critical value for all homologous series was observed at carbon number 12 – 13 for the butadecylsilica phase, and carbon number 14 – 15 for the octadecylsilica phase. From these plots, the change in molar enthalpy decreased while the change in molar entropy increased with increasing solute carbon number in the homologous series. However, a discontinuity was observed in each plot at the same critical carbon numbers cited above. All of these trends were viewed to be consistent with the previous explanation of vertical insertion of the solute into the stationary phase, where changes in both enthalpy and entropy were altered at the critical carbon number. These studies suggest a consistency in the retention mechanism of alkylsilica stationary phases.

Miyabe and Guiochon [55] studied the kinetic properties of silica bonded phases with alkyl chain lengths ranging from 1 to 18 carbons. By using the plate height model, they determined the intraparticle diffusion (Equation 1.31) and the components of pore diffusion and surface diffusion for homologous alkylbenzenes. From the measured values of the surface diffusion coefficient, they calculated a hypothetical surface diffusion coefficient normalized for the carbon content of the stationary phase. A simple model was derived that permitted estimation of surface diffusion coefficients under different experimental conditions with an accuracy of approximately ± 20 %. These results confirm that the kinetic behavior arising from surface diffusion was similar for alkylsilica materials with varying alkyl chain length.

The bond

rat's of critical

examined the pa

ases with bon

ation coeffic e

reafter it beg

atic solutes

ases (methanc

). In the low c

ucture had litt

>31 μmol m^{-2}).

ecting into t

del of Dill [46]

pared the se

ding density.

ethanol-water).

ctions ar

logous ser

stant at 1.96

ever, for a

henyl selec

With increas

trade select

The bonding density of alkylsilica stationary phases is another parameter that is of critical importance to the retention mechanism. Sentell and Dorsey [56] examined the partition coefficient for a series of monomeric octadecylsilica phases with bonding densities of 1.6 to 4.1 $\mu mol/m^2$. They found that the partition coefficient increased linearly with bonding density up to 3.1 $\mu mol/m^2$, whereafter it began to decrease. This trend was observed for a variety of aromatic solutes (ethylbenzene, biphenyl, p-terphenyl, naphthalene), mobile phases (methanol-water and acetonitrile-water), and temperatures (298 to 313 K). In the low density region (< 3.1 $\mu mol/m^2$), the alkyl chain order or packing structure had little effect on solute retention, whereas in the high density region (> 3.1 $\mu mol/m^2$), the chain packing was constrained and interfered with the solute partitioning into the phase. These results confirmed the prediction of the lattice model of Dill [46], as discussed previously. Sentell and Dorsey [57] subsequently compared the selectivity of monomeric octadecylsilica phases as a function of bonding density. When the mobile phase composition was held constant (55 % methanol-water), all changes in selectivity were attributed to free energy contributions arising from solute interactions with the stationary phase. For a homologous series of alkylbenzenes, the methylene selectivity was nearly constant at 1.96 $\pm$ 0.03 for all bonding densities from 1.74 to 4.07 $\mu mol/m^2$. However, for a homologous series of polycyclic aromatic hydrocarbons (PAHs), the phenyl selectivity increased in an approximately linear manner from 7.05 to 8.18 with increasing bonding density. This increase was attributed to an increase in shape selectivity for the solutes (benzene, biphenyl, and p-terphenyl) as the

bonding density inc

these observations.

different annelation

electivity and bon

he PAHs. The s

nonplanar PAHs p

Sander and Wise

electivity of tetrac

however for bon

decreased to 1.5

der was obser

ctative of a sig

suggested that

hydrocyclisation ph

the degree of poly

More deta

performed by Co

PAHs as model

phenanthrene octa

ene. On the

kcal/m

kcal/m and

kcal/m

bonding density increased and the alkyl chains became more ordered. Based on these observations, selectivity was determined for a series of four-ring PAHs with different annelation structure. A distinct correlation was observed between selectivity and bonding density that was related to the length-to-breadth ratio of the PAHs. The selectivity was also determined for the series of planar and nonplanar PAHs previously identified for stationary phase characterization by Sander and Wise [58]. For bonding densities from 1.74 to 3.56 $\mu mol/m^2$, the selectivity of tetrabenzonaphthalene and benzo[a]pyrene was approximately 1.7. However for bonding densities of 3.60 and 4.07 $\mu mol/m^2$, the selectivity decreased to 1.56 and 1.63, respectively. Concurrently, a change in elution order was observed for benzo[a]pyrene and phenanthro[3,4-c]phenanthrene, indicative of a significant change in the stationary phase structure. The authors suggested that the shape selectivity observed for these monomeric octadecylsilica phases could be due to ordering of the alkyl chains rather than the degree of polymerization or thickness of the stationary phase.

More detailed thermodynamic studies of the effect of bonding density were performed by Cole and Dorsey [59] using alkylbenzenes, nitroalkanes, and small PAHs as model solutes. The van't Hoff plots were linear for all solutes on monomeric octadecylsilica phases with bonding densities of 1.60 and 2.84 $\mu mol/m^2$. On these phases, the change in molar enthalpy for benzene was -3.07 and -2.19 kcal/mol, respectively, and the change in molar entropy for benzene was -6.36 and -2.61 cal/mol K, respectively. Phases with bonding densities of 3.06 to 4.07 $\mu mol/m^2$ were also examined, however linear van't Hoff plots were

not observed ove

arsity increased

the entropic contr

as the bonding de

were compared to

were reported by

335 K) [60]. He

environment (benz

opposite that of th

ert Dorsey conc

romatographic sy

Other invest

from the alkyls lica

a series of bonded

silicon polymeriz

support. Each alky

ifferent phases. T

3.84 μmol m^{-2}. T

densities of 4.21 to

Phase variation in

ere compared with

bonding. No s

for the different s

not observed over the temperature range from 273 to 358 K. As the bonding density increased, both ΔH and ΔS became less negative. This suggested that the entropic contribution became more significant than the enthalpic contribution as the bonding density increased. The chromatographic values for ΔH and ΔS were compared to thermodynamic values for dissolution of liquid benzene in water reported by Gill and Wadso (ΔH = 0.497 kcal/mol, ΔS = -13.8 cal/mol K at 298 K) [60]. Here, ΔH and ΔS represent the transfer from the nonpolar environment (benzene) to the polar environment (water), so the sign should be opposite that of the chromatographic system. When this was considered, Cole and Dorsey concluded that the thermodynamic values obtained for the chromatographic system were similar to those for dissolution.

Other investigators have examined the effect of the synthetic method by which the alkylsilica stationary phase is prepared. Rimmer et al. [61] synthesized a series of bonded phases, tridecylsilica to octadecylsilica, using monomeric, solution polymerized, and surface polymerized methods on the same silica support. Each alkyl chain length was synthesized by each method to yield 20 different phases. The monomeric phases had similar bonding densities of 1.19 to 3.64 $\mu mol/m^2$. The solution polymerized phases had slightly higher bonding densities of 4.21 to 5.92 $\mu mol/m^2$. The surface polymerized phases had the greatest variation in bonding density from 1.90 to 7.97 $\mu mol/m^2$. The phases were compared with respect to methylene selectivity, shape selectivity, and band broadening. No significant chromatographic differences were found to result from the different synthetic routes, other than the changes in bonding density

mentioned above. The methylene selectivity, measured with homologous alkylbenzenes, was observed to increase slightly from 1.28 to 1.71 with bonding density. In contrast, selectivity for tetrabenzonaphthalene and benzo[a]pyrene decreased from 1.67 for a monomeric heptadecylsilica phase (3.56 $\mu mol/m^2$), to 0.64 for a solution-polymerized heptadecylsilica phase (5.50 $\mu mol/m^2$), to 0.19 for a surface-polymerized heptadecylsilica phase (7.28 $\mu mol/m^2$). The concomitant inversion in retention order indicated a significant change in the stationary phase structure.

To further understand the influence of the synthetic method, Jinno et al. [62] examined the temperature dependence of monomeric octadecylsilica, monomeric octadecylsilica with endcapping, polymeric octadecylsilica, and diphenylsilica phases. The van't Hoff plots for PAHs on the monomeric octadecylsilica phases and the diphenylsilica phase were linear in the temperature range from 298 to 473 K, yet showed very high curvature on the polymeric phases. The selectivity was calculated for each solute pair at each temperature on each of the stationary phases. The authors concluded that polymeric phases were more capable of discriminating the planar/nonplanar character of PAHs than monomeric phases. This distinction was more marked with polymeric phases synthesized from trichlorosilanes than those synthesized from dichlorosilanes. This selectivity decreased with temperature, with a critical point between 313 and 333 K, which coincided with the temperature range where a phase transition was proposed to occur.

The o

aqueous ph

and polymer

erature in

hromatogra

ransition na

uggests tha

ence that

onstant (6

ransition.

ifferential

emperature

rans bon

Tiemburg

econd orc

hysica a

hase trans

biquitous

ation-bear

ition of

tagent a

Tailored

ther cons

The occurrence of a phase transition has frequently been proposed for alkylsilica phases, particularly those with long alkyl chains, high bonding density, and polymeric synthesis method. Wheeler et al. [63] reviewed the published literature in this area derived from calorimetric, spectroscopic, and chromatographic studies. The primary chromatographic evidence of a phase transition has been the nonlinear nature of van't Hoff plots. Nonlinearity suggests that the change in molar enthalpy is not constant with temperature and, hence, that the heat capacity at constant pressure ($\Delta C_P = (\partial \Delta H/\partial T)_P$) is also not constant [64]. A change in heat capacity is the clearest indication of a phase transition. Morel and Serpinet [65-67] directly confirmed this conclusion using differential scanning calorimetry and NMR spectroscopy. The transition temperature was observed to increase with the length and density of the alkyl chains bonded to the silica surface. By using adiabatic calorimetry, Van Miltenburg and Hammers [68] demonstrated that the phase transition is actually second order and extends over a broad temperature range from 70 to 310 K for octylsilica and from 150 to 305 K for octadecylsilica phases. This second-order phase transition is viewed as an order-disorder transition, rather than a traditional solid-liquid or melting transition. An ordered alkyl chain consists of all *trans* carbon-carbon bonds and the degree of disorder is indicated by the number and position of *gauche* bonds. The ordered state, in which the contact area between adjacent alkyl chains is maximized, is enthalpically preferred but entropically unfavored. In contrast, the highly disordered state, in which the chains have a great conformational diversity with many *gauche* bonds, is entropically preferred

ut enthalpica

ogressively, be

evailing to the

ectroscopy th

(with high proc

e proximal e

orresponding r

tal of the n-alka

McGuffin

the polymeric c

emperature (31

C to C_{22} n

ders of magn

88 % respec

e phase tran

ease in rete

e rate consta

e order of

ile phase

e stationary

behavior. The

order for C

is constrs

but enthalpically unfavored. The phase transition is thought to occur progressively, beginning at the distal or free end of the alkyl chain then gradually prevailing to the proximal or bound end. Sander et al. [69] confirmed by FTIR spectroscopy that the bonded alkyl chains contain several *gauche* bonds at 317 K, with high probability of occurrence at the distal end and very low probability at the proximal end. The degree of disorder is comparable to that of the corresponding n-alkane coated in a thin film on the silica surface, but less than that of the n-alkane in bulk solution.

McGuffin and Lee [70] compared the thermodynamic and kinetic behavior of a polymeric octadecylsilica phase (5.4 $\mu mol/m^2$) in the vicinity of the transition temperature (318 K). The retention factors for a homologous series of fatty acids (C_{10} to C_{22}) increased systematically with carbon number by approximately two orders of magnitude. The retention factors for C_{10} to C_{22} decreased by 84.4 to 99.6 %, respectively, as temperature was increased from 293 to 333 K. Hence, the phase transition had a significant effect on thermodynamic behavior. The increase in retention factor with carbon number was accompanied by changes in the rate constant for transfer from mobile to stationary phase by approximately one order of magnitude and the rate constant for transfer from stationary to mobile phase by approximately three orders of magnitude. Hence, the transition from stationary to mobile phase seemed to have the greatest effect on kinetic behavior. The characteristic time ($t = 1/(k_{ms} + k_{sm})$) increased with carbon number for C_{10} to C_{18} fatty acids, but remained relatively constant thereafter. This is consistent with the mechanism described by Tchapla et al. [53,54],

wherein the solute

carbon number g

istance into the

ne transition ter

omparable to tho

In subsequ

aration of PAH

octadecylsilica pr

hase were gen

hase. However

were generally sm

ther words, it w

ore difficult for

ensity. All so

ecrease in rate

Finally, a

eriods that m

ompared six c

hases stericall

ntercalated p

ased on linear

ompounds sho

nge from 280

wherein the solutes insert vertically in the stationary phase. Hence, solutes with carbon number greater than that of the stationary phase (C_{18}) inserted the same distance into the stationary phase and had comparable kinetic behavior. Above the transition temperature, the rate constants increased significantly and were comparable to those for monomeric octadecylsilica phases.

In subsequent studies, Howerton and McGuffin [37] compared the kinetic behavior of PAHs on monomeric (2.7 $\mu mol/m^2$) and polymeric (5.4 $\mu mol/m^2$) octadecylsilica phases. The rate constants for transfer from mobile to stationary phase were generally larger for the polymeric phase than for the monomeric phase. However, the rate constants for transfer from stationary to mobile phase were generally smaller for the polymeric phase than for the monomeric phase. In other words, it was faster and more facile for solutes to enter, but slower and more difficult for them to exit the polymeric stationary phases with higher bonding density. All solutes on both monomeric and polymeric phases showed a decrease in rate constants as the retention factor was increased.

Finally, a number of studies have examined the effect of other synthetic methods that modify the stationary phase structure. Vervoort et al. [71] compared six different octadecylsilica stationary phases, including polymeric phases, sterically protected phases, phases with bidentate bonded alkyl chains and embedded polar groups, as well as those synthesized with high-purity silica. Based on linear van't Hoff plots, it was concluded that basic pharmaceutical compounds showed no change in retention mechanism over the temperature range from 280 to 360 K. The degree to which each compound interacted with

the stationary phase depended on the stationary phase properties. For example, neutral compounds (benzene, phenol) showed similar ΔH values on each stationary phase, whereas the more basic compounds (nortriptyline) showed more negative ΔH and ΔS values on the polar embedded phases and those synthesized with high-purity silica. Neue et al. [72,73] classified these various octadecylsilica materials using graphs of ln k_1 versus ln k_2 and graphs of ln α_1 versus ln α_2 where 1 and 2 correspond to two different stationary phases. This idea was previously introduced by Vailaya and Horvath [74]. Layne [75] has similarly compared conventional, polar-embedded, and polar-endcapped octadecylsilica phases by using various selectivity values for nonpolar, polar, and hydrogen-bonding solutes. These studies illustrated the importance of the synthetic method and the incorporation of polar groups, particularly for the separation of acidic and basic solutes.

1.4.3. Effect of support

The underlying solid support also has a very significant influence on retention in reversed-phase separations. As noted in the previously-discussed studies, the most common support material is silica. Sander and Wise [76] compared bonded phases prepared on 22 silica materials with differing particle shape, diameter, density, surface area, and pore diameter. They observed large variations in bonding density on the silica materials when performed under the same synthetic conditions, 1.26 to 2.78 $\mu mol/m^2$ for monomeric octadecylsilica phases and 2.57 to 5.35 $\mu mol/m^2$ for polymeric octadecylsilica phases. Two parameters were found to have the greatest influence: pore diameter and silica

pretreatment with

PAHs were most

sample the rete

selectivity of tet

133. The autho

effect often unp

physical phases

In addition

sis and its det

a seminal stu

surface on the r

down-flow mes

and decreased

facing. The co

-8.397, -8.433,

predominant mec

of carbon load

the highest carb

respective sites a

the retention of

is largely con

facing of the bo

pretreatment with acid or base. Differences in retention factor and selectivity of PAHs were most pronounced for these parameters on the polymeric phases. For example, the retention factor of benzo[a]pyrene varied from 1.56 to 13.60 and the selectivity of tetrabenzonaphthalene and benzo[a]pyrene varied from 0.62 to 1.33. The authors concluded that the underlying silica substrate has a great effect, often unpredictable and uncontrollable, on retention and selectivity of alkylsilica phases.

In addition, much attention has been drawn to the adsorptive nature of silica and its detrimental effect on the partition mechanism of alkylsilica phases. In a seminal study, Nahum and Horvath [77] examined the effect of the silica surface on the retention factor and change in molar enthalpy for dibenzo-18-crown-6 in a methanol mobile phase. The retention factor was greatest on silica and decreased progressively on octadecylsilica with 5 % and 12 % carbon loading. The corresponding changes in molar enthalpy were determined to be -8.797, -8.433, and -7.356 kcal/mol, respectively. If partition was the predominant mechanism here, then retention and molar enthalpy should increase with carbon loading. However, if adsorption was dominant, then the phase with the highest carbon loading should have the lowest concentration of residual adsorptive sites and, thus, the smallest effect of these sites on retention. Hence, the retention of hydrogen bonding solutes such as the crown ethers was shown to be largely controlled by the underlying silica support, even with high carbon loading of the bonded phase. In a two-part review by Nawrocki [5,6], the nature

of the silo

package an

Altho

supports su

2 ions a su

of pH and t

surface is e

deformed

charges in

rated (PB

anged fro

ffective

rimarily d

.09 kca

.41 kcal

was found

ily by

rabecyl-

temperatu

hylbenze

ilage to

ffect pra

electrole

of the silica adsorption sites was discussed and several methods for their blockage and removal were reviewed and compared.

Although the most common underlying support is silica, many other supports such as zirconia, titania, and synthetic polymers have been used. Zirconia supports are more stable than silica supports, and can handle extremes of pH and temperature that silica cannot. However, complete coverage of the surface is essential to avoid deleterious adsorption. Li and Carr [78,79] have performed a number of studies on zirconia-based reversed-phase systems. Changes in molar enthalpy were determined for alkylbenzenes on polybutadiene-coated (PBD) zirconia in a temperature range of 313 to 373 K. The values ranged from -2.07 to -4.00 kcal/mol for benzene to n-pentylbenzene, respectively, and are similar to those reported for octadecylsilica phases. The enthalpy of transfer of a methylene group for the PBD-zirconia phase (-0.39 kcal/mol) was comparable to those for octadecylsilica phases (-0.27 and -0.41 kcal/mol) as well. In fact, the hydrophobic selectivity of the PBD-zirconia was found to be comparable to conventional bonded phases [78]. A temperature study by Guillarme et al. [80] compared the thermodynamic behavior of octadecyl- and PBD-zirconia with octadecylsilica phases. Over a limited temperature range of 298 to 353 K, the van't Hoff plots were linear for alkylbenzenes and other solutes on all phases. Over a wider temperature range of 298 to 473 K, however, distinct differences were observed. Typical silica-based phases showed linear van't Hoff plots for both methanol-water and acetonitrile-water mobile phases. However, slight curvature in the van't Hoff

ots was obser

ater mobile ph

ater mobile ph

ere not due to

ssure the true

re detailed

Jorsey [81].

omatic solutes

ots the chang

ermeric) at

range in mol

mperature ra

38 to 448 K.

range in the r

esolute. In s

ere significar

mperature ra

Organ

several years.

surements, o

haracterizatio

orted. A the

ification of te

plots was observed for zirconia-based phases with pure water and acetonitrile-water mobile phases, while a linear relationship was observed with methanol-water mobile phases. The authors demonstrated that the curved van't Hoff plots were not due to changes in the system pressure with temperature, which could obscure the true temperature dependence of retention. A confirming study with more detailed thermodynamic measurements was performed by Coym and Dorsey [81]. They observed curvature in the van't Hoff plots for nonpolar aromatic solutes on PBD-zirconia using a pure water mobile phase. From these plots, the changes in molar enthalpy were found to be significantly more negative (exothermic) at high temperature than at low temperature. For example, the change in molar enthalpy for toluene was reported to be -5.7 kJ/mol in the temperature range of 288 to 328 K and -31.3 kJ/mol in the temperature range of 398 to 448 K. The authors attributed the differences in molar enthalpy to a change in the hydrogen-bonding network in water that influences the solvation of the solute. In spite of this large difference in molar enthalpy, the retention factors were significantly smaller in the high temperature range than in the low temperature range.

Organic-inorganic hybrid supports have seen increasing use in the past several years. While the hybrid phase has been employed in numerous experiments, only a few studies have made an effort to provide a thermodynamic characterization of the material [82,83] and kinetic characterization has not been reported. A thermodynamic evaluation of a C_{18} hybrid phase was performed as a function of temperature from 423 to 473 K in an aqueous mobile phase using

alkyl benzenes and aromatic alcohols [82] and substituted anilines [83]. Linear van't Hoff plots were obtained and negative changes in molar enthalpy were reported for all solutes. Further investigation of toluene at a wider temperature range from 303 to 473 K yielded a change in slope of the van't Hoff plot near 370 K. Solid state NMR of the dry stationary phase indicated that no change in the stationary phase structure occurred [82]. However, the change in slope in the low temperature region (ΔH = -17.6 kJ/mol) was half that of the slope in the high temperature region (ΔH = -33.5 kcal/mol). This observation was similar to that seen by Coym and Dorsey [81] with PBD-zirconia, where the difference was attributed to a change in the hydrogen-bonding network with temperature.

Additional studies have investigated the effect of alkyl chain length on a hybrid support material containing a polar embedded group in the chain. O'Gara et al. [84] investigated the retention of nonpolar, polar, and basic compounds on a series of phases ranging from C_8 to C_{18}. Retention increased from C_8 to C_{16} but decreased for the C_{18} length, similar to silica-based materials. Tailing of the basic compounds was studied as a function of chain length and surface concentration. Tailing was independent of chain length, but decreased with increasing bonding density for a set of C_{18} phases. These studies suggest that the hybrid material may be quite similar to silica materials. However, a direct comparison of hybrid and silica has not yet been performed.

1.4.4. Effect of mobile phase composition

Whereas the contributions of the alkylsilica stationary phase clearly predominate [50,51], the contributions of the mobile phase also greatly influence

retention and selectivity of reversed-phase separations. To elucidate these contributions, many investigators have varied the type and composition of the mobile phase to examine changes in the thermodynamic and kinetic behavior.

The most common mobile phases in RPLC are aqueous mixtures of methanol, tetrahydrofuran, or acetonitrile. These solvents are chosen to enhance acid, base, or dipole interactions, respectively, and hence can influence the selectivity. To influence the retention, the proportion of water in the mobile phase is varied. The effect of water on retention has been investigated extensively. Grushka et al. [85] studied the effect of water on retention factor, selectivity, and the concomitant changes in molar enthalpy and entropy. As the water content was increased, the retention factors for a series of alkylbenzenes increased and the methylene selectivity increased. The selectivity was found to be more strongly dependent on the mobile phase composition than on the temperature. Values for ΔH became more negative as the water content increased, ranging from -1.82 to -4.39 kcal/mol in 90 % methanol-water and ranging from -2.06 to -6.21 kcal/mol in 80 % methanol-water for ethylbenzene to dodecylbenzene, respectively. The differential change in molar enthalpy ($\Delta\Delta H$) per methylene group was determined as -0.267 and -0.405 kcal/mol in 90 % and 80 % methanol-water, respectively. Therefore, it is energetically more favorable for the solute to be in the stationary phase as the water content of the mobile phase is increased.

Cole et al. [86] investigated the role of the mobile phase by means of van't Hoff plots for benzene. When water-rich mobile phases of protic solvents (e.g.,

methanol-

bined ov

ositive fo

300 to 35

were use

ral the

solvents

situations

rough t

lenes co

hanged

to e pr

Methanol-

e rotary

emperatu

Then ent

were reg

ection

reacted

hange

released

became

Then en

methanol-water and propanol-water) were used, the van't Hoff plots were highly curved over the temperature range from 268 to 353 K. The values of ΔH were positive for temperatures from 268 to 293 K and negative for temperatures from 303 to 353 K. When mobile phases with aprotic solvents (e.g., acetonitrile-water) were used, the van't Hoff plots were more nearly linear. The authors concluded that the hydrophobic (solvophobic) mechanism may be reasonable for protic solvents, but is not adequate to explain the retention mechanism in other situations. A related mobile phase effect was observed by Sentell et al. [87] through the examination of retention and selectivity for several homologous series consisting of alkylbenzenes, phenylenes, and PAHs. The selectivity changed more with temperature for methanol-water than for acetonitrile-water mobile phases. This was attributed to the hydrogen-bonding capability of the methanol-water mobile phases, which led to a more structured mobile phase. It is noteworthy that the graphs of the logarithm of selectivity versus inverse temperature were linear and the reported values for the differential change in molar enthalpy ($\Delta\Delta H$) and molar entropy ($\Delta\Delta S$) per methylene and phenyl groups were negative over all temperature ranges. Sander and Field [88] examined the retention behavior of N,N-diethylaniline and 2-propylbenzene on an octadecylsilica phase over a wide range of methanol-water compositions. The change in molar enthalpy values for both solutes, although all negative, increased with an increase in the methanol concentration. That is, the transfer became less favorable for higher concentrations of methanol. The change in molar entropy for both solutes, although negative, slightly increased with an

increase in the methanol concentration. The enthalpy term was found to be the predominant contribution to retention. Barman and Martire [89] examined the effect of methanol-water and ethanol-water composition on the retention of a series of alkylbenzenes by using a semi-empirical relationship between the retention volume and the temperature and mobile phase composition. Through graphs of the logarithm of retention volume versus the volume of fraction of water in the mobile phase, the enthalpic contribution was found to be greater and opposite the entropic contribution. That is, as the volume fraction of water was increased, the enthalpic contribution to the retention volume systematically increased, while the entropic contribution systematically decreased for xylenes, ethyltoluenes, and diethylbenzenes. In all cases, the enthalpic term was the predominant contribution to retention.

Wu et al. [90] examined the thermodynamic behavior of methanol-water and acetonitrile-water mobile phases as a function of pH. The mobile phase type and composition greatly affected both the retention and selectivity of piperazine diastereomers. The neutral form of the diastereomers is predominant at pH 6.4, whereas the protonated form of the diastereomers is predominant at pH 3.0. At both pH values, the logarithm of the retention factor decreased monotonically with an increase in methanol-water or acetonitrile-water composition. However, the logarithm of the diastereomeric selectivity showed interesting behavior as a function of the mobile phase composition. For methanol-water systems at pH 6.4, the selectivity decreased linearly with composition. For acetonitrile-water systems at pH 3.0 and 6.4 and for methanol-water systems at pH 3.0, the

selectivity in t

composition.

passing from

rotety at low

y more gene

nsfer. Thro

behavior of th

ne vant Hoff

ture phases

diastereomers

was more h

predominant.

ogarithm of

thanol-wat

ogarithm of t

thanol-wat

ormated.

ystem. Sugg

Compa

ure to eluc

ected the e

ther potatoe

ite of the a

selectivity initially increased, reached a maximum value, and then decreased with composition. The authors suggested that the retention mechanism is complex, passing from a region that is dominated by selective solvation of the piperazine moiety at low concentration of the organic modifier to a region that is dominated by more general solvent strength effects at high concentration of the organic modifier. Through examination of the temperature behavior, the thermodynamic behavior of the mobile phases was also found to differ. At pH 3.0, the slope of the van't Hoff plot was negative for both methanol-water and acetonitrile-water mobile phases. This was attributed to a change in the pK_a of the piperazine diastereomers with increasing temperature, which favored the neutral form that was more highly retained. At pH 6.4, where the neutral form was already predominant, the behavior of the two mobile phases was distinctly different. The logarithm of the retention factor decreased with increasing temperature in methanol-water but slightly increased in acetonitrile-water. The slope of the logarithm of the selectivity factor versus inverse temperature was positive in the methanol-water system, suggesting that the retention process was enthalpy-dominated. In contrast, the slope was slightly negative in the acetonitrile-water system, suggesting that the retention process was entropy-dominated.

Compared with the thermodynamic effects, relatively little work has been done to elucidate the kinetic effects of the mobile phase. Miyabe et al. [91] studied the effect of the organic modifier on retention and mass transfer kinetics for an octadecylsilica phase. The equilibrium constant increased with the surface area of the alkylbenzene solutes for mobile phases of 50 % tetrahydrofuran-

water. T

ractive

ly a c s

contac

35 %. S

ically

contac

ignifica

he mola

olute v

f the or

ncreas

ifferen

as a d

Ba

ell as t

hermod

effect on

4.5. Eff

The

hermod

ly solu

hermod

water, 70 % methanol-water, and 70 % acetonitrile-water. In addition, the relative importance of the individual mass transfer processes was evaluated. Axial dispersion (δ_{ax}) contributed around 30 %, fluid to particle mass transfer (δ_f) contributed from 30 to 40 %, and intraparticle diffusion (δ_d) contributed from 30 to 35 %. Since each of these mass transfer processes contributed approximately equally to the second moment, none could be neglected. Among the contributions to intraparticle diffusion, surface diffusion was shown to be more significant than pore diffusion. The surface diffusion coefficient was correlated to the molar volume of the solute through the use of an empirical equation. As the solute volume increased, the surface diffusion coefficient increased. The effect of the organic modifier was also observed, where the surface diffusion coefficient increased in the order methanol < tetrahydrofuran < acetonitrile. As this order is different from the order of retention strength, this suggests that the mobile phase has a different effect on surface diffusion than on retention.

Based on these studies, the type and concentration of organic modifier as well as the type and concentration of buffer and pH have a significant effect on thermodynamic behavior. Presumably, these parameters also have a significant effect on kinetic behavior, however much work remains to be done in this area.

1.4.5. Effect of solute structure and concentration

The retention mechanism is dependent not only on the characteristics of the mobile and stationary phases, but also on the solute structure and properties. Many solutes are helpful for characterization of the retention process, particularly homologous series of aliphatic and aromatic solutes. These series provide

information about the contributions to retention and selectivity from an individual methylene or benzene group. McGuffin and Chen [64] determined the changes in molar enthalpy and molar volume for a homologous series of saturated fatty acids. On a monomeric octadecylsilica phase (2.7 $\mu mol/m^2$), the change in molar enthalpy ranged from -1.7 to -4.2 kcal/mol for C_{10} to C_{22}, respectively. The differential change in molar enthalpy ($\Delta\Delta H$) per ethylene group was relatively constant at -0.41 $\pm$ 0.02 kcal/mol. This suggests that each ethylene group contributes equally to the retention process from an energetic perspective. On a polymeric octadecylsilica phase (5.4 $\mu mol/m^2$), the change in molar enthalpy was much greater and ranged from -10.6 to -30.5 kcal/mol for C_{10} to C_{22}, respectively. The differential change in molar enthalpy per ethylene group was relatively constant at -3.65 $\pm$ 0.13 kcal/mol, approximately an order of magnitude greater than that on the monomeric phase. The changes in molar volume were similarly distinctive and informative. On the monomeric phase, the changes in molar volume ranged from 1.9 to -4.3 mL/mol for C_{10} to C_{22}, respectively. A positive change indicates that the solute occupies greater volume in the mobile phase than in the stationary phase, whereas a negative change indicates the converse. The differential change in molar volume ($\Delta\Delta V$) per ethylene group was -1.0 $\pm$ 0.4 mL/mol, which confirmed that each ethylene group contributes equally to the retention process from a volumetric perspective. On the polymeric phase, the changes in molar volume ranged from -27.1 to -104 mL/mol for C_{10} to C_{22}, respectively. This change in molar volume is a significant proportion of the total

near w

respect

441 = 2

rocome

remod

T

polymer

ns stud

decrease

ym mo

ragnitud

h adsro

proton

The re

ym mo

nstant

tationary

ns was a

tationary

ne the n

ther and

d rather

rogress w

molar volume, which is approximately 201 to 441 mL/mol for C_{10} to C_{22}, respectively. The differential change in molar volume per ethylene group was -14.1 ± 2.8 mL/mol, approximately an order of magnitude greater than that on the monomeric phase. These studies provide a clear indication of the thermodynamic contributions of the methylene group to retention.

The kinetic contributions to retention for the homologous fatty acids on the polymeric octadecylsilica phase were examined by McGuffin and Lee [70]. In this study, the retention factor increased logarithmically and the rate constants decreased logarithmically with increasing carbon number. The rate constants from mobile to stationary phase decreased by approximately one order of magnitude, while the rate constants from stationary to mobile phase decreased by approximately three orders of magnitude for C_{10} to C_{22}. Hence, under most conditions, the transfer from stationary to mobile phase was the rate-limiting step in the retention mechanism. The concomitant changes in activation enthalpy from mobile phase to transition state showed small variations, but was roughly constant with increasing carbon number. In contrast, the activation enthalpy from stationary phase to transition state increased monotonically with carbon number and was approximately two-fold larger than the activation enthalpy from mobile to stationary phase. These activation enthalpies were also substantially greater than the net change in molar enthalpy. Hence, it is likely that the solutes do not enter and leave the stationary phase in a single step (as shown in Figure 1.3), but rather in a stepwise or progressive manner. When considered as a progressive process, the average increase in activation enthalpy was 1.6 ± 0.6

kcal/mol per ethylene group, which is energetically feasible within the chromatographic system. The activation volume from mobile phase to transition state increased monotonically by 11 ± 4 mL/mol per ethylene group. The activation volume from stationary phase to transition state was approximately two-fold larger, and increased by 24 ± 9 mL/mol per ethylene group. These activation volumes were also substantially greater than the net change in molar volume. Again, this suggests that the solutes do not enter and leave the stationary phase in a single step, but rather in a stepwise or progressive manner.

Zhao and Carr [92] examined the thermodynamic contributions of the methylene group for several nonpolar homologous series. The differential change in molar free energy ($\Delta\Delta G$) per methylene group was determined for alkylbenzenes, alkylacetates, alkylphenones, alkylanilines, and nitroalkanes. The $\Delta\Delta G$ values were very similar, ranging from 0.303 to 0.322 kcal/mol, with an average deviation of ±0.007 kcal/mol. Hence, the authors concluded that the terminal functional group of the homologous series has little effect on the net retention of the methylene group for alkylsilica phases. More detailed studies by Chen et al. [93] evaluated the changes in molar enthalpy and entropy for an extensive set of solutes. For homologous alkylbenzenes, p-alkylphenols, p-alkyliodobenzenes, p-alkylacetophenones, and p-alkylanilines, ΔH became systematically more negative as the alkyl chain length was increased. Although there were small variations between these homologous series, the differential change in molar enthalpy for the methylene group ranged from 1.69 to 1.91 kJ/mol, with an average deviation of ±0.09 kJ/mol. In addition, the intercept of

the van't Hoff plot became more negative with increasing alkyl chain length. These values were also relatively similar, ranging from 0.224 to 0.314. Hence, the terminal functional group of the homologous series appeared to have little effect on the enthalpic and entropic contributions to retention of the methylene group for alkylsilica phases.

Carr et al. [94] examined the retention behavior of more polar functional groups, such as methoxyl, methyl ester, aldehyde, nitro, and cyano. Unlike methylene groups, these polar groups exhibited different values for the change in molar free energy in the chromatographic system and in a liquid-liquid extraction system using hexadecane as a model of the stationary phase. This suggests that a simple partition mechanism may not be sufficient to describe the retention of polar functional groups. Moreover, unlike methylene groups, the interactions of the polar groups with the mobile phase were energetically favorable and much greater than their interactions with hexadecane. This observation may suggest that the retention process is, in fact, driven by the mobile phase for polar groups. However, these interactions are not solvophobic, as suggested in the model of Horvath et al. [43,44], but solvophilic in nature. Chen et al. [93] examined the changes in molar enthalpy and entropy for substituted benzenes. These values provide insight into the enthalpic and entropic contributions for individual functional groups. For solutes with a more negative change in molar enthalpy than benzene, their functional groups have a more energetically favorable interaction with the stationary phase or, equivalently, a less favorable interaction with the mobile phase. The most negative values were observed for chloro,

bromo, iodo, and phenylketone functional groups. Conversely, for solutes with a less negative change in molar enthalpy than benzene, their functional groups have a more energetically favorable interaction with the mobile phase or, equivalently, a less favorable interaction with the stationary phase. The least negative values were observed for hydroxyl, methylenehydroxyl, and methylketone functional groups. Similar insight can be gained from the entropy term, provided that the accessible phase ratio remains constants for these solutes. For solutes with a more negative change in this term than benzene, their functional groups have a less favorable entropic contribution to retention. The most negative values were observed for amide, hydroxyl, nitrile, methylenehydroxyl, and phenylketone functional groups. Conversely, solutes with a less negative change in this term than benzene will have a more favorable entropic contribution. For these experimental conditions, no solutes had a less negative value than benzene.

In other studies, homologous series that vary in the number and position of benzene groups have been examined. McGuffin and Chen [64] determined the changes in molar enthalpy and molar volume for a series of PAHs. On a monomeric octadecylsilica phase (2.7 $\mu mol/m^2$), the change in molar enthalpy for the homologous series of phenanthrene, chrysene, and picene ranged from -0.8 to -2.9 kcal/mol. The change in molar enthalpy per benzene group was not constant, which suggests that each additional benzene group did not contribute equally to the retention process from an energetic perspective. Benzo[a]pyrene, with the same number (five) of aromatic rings but a more condensed structure

than picene, had a slightly less negative change in molar enthalpy of -2.2 kcal/mol. The nonplanar PAHs, phenanthro[3,4-c]phenanthrene and tetrabenzonaphthalene, have significantly less negative changes in molar enthalpy than would be expected based on their six-ring structure. In fact, they are more comparable to the three- and four-ring homologous PAHs. On a polymeric octadecylsilica phase (5.4 $\mu mol/m^2$), the changes in molar enthalpy were significantly greater, but exhibited the same trends as the monomeric octadecysilica phase. The changes in molar volume were similarly distinctive and informative. On the monomeric phase, the change in molar volume for the cata-annelated homologous series of phenanthrene, chrysene, and picene ranged from -1.9 to -3.1 mL/mol. The change in molar volume per benzene group was not constant, which suggests that each additional benzene group did not contribute equally to the retention process from a volumetric perspective. Benzo[a]pyrene, with the same number (five) of aromatic rings but a more condensed annelation structure than picene, had a slightly less negative change in molar volume of -2.1 mL/mol. In contrast, the nonplanar PAHs, phenanthro[3,4-c]phenanthrene and tetrabenzonaphthalene, exhibit positive changes in molar volume. Hence, these solutes occupy a greater volume in the stationary phase than in the mobile phase. On the polymeric phase, the changes in molar volume were greater, but exhibited the same trends as the monomeric octadecysilica phase. These studies, as well as others [87,93,95], provide a clear indication of the thermodynamic contributions of the benzene group to retention.

The kinetic contributions to retention for the PAHs on the polymeric octadecylsilica phase were examined by Howerton and McGuffin [37]. The rate of transfer for the three-ring PAH phenanthrene and the six-ring nonplanar PAHs phenanthro[3,4-c]phenanthrene and tetrabenzonaphthalene were very fast and, in fact, were greater than the capabilities of the chromatographic measurement method ($\geq$400 s^{-1}). For the remaining PAHs, the rate constants decreased with increasing ring number and increased for more condensed annelation structure. The transfer from mobile to stationary phase was the rate-limiting step for the monomeric octadecylsilica phase, whereas the transfer from stationary to mobile phase was the rate-limiting step for the polymeric octadecylsilica phase. The concomitant changes in activation enthalpy increased with ring number and decreased for more condensed annelation structure. A more detailed examination of the effect of annelation structure was reported by Howerton and McGuffin [87]. The activation enthalpies and volumes were substantially greater than the net changes in molar enthalpy and volume. As noted previously, this suggests that the solutes do not enter and leave the stationary phase in a single step, but rather in a stepwise or progressive manner.

The thermodynamic and kinetic behavior of nitrogen-containing PAHs (NPAHs) has also been elucidated on a polymeric octadecylsilica phase by McGuffin et al. [96]. The retention factors for the NPAHs were smaller than those for the parent PAHs in methanol mobile phase, while the converse was true in acetonitrile. In fact, retention factors for aza-PAHs increased by approximately an order of magnitude in acetonitrile compared to methanol. This was attributed

to the a

re sl c

solvent

ben the

re ora

hases

remain

remov

empty

off a c

by two

ate co

were 47

The co

were 80

ves the

ctate

hases.

by emp

Place a

ube re

Press n

to the ability of the NPAHs to interact only weakly with residual silanol groups on the silica surface in the protic solvent, but much more strongly in the aprotic solvent. In general, the NPAHs had more negative changes in molar enthalpy than their parent PAHs owing to this adsorption. It is noteworthy, however, that the changes in molar enthalpy were relatively comparable in the two mobile phases. For example, benz[a]acridine had ΔH values of -6.6 $\pm$ 0.1 kcal/mol in methanol and -8.3 $\pm$ 2.1 kcal/mol in acetonitrile. Hence, the differences in thermodynamic behavior were attributed to changes in the intercept (e.g., molar entropy or phase ratio) rather than the slope (e.g., molar enthalpy) of the van't Hoff plot. The kinetic behavior was equally dramatic, with rate constants differing by two to four orders of magnitude in the two mobile phases. For example, the rate constants for transfer of benz[a]acridine from mobile to stationary phase were 47 and 1.3 x 10^{-2} s^{-1} in methanol and acetonitrile, respectively, at 303 K. The corresponding rate constants for transfer from stationary to mobile phase were 80 and 2.9 x 10^{-3} s^{-1}, respectively. In nearly all cases, the latter process was the rate-limiting step of the retention mechanism. These results clearly indicate the importance of adsorption on the underlying support in alkylsilica phases. Further studies with aqueous mobile phases and additives are desirable for more thorough characterization.

The effect of solute concentration on kinetic behavior was examined by Miyabe and Guiochon [97] for an octadecylsilica phase. From the estimation of plate height, the axial dispersion coefficient was found to increase linearly with increasing concentration in the range of 0 to 10^2 g/mL of 4-(2-methyl-2-

propyl)phenol. The mass transfer rate constant was also found to increase linearly with concentration. Among the kinetic contributions to the rate constant, the sorption/desorption and external mass-transfer processes were negligibly small and intraparticle diffusion was dominant. Moreover, among the contributions to intraparticle diffusion, surface diffusion was shown to be much more significant than pore diffusion. Hence, the authors concluded that the concentration dependence of the rate constant arises primarily from the surface diffusion coefficient. This concentration dependence of the surface diffusion coefficient was explained by the chemical potential driving force model. These results are significant because they clearly indicate the important role of surface diffusion processes in the kinetic behavior of alkylsilica phases.

1.5. Conclusions

Alkylsilica stationary phases operate predominantly by a partition mechanism, where the solute interacts more strongly with the stationary phase than with the mobile phase. The underlying support plays an important role in both the thermodynamic and kinetic behavior, often leading to a combined partition – adsorption mechanism. As the alkyl chain length and bonding density increase, the changes in molar enthalpy increase and kinetic rate constants decrease. The mobile phase composition, likewise, influences the changes in molar enthalpy by means of the water content and the type of organic modifier. The kinetic behavior is influenced by the organic modifier and its effect upon the surface diffusion coefficient. Finally, the solute structure provides a broad view of the retention mechanism from both a thermodynamic and kinetic perspective.

This deep understanding of the retention mechanism in liquid chromatography is necessary in order to maximize the beneficial contributions and minimize the detrimental contributions to the separation. While a vast amount is known about silica-based materials, little is known about hybrid-based materials. Thus, the goal of this research is to investigate hybrid stationary phases using thermodynamic and kinetic properties. Experimental methods to extract thermodynamic and kinetic information from zone profiles will be developed and compared in Chapter 3. The effect of temperature and mobile phase will be examined in Chapter 4 and the effect of mobile phase modifiers will be examined in Chapter 5. These investigations will lead to a better understanding of the retention processes on hybrid stationary phases.

1.6. References

[1] L.R. Snyder, J.J. Kirkland, Introduction to Modern Liquid Chromatography, John Wiley & Sons, New York, NY, **1974**.

[2] High Performance Liquid Chromatography Fundamental Principles & Practice, Blackie Academic & Professional, Glasgow, United Kingdom, **1996**.

[3] L.C. Sander, M. Pursch, S.A. Wise, *Anal. Chem. 71* (**1999**) 4821-4830.

[4] L.C. Sander, S.A. Wise, *CRC Crit. Rev. Anal. Chem. 18* (**1987**) 299-415.

[5] J. Nawrocki, *Chromatographia 31* (**1991**) 177-192.

[6] J. Nawrocki, *Chromatographia 31* (**1991**) 193-205.

[7] J. Nawrocki, *J. Chromatogr. A 779* (**1997**) 29-72.

[8] C. Stella, S. Rudaz, J.L. Veuthey, A. Tchapla, *Chromatographia 53(Suppl.)* (**2001**) S113-S131.

[9] V.L. McGuffin, E. Heftmann (Editor), Theory of chromatography, Elsevier, Amsterdam, Netherlands, **2004**, 1-93.

[10] J.W. Dolan, *LCGC North America 23* (**2005**) 470-475.

[11] T.V. Koval'chuk, U. Lewin, V.N. Zaitsev, W. Engewald, *J. Anal. Chem. 54* (**1999**) 115-121.

[12] J.J. Kirkland, J.L. Glajch, R.D. Farlee, *Anal. Chem. 61* (**1989**) 2-11.

[13] N. Sagliano, T.R. Floyd, R.A. Hartwick, J.M. Dibussolo, N.T. Miller, *J. Chromatogr. A 443* (**1988**) 155-172.

[14] J. Layne, *J. Chromatogr. A 957* (**2002**) 149-164.

[15] U.D. Neue, Y.-F. Cheng, Z. Lu, B.A. Alden, P.C. Iraneta, C.H. Phoebe, K. Van Tran, *Chromatographia 54* (**2001**) 169-177.

[16] J.W. Coym, *J. Sep. Sci. 31* (**2008**) 1712-1718.

[17] K.D. Wyndham, J.E. O'Gara, T.H. Walter, K.H. Glose, N.L. Lawrence, B.A. Alden, G.S. Izzo, C.J. Hudalla, P.C. Iraneta, *Anal. Chem. 75* (**2003**) 6781-6788.

[18] J.E. O'Gara, K.D. Wyndham, *J. Liq. Chromatogr. Relat. Technol. 29* (**2006**) 1025-1045.

[19] X. Li, A.M. Hupp, V.L. McGuffin, *Adv. Chromatogr. 45* (**2007**) 1-88.

[20] J.C. Giddings, Dynamics of Chromatography Part 1 Principles and Theory, Marcel Dekker, New York, **1965**.

[21] P.W. Atkins, Physical Chemistry, W. H. Freeman, New York, NY, **1997**.

[22] K. Miyabe, G. Guiochon, *J. Sep. Sci. 26* (**2003**) 155-173.

[23] C.F. Bernasconi, Relaxation Kinetics, Academic Press, New York, NY, **1976**.

[24] J.M. Harris, D.B. Marshall, *J. Microcolumn Sep. 9* (**1997**) 185-191.

[25] A. Dawson, J. Gormally, E. Wyn-Jones, J. Holzwarth, *J. Chem. Soc., Chem. Commun. 8* (**1981**) 386-387.

[26] S.W. Waite, D.B. Marshall, J.M. Harris, *Anal. Chem. 66* (**1994**) 2052-2061.

[27] E.H. Ellison, S.W. Waite, D.B. Marshall, J.M. Harris, *Anal. Chem. 65* (**1993**) 3622-3630.

[28] S.W. Waite, J.M. Harris, E.H. Ellison, D.B. Marshall, *Anal. Chem. 63* (**1991**) 2365-2370.

[29] E.F. Caldin, J.P. Field, *J. Chem. Soc., Faraday Trans. 78* (**1982**) 1923-1935.

[30] S.W. Waite, J.F. Holzwarth, J.M. Harris, *Anal. Chem. 67* (**1995**) 1390-1399.

[31] D.B. Marshall, J.W. Burns, D.E. Connolly, *J. Chromatogr. A 360* (**1986**) 13-24.

[32] S.R. Shield, J.M. Harris, *Anal. Chem. 74* (**2002**) 2248-2256.

[33] D. Gowanlock, R. Bailey, F.F. Cantwell, *J. Chromatogr. A 726* (**1996**) 1-23.

[34] J. Li, L.M. Litwinson, F.F. Cantwell, *J. Chromatogr. A 726* (**1996**) 25-36.

[35] J. Li, F.F. Cantwell, *J. Chromatogr. A 726* (**1996**) 37-44.

[36] R. Bujalski, F.F. Cantwell, *J. Chromatogr. A 1048* (**2004**) 173-181.

[37] S.B. Howerton, V.L. McGuffin, *Anal. Chem. 75* (**2003**) 3539-3548.

[38] H.C. Thomas, *J. Am. Chem. Soc. 66* (**1944**) 1664-1666.

[39] J.L. Wade
[40] S. Golshar
[41] G. Gu och
[42] R. Tijssen
J. Chroma
[43] C. Horvát
[44] C. Horvat
[45] D.E. Mart
[46] K.A. Dill. J
[47] L.C. Tan, P
[48] J.H. Park,
Carr. J. Ch
[49] C. Horvat
[50] P.W. Carr,
(1993) 113
[51] R.P.J. Ran
[52] A.M. Krstu
(1983) 228
[53] A. Tchapla
[54] A. Tchapla
1443-1448
[55] K. Miyabe,
[56] K.B. Sente
[57] K.B. Sente
[58] L.C. Sander
[59] L.A. Cole. J.
[60] S.J. Gill. I. V.

[39] J.L. Wade, A.F. Bergold, P.W. Carr, *Anal. Chem. 59* (**1987**) 1286-1295.

[40] S. Golshan-Shirazi, G. Guiochon, *J. Chromatogr. A 603* (**1992**) 1-11.

[41] G. Guiochon, *J. Chromatogr. A 965* (**2002**) 129-161.

[42] R. Tijssen, P.J. Schoenmakers, M.R. Böhmer, L.K. Koopal, H.A.H. Billiet, *J. Chromatogr. A 656* (**1993**) 135-196.

[43] C. Horváth, W. Melander, I. Molnár, *J. Chromatogr. A 125* (**1976**) 129-156.

[44] C. Horvath, W. Melander, *J. Chromatogr. Sci. 15* (**1977**) 393-404.

[45] D.E. Martire, R.E. Boehm, *J. Phys. Chem. 87* (**1983**) 1045-1062.

[46] K.A. Dill, *J. Phys. Chem. 91* (**1987**) 1980-1988.

[47] L.C. Tan, P.W. Carr, *J. Chromatogr. A 775* (**1997**) 1-12.

[48] J.H. Park, Y.K. Lee, Y.C. Weon, L.C. Tan, J. Li, L. Li, J.F. Evans, P.W. Carr, *J. Chromatogr. A 767* (**1997**) 1-10.

[49] C. Horvath, W. Melander, *Am. Lab. 10* (**1978**) 17-36.

[50] P.W. Carr, J. Li, A.J. Dallas, D.I. Eikens, L.C. Tan, *J. Chromatogr. A 656* (**1993**) 113-133.

[51] R.P.J. Ranatunga, P.W. Carr, *Anal. Chem. 72* (**2000**) 5679-5692.

[52] A.M. Krstulovic, H. Colin, A. Tchapla, G. Guiochon, *Chromatographia 17* (**1983**) 228-230.

[53] A. Tchapla, H. Colin, G. Guiochon, *Anal. Chem. 56* (**1984**) 621-625.

[54] A. Tchapla, S. Heron, H. Colin, G. Guiochon, *Anal. Chem. 60* (**1988**) 1443-1448.

[55] K. Miyabe, G. Guiochon, *J. Phys. Chem. B 109* (**2005**) 12038-12048.

[56] K.B. Sentell, J.G. Dorsey, *Anal. Chem. 61* (**1989**) 930-934.

[57] K.B. Sentell, J.G. Dorsey, *J. Chromatogr. A 461* (**1989**) 193-207.

[58] L.C. Sander, S.A. Wise, *Anal. Chem. 56* (**1984**) 504-510.

[59] L.A. Cole, J.G. Dorsey, *Anal. Chem. 64* (**1992**) 1317-1323.

[60] S.J. Gill, I. Wadso, *Proc. Natl. Acad. Sci. U. S. A. 73* (**1976**) 2955-2958.

[61] C.A. Rimmer, L.C. Sander, S.A. Wise, J.G. Dorsey, *J. Chromatogr. A 1007* (**2003**) 11-20.

[62] K. Jinno, T. Nagoshi, N. Tanaka, M. Okamoto, J.C. Fetzer, W.R. Biggs, *J. Chromatogr. A 436* (**1988**) 1-10.

[63] J.F. Wheeler, T.L. Beck, S.J. Klatte, L.A. Cole, J.G. Dorsey, *J. Chromatogr. A 656* (**1993**) 317-333.

[64] V.L. McGuffin, S.-H. Chen, *J. Chromatogr. A 762* (**1997**) 35-46.

[65] D. Morel, J. Serpinet, *J. Chromatogr. A 200* (**1980**) 95-104.

[66] D. Morel, J. Serpinet, *J. Chromatogr. A 214* (**1981**) 202-208.

[67] P. Claudy, J.M. Letoffé, C. Gaget, D. Morel, J. Serpinet, *J. Chromatogr. A 329* (**1985**) 331-349.

[68] J.C. Van Miltenburg, W.E. Hammers, *J. Chromatogr. A 268* (**1983**) 147-155.

[69] L.C. Sander, J.B. Callis, L.R. Field, *Anal. Chem. 55* (**1983**) 1068-1075.

[70] V.L. McGuffin, C. Lee, *J. Chromatogr. A 987* (**2003**) 3-15.

[71] R.J.M. Vervoort, E. Ruyter, A.J.J. Debets, H.A. Claessens, C.A. Cramers, G.J. de Jong, *J. Chromatogr. A 964* (**2002**) 67-76.

[72] U.D. Neue, B.A. Alden, T.H. Walter, *J. Chromatogr. A 849* (**1999**) 101-116.

[73] U.D. Neue, V.T. K., P.C. Iraneta, B.A. Alden, *J. Sep. Sci. 26* (**2003**) 174-186.

[74] A. Vailaya, C. Horvath, *J. Phys. Chem. 102* (**1998**) 701-718.

[75] J. Layne, *J. Chromatogr. A 957* (**2002**) 149-164.

[76] L.C. Sander, S.A. Wise, *J. Chromatogr. A 316* (**1984**) 163-181.

[77] A. Nahum, C. Horváth, *J. Chromatogr. 203* (**1981**) 53-63.

[78] J. Li, P.W. Carr, *Anal. Chem. 69* (**1997**) 837-843.

[79] J. Li, P.W. Carr, *Anal. Chem. 68* (**1996**) 2857-2868.

[80] D. Guillarme, S. Heinisch, J.L. Rocca, *J. Chromatogr. A 1052* (**2004**) 39-51.

[81] J.W. Coym, J.G. Dorsey, *J. Chromatogr. A 1035* (**2004**) 23-29.

[82] Y. Liu, N. Grinberg, K.C. Thompson, R.M. Wenslow, U.D. Neue, D. Morrison, T.H. Walter, J.E. O'Gara, K.D. Wyndham, *Anal. Chim. Acta 554* (**2005**) 144-151.

[83] S. Shen, H. Lee, J. McCaffrey, N. Yee, C. Senanayake, N. Grinberg, *J. Liq. Chromatogr. Relat. Technol. 29* (**2006**) 2823-2834.

[84] J.E. O'Gara, D.P. Walsh, B.A. Alden, P. Casellini, T.H. Walter, *Anal. Chem. 71* (**1999**) 2992-2997.

[85] E. Grushka, H. Colin, G. Guiochon, *J. Chromatogr. A 248* (**1982**) 325-339.

[86] L.A. Cole, J.G. Dorsey, K.A. Dill, *Anal. Chem. 64* (**1992**) 1324-1327.

[87] K.B. Sentell, N.I. Ryan, A.N. Henderson, *Anal. Chim. Acta 307* (**1995**) 203-215.

[88] L.C. Sander, L.R. Field, *Anal. Chem. 52* (**1980**) 2009-2013.

[89] B.N. Barman, D.E. Martire, *Chromatographia 34* (**1992**) 347-356.

[90] N. Wu, P.M. Yehl, D. Gauthier, A. Dovletoglou, *Chromatographia 59* (**2004**) 189-195.

[91] K. Miyabe, S. Sotoura, G. Guiochon, *J. Chromatogr. A 919* (**2001**) 231-244.

[92] J. Zhao, P.W. Carr, *Anal. Chem. 72* (**2000**) 302-309.

[93] Z. Chen, T. Nakayama, T. Nakagama, K. Uchiyama, T. Hobo, *J. Liq. Chromatogr. Relat. Technol. 26* (**2003**) 2809-2838.

[94] P.W. Carr, L.C. Tan, J.H. Park, *J. Chromatogr. A 724* (**1996**) 1-12.

[95] S.B. Howerton, V.L. McGuffin, *J. Chromatogr. 1030* (**2004**) 3-12.

[96] V.L. McGuffin, S.B. Howerton, X. Li, *J. Chromatogr. A 1073* (**2005**) 63-73.

[97] K. Miyabe, G. Guiochon, *Anal. Chem. 72* (**2000**) 5162-5171.

CHAPTER 2

EXPERIMENTAL METHODS

2.1 Introduction

This chapter details the experimental methods used for the subsequent research. Column preparation and packing are discussed, along with physical properties of the stationary phases, followed by the two chromatographic systems utilized throughout the research.

2.2 Column preparation and packing

In order to accurately determine thermodynamic and kinetic information regarding a separation, a well-behaved and well-characterized chromatographic column is needed. To this end, capillary columns that are packed in-house are used throughout this research. An optically transparent, fused-silica capillary is used for the column. Detection windows are created by burning off the polyimide coating on the outside of the capillary, followed by removal of the charred residue with high purity methanol (Burdick and Jackson Division, Honeywell). The column is terminated with a quartz wool frit. The stationary phase is packed using the slurry method, as columns packed by this method have uniform packing across the diameter and length of the column [1]. To do this, the stationary phase is suspended in a solvent that prevents immediate precipitation. The slurry is stirred for 0.5 hours and subsequently transferred to a metal reservoir connected between a single-piston reciprocating pump (Model 114M, Beckman Instruments) and the prepared fused-silica capillary. The reservoir is brought to a high pressure (4000 psi) in an effort to quickly load the stationary

phase into the capillary column; packing is usually complete in less than twenty minutes. The highest pressure is maintained for three to five hours and gradually lowered to 1000 psi overnight. The lower pressure allows the packed bed to compress, removing any voids left during the initial packing step.

The efficiency or plate height (H) of each column is investigated using a well-behaved series of coumarin-labeled fatty acid solutes (Figure 2.1). After separation, the zone profile for each solute is fit to the Gaussian function (Equation 1.33). The fit equation is regenerated in Microsoft Excel where the first and second statistical moments are calculated (Equations 1.20 and 1.21), followed by the calculation of plate height (Equation 1.23). For an efficient column, the plate height should be close to two times the particle diameter of the packing material. If an inefficient column is produced, the slurry density and solvent can be adjusted in an effort to improve the column efficiency. In addition, the column porosity can be useful for column characterization as it gives an indication of the void space between particles relative to the total column volume. The interparticle porosity (ε_u) can be calculated from

$$\frac{\varepsilon_u^3}{(1-\varepsilon_u)^2} = \frac{180\,\mu\eta L}{d_p^2\,\Delta P} \tag{2.1}$$

where μ is the linear velocity, η is the solvent viscosity, d_p is the particle size, and ΔP is the pressure drop along the column. Typically for randomly packed spheres, ε_u will be 0.38. The total porosity (ε_T) is the sum of the inter- and intraparticle porosities. Many porous, silica particles have intraparticle porosities of 0.5 [2]. Thus, ε_T for a typical, silica-based porous particle is 0.88.

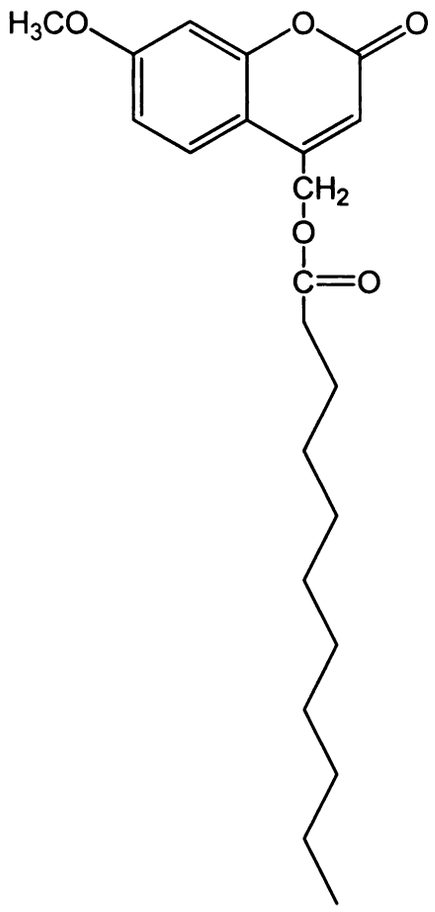

Figure 2.1. C_{10} coumarin-labeled fatty acid.

2.3 Stationary phases

Several different stationary phases were used throughout the course of the research. For the first investigation (Chapter 3), a polymeric octadecylsilica phase custom synthesized by Lane Sander at the National Institute of Standards and Technology was employed. This packing material is characterized by a 5.5 μm particle size, 190 Å pore size, and 240 m^2/g surface area (IMPAQ 200, PQ Corp.). It is prepared by reaction of the silica support with triethoxyoctadecylsilane at a bonding density of 5.4 $\mu mol/m^2$. This phase was packed in an acetone slurry to yield of a plate height of 15 μm and an interparticle porosity of 0.44.

For the subsequent investigations (Chapters 4 and 5), three organic – silica hybrid phases were used. The bridged-ethylene hybrid (BEH) support is prepared by the co-condensation reaction of tetraethoxysilane and 1,2-bis(triethoxysilyl)ethane. The alkyl-bonded phases are then produced through derivatization of the hybrid support. Each phase is endcapped with trimethylchlorosilane. An illustration of the phase chemistry is given in Figure 2.2. The C_{18} phase (Figure 2.2A) is prepared by reaction of the hybrid support with a trifunctional silane at a bonding density of 3.06 $\mu mol/m^2$. It is characterized by a 5.2 μm particle size, 141 Å pore size, and 189 m^2/g surface area (XBridge C_{18}, Waters Corporation). This phase is packed in an acetone slurry to yield of a plate height of 10 μm and an interparticle porosity of 0.39. Another C_{18} phase (Figure 2.2B) contains a carbamate (polar) group embedded

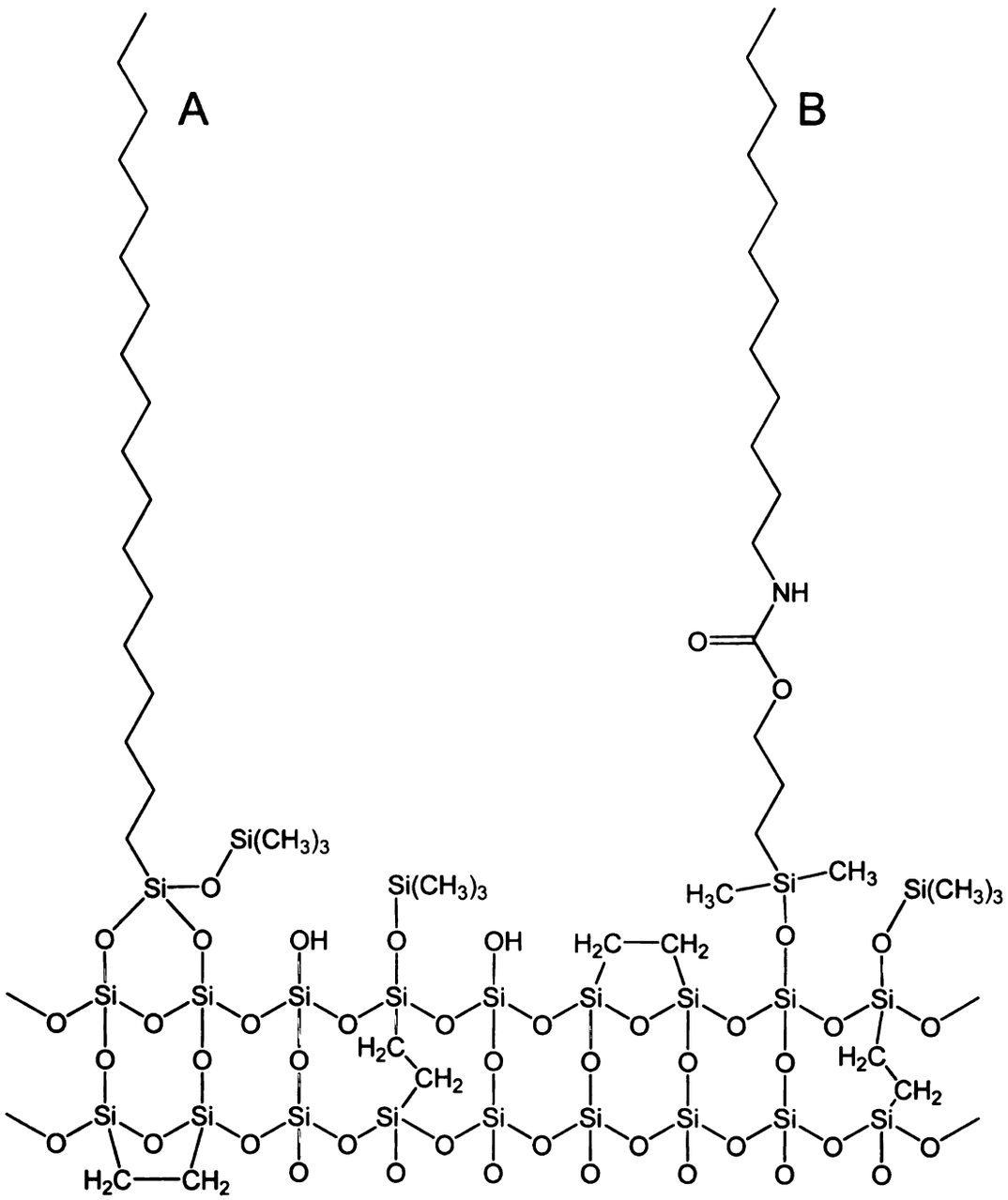

Figure 2.2. Chemical structure of the bridged-ethylene hybrid (BEH) phases showing derivatization of each C_{18} phase on the BEH support. (A) XBridge C_{18} (B) XBridge Shield RP_{18}

in the C_{18} chain and is prepared by reaction of the silica support with a monofunctional silane at a bonding density of 3.23 μmol/m^2. It is characterized by a 5.4 μm particle size, 154 Å pore size, and 194 m^2/g surface area (XBridge Shield RP_{18}, Waters Corporation). This phase is packed in an acetone slurry to yield of a plate height of 9 μm and an interparticle porosity of 0.39. In addition to the C_{18} phases, the underivatized underlying hybrid particle is examined (Figure 1.2). The hybrid support was produced from the same lot as the XBridge Shield RP_{18} material and is characterized by a 5.1 μm particle size (Bridged-ethylene hybrid support, Waters Corporation). This phase is packed in an acetone slurry to yield of a plate height of 25 μm and an interparticle porosity of 0.43.

2.4 Chromatographic systems

2.4.1 One-detector system for mobile phase modifier study

A one-detector system (Figure 2.3) was used for all mobile phase modifier studies (Chapter 5). A capillary column is prepared as described in Section 2.2, where the polyimide coating has been removed at a length near 82 cm. The mobile phase is delivered by a single-piston reciprocating pump (Model 114M, Beckman Instruments), operated in the constant-pressure mode. After injection (Model ECI4W1, Valco Instruments), the samples are split between the column and a fused-silica splitting capillary (50 μm i.d., Polymicro Technologies). The length of the splitter is carefully controlled, as it controls the amount of sample introduced onto the column. In order to avoid overloading the stationary phase in

Pump

igure 2.3.
matograp
e phase
ary, F

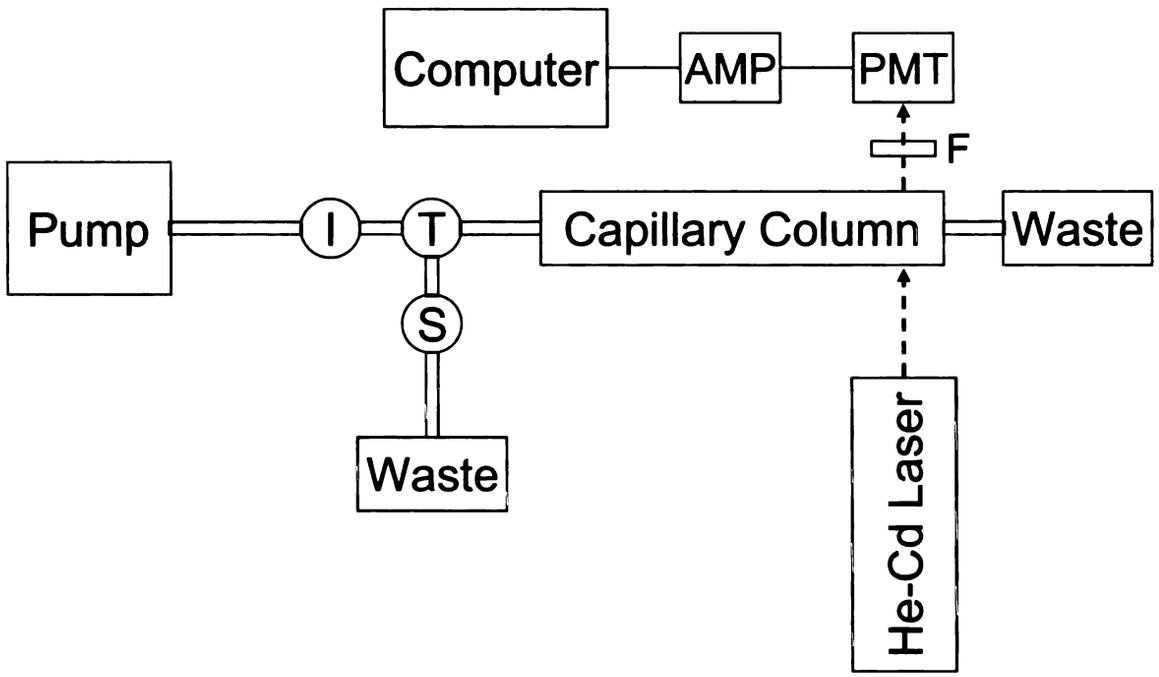

Figure 2.3. Schematic diagram of the experimental system for capillary liquid chromatography with one on-column laser-induced fluorescence detector for mobile phase modifier study. I: injection valve, T: splitting tee, S: splitting capillary, F: filter, PMT: photomultiplier tube, AMP; current to voltage amplifier.

re capillary

diaccrox ma

Solute

ant aous-w

accrox mate

fuorescence

reference

proportiple

suring pho

struments)

struments)

struments)

24.2 Four-c

A four

ressure con

sorbed in S

ases along

livered by

struments).

24.4.1. Valc

ases loca sp

e solver is c

15 nL. At th

the capillary column, the 1 μL injection is split 100:1 to yield an injection volume of approximately 10 nL.

Solute detection is achieved by on-column laser-induced fluorescence. A continuous-wave helium-cadmium laser (Model 3074-20M, Melles Griot), with approximately 24 mW power at 325 nm, is used as the excitation source. The fluorescence emission is isolated by a liquid filter (1 % aqueous $NaNO_3$) and two interference filters (420 nm, S10-410-F, Corion) and is detected by a photomultiplier tube (Centronic Model Q4249BA, Bailey Instruments). The resulting photocurrent is amplified using a gain of 10 μA/V (Model 480, Keithley Instruments), converted to the digital domain (Model PCI-MIO-16XE-50, National Instruments) and stored by a user-defined program (Labview v5.1, National Instruments).

2.4.2 Four-detector system for temperature and pressure study

A four-detector system (Figure 2.4) was used for all temperature and pressure controlled studies (Chapter 3 and 4). A capillary column is prepared as described in Section 2.2, where the polyimide coating has been removed at four places along the column (~23, 29, 53, and 58 cm). The mobile phase is delivered by a single-piston reciprocating pump (Model 114M, Beckman Instruments), operated in the constant-pressure mode. After injection (Model EC14W1, Valco Instruments), the samples are split between the column and a fused-silica splitting capillary (50 μm i.d., Polymicro Technologies). The length of the splitter is carefully controlled to yield an injection volume of approximately 10 - 15 nL. At the end of the column, another fused-silica capillary (20 μm i.d.,

Figure 2.4. S
atograph
perature a
ay. R

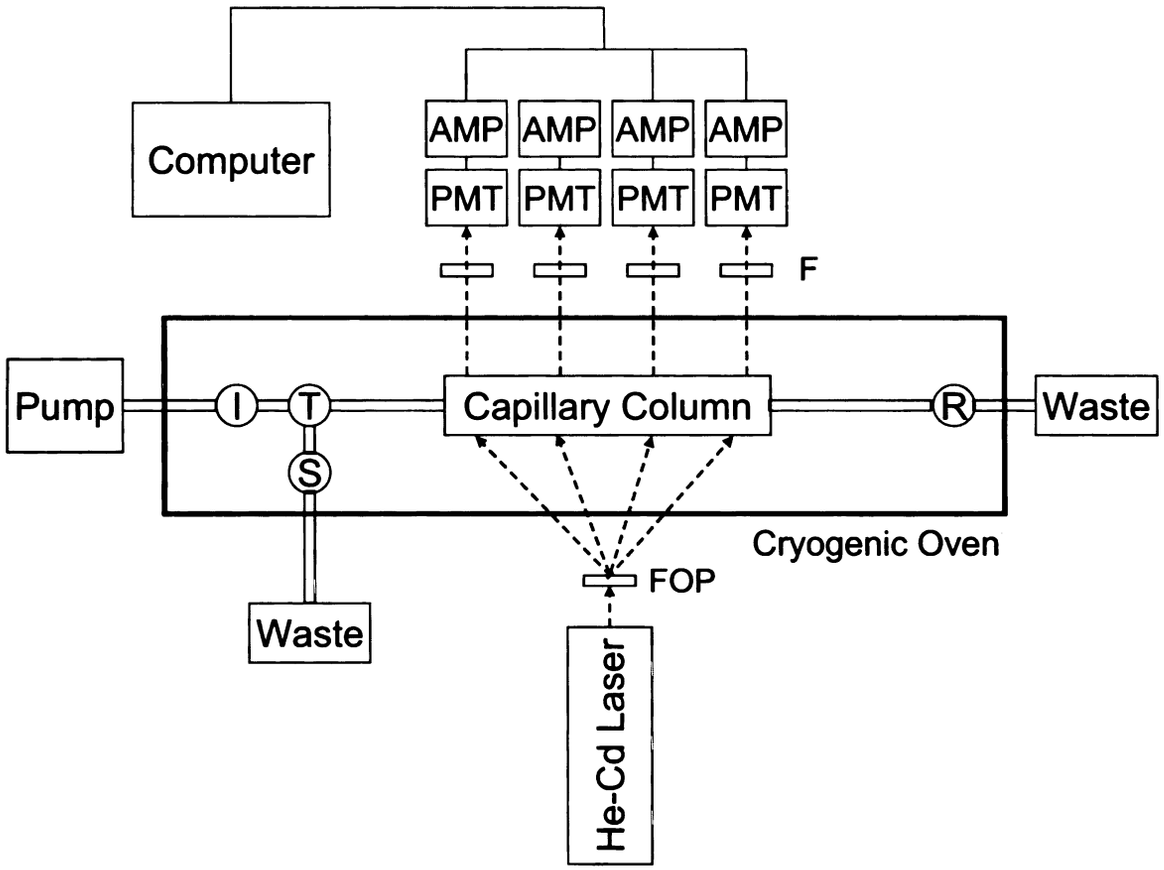

Figure 2.4. Schematic diagram of the experimental system for capillary liquid chromatography with four on-column laser-induced fluorescence detectors for temperature and pressure study. I: injection valve, T: splitting tee, S: splitting capillary, R: restricting capillary, FOP: fiber-optic positioner, F: filter, PMT: photomultiplier tube, AMP; current to voltage amplifier.

Polymicro Tec

Chapter 3. the

low rate alon

solter. colum

3300. Varian A

the use of liqu

Solute

continuous-wa

with power at

into UV-gras

transmitted to

been remove

orthogonally

to transmitte

photomultiplie

ding a gain

converted to t

is stored by

3.5 Conclu

In orde

experimental p

designed expe

procedures and

Polymicro Technologies) is attached to serve as a restrictor. For the study in Chapter 3, the length of the restrictor is systematically decreased to adjust the flow rate along the column while maintaining constant pressure. The injector, splitter, column, and restrictor are contained within a cryogenic oven (Model 3300, Varian Associates) that maintains a constant temperature (± 0.1 K) through the use of liquid nitrogen aspiration and resistive heating coils.

Solute detection is achieved by on-column laser-induced fluorescence. A continuous-wave helium-cadmium laser (Model 3074-20M, Melles Griot), with 30 mW power at 325 nm, is used as the excitation source. The laser is focused onto UV-grade optical fibers (100 μm, Polymicro Technologies) and is transmitted to four locations along the column where the polyimide coating has been removed. The fluorescence power at each location is collected orthogonally by large diameter optical fibers (500 μm, Polymicro Technologies) and transmitted through a 420 nm interference filter (S10-410-F, Corion) to a photomultiplier tube (Model R760, Hamamatsu). The photocurrent is amplified using a gain of 100 nA/V and a time constant of 10 ms (Model 556, Ortec), converted to the digital domain (Model PCI-MIO-16XE-50, National Instruments), and stored by a user-defined program (Labview v5.1, National Instruments).

2.5 Conclusions

In order to accurately characterize the retention event, adequate experimental procedures for packing have been developed and a judiciously designed experiment system has been used. This chapter details the packing procedures and the chromatographic systems utilized throughout the research.

J.C. G
(1983

R. O

2.6 References

[1] J.C. Gluckman, A. Hirose, V.L. McGuffin, M. Novotny, *Anal. Chim. Acta 17* (**1983**) 303-309.

[2] R. Ohmacht, I. Halász, *Chromatographia 14* (**1981**) 155-162.

EXPERIM
RETE

3.1. Introdu

A dee

es both

ontrol the re

f zone broad

separation. A

aviour wh

aviour has

retic behav

separation sp

derstand k

associated k

accomplishec

Sectio

formation, b

mpare exp

omatograp

heral metho

ies [6] as a f

s a function

CHAPTER 3

EXPERIMENTAL EVALUATION OF METHODS FOR EXTRACTING RETENTION FACTORS AND KINETIC RATE CONSTANTS IN LIQUID CHROMATOGRAPHY

3.1. Introduction

A deep understanding of chromatographic and related separations requires both thermodynamic and kinetic information [1]. Thermodynamic factors control the retention and selectivity, whereas kinetic processes dictate the extent of zone broadening and asymmetry, each of which affect the resolution of the separation. A number of studies have been performed to elicit thermodynamic behavior, which is now well understood for many systems [2-5]. However, kinetic behavior has not been studied in as much detail. A detailed understanding of the kinetic behavior is necessary to identify the rate-limiting processes so that separation speed may be increased without sacrificing resolution. To better understand kinetic processes, accurate measurement of rate constants and the associated kinetic parameters (i.e. activation enthalpy and volume) must be accomplished.

Section 1.3 contained methods for extracting thermodynamic and kinetic information, but to date, there have been no studies that directly validate and compare experimental methods for extracting kinetic parameters from real chromatographic peaks. Using stochastic simulation, Li and McGuffin evaluated several methods for extracting kinetic rate constants by comparison to the "true" value [6] as a function of column length, linear velocity, and equilibrium constant. As a function of both column length and linear velocity, calculated retention

factors were

from the EMG

model. Kinet

parameters.

for the stat

method. Th

along the co

profile than t

torrent and

a smaller re

constants tha

The authors

thermodynam

stochastic s

thermodynam

and extra-co

calculated.

The go

the profiles

fibre carbon

ing several t

other advanta

factors were most reliable from the statistical moment model, somewhat reliable from the EMG model, and least reliable (with the greatest error) from the Thomas model. Kinetic rate constants were more inconsistent with the various separation parameters. As column length was increased, the rate constants were constant for the statistical moment and Thomas methods and increased for the EMG method. This behavior was attributed to the change in shape of the zone profile along the column, becuase the EMG method more strongly depends on the zone profile than the other methods. As a function of linear velocity, the statistical moment and Thomas models provided rate constants approximately 10 and 15 % smaller, respectively, than the true value, while the EMG model provided rate constants that decreased with increasing linear velocity. Based on their results, the authors deemed each method capable of accurately evaluating thermodynamic and kinetic parameters under the conditions specified in the stochastic simulation. However, the ability of the methods to extract thermodynamic and kinetic information under practical conditions, where column and extra-column contributions affect broadening and asymmetry, is yet to be evaluated.

The goals of this research are as follows: (1) to generate experimental zone profiles as a function of column length, mobile phase linear velocity, and solute carbon number, (2) to extract retention factors and kinetic rate constants using several theoretical methods and (3) to compare the methods with respect to their advantages and limitations.

3.2. Theory

The retention factor is a thermodynamic description of the interaction strength of a solute with the mobile and stationary phases. The retention factor is calculated from measurable chromatographic parameters by

$$k = \frac{t_r - t_0}{t_0} \tag{3.1}$$

where t_r is the retention time of the solute and t_0 is the elution time of a non-retained compound. The kinetic rate constants quantify kinetic aspects of the rate of solute transfer, and are related to the retention factor by

$$k = \frac{k_{sm}}{k_{ms}} \tag{3.2}$$

where k_{sm} is the rate constant for the transfer from mobile to stationary phase and k_{ms} is the rate constant for the transfer from stationary to mobile phase. Three data analysis methods are examined in this study; each method is discussed in detail in Chapter 1.3.3, while experimental details are provided here.

3.2.1. Plate height model

In the statistical moment method, the moments may be calculated directly from the zone profiles (i.e. without regression to specific equations). The first and second statistical moments in time units are defined as

$$M_1 = \frac{\int C(t)\, t\, dt}{\int C(t) dt} \tag{3.3}$$

$$M_2 = \frac{\int C(t)(t - M_1)^2 dt}{\int C(t) dt} \tag{3.4}$$

where C(t) is the solute concentration at the detector as a function of time, M_1 is the mean retention time, and M_2 is the peak variance. The retention factor is determined from the first moment by

$$k = \frac{M_1 - t_0}{t_0} \tag{3.5}$$

As discussed in Chapter 1.3.3, the method of calculating kinetic rate constants is derived by extension of Giddings' work [1]. The plate height in length units (H_L) can be related to the second moment by

$$H_L = \frac{M_2 L}{M_1^2} \tag{3.6}$$

where L is the column length. The mass transfer term (C_s) for slow kinetics is derived from the generalized nonequilibirum theory of Giddings [1] and is given by

$$C_s = \frac{2k}{(1+k)^2 k_{ms}} \tag{3.7}$$

Thus, the rate constants are related to the plate height by

$$k_{ms} = \frac{2ku}{(1+k)^2 dH_L} \quad \text{and} \quad k_{sm} = \frac{2k^2u}{(1+k)^2 dH_L} \tag{3.8}$$

where u is the linear velocity and dH_L is the corrected plate height. The corrected plate height represents slow mass transfer in the stationary phase (C_s), and is calculated by

$$dH_L = H_L - A - \frac{B_m}{u} - \frac{B_s}{u} - C_m u \tag{3.9}$$

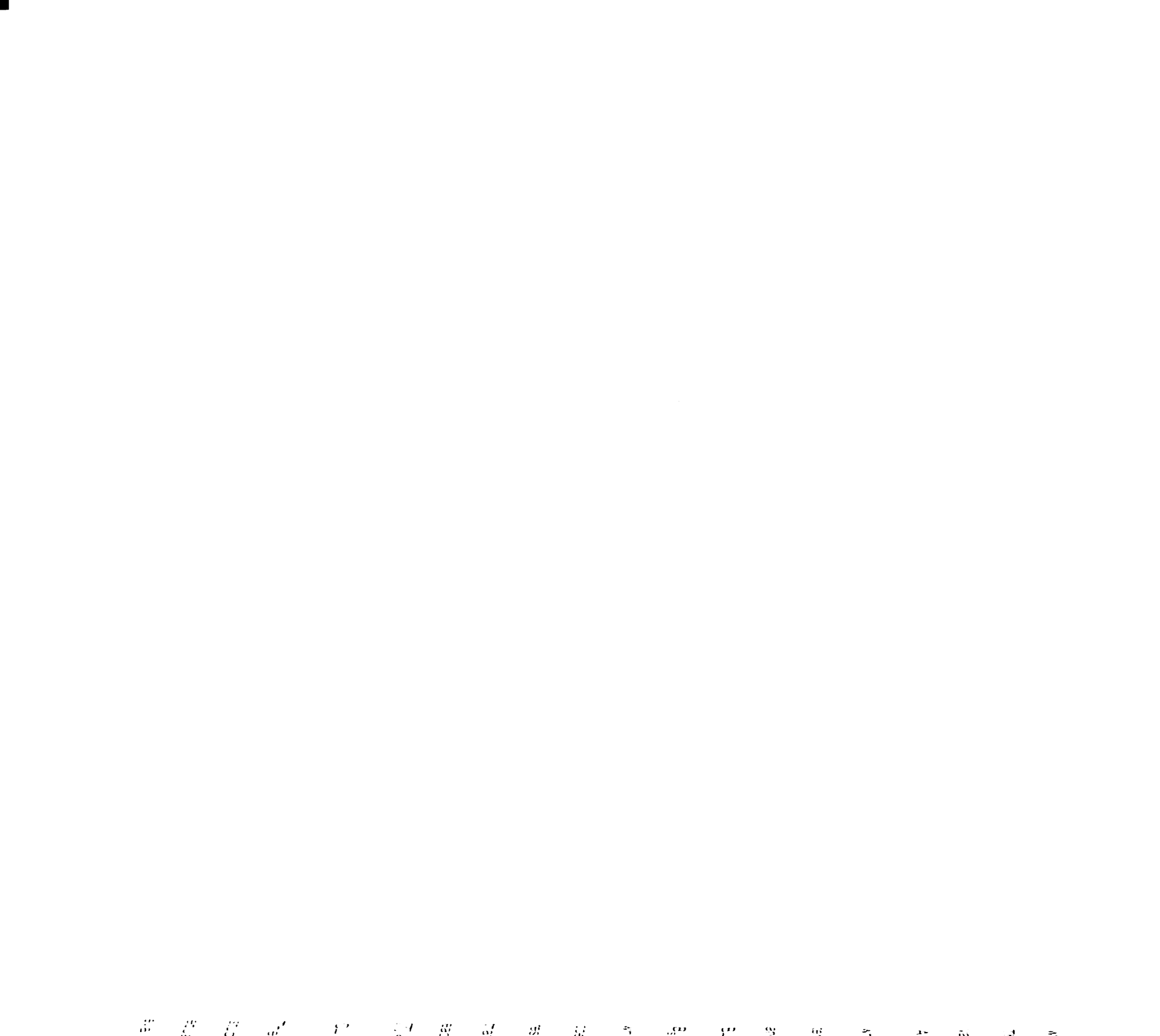

where A, B_m, B_s, and C_m are the classical contributions to zone broadening [1]. The multiple paths term (A) characterizes the broadening that arises from the variety of flow paths available in the packed column, and is given by

$$A = 2\lambda d_p \tag{3.10}$$

where λ is a packing factor and d_p is the particle size. The longitudinal diffusion terms (B_m and B_s) characterize the random motion of molecules in the mobile and stationary phases, respectively, and are given by

$$B_m = 2\gamma_m D_m \tag{3.11}$$

$$B_s = 2\gamma_s D_s k \tag{3.12}$$

where γ_m and γ_s are obstruction factors and D_m and D_s are the diffusion coefficient of the solute in the mobile and stationary phases, respectively. The resistance to mass transfer term in the mobile phase (C_m) represents broadening that arises because solute molecules tend to remain in the same flow stream, each of which has a different velocity. This contribution is given by van Deemter [7] as

$$C_m = \frac{k^2 {d_p}^2}{100(1+k)^2 D_m} \tag{3.13}$$

The van Deemter form was chosen as it performed more consistently in this study than the the Purnell [8], Giddings [1], and Giddings coupling [9,10] equations, as well as the method developed by Miyabe and Guiochon [11]. The evaluation of these equations is discussed in detail in Appendix 3A.1.

A

Equation

orrected

ased on

mer of

equation

hese em

ply extra

detector.

calculato

corrected

ormatio

detector.

$$\eta = \frac{\Delta M_2}{\Delta M_1}$$

here Δt_2

he differe

ce ΔL is t

2.2. Exp

The

ibution

As shown in Equation 3.9, each of the broadening contributions in Equations 3.10 to 3.13 is subtracted from the plate height in order to give the corrected plate height. However, each contribution includes a parameter that is based on estimation. For this study, λ, γ_m, and γ_s are taken as unity, D_m is on the order of 10^{-5} cm^2/s and D_s values, which were estimated using the Wilke–Chang equation [12], range from 10^{-6} to 10^{-9} cm^2/s for solutes C_{10} to C_{20}. Unfortunately, these empirical estimations will introduce errors in the measurement. In addition, any extra-column contributions to broadening, including those from the injector, detector, connections, etc., must be minimized or eliminated to assure accurate calculation of thermodynamic and kinetic parameters. In this work, extra-column contributions were eliminated through detection at several points along the chromatographic column with subtraction of the parameters determined at each detector. Thus, Equations 3.5 and 3.6 become

$$k = \frac{\Delta M_1 - \Delta t_0}{\Delta t_0} \tag{3.14}$$

$$H_L = \frac{\Delta M_2 \, \Delta L}{(\Delta M_1)^2} \tag{3.15}$$

where Δt_0 is the difference in the elution time of a non-retained species, ΔM_1 is the difference in the first moment, ΔM_2 is the difference in the second moment, and ΔL is the distance between two on-column detectors.

3.2.2. Exponentially modified Gaussian (EMG) model

The EMG model is a convolution of the Gaussian and exponential contributions as described in the following equation

$$k_{1}=\frac{A_{0}}{2A_{3}}$$

ware eff

ecation

egression

me this

$=A_{1}+A$

and the co

onstants

$$k_{3}=\frac{2kt_{3}}{A_{3}^{2}}$$

his meth

lasses by

has been

MCS_Em

In

mized

nts alg

determine

$$k_{2}=\frac{}{}$$

$$k_{3}=\frac{2k}{}$$

$$C(t) = \frac{A_0}{2A_3} \exp\left(\frac{A_2^2}{2A_3^2} + \frac{A_1 - t}{A_3}\right)\left(\text{erf}\left(\frac{t - A_1}{\sqrt{2}A_2} - \frac{A_2}{\sqrt{2}A_3}\right) + 1\right) \quad (3.16)$$

where erf is a statistical error function. The zone profile is fit to the EMG equation by nonlinear regression (PeakFit, Jandel Scientific) to extract the regression parameters, A_0, A_1, A_2, A_3. From these parameters, the retention time (t_r) is calculated as

$$t_r = A_1 + A_3 \quad (3.17)$$

and the corresponding retention factor is calculated from Equation 3.1. The rate constants are calculated by

$$k_{ms} = \frac{2kt_0}{A_3^2} \text{ and } k_{sm} = \frac{2k^2 t_0}{A_3^2} \quad (3.18)$$

This method of determining the rate of transfer between mobile and stationary phases by adjusting an exponential equation on the tail of an asymmetric peak has been justified by Vidal-Madjar and Guiochon [13] and applied extensively by McGuffin et al. [6,14-17].

In the EMG method, any extra-column contributions to asymmetry must be minimized or eliminated. This can be accomplished by detection at several points along the chromatographic column with subtraction of the parameters determined at each detector. Thus, Equations 3.1 and 3.18 become

$$k = \frac{\Delta t_r - \Delta t_0}{\Delta t_0} \quad (3.19)$$

$$k_{ms} = \frac{2k\,\Delta t_0}{\Delta A_3^2} \text{ and } k_{sm} = \frac{2k^2\,\Delta t_0}{\Delta A_3^2} \quad (3.20)$$

where Δt_r is the difference in the retention time and ΔA_3^2 is the difference in A_3^2 between two on-column detectors.

3.2.3. Thomas nonlinear chromatography model

The Thomas method describes the concentration (C(x)) as

$$C(x) = \frac{A_0}{A_2 A_3}\left(1-\exp\left(-\frac{A_3}{A_2}\right)\right)\left(\frac{\sqrt{\frac{A_1}{x}}\, I_1\left(\frac{2\sqrt{A_1 x}}{A_2}\right)\exp\left(\frac{-x-A_1}{A_2}\right)}{1-T\left(\frac{A_1}{A_2},\frac{x}{A_2}\right)\left(1-\exp\left(-\frac{A_3}{A_2}\right)\right)}\right) \tag{3.21}$$

where

$$T(u,v) = \exp(-v)\int_0^u \exp(-x)\, I_0\left(\sqrt{2vx}\right)dx \tag{3.22}$$

and I_0 and I_1 are modified Bessel functions of the first kind. After conversion from the time domain (t) to the retention factor domain (x), the zone profile is fit by nonlinear regression to Equation 3.21 (PeakFit, Jandel Scientific). From the regression parameters (A_0, A_1, A_2, and A_3), the corresponding retention factor and rate constants are obtained as shown

$$k = A_1 \tag{3.23}$$

$$k_{ms} = \frac{1}{A_2 t_0} \text{ and } k_{sm} = \frac{k}{A_2 t_0} = \frac{A_1}{A_2 t_0} \tag{3.24}$$

For accurate calculation of retention factor and rate constants, any extra-column contributions, including those from the injector, detector, connections, etc., must be negligible. However, unlike the moment and EMG models, there is no *a posteriori* method to correct for these contributions.

3.3. M

3.3.1. R

A

Acromeg

ndividual

ssue occ

mple pr

nitrogen

ackson D

3.3.2. Ex

The

AT mut

base is

Chapter 2

ecretary o

Technolog

Technolog

Director

ne ma

temperatu

3.3.3. Da

Alle

be chrom

3.3. Methods

3.3.1. Reagents

A series of fatty acids (Sigma) ranging from C_{10} to C_{20} are derivatized with 4-bromomethyl-7-methoxycoumarin (Sigma), as shown in Figure 2.1 [18]. Individual fatty acid derivatives are isolated and purified using a conventional-scale octadecylsilica column (ODS-224, Applied Biosystems) with methanol mobile phase [19]. The resulting fractions are evaporated in a stream of dry nitrogen at 313 K and are redissolved in high-purity methanol (Burdick and Jackson Division, Honeywell) at a concentration of 5×10^{-4} M.

3.3.2. Experimental system

The solutes are separated on a capillary liquid chromatography system with multiple on-column detectors as illustrated in Figure 2.4. The stationary phase is a silica-based C_{18} material (IMPAQ 200, PQ Corp.) described in Chapter 2.3 and the mobile phase is methanol. The sample is split between the capillary column and a 50 μm i.d. fused-silica capillary (0.6 m length, Polymicro Technologies). A 20 μm i.d. fused-silica capillary (2 m length, Polymicro Technologies) is attached post-column to serve as a restrictor. The length of the restrictor is systematically decreased to adjust the flow rate along the column while maintaining constant pressure. The separation was performed in constant temperature (303 K) and pressure (4000 psi) mode.

3.3.3. Data analysis

After separation, the solute zone profiles are individually extracted from the chromatogram and then analyzed. In preliminary studies, several models

were examined for experimental data analysis. Each profile was fit by nonlinear regression to the Gaussian and Giddings functions (Equations 1.33 and 1.39, respectively) by a commercially available program (Peakfit v4.14, SYSTAT Software, Inc.). The Gaussian model assumes a symmetric peak shape, while the Giddings model assumes negligible column contributions from multiple paths and diffusion in the mobile and stationary phases; both assumptions are not valid for all solutes in this experiment. The Gaussian model contained nonrandom residuals with correlation coefficients ranging from 0.990 to 0.813 for C_{10} to C_{20}, respectively. The Giddings model also produced nonrandom residuals with correlation coefficients ranging from 0.990 to 0.830 for C_{10} to C_{20}, respectively. Due to the poor quality of fit, these models were not used for further analysis of the zone profiles. Other models that can account for asymmetric peak shapes were then evaluated and determined to be more suitable. For the plate height method, the profile is fit to an asymmetric double sigmoidal function (ADS)

$$y = \frac{A_0}{1+\exp\left[-\left(\frac{X-A_1+\frac{A_2}{2}}{A_3}\right)\right]}\left[1-\frac{1}{1+\exp\left[-\left(\frac{X-A_1-\frac{A_2}{2}}{A_4}\right)\right]}\right] \tag{3.25}$$

where A_0 is the amplitude, A_1 is the peak center, and A_2, A_3, and A_4 are peak widths. A commercially available program (Tablecurve v2.02, SYSTAT Software, Inc.) is used to fit the zone profile. The fit equation is regenerated in Microsoft Excel, from which the statistical moments are calculated. This method produces high quality fits (correlation coefficients ranging from 0.999 to 0.979), reduces noise, and allows control of peak integration limits. In this work, the integration

nts are ident

culation of t

trail under the

ore EMG and

ommercially a

gression of t

rrelation coe

1.936 to 0.942

ore profile d

he peak ma

n the Tho

efficients

EMG and T

Physical and

3.4. Res

3.4.1. Ret

The

ecity a

ace-volu

ction o

creases

he Thoma

ecur the

limits are identified at 0.1 % of the maximum peak height, as the error in the calculation of the moments, particularly the second moment, has been proven small under these conditions [20]. Each profile is also fit by nonlinear regression to the EMG and Thomas functions (Equations 3.16 and 3.21, respectively) by a commercially available program (Peakfit v4.14, SYSTAT Software, Inc.). The regression of the zone profiles to each of these equations is excellent, with correlation coefficients ranging from 0.999 to 0.941 for the EMG equation and 0.998 to 0.942 for the Thomas equation. However, each of the models fits the zone profile differently. As shown in Figure 3.1, the EMG model overestimates the peak maximum and tail and underestimates the region around the mean, while the Thomas model behaves in the opposite manner. The high correlation coefficients result from the average of positive and negative error in both the EMG and Thomas models. The ADS fit is most accurate, however it lacks physical and chromatographic significance.

3.4. Results and discussion

3.4.1. Retention factor

The retention factors at each on-column detector at a representative linear velocity are plotted in Figure 3.2. These retention factors are not corrected for extra-column effects. For all methods, the retention factor increases slightly as a function of column length. For example, for the C_{16} fatty acid, the retention factor increases by 4.8 % for the statistical moment, 4.6 % for the EMG, and 3.5 % for the Thomas methods. To further examine the effect of distance on retention factor, the difference method was used, as this method corrects for extra-column

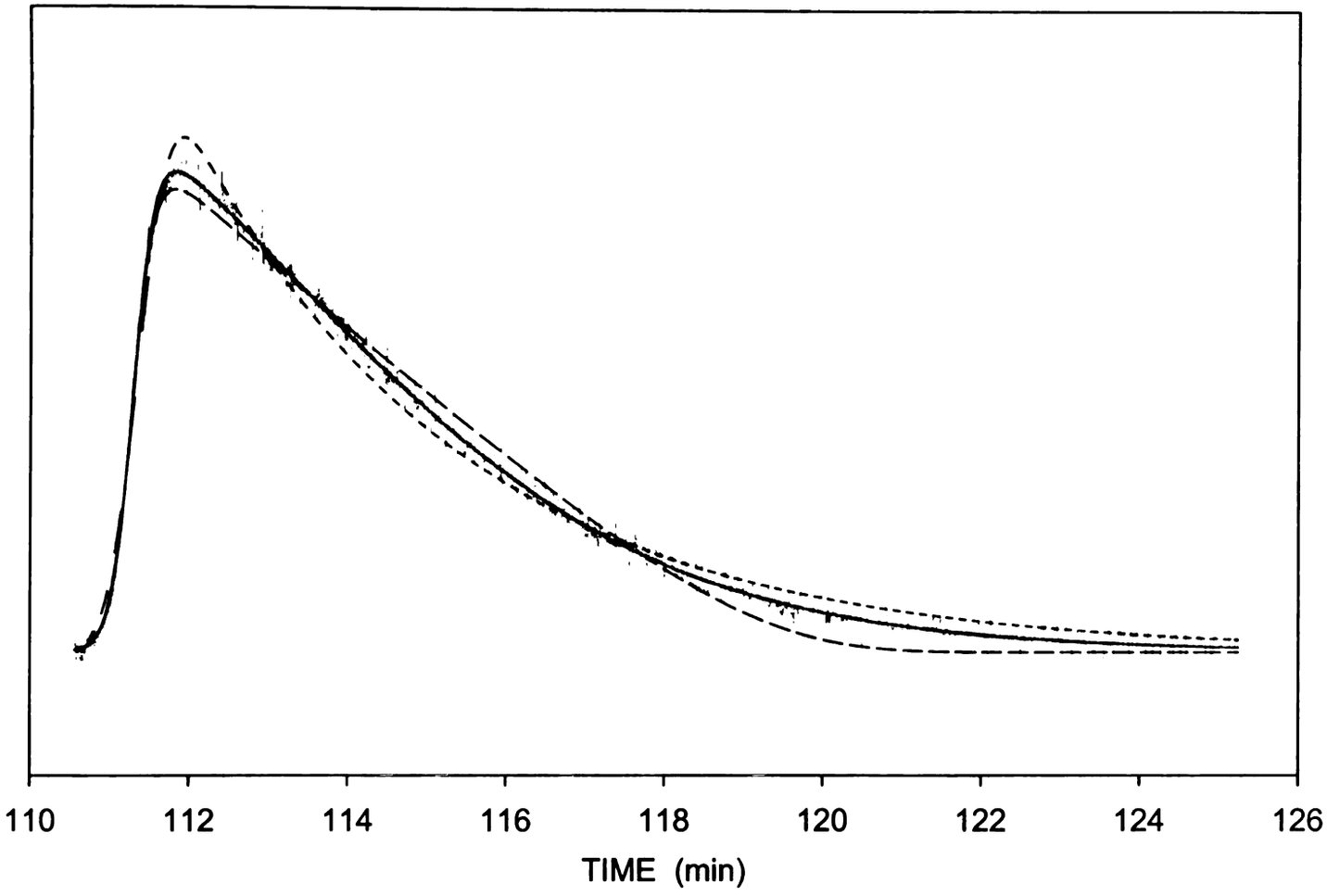

Figure 3.1. Regression analysis of the C_{18} coumarin-labeled fatty acid at a linear velocity of 0.062 cm/s. Peak (·-·-·), EMG (------), NLC (— —), ADS (——)

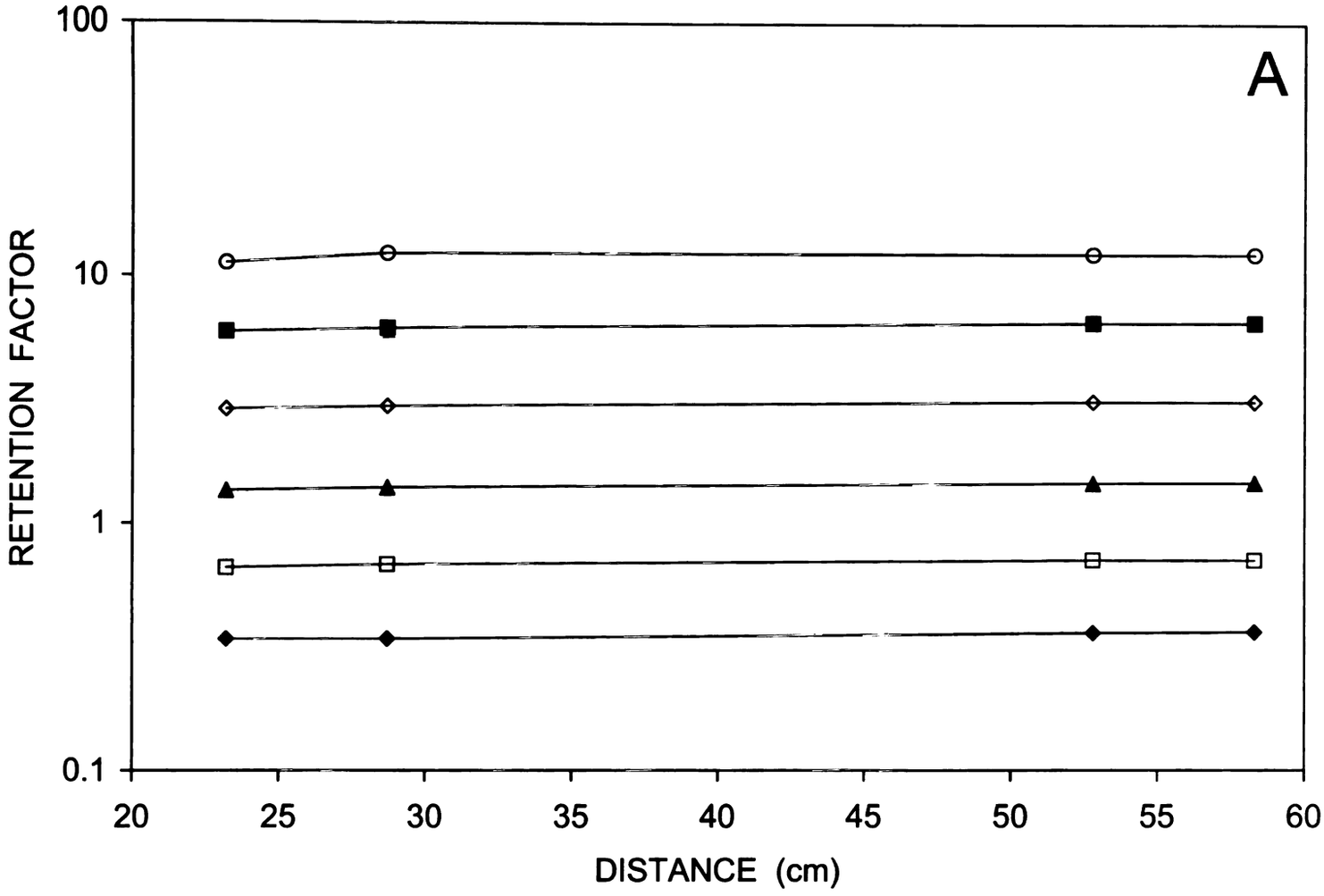

Figure 3.2A: Retention factor plotted versus distance. The retention factors were calculated with the moment model at a linear velocity of 0.088 cm/s. C_{10} (◆) C_{12} (□) C_{14} (▲) C_{16} (◇) C_{18} (■) C_{20} (○)

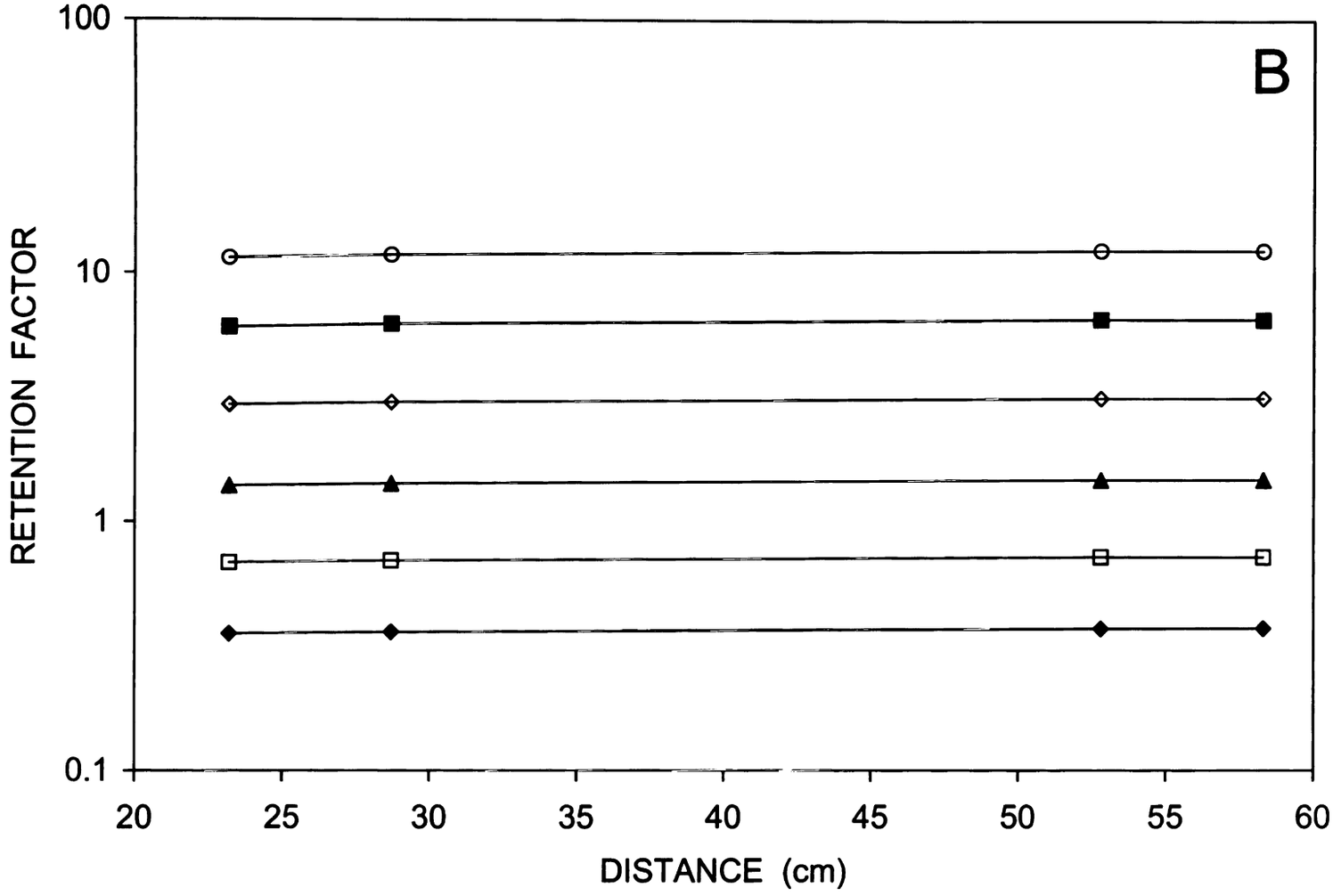

Figure 3.2B: Retention factor plotted versus distance. The retention factors were calculated with the EMG model at a linear velocity of 0.088 cm/s. C_{10} (◆) C_{12} (□) C_{14} (▲) C_{16} (◇) C_{18} (■) C_{20} (○)

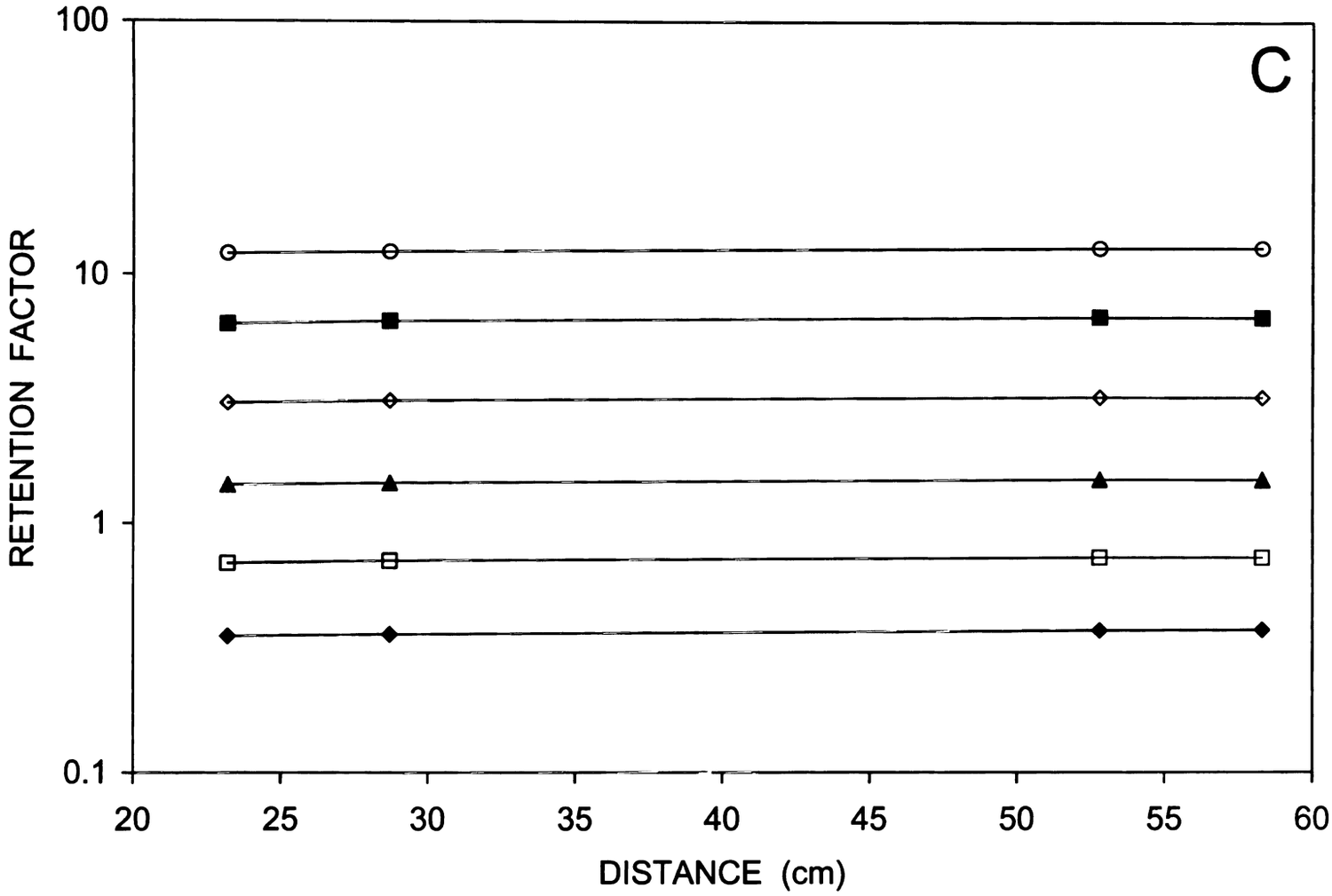

Figure 3.2C: Retention factor plotted versus distance. The retention factors were calculated with the Thomas model at a linear velocity of 0.088 cm/s. C_{10} (◆) C_{12} (□) C_{14} (▲) C_{16} (◇) C_{18} (■) C_{20} (○)

variance. The retention factors are calculated between detectors 4 and 1 (35.1 cm), detectors 4 and 2 (29.6 cm), and detectors 3 and 2 (24.1 cm), as summarized for the EMG model in Table 3.1. As the distance between the detectors increases, there is no significant change in the retention factor (0 to 1.4 %). This decrease in the variation relative to 4.6 % (*vida supra*) illustrates the advantage of using the difference approach. Because the retention factor is a measure of thermodynamic conditions, the constancy along the column implies that steady state has been achieved and reliable extraction of the kinetic information can occur.

Representative values for the retention factor calculated by difference (between detectors 4 and 1) at each velocity are summarized for each model in Tables 3.2 – 3.4. Retention factors are quite similar for all models and show the same trends with velocity and carbon number. The retention factor decreases with increasing linear velocity for all solutes. It may be noted that at any velocity, the solute transfers between the stationary and mobile phases toward equilibrium. At higher velocities, equilibrium conditions are more difficult to achieve because the mobile phase is moving faster, yet the stationary phase remains immobile, which leads to a decrease in retention. The effect is most apparent for solutes with longer alkyl chains, which on average spend a longer time in the stationary phase. For example, using the statistical moment model, the retention factor for C_{10} decreases by approximately 13 %, whereas the retention factor for C_{20} decreases by approximately 26 % as the velocity is

Table 3.
were ca

Table 3.1: Retention factors as a function of length (L). The retention factors were calculated with the EMG difference model at a linear velocity of 0.088 cm/s.

Carbon Number	Retention factor, k		
	L4 – L1 = 35.1 cm	L4 – L2 = 29.6 cm	L3 – L2 = 24.1 cm
10	0.38	0.38	0.38
12	0.74	0.74	0.74
14	1.50	1.50	1.51
16	3.19	3.18	3.21
18	6.60	6.58	6.67
20	12.4	12.4	12.5

Table 3.2: Retention factors for coumarin-labeled fatty acids as a function of linear velocity (u). The retention factors were calculated with the moment model by difference between detectors 4 and 1.

Carbon Number	Retention factor, k				
	u = 0.045 cm/s	u = 0.062 cm/s	u = 0.088 cm/s	u = 0.150 cm/s	u = 0.368 cm/s
10	0.39	0.39	0.38	0.37	0.34
12	0.76	0.75	0.74	0.71	0.64
14	1.55	1.53	1.51	1.43	1.21
16	3.33	3.27	3.18	2.99	2.41
18	6.85	6.79	6.58	6.12	4.69
20	12.9	12.8	12.3	11.5	8.52

Table 3.3: Retention factors for coumarin-labeled fatty acids as a function of linear velocity (u). The retention factors were calculated with the EMG model by difference between detectors 4 and 1.

Carbon Number	Retention factor, k				
	u = 0.045 cm/s	u = 0.062 cm/s	u = 0.088 cm/s	u = 0.150 cm/s	u = 0.368 cm/s
10	0.39	0.39	0.38	0.37	0.34
12	0.76	0.75	0.74	0.71	0.63
14	1.56	1.54	1.50	1.43	1.21
16	3.34	3.28	3.19	2.99	2.41
18	6.95	6.81	6.60	6.15	4.70
20	13.2	12.9	12.4	11.5	8.60

Table 3.4: Retention factors for coumarin-labeled fatty acids as a function of linear velocity (u). The rate constants were calculated with the Thomas model at detector 4.

Carbon Number	Retention factor, k				
	u = 0.045 cm/s	u = 0.062 cm/s	u = 0.088 cm/s	u = 0.150 cm/s	u = 0.368 cm/s
10	0.38	0.37	0.37	0.36	0.34
12	0.74	0.72	0.72	0.71	0.65
14	1.54	1.50	1.48	1.42	1.27
16	3.25	3.22	3.15	3.01	2.57
18	6.78	6.72	6.58	6.23	5.11
20	12.9	12.8	12.5	11.8	9.49

increased. Thus, a change in linear velocity plays a more significant role retention of solutes that are highly retained.

The retention factor increases logarithmically with an increase in carbon number, as shown in Figure 3.3. Each additional ethylene group systematically adds to the interaction of the solute with the stationary phase, causing the solute to become more retained as the carbon number increases. The retention factors for each solute calculated with each model are within 3 % of one another at all velocities, except the Thomas model at the highest velocity. At a linear velocity of 0.368 cm/s, values for the Thomas model differ by 0 to 9.4 % from those for the moment and EMG models. Overall, each model provides reasonably consistent thermodynamic information

3.4.2. Kinetic rate constants

While retention factors provide information about the equilibrium or steady-state chromatographic behavior, rate constants provide information about the non-equilibrium and kinetic behavior. The rate of solute transfer between mobile and stationary phases depends not only on the chemical structure of the solute, but also on the experimental conditions. Thus, the distance the solute has traveled along the column, the velocity of the mobile phase, and the chemical structure of the solute are important with regard to their impact on the rate of solute transfer.

3.4.2.1. Effect of column length

If the system is at steady state, both the thermodynamic and kinetic properties should remain constant with distance. The preceding investigation of

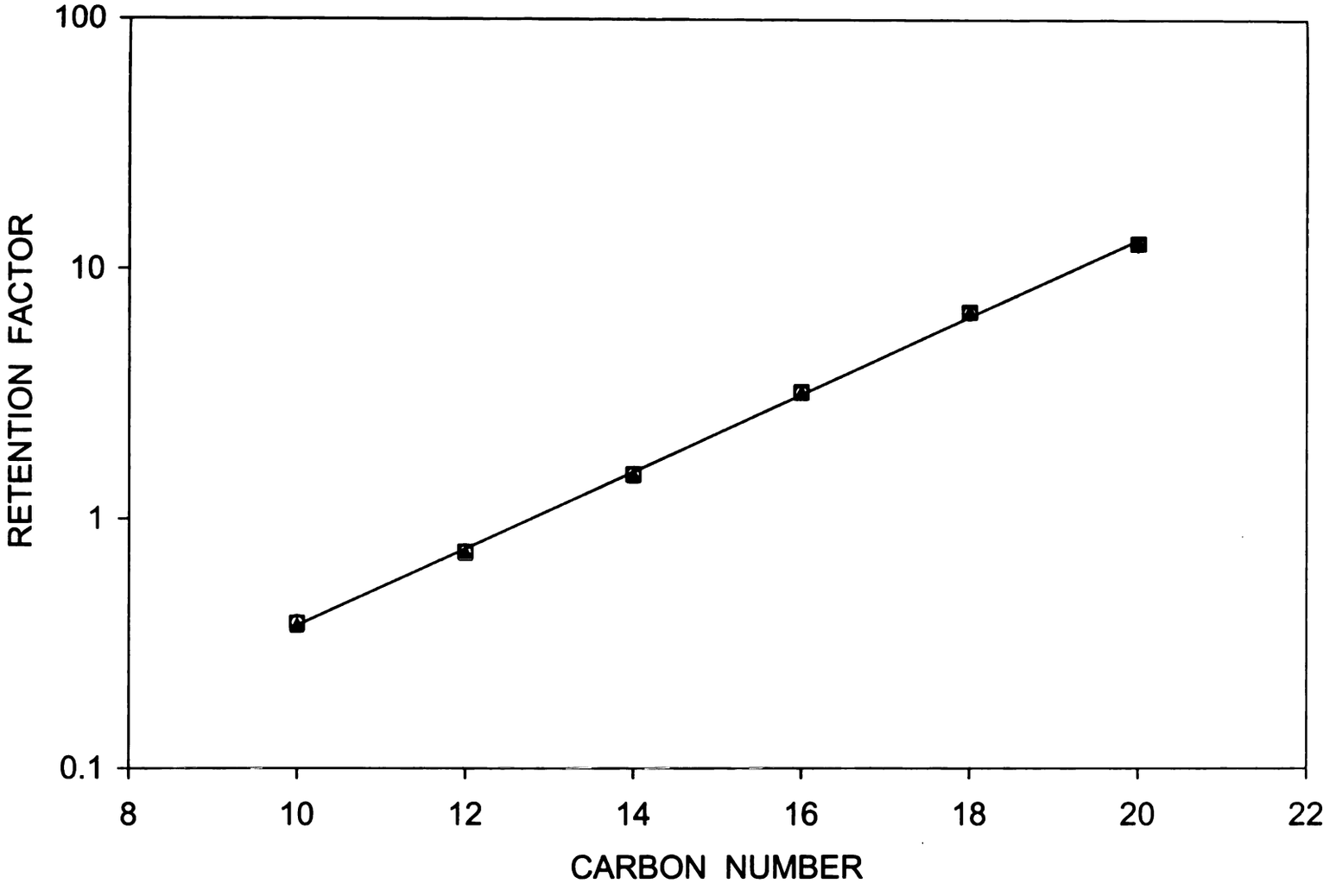

Figure 3.3: Retention factor plotted versus carbon number. The retention factors were calculated with the moment (○), EMG (□),and Thomas (▲) models at a linear velocity of 0.088 cm/s.

retention factor suggests that the system has achieved steady state. To investigate the effect of column length on kinetic factors, the rate constants from stationary to mobile phase (k_{ms}) at each on-column detector at a representative linear velocity are plotted in Figure 3.4. These rate constants are not corrected for extra-column effects. Obvious differences in the values for the rate constants using the three methods can be observed. First, rate constants for the moment model fluctuate with increasing column length, while they decrease slightly for the EMG model, and are constant for the Thomas model. In addition, the rate constants for C_{10} to C_{20} in the moment and EMG models span several orders of magnitude, while in the Thomas model they span only one order of magnitude. Moreover, rate constants fluctuate with distance by as much as 86 % for the moment method, 48 % for the EMG method, and 39 % for the Thomas method.

The difference method is utilized to gain more information concerning the effect of distance on rate constant. The rate constants between detectors 4 and 1 (35.1 cm), detectors 4 and 2 (29.6 cm), and detectors 3 and 2 (24.1 cm) using the EMG method are calculated in Table 3.5. As the distance between detectors increases, there is still some fluctuation in the rate constant for each solute (3 to 20 %). However, the decrease in the amount of fluctuation with distance relative to 48 % at an individual detector (*vide supra*) illustrates the advantage of using the difference method.

3.4.2.2. Effect of linear velocity

Representative values for rate constants as a function of linear velocity are summarized in Tables 3.6 – 3.8. Both rate constants (k_{sm} and k_{ms})

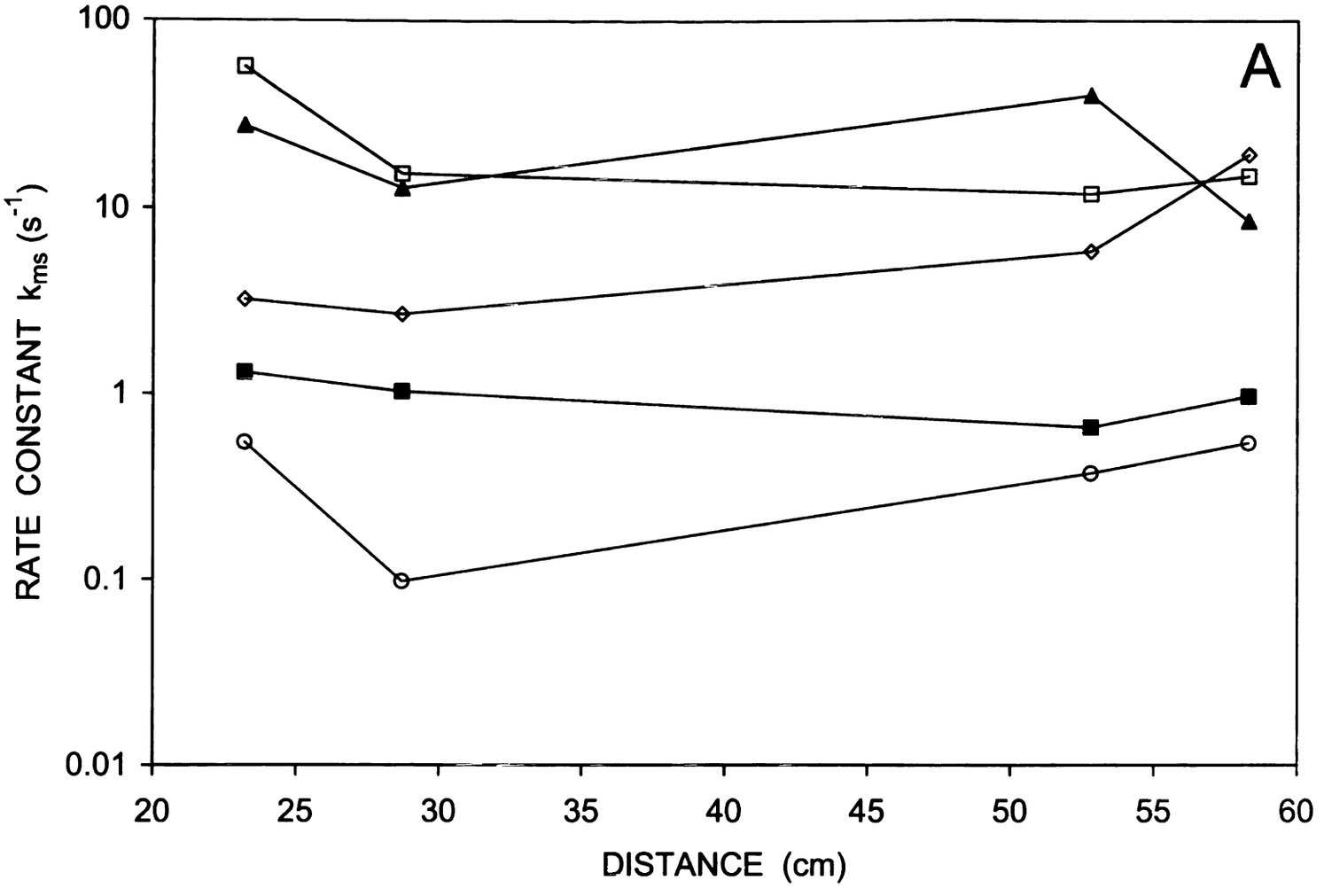

Figure 3.4A: Rate constant plotted versus distance. The rate constants were determined with the moment model using data collected at a linear velocity of 0.088 cm/s. C_{12} (□) C_{14} (▲) C_{16} (◇) C_{18} (■) C_{20} (○)

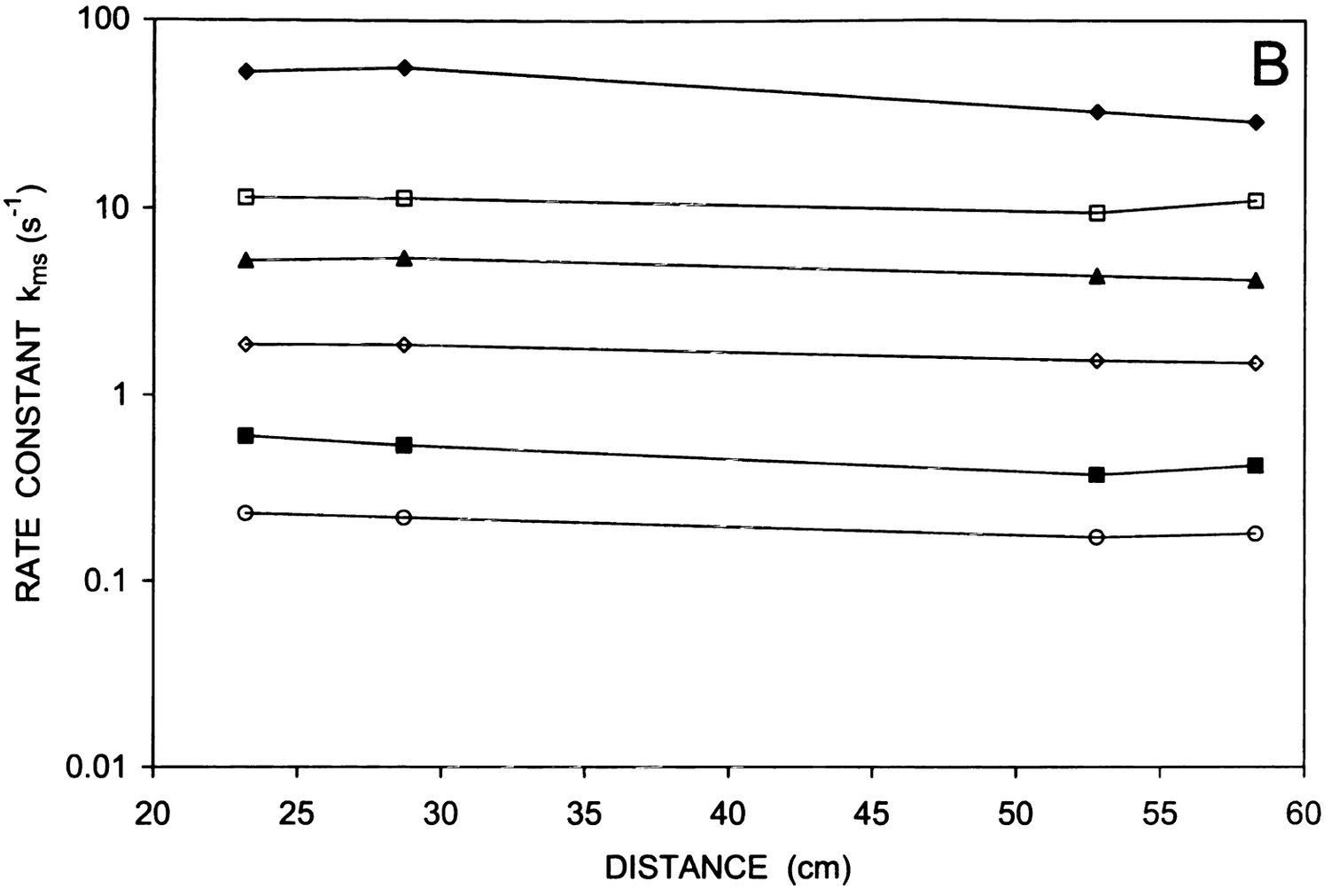

Figure 3.4B: Rate constant plotted versus distance. The rate constants were determined with the EMG model using data collected at a linear velocity of 0.088 cm/s. C_{10} (◆) C_{12} (□) C_{14} (▲) C_{16} (◇) C_{18} (■) C_{20} (○)

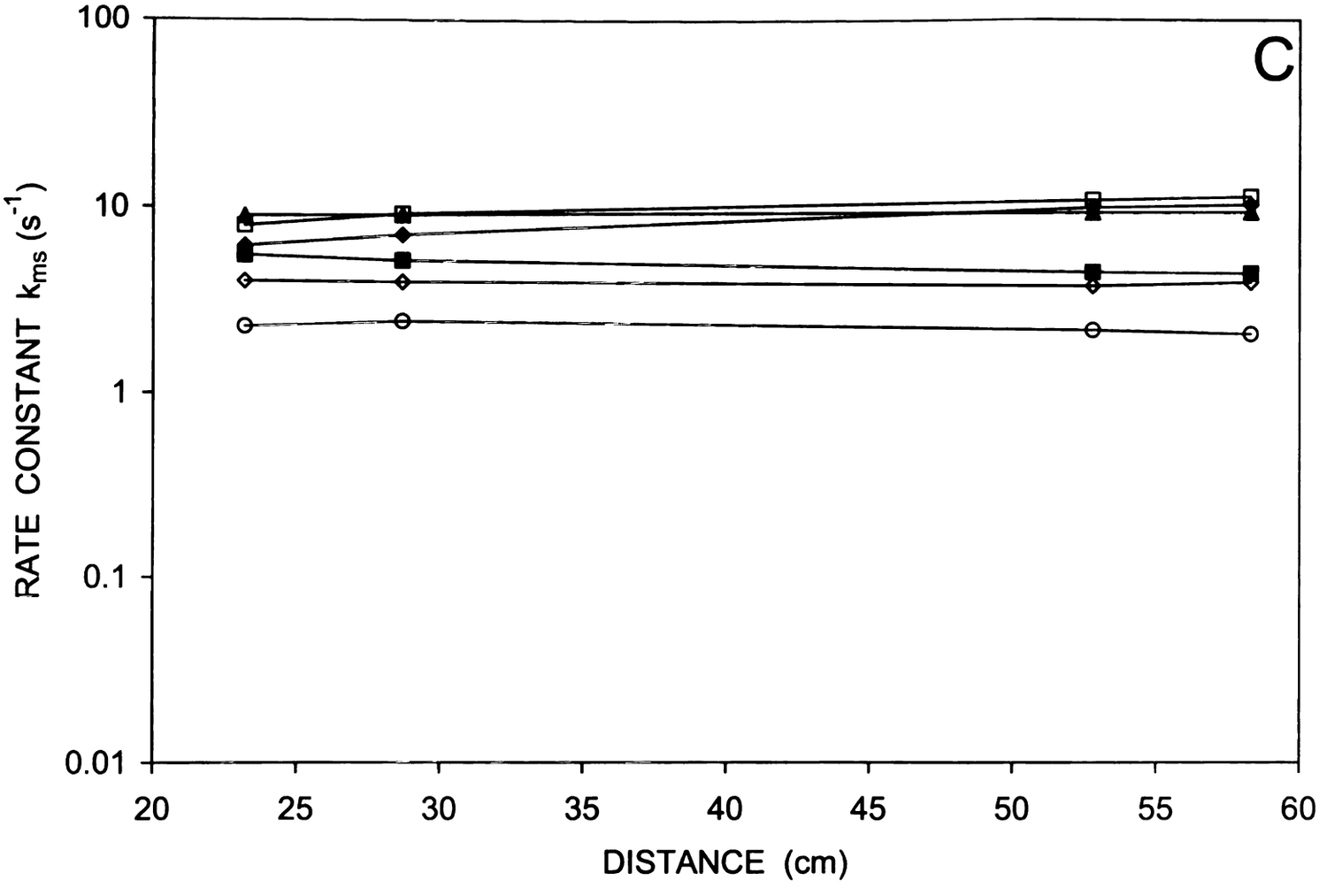

Figure 3.4C: Rate constant plotted versus distance. The rate constants were determined with the Thomas model using data collected at a linear velocity of 0.088 cm/s. C_{10} (◆) C_{12} (□) C_{14} (▲) C_{16} (◇) C_{18} (■) C_{20} (○)

Table 3
were de
detected

Carbo Numb
10
12
14
16
18
20

Table 3.5: Rate constants calculated as a function of length (L). The constants were determined with the EMG difference method using data collected at a linear velocity of 0.088 cm/s.

Carbon Number	Rate constant, k_{ms} (s^{-1})			Rate constant, k_{sm} (s^{-1})		
	L4 – L1 = 35.1 cm	L4 – L2 = 29.6 cm	L3 – L2 = 24.1 cm	L4 – L1 = 35.1 cm	L4 – L2 = 29.6 cm	L3 – L2 = 24.1 cm
10	22	19.5	26.9	8.4	7.4	10.2
12	11	10.6	9.7	7.8	7.8	7.2
14	3.6	3.3	4.3	5.3	5.0	6.5
16	1.3	1.2	1.5	4.1	3.9	5.0
18	0.35	0.34	0.34	2.3	2.3	2.3
20	0.16	0.15	0.17	1.9	1.9	2.1

Table 3.6: Rate constants for coumarin-labeled fatty acids as a function of linear velocity (u). The rate constants were calculated using the moment model by difference between detectors 4 and 1.

Carbon Number	Rate constant, k_{ms} (s^{-1})					Rate constant, k_{sm} (s^{-1})				
	u = 0.045 cm/s	u = 0.062 cm/s	u = 0.088 cm/s	u = 0.150 cm/s	u = 0.368 cm/s	u = 0.045 cm/s	u = 0.062 cm/s	u = 0.088 cm/s	u = 0.150 cm/s	u = 0.368 cm/s
10	--	--	--	--	43	--	--	--	--	15
12	16	9.7	13	15	50	12	7.3	9.8	11	32
14	3.6	4.0	3.6	6.2	18	5.6	6.1	5.5	8.8	22
16	0.98	1.3	2.5	2.6	4.7	3.2	4.2	8.1	7.9	11
18	0.15	0.40	0.67	0.85	2.9	1.7	2.7	4.4	5.2	13
20	0.13	0.16	0.26	0.32	1.0	1.6	2.1	3.2	3.7	8.6

Table 3.7: Rate constants for coumarin-labeled fatty acids as a function of linear velocity (u). The rate constants were calculated using the EMG model by difference between detectors 4 and 1.

Carbon Number	Rate constant, k_{ms} (s^{-1})					Rate constant, k_{sm} (s^{-1})				
	u = 0.045 cm/s	u = 0.062 cm/s	u = 0.088 cm/s	u = 0.150 cm/s	u = 0.368 cm/s	u = 0.045 cm/s	u = 0.062 cm/s	u = 0.088 cm/s	u = 0.150 cm/s	u = 0.368 cm/s
10	17	19	22	65	--	6.7	7.4	8.4	24	--
12	5.4	6.0	11	15	24	4.1	4.5	7.8	11	15
14	1.8	2.8	3.6	6.9	12	2.9	4.3	5.3	9.8	15
16	0.45	1.0	1.3	2.0	4.1	1.5	3.4	4.1	5.9	9.9
18	0.11	0.23	0.35	0.47	1.6	0.78	1.5	2.3	2.9	7.4
20	0.05	0.09	0.16	0.17	0.49	0.68	1.2	1.9	2.0	4..2

Table 3.8: Rate constants for coumarin-labeled fatty acids as a function of linear velocity (u). The rate constants were calculated using the Thomas model at detector 4.

Carbon Number	Rate constant, k_{ms} (s^{-1})					Rate constant, k_{sm} (s^{-1})				
	u = 0.045 cm/s	u = 0.062 cm/s	u = 0.088 cm/s	u = 0.150 cm/s	u = 0.368 cm/s	u = 0.045 cm/s	u = 0.062 cm/s	u = 0.088 cm/s	u = 0.150 cm/s	u = 0.368 cm/s
10	8.5	9.6	10	13	13	3.2	3.6	3.7	4.7	4.4
12	9.1	10	11	13	18	6.7	7.5	8.1	9.0	12
14	7.5	8.3	92	12	17	11	12	14	17	22
16	2.7	3.1	3.9	4.9	9.6	8.9	10	12	15	25
18	3.1	3.7	4.3	5.8	10	21	25	28	36	52
20	1.5	1.7	2.0	2.6	5.0	19	22	25	31	47

calculated with each of the models show an overall increase with an increase in velocity. Bujalski experimentally investigated the diffusion-film thickness around an octadecylsilica particle using the shallow-bed technique [21]. As the flow rate was increased from 2.2 to 3.9 cm/s, the diffusion-film thickness decreased from 0.51 to 0.44 μm. If the stagnant mobile phase layer is thinner at higher velocities, the solute may be able to traverse through the layer faster. This suggests that the decrease in the thickness of the stagnant mobile phase layer surrounding the particle could cause k_{ms} and k_{sm} to increase with velocity, as observed in the present study. Although the rate constants calculated using each of the three models show the same overall trends, their magnitudes vary. For example, if k_{ms} for the C_{16} fatty acid is considered, values range from 0.98 to 4.7 s^{-1} for the statistical moment model, from 0.45 to 4.1 s^{-1} for the EMG model, and from 2.7 to 9.6 s^{-1} for the Thomas model for a linear velocity range of 0.045 cm/s to 0.368 cm/s. If k_{sm} for the same solute is then examined, values range from 3.2 to 11 s^{-1} for the moment model, from 1.5 to 9.9 s^{-1} for the EMG model, and from 8.9 to 25 s^{-1} for the Thomas model. The observed differences in rate constants demonstrate the intrinsic capabilities and limitations of each model. For instance, rate constants for the C_{10} fatty acid could not be obtained at most velocities using the moment method.

In this method, the rate constants are calculated directly from dH_L, the corrected plate height. If the sum of the theoretical A, B, and C_m terms in Equations 3.10 to 3.13 is larger than the observed plate height, an overcorrection

will occur that causes dH_L and the rate constants to be negative and, thus, indeterminate. This is common for very narrow peaks, as the theoretical correction terms overestimate the experimental zone profile. This effect is an outcome and ultimate limitation of the moment model. Additionally, several assumptions of the Thomas model limit its ability to accurately calculate kinetic rate constants. First, as stated previously, the model assumes that all contributions to broadening arise from nonlinear isotherms and slow kinetics of adsorption/desorption. However, the concentrations used in this study are well within the linear region of the isotherm and the mechanism of retention is purely partition. Second, the method assumes column contributions to variance from multiple paths and diffusion are negligible. However, in a packed column, these processes will be present and most assuredly will affect the peak broadening. Last, it should also be noted that the rate constants from the Thomas model are given only at the last on-column detector, while the moment and EMG models are calculated by taking the difference between the first and last detector. There is no direct way to use the difference approach with the Thomas model. Thus, any values calculated from the Thomas model inherently include extra-column contributions, which could lead to incorrect values for both thermodynamic and kinetic parameters.

3.4.2.3. Effect of solute carbon number

The rate of transfer between mobile and stationary phases is controlled by several factors related to the solute structure and properties. These factors primarily include the solute affinity for the mobile and stationary phases, diffusion

in the stagnant mobile phase layer, diffusion in the stationary phase, and interfacial resistance to mass transfer. Each of these factors is dependent upon the solute carbon number and will affect the kinetic behavior.

Rate constants for solute transfer from the stationary to mobile phase (k_{ms}) decrease with higher carbon number. However, the magnitude and rate of change are different for each model. For the statistical moment model, the rate constants for the C_{10} fatty acid could not be determined successfully due to overcorrection, as previously discussed. For the other solutes, the rate constants decrease over two orders of magnitude on going from C_{12} to C_{20}. The EMG model shows a decrease in rate constant of over three orders of magnitude. For the same solute, rate constants from the moment model are consistently larger than those from the EMG model. Rate constants from the Thomas model also decrease with carbon number. However, inconsistencies in this general trend are prevalent throughout the data. That is, the contribution to the rate constant from each additional ethylene unit is relatively constant for both the moment and EMG models, while it is not constant for the Thomas model, as seen in a graph of the logarithm of k_{ms} versus carbon number (Figure 3.5A).

Rate constants for solute transfer from mobile to stationary phase (k_{sm}) decrease with increasing carbon number for the moment and EMG models, but increase for the Thomas model. Again, the contribution to the rate constant from each additional ethylene unit is relatively constant for both the moment and EMG models, while it varies for the Thomas model (Figure 3.5B).

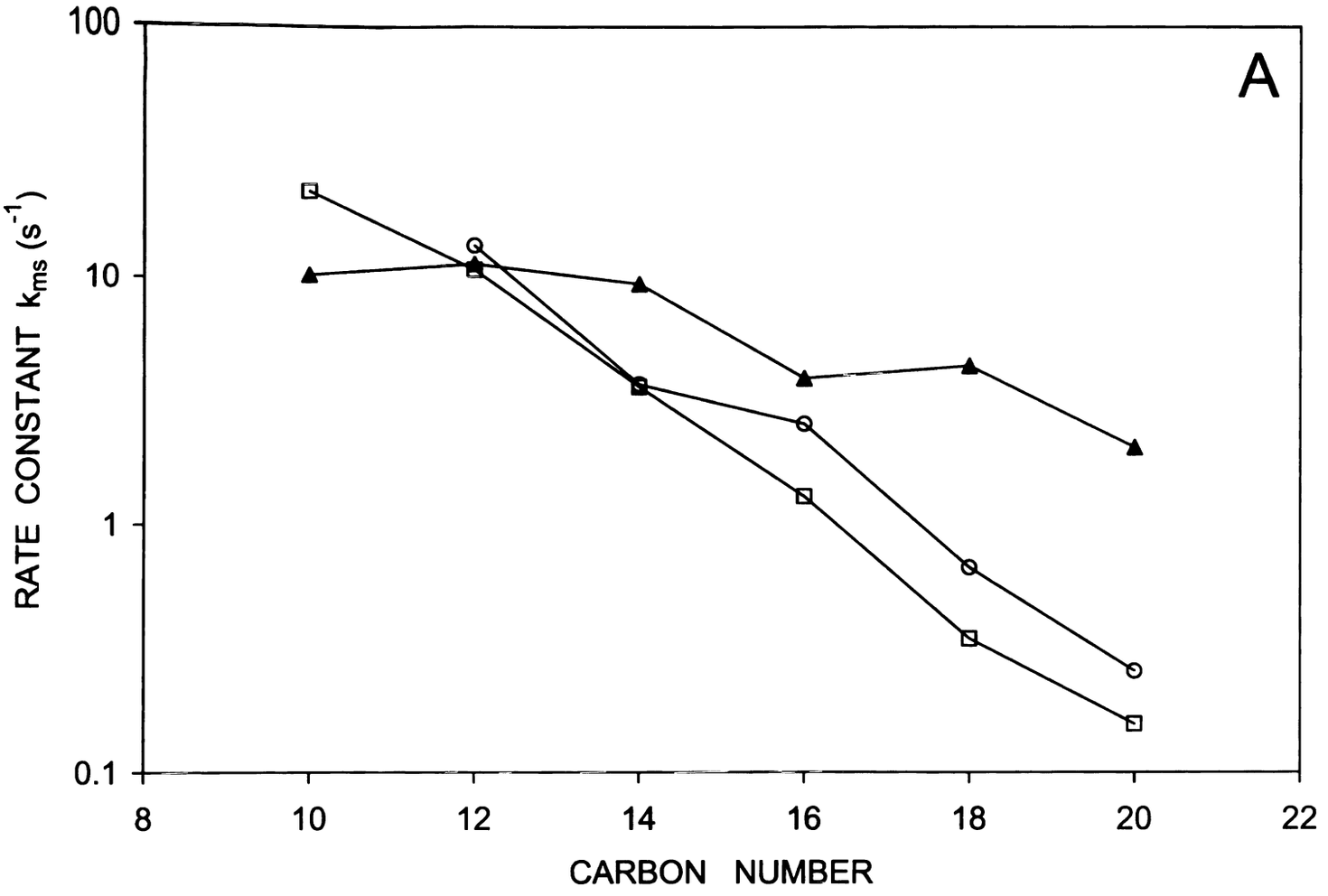

Figure 3.5A: Rate constant from stationary to mobile phase plotted versus carbon number. The rate constants were calculated using moment (○), EMG (□),and Thomas (▲) models at a linear velocity of 0.088 cm/s.

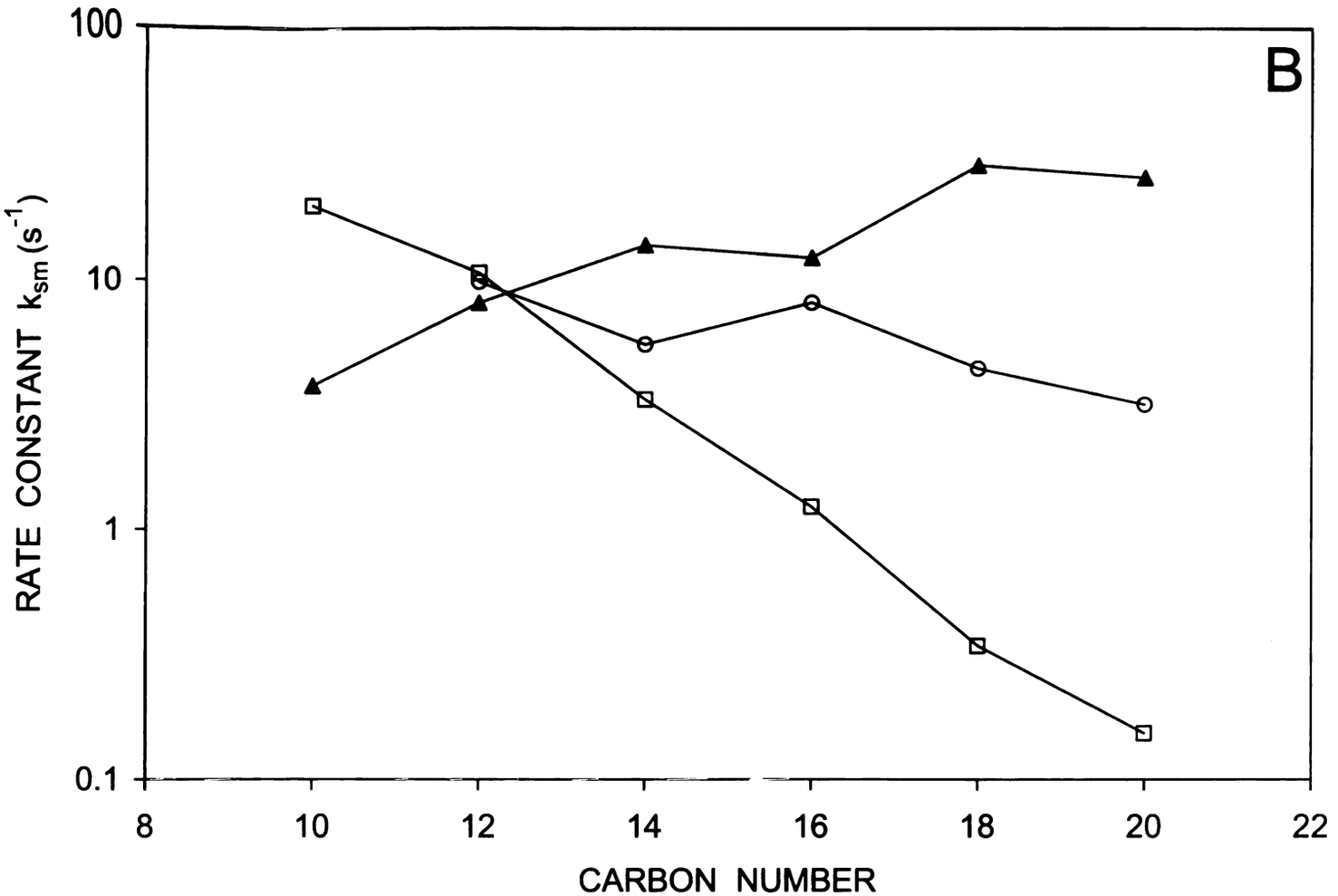

Figure 3.5B: Rate constant from mobile to stationary phase plotted versus carbon number. The rate constants were calculated using moment (○), EMG (□),and Thomas (▲) models at a linear velocity of 0.088 cm/s.

3.5. Conclusions

This study is the first to validate and compare theoretical methods to extract retention factors and kinetic rate constants from experimental data. In this experiment, the effect of column length, linear velocity, and solute chain length have been evaluated. Overall, values for the retention factor are similar for each model. Retention factors are constant with distance, decrease with velocity, and increase with solute carbon number. However, the values for the kinetic rate constants differ for each model. The statistical moment and EMG models show the largest variation in rate constant as a function of distance. However, the variation decreases substantially when the rate constants are calculated by difference between two detectors. The moment and EMG methods by difference are more reliable than the Thomas model at one detector. As a function of velocity and carbon number, the moment and EMG models show more consistent and reliable trends in rate constants, as compared with the Thomas method. Problems with the Thomas model could be related to the inherent assumptions that broadening arises due to nonlinear isotherms and slow kinetics, and that all column and extra-column effects are negligible. However, due to the nature of the model, extra-column effects cannot be eliminated using the difference approach. Based on these results, the statistical moment and EMG models yield reasonable values for retention factors and rate constants in an experimental liquid chromatographic system.

3.6. References

[1] J.C. Giddings, Dynamics of Chromatography Part 1 Principles and Theory, Marcel Dekker, New York, **1965**.

[2] K. Miyabe, G. Guiochon, *Adv. Chromatogr. 40* (**2000**) 1-113.

[3] X. Li, A.M. Hupp, V.L. McGuffin, *Adv. Chromatogr. 45* (**2007**) 1-88.

[4] J.F. Wheeler, T.L. Beck, S.J. Klatte, L.A. Cole, J.G. Dorsey, *J. Chromatogr. A 656* (**1993**) 317-333.

[5] R.P.J. Ranatunga, P.W. Carr, *Anal. Chem. 72* (**2000**) 5679-5692.

[6] X. Li, V.L. McGuffin, *J. Chromatogr. A 1203* (**2008**) 67-80.

[7] J.J. van Deemter, F.J. Zuiderweg, A. Klinkenberg, *Chem. Eng. Sci. 5* (**1956**) 271-289.

[8] H. Purnell, Gas Chromatography, John Wiley & Sons, New York, **1962**, 117-164.

[9] J.C. Giddings, R.A. Robinson, *Anal. Chem. 34* (**1962**) 885-890.

[10] J.C. Giddings, *Anal. Chem. 35* (**1963**) 2215-2216.

[11] K. Miyabe, G. Guiochon, *J. Sep. Sci. 26* (**2003**) 155-173.

[12] C.R. Wilke, P. Chang, *A.I.Ch.E. 1* (**1955**) 264-270.

[13] C. Vidal-Madjar, G. Guiochon, *J. Chromatogr. 142* (**1977**) 61-86.

[14] V.L. McGuffin, C. Lee, *J. Chromatogr. A 987* (**2003**) 3-15.

[15] S.B. Howerton, V.L. McGuffin, *Anal. Chem. 75* (**2003**) 3539-3548.

[16] S.B. Howerton, V.L. McGuffin, *J. Chromatogr. 1030* (**2004**) 3-12.

[17] V.L. McGuffin, S.B. Howerton, X. Li, *J. Chromatogr. A 1073* (**2005**) 63-73.

[18] V.L. McGuffin, R.N. Zare, *Appl. Spectrosc. 39* (**1985**) 847.

[19] S.-H. Chen, Ph.D. Dissertation, Michigan State University, East Lansing, Michigan, **1993**.

[20] S.B. Howerton, C. Lee, V.L. McGuffin, *Anal. Chim. Acta 478* (**2003**) 99-110.

[21] R. Bujalski, Ph.D. Dissertation, University of Alberta, Edmonton, **2005**.

APPENDIX 3A.1

COMPARISON OF VARIOUS APPROACHES TO THE PLATE HEIGHT MODEL USING STATISTICAL MOMENTS

3A.1. Introduction

As discussed in Chapter 3.2.1, the plate height model accounts for contributions to band broadening from multiple paths, diffusion, and mass transfer. Accurate estimation of each band broadening term is essential to the model. While the multiple paths (A) and longitudinal diffusion (B_m, B_s) terms are straightforward, a variety of alternative methods have been proposed for the mass transfer contribution to broadening in the mobile phase (C_m). Therefore, in this work, several different methods for determining the mass transfer term, including classical and modern, are evaluated and compared. In this appendix, each method is developed to utilize the difference approach. The difference between two on-column detectors is used to subtract extra-column contributions to broadening.

3A.2. Classical kinetic approaches

The corrected plate height (dH_L) is derived by subtraction of the classical contributions to broadening, such as the A, B_m, B_s, and C_m terms (Equation 3.9). In this appendix, the values for A, B_m, and B_s are fixed (Equations 3.10 – 3.12), while those for C_m are compared. That is, the calculated plate heights only differ in their expression for C_m.

The van Deemter [1] form of the mass transfer contribution to plate height in a packed column can be expressed as

$$H_{van\ Deemter} = C_m u = \left(\frac{k^2}{100(1+k)^2} \right) \frac{d_p^2\ u}{D_m} \qquad (3A.1)$$

where u is the linear velocity calculated by difference ($u = \Delta L/\Delta t_0$), k is the retention factor calculated by difference (Equation 3.14), d_p is the particle diameter, and D_m is the diffusion coefficient in the mobile phase.

Based on the model originally developed by Golay [2] for open tubular columns, Purnell [3] developed the following expression for the mass transfer contribution to plate height

$$H_{Purnell} = C_m u = \left(\frac{\chi(1+6k+11k^2)}{96(1+k)^2} \right) \frac{d_p^2\ u}{D_m} \qquad (3A.2)$$

where χ is a factor equal to 0.05. In this approach, the packed column is treated as a bundle of open tubes of the same nominal diameter.

An alternative equation was developed by Giddings [4], in which a single adjustable parameter, ω, is used to represent the first parenthetical term.

$$H_{Giddings} = C_m u = \omega \frac{d_p^2\ u}{D_m} \qquad (3A.3)$$

Typical values for ω range from 0.5 to 5.

Later, Giddings challenged the idea that each of the sources of broadening is independent and concluded that multiple paths and mass transfer in the mobile phase are coupled to one another [5]. Giddings expressed this coupling as

$$H_{Giddings\ coupling} = \left(\frac{1}{A} + \frac{1}{C_m u} \right)^{-1} \qquad (3A.4)$$

where A is the multiple paths term (Equation 3.10) and C_m is the Giddings contribution to mobile phase mass transfer (Equation 3A.3).

Each of the mass transfer terms (van Deemter, Purnell, Giddings, and Giddings coupling) can be directly subtracted from the plate height (Equation 3.9) in order to obtain the corrected plate height.

3A.3. Modern kinetic approaches

More recently, Miyabe and Guiochon have investigated the individual mass transfer processes that contribute to band broadening [6]. This method does not use the classical expressions for A, B_m, B_s, and C_m. Instead, contributions from axial dispersion (δ_{ax}) external mass transfer (δ_f) and intraparticle diffusion (δ_d) are estimated from the experimental data and used to calculate a corrected plate height.

The sorption equilibrium constant (K) is derived from

$$\frac{\Delta M_1 - \Delta t_0}{1-\varepsilon} = \left(\frac{\Delta L}{u_s}\right)\rho_p K \qquad (3A.5)$$

where ε is the interparticle void fraction, ρ_p is the density of the packing material, and u_s is the superficial velocity. In addition, ΔM_1 is the first statistical moment and Δt_0 is the elution time of a non-retained component, both calculated by difference, and ΔL is the distance between two on-column detectors. The values for ε and the porosity of the packing material (ε_p) are estimated from Δt_0 using

$$\Delta t_0 = \left(\frac{\Delta L}{u_s}\right)\left(\varepsilon + (1-\varepsilon)\varepsilon_p\right) \qquad (3A.6)$$

The value of K is subsequently obtained from the slope of a plot of the left side of Equation 3A.5 versus $\Delta L/u_s$. This equilibrium constant is used to characterize the thermodynamic behavior of the system.

The plate height is calculated from

$$H = \left(\frac{\Delta M_2}{(\Delta M_1)^2}\right)\left(\frac{\Delta L}{2u_s}\right) \tag{3A.7}$$

where ΔM_2 is the second statistical moment calculated by difference. The contribution from external mass transfer is calculated from

$$\delta_f = (1-\varepsilon)\left(\frac{R_p}{3K_f}\right)\left(\varepsilon_p + \rho_p K\right)^2 \tag{3A.8}$$

where R_p is the particle radius and k_f is the external mass transfer coefficient. This coefficient is given by

$$k_f = \left(\frac{1.09}{\varepsilon}\right)\left(\frac{\eta}{\rho D_m}\right)^{1/3}\left(\frac{u_s d_p \rho}{\eta}\right)^{1/3}\left(\frac{D_m}{d_p}\right) \tag{3A.9}$$

where η and ρ are the viscosity and the density of the mobile phase, respectively. The diffusion coefficient of the solute (D_m) is determined from the Wilke-Chang equation [7]. A dimensionless retention parameter (δ_0) is estimated from Equation 3A.10 and subsequently used in Equation 3A.11 to afford information about the contributions from axial dispersion and intraparticle diffusion.

$$\delta_0 = \varepsilon + (1-\varepsilon)\left(\varepsilon_p + \rho_p K\right) \tag{3A.10}$$

$$\left(H-\frac{\delta_f}{\delta_0^2}\right)=\left(\frac{D_L}{u_s^2}\right)+\left(\frac{\delta_d}{\delta_0^2}\right) \tag{3A.11}$$

From a linear correlation of $(H - \delta_f/\delta_0^2)$ versus $1/u_s$, δ_d can be determined from the intercept. The axial dispersion coefficient (D_L) can be identified from the slope, and subsequently, be used to calculate δ_{ax} as

$$\delta_{ax}=\left(\frac{D_L}{u_s^2}\right)\delta_0^2 \tag{3A.12}$$

It should be noted that the value for δ_{ax} is indirectly dependent on the value for δ_f, according to Equation 3A.11. Finally, the corrected plate height is calculated by

$$dH_L = H-\frac{\delta_{ax}}{\delta_0^2}-\frac{\delta_f}{\delta_0^2}-\frac{\delta_d}{\delta_0^2} \tag{3A.13}$$

3A.4. Comparison of plate height models

In an effort to accurately determine the plate height for the purposes of kinetic measurement, each of the aforementioned models are examined and compared. Representative values for each mass transfer term and the corresponding corrected plate height are given in the following tables with respect to varying solute carbon number and linear velocity. The solutes are coumarin-labeled fatty acids ranging from C_{10} to C_{20}. The linear velocity is varied from 0.045 – 0.368 cm/s. All other experimental details are given in Chapter 3.3.

As seen in Table 3A.1, the van Deemter and Purnell contributions to mass transfer are small and similar in magnitude to one another. For both, the contribution increases with increasing carbon number and increasing linear

Table 3A.1: Mass transfer contributions to plate height according to van Deemter and Purnell calculated using Equations 3A.1 and 3A.2, respectively.

Carbon Number	$H_{van\ Deemter} = C_m\ u$ ($\times 10^{-6}$ cm)		$H_{Purnell} = C_m\ u$ ($\times 10^{-6}$ cm)	
	u = 0.045 cm/s	u = 0.368 cm/s	u = 0.045 cm/s	u = 0.368 cm/s
10	0.319	2.18	0.551	4.23
12	0.804	5.42	0.866	6.46
14	1.69	1.13	1.34	9.82
16	2.83	1.98	1.90	14.1
18	3.82	28.2	2.37	18.1
20	4.51	34.6	2.69	21.1

velocity. However, each contribution is 5 orders of magnitude less than the combined contribution from the A, B_m, and B_s terms. Therefore, the subtraction of C_m yields equivalent corrected plate heights for both equations, as seen in Table 3A.2. Negative values for the corrected plate height indicate overcorrection from the A, B_m, and B_s terms, where the correction is larger than the original plate height. Rate constants cannot be calculated from negative plate heights.

The Giddings mass transfer terms for ω = 0.5 and 5 are summarized in Table 3A.3. The Giddings correction increases with increasing carbon number and increasing linear velocity. The term is an order of magnitude smaller for ω = 0.5 compared to ω = 5. At ω = 5, the Giddings contribution is the same order of magnitude as the combined contribution from the A, B_m, and B_s terms. This results in overcorrection of the plate height for several solutes, as seen in Table 3A.4. When ω is decreased to ω = 0.5, the corrected plate height increases, which is due to a smaller correction for the C_m term. Although the Giddings mass transfer term is one order of magnitude lower for ω = 0.5 than ω = 5 (Table 3A.3), the corrected plate height is relatively similar at the slowest linear velocity (Table 3A.4). In contrast, at the fastest linear velocity, the corrected plate heights for the two values of ω are substantially different. At the slowest linear velocity, the corrected plate heights for the Giddings equation for both values of ω are similar in magnitude to those calculated using the van Deemter and Purnell equations (Table 3A.2). However, at the fastest linear velocity, only the corrected plate

Table 3A.2: Corrected plate height (dH_L) using van Deemter and Purnell Equations 3A.1 and 3A.2, respectively.

Carbon Number	dH_L (cm)			
	van Deemter		Purnell	
	u = 0.045 cm/s	u = 0.368 cm/s	u = 0.045 cm/s	u = 0.368 cm/s
10	-0.0010	0.0032	-0.0010	0.0032
12	0.0014	0.0035	0.0014	0.0035
14	0.0059	0.0099	0.0059	0.0099
16	0.0164	0.0322	0.0164	0.0322
18	0.0394	0.0375	0.0394	0.0375
20	0.0477	0.0685	0.0477	0.0686

Table 3A.3: Mass transfer contributions to plate height according to Giddings Equation 3A.3.

Carbon Number	$H_{Giddings} = C_m u$ (x 10^{-3} cm)			
	$\omega = 5$		$\omega = 0.5$	
	u = 0.045 cm/s	u = 0.368 cm/s	u = 0.045 cm/s	u = 0.368 cm/s
10	2.05	16.9	0.205	1.69
12	2.17	17.9	0.217	1.79
14	2.29	18.9	0.229	1.89
16	2.40	19.8	0.240	1.98
18	2.51	20.7	0.251	2.07
20	2.62	21.6	0.262	2.16

Table 3A.4: Corrected plate height (dH_L) using Giddings Equation 3A.3

Carbon Number	dH_L (cm)			
	Giddings, $\omega = 5$		Giddings, $\omega = 0.5$	
	u = 0.045 cm/s	u = 0.368 cm/s	u = 0.045 cm/s	u = 0.368 cm/s
10	-0.0030	-0.0136	-0.0012	0.0016
12	-0.0008	-0.0144	0.0012	0.0017
14	0.0037	-0.0090	0.0057	0.0080
16	0.0140	0.0124	0.0162	0.0303
18	0.0370	0.0168	0.0392	0.0355
20	0.0451	0.0470	0.0474	0.0664

heights for the Giddings model for ω = 0.5 are similar to those calculated using the other models. Since ω represents the retention factor dependence of the mass transfer term, a value of 0.5 appears to be more similar to the k dependence of the van Deemter and Purnell equations.

The values for the Giddings coupling contribution calculated using Equation 3A.4 are summarized in Table 3A.5. These values are a combination of the contribution from both A and C_m terms. Values for the Giddings coupling contribution increase with increasing carbon number and increasing linear velocity. The term is smaller for ω = 0.5 compared to ω = 5. The corrected plate heights for the Giddings coupling method are summarized in Table 3A.6. The coupling method yields no negative or overcorrected plate heights. However, the plate heights for the Giddings coupling method are approximately half the magnitude of those from the van Deemter and Purnell equations.

The modern method advocated by Miyabe and Guiochon [6], summarized in Equations 3A.5 – 3A.13, is quite different from the classical approach to the plate height model. Values for the corrected plate height are shown in Table 3A.7. The corrected plate height increases with increasing carbon number yet, in contrast to the classical models, decreases with increasing linear velocity. Corrected plate heights for the Guiochon method are one to two orders of magnitude larger than those for the classical models. Some overcorrection, primarily due to axial dispersion, is observed for narrow peaks. The parameters in this method are determined from the flow rate, rather than the linear velocity ($\Delta L/\Delta t_0$), and errors may arise from inaccuracies in the flow rate measurement.

Table 3A.5: Mass transfer contributions to plate height according to Giddings coupling Equation 3A.4.

Carbon Number	$H_{Giddings\ coupling} = C_m u$ (x 10^{-3} cm)			
	$\omega = 5$		$\omega = 0.5$	
	u = 0.045 cm/s	u = 0.368 cm/s	u = 0.045 cm/s	u = 0.368 cm/s
10	0.7154	1.033	0.1725	0.6664
12	0.7299	1.036	0.1812	0.6817
14	0.7426	1.039	0.1893	0.6951
16	0.7544	1.042	0.1971	0.7076
18	0.7648	1.044	0.2044	0.7187
20	0.7744	1.046	0.2113	0.7289

Table 3A.6: Corrected plate height (dH_L) using Giddings coupling Equation 3A.4.

Carbon Number	dH_L (cm)			
	ω = 5		ω = 0.5	
	u = 0.045 cm/s	u = 0.368 cm/s	u = 0.045 cm/s	u = 0.368 cm/s
10	0.0000	0.0008	0.0005	0.0012
12	0.0009	0.0009	0.0015	0.0013
14	0.0029	0.0035	0.0034	0.0038
16	0.0074	0.0122	0.0080	0.0126
18	0.0178	0.0141	0.0183	0.0144
20	0.0214	0.0255	0.0219	0.0259

Table 3A.7: Corrected plate height (dH_L) for modern kinetic method.

Carbon Number	dH_L (cm)	
	Guiochon	
	u = 0.045 cm/s	u = 0.368 cm/s
10	-0.027	0.005
12	0.021	0.002
14	0.140	0.020
16	0.377	0.100
18	0.857	0.110
20	1.018	0.203

3A.5. Discussion

It is important to note that most of the methods examined in this appendix yield comparable values for the corrected plate height and, hence, comparable kinetic rate constants. However, the number of variables and the accuracy with which they are known can limit the accuracy of each method. The van Deemter equation is straightforward, having no adjustable parameters. The Purnell equation generates comparable values to the van Deemter equation, however, it relies on a proportionality constant (χ) that dictates the magnitude of the mass transfer term. While the Giddings mass transfer equation is straightforward, it also relies on a proportionality constant (ω). Depending upon the magnitude of this constant, it can cause an overcorrection in the plate height for some solutes at some flow rates, making it less useful in practice. The Giddings coupling theory, with a similar adjustable parameter, provides corrected plate heights that are approximately half the magnitude of the other classical models. On the other hand, the modern approach developed by Miyabe and Guiochon yields corrected plate heights that are substantially larger than those from the classical methods. This method is more challenging to use, as it relies on experimentally derived values for numerous variables. Thus, after investigation of each method, the van Deemter equation is deemed most suitable for these chromatographic conditions and, thus, was selected for primary use in the study in Chapter 3.

3A.6. References

[1] J.J. van Deemter, F.J. Zuiderweg, A. Klinkenberg, *Chem. Eng. Sci. 5* (**1956**) 271-289.

[2] M.J.E. Golay, Gas Chromatography, Butterworths, London, **1958**.

[3] R.H. Perrett, J.H. Purnell, *Anal. Chem. 35* (**1963**) 430-439.

[4] J.C. Giddings, Dynamics of Chromatography Part 1 Principles and Theory, Marcel Dekker, New York, **1965**.

[5] J.C. Giddings, *Nature 187* (**1960**) 1023-1024.

[6] K. Miyabe, G. Guiochon, *J. Sep. Sci. 26* (**2003**) 155-173.

[7] C.R. Wilke, P. Chang, *A.I.Ch.E. 1* (**1955**) 264-270.

CHAPTER 4

THERMODYNAMIC AND KINETIC CHARACTERIZATION OF A BRIDGED-ETHYLENE HYBRID C_{18} STATIONARY PHASE

4.1 Introduction

Silica-based supports remain the most widely used materials for reversed-phase liquid chromatography (RPLC) separations. However, a number of improvements have been made to these phases in recent years that address chromatographic problems related to the silica support [1-7]. These improvements have significantly influenced the types of separations that can currently be performed. Nevertheless, problems with silica-based materials continue to exist at high and low pH, extreme temperature, and for basic solutes interacting with residual silanol groups. For this reason, a support material based on a hybrid organic – inorganic particle has been developed and widely used as an RPLC stationary phase. This bridged-ethylene hybrid (BEH) particle is synthesized by the co-condensation of 1,2-bis(triethoxysilyl)ethane with tetraethoxysilane (Figure 1.2) [8]. This support particle has the mechanical strength of silica yet the pH stability of polymeric particles [8,9]. In addition, the ethylene bridge in the backbone is thought to decrease the number of silanols available to bind to basic solutes.

The hybrid phase has been employed in many studies under numerous experimental conditions. However, only a few reported studies afford thermodynamic information about the hybrid material [10,11] while no studies provide kinetic information. A thermodynamic evaluation of a C_{18} hybrid phase was performed as a function of temperature (423 to 473 K) in an aqueous mobile

phase using alkyl benzenes and aromatic alcohols [10] and substituted anilines [11]. Linear van't Hoff plots were obtained and negative changes in molar enthalpy were reported. Further investigation of toluene at a wider temperature range (303 to 473 K) was performed. A change in slope of the van't Hoff plot near 370 K was seen and was attributed to a change in the conformation of the stationary phase in the presence of the mobile phase [10]. Nevertheless, a direct comparison to silica-based materials was not performed and has not been reported in the literature.

Nitrogen-containing polycyclic aromatic hydrocarbons (NPAHs) are an interesting set of basic compounds that have been thoroughly investigated on silica-based materials [12,13]. NPAHs are commonly found in tobacco smoke [14,15], automobile exhaust [16], fossil fuels [17,18], and even lake sediment [19], and have been identified as carcinogens [20]. RPLC has proven useful for the separation of complex NPAHs. Their asymmetric peak shapes make them a suitable set of solutes for examination of the thermodynamic and kinetic behavior of hybrid stationary phases.

The goals of this research are as follows: (1) to separate a series of NPAHs and their parent polycyclic aromatic hydrocarbons (PAHs) using a hybrid C_{18} packing material, (2) to observe the effect of temperature on thermodynamic and kinetic behavior, (3) to examine the effect of protic and aprotic mobile phase on thermodynamic and kinetic behavior, and (4) to compare specific thermodynamic and kinetic parameters to silica-based C_{18} phases in an effort to identify the retention mechanism of the hybrid C_{18} material.

4.2 Theory

The determination of thermodynamic and kinetic contributions to retention requires a synthesis of traditional thermodynamic and transition state theories [21,22]. In this evaluation, the transfer between mobile and stationary phases is treated as a chemical reaction. The thermodynamic and kinetic theory utilized within this chapter was explained in Chapter 1.2.

4.3 Methods

4.3.1 Reagents

As shown in Figure 4.1, two PAHs and six nitrogen-containing NPAHs are chosen to study the effect of nitrogen position, ring number, and annelation structure on the thermodynamics and kinetics of retention. Pyrene, benz[a]anthracene, 1-aminopyrene (Sigma-Aldrich), 1-azapyrene, 4-azapyrene, benz[a]acridine, dibenz[c,h]acridine, and dibenz[a,j]acridine (Institute für PAH Förschung) are obtained as solids and dissolved in high-purity methanol and acetonitrile (Burdick and Jackson Division, Honeywell) to yield standard solutions with concentrations between 10^{-3} M and 10^{-5} M. A non-retained marker, 4-bromomethyl-7-methoxycoumarin (Sigma), is added to each solution at a concentration of 10^{-3} M.

4.3.2 Experimental system

The solutes are separated on a capillary liquid chromatography system with multiple on-column detectors as illustrated in Figure 2.4. The stationary phase is a hybrid-based C_{18} material (XBridge C_{18}, Waters Corporation) described in Chapter 2.2. The mobile phase consists of methanol or acetonitrile.

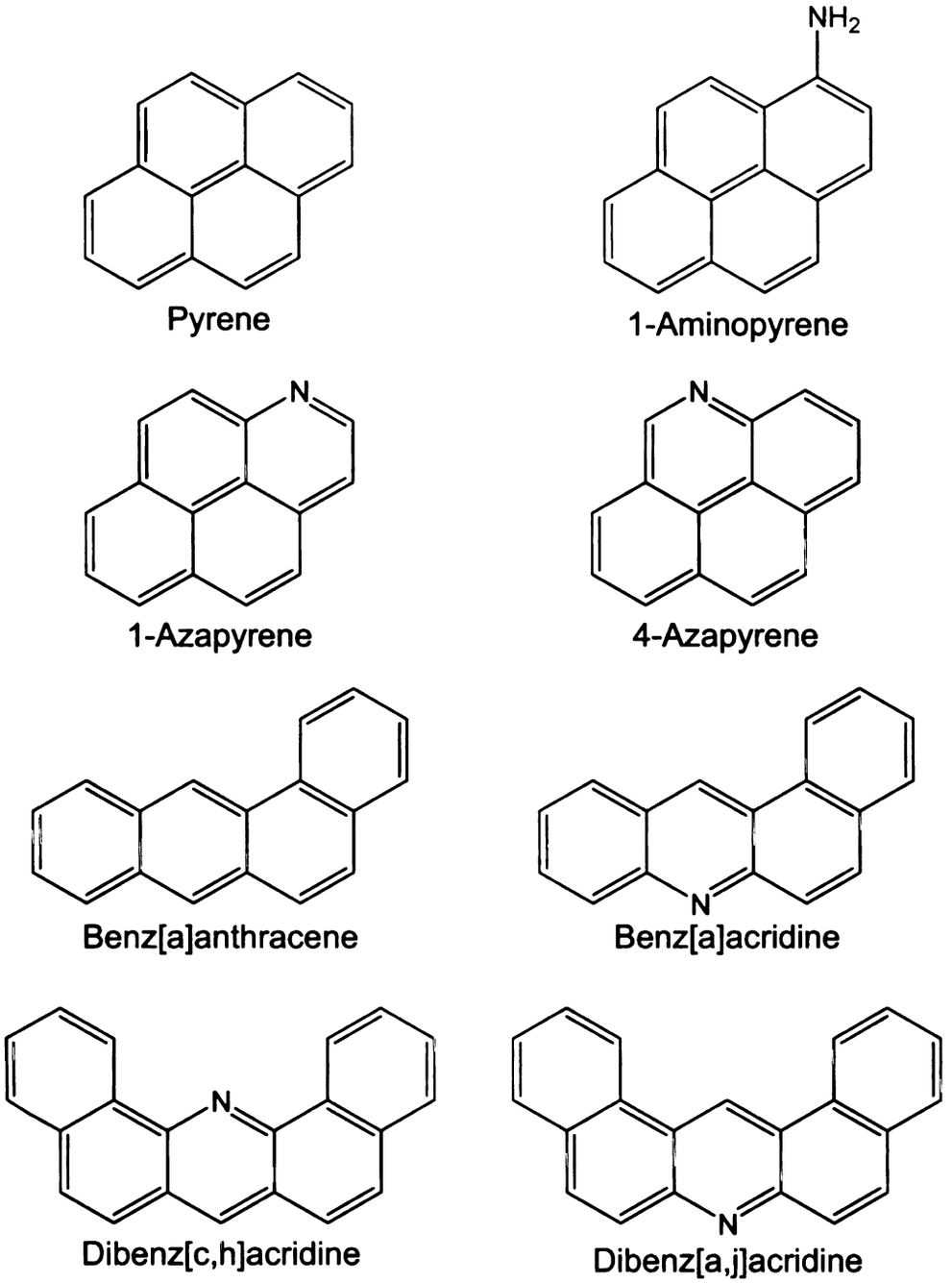

Figure 4.1. Structures of the polycyclic aromatic hydrocarbons (PAHs) and nitrogen-substituted polycyclic aromatic hydrocarbons (NPAHs) examined in this study.

The sample is split between the capillary column and a fused-silica capillary (50 μm i.d., Polymicro Technologies), resulting in an injection volume of 10 nL. A fused-silica capillary (20 μm i.d., Polymicro Technologies) is attached post-column to serve as a restrictor. The temperature was varied from 283 to 313 K (± 0.1 K), while the pressure was maintained at 2000 psi.

4.3.3 Data analysis

After separation, the zone profile for each solute is extracted from the chromatogram. Each profile is fit by nonlinear regression to a combination of Gaussian (Equation 1.33) and asymmetric double sigmoidal (Equation 3.25) equations using a commercially available program (Peakfit v4.14, SYSTAT Software). This method produces high quality fits (correlation coefficients ranging from 0.999 to 0.956), reduces noise, and allows control of peak integration limits. The fit is regenerated in Microsoft Excel, from which the statistical moments are calculated. In this work, the peak boundaries are identified at 0.1 % of the maximum peak height, as the error in the calculation of the statistical moments has been proven small at this integration limit [23]. The data are analyzed using the plate height model (statistical moment model) as described in Chapter 3.2.1.

4.4 Results and discussion

The choice of mobile phase has been shown to be very relevant to separation behavior on silica-based stationary phases [12]. In this study, both protic (methanol) and aprotic (acetonitrile) solvents are evaluated. The methanol mobile phase can form hydrogen bonds with the NPAHs, inhibiting their ability to

adsorb at silanol sites. Methanol can also form hydrogen bonds with silanol sites in the hybrid support, displacing or competing with the NPAHs. In these ways, methanol reduces the interactions of the NPAHs with silanol sites. However, acetonitrile cannot undergo hydrogen-bonding interactions, and, therefore retention behavior under such conditions is of interest.

4.4.1 Methanol mobile phase

Figure 4.2 shows a representative set of chromatograms. In methanol, a neutral solute, such as pyrene (Figure 4.2A) has a symmetric peak shape. However, a basic solute, such as 4-azapyrene (Figure 4.2B) has a tailing peak shape. The peak shape for pyrene is representative of benz[a]anthracene, 1-aminopyrene, and dibenz[c,h]acridine. The peak shape for 4-azapyrene is representative of the remaining NPAHs.

4.4.1.1 Thermodynamic behavior

4.4.1.1.1 Retention factor

Table 4.1 summarizes the retention factors for the PAHs and NPAHs. For the most part, retention factors for the NPAHs are notably smaller than those for the parent PAHs. The retention factors for 1-aminopyrene and 4-azapyrene are smaller by 76 % and 20 % than pyrene, respectively. In addition, the retention factor for benz[a]acridine is smaller by 45 % than benz[a]anthracene. This decreased retention behavior is due to the increased polarity of the NPAHs relative to the PAHs and is consistent with a partition mechanism. This behavior was also observed with stationary phases built on silica supports [12]. In addition, retention increases with the number of aromatic rings and less

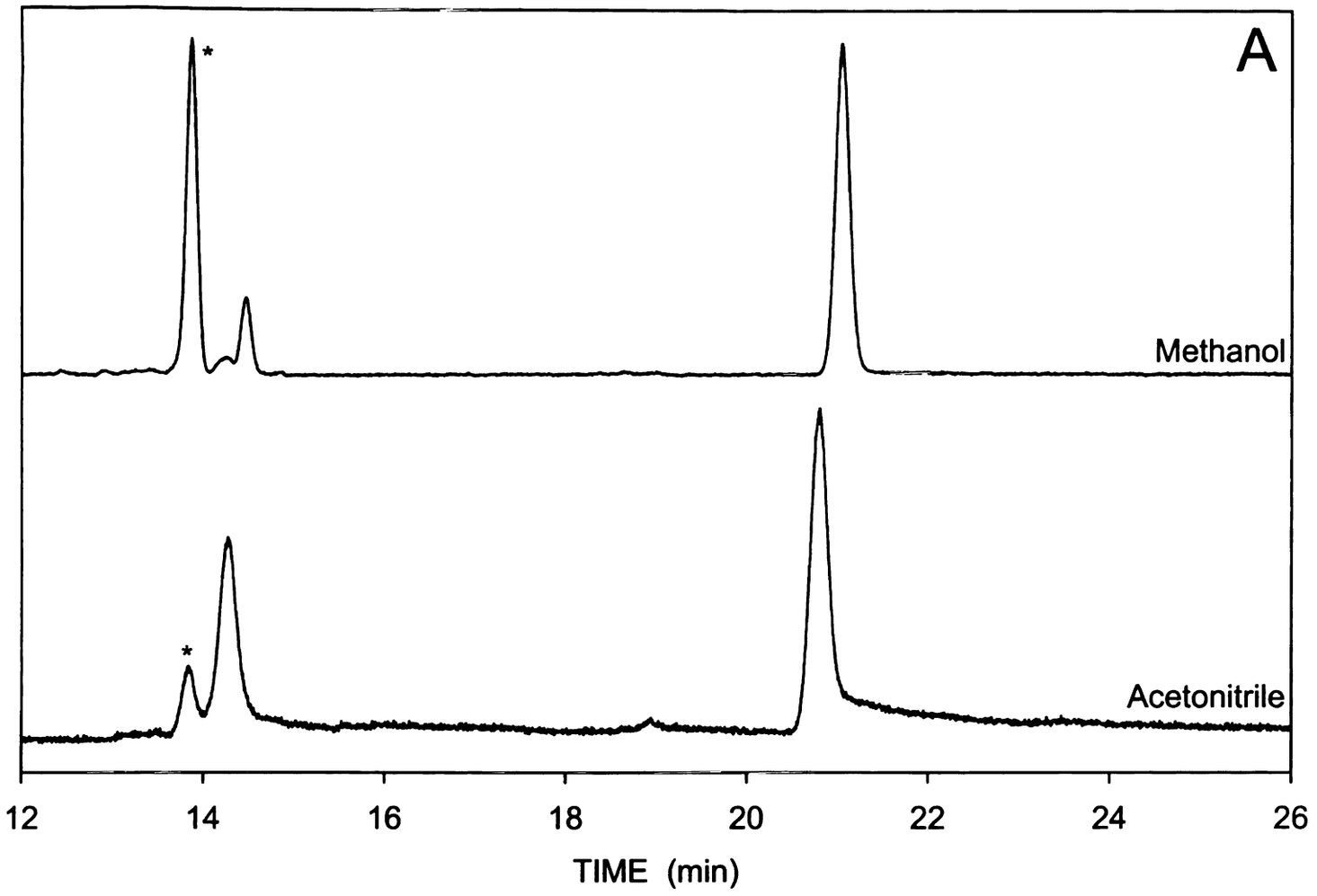

Figure 4.2A: Representative chromatograms of pyrene in methanol (303 K) and acetonitrile (303 K) mobile phases. The void time marker (4-bromomethyl-7-methoxy coumarin) is represented by *.

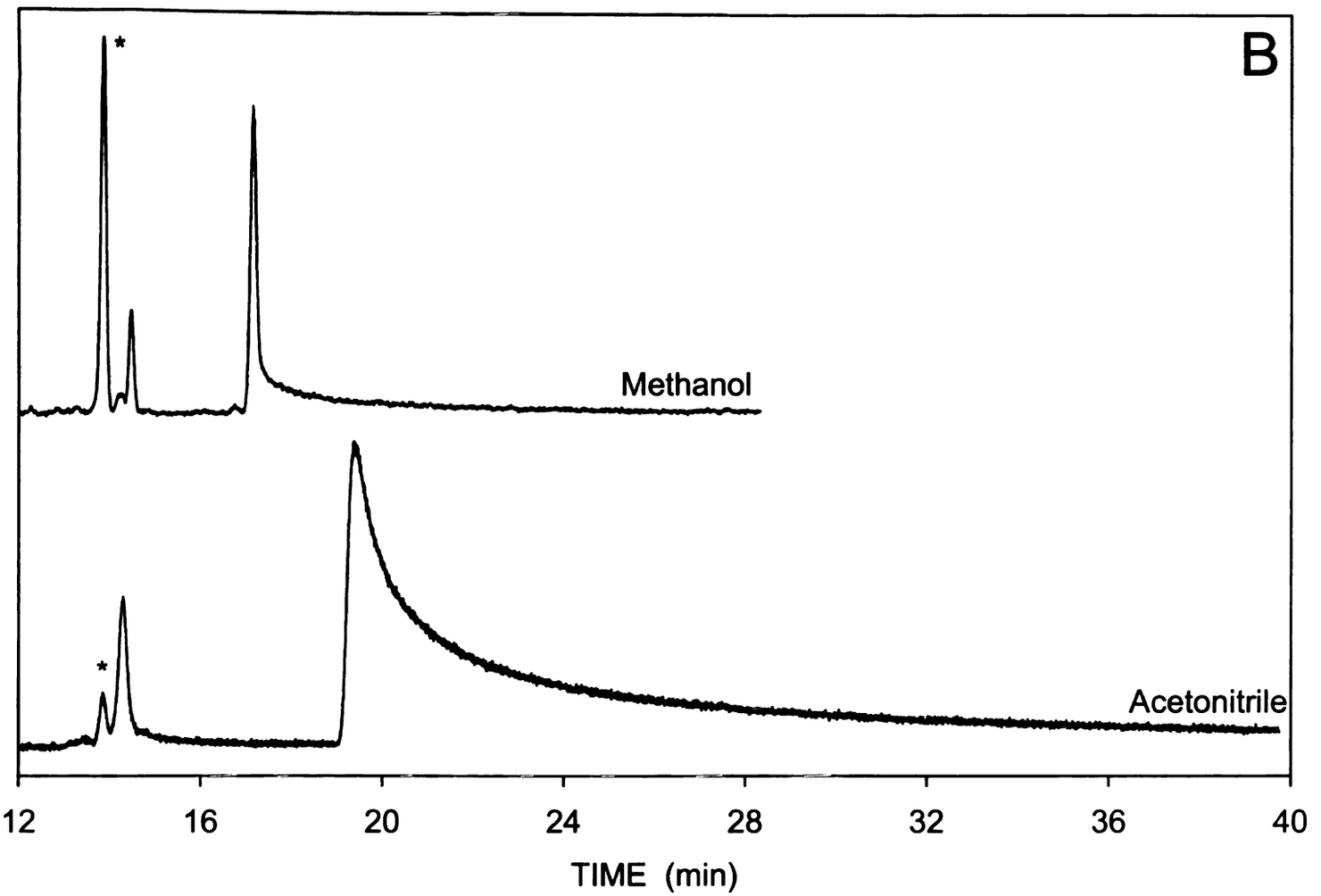

Figure 4.2B: Representative chromatograms of 4-azapyrene in methanol (303 K) and acetonitrile (303 K) mobile phases. The void time marker (4-bromomethyl-7-methoxy coumarin) is represented by *.

Table 4.1: Retention factor (k) and change in molar enthalpy (ΔH) for PAH and NPAH solutes in methanol (2000 psi). Values in parentheses have large errors and are given for illustrative purposes only. Solutes: pyrene (P), 1-aminopyrene (1AmP), 1-azapyrene (1AzaP), 4-azapyrene (4AzaP), benz[a]anthracene (B[a]A), benz[a]acridine (B[a]Ac), dibenz[a,j]acridine (D[aj]Ac), dibenz[c,h]acridine (D[ch]Ac)

Solute	Retention factor, k		Molar Enthalpy ΔH (kcal/mol)
	T = 288 K	T = 313 K	
P	0.78	0.55	-2.5 ± 0.1
1AmP	0.15	0.13	-1.4 ± 0.1
1AzaP	0.62	0.82	(3.1 ± 1.4)
4AzaP	0.45	0.44	(1.6 ± 1.1)
B[a]A	0.92	0.62	-3.0 ± 0.1
B[a]Ac	0.43	0.34	-1.6 ± 0.1
D[aj]Ac	0.92	0.51	-4.0 ± 0.3
D[ch]Ac	1.80	1.02	-4.3 ± 0.2

condensed annelation structure. These trends are again, consistent with a partition mechanism and with phases built on silica supports.

Table 4.1 demonstrates the effect of temperature. Retention factors decrease significantly (13 – 45 %) with increasing temperature, except for 1-azapyrene and 4-azapyrene, which fluctuate, yet increase (32 %) or remain the same with temperature, respectively. A decrease in retention factor with temperature is expected under a partition-dominated mechanism.

4.4.1.1.2 Molar enthalpy

Figure 4.3 displays a representative graph of the logarithm of the retention factor versus inverse temperature (van't Hoff plot). The graph for each solute in Figure 4.3A is linear (R^2 = 0.973 – 0.997) and the slope is positive. A linear graph indicates that the change in molar enthalpy is constant over the temperature range of the study (283 – 313 K), which suggests that there is no significant change in retention mechanism in this region. A positive slope indicates a negative change in molar enthalpy, suggesting the transfer from mobile to stationary phase is an enthalpically favorable process. The graph of 1-azapyrene and 4-azapyrene in Figure 4.3B is roughly linear (R^2 = 0.554 and 0.346), however the slope is negative. A negative slope indicates a positive change in molar enthalpy, suggesting the transfer from mobile to stationary phase is not enthalpically favorable. This will be discussed in more detail in the following paragraph.

The change in molar enthalpy is calculated from the slope of Figure 4.3, according to Equation 1.7, and is summarized for all solutes in Table 4.1. The

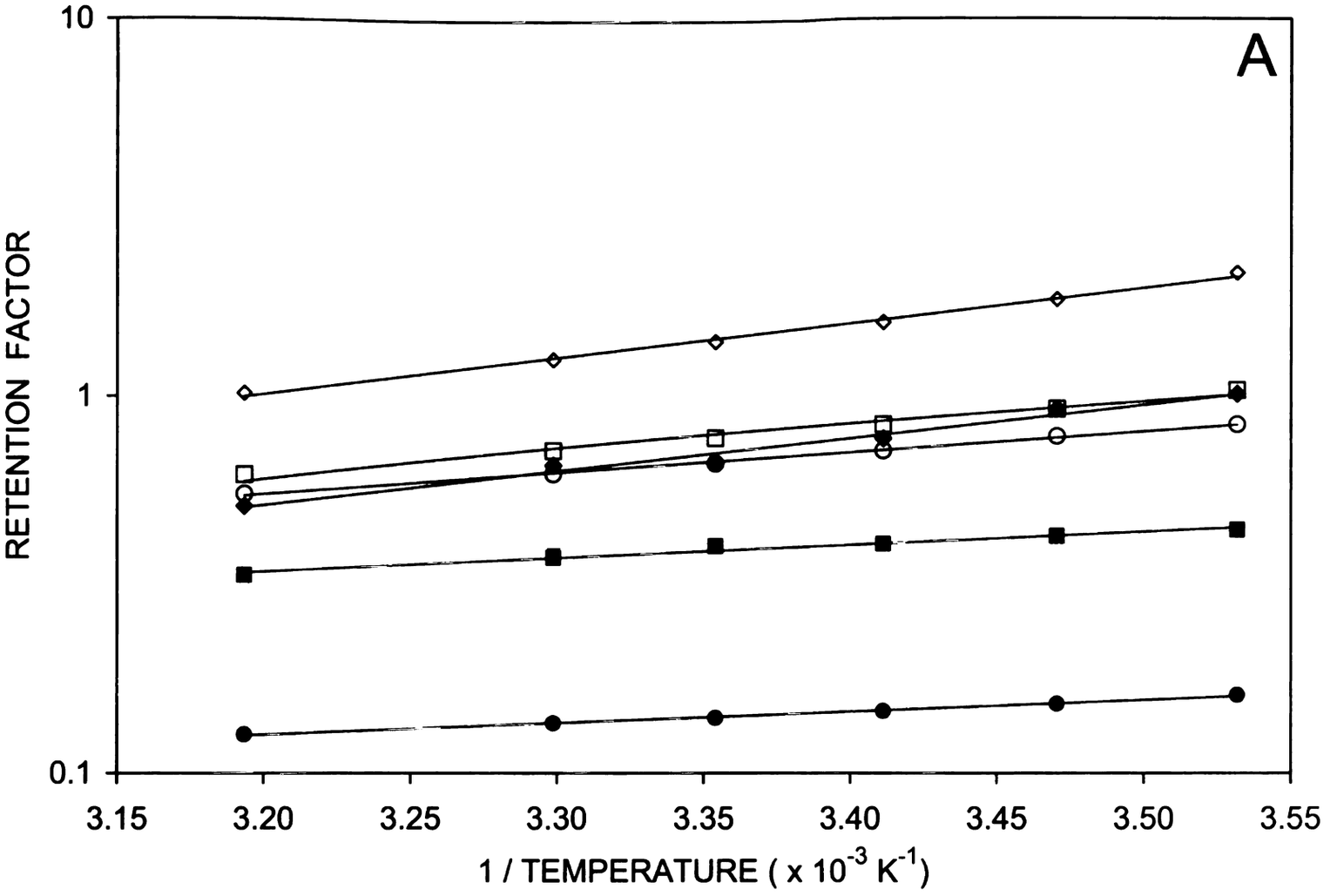

Figure 4.3A: Representative graph of retention factor versus inverse temperature for methanol mobile phase. pyrene (○), 1-aminopyrene (●), benz[a]anthracene (□), benz[a]acridine (■), dibenz[a,j]acridine (◆), dibenz[c,h]acridine (◇)

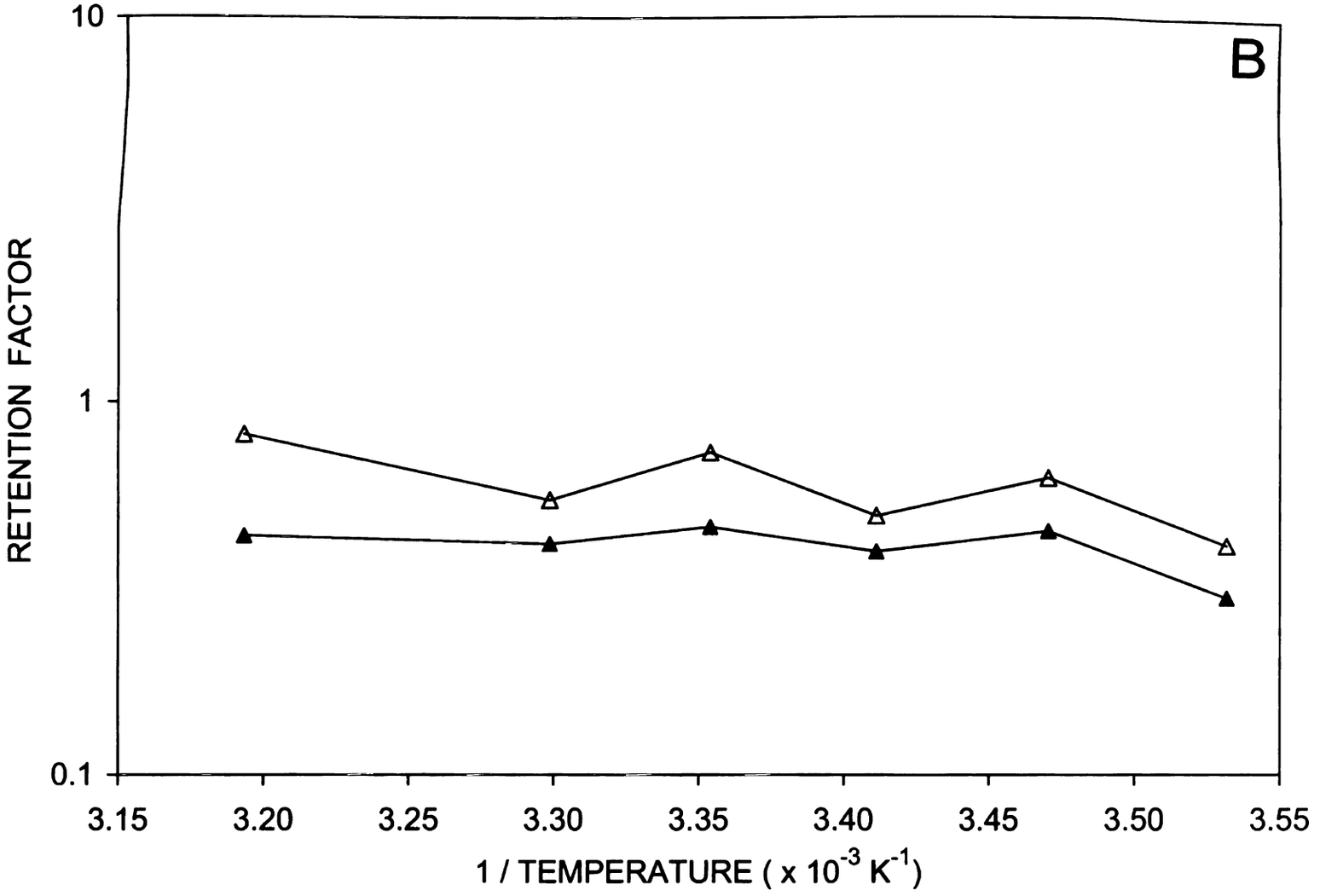

Figure 4.3B: Representative graph of retention factor versus inverse temperature for methanol mobile phase. 1-azapyrene (△), 4-azapyrene (▲)

changes in molar enthalpy are least negative for 1-aminopyrene and benz[a]acridine, followed by pyrene and benz[a]anthracene, and become even more negative for dibenz[a,j]acridine and dibenz[c,h]acridine. These trends indicate that the change in molar enthalpy becomes more negative with increasing ring number and with less condensed annelation structure. These trends also were observed on silica-based stationary phases and have been discussed in depth previously [12,24]. The change in molar enthalpy may be attributed to the depth to which each PAH can penetrate into the stationary phase. The proximal regions, where the alkyl group is bound to the silica surface, are highly ordered with all trans carbon – carbon bonds. As the distance from the surface increases, there are more gauche bonds and greater disorder [25-27]. The more condensed PAHs, such as pyrene, probe only the distal regions of the alkyl chain, while less condensed PAHs, such as benz[a]anthracene, penetrate more deeply into the ordered regions of the alkyl chain. Therefore, the change in molar enthalpy becomes more negative the farther the PAH can access in the inner region of the stationary phase.

The change in molar enthalpy is positive for 1-azapyrene and 4-azapyrene, corresponding to the negative slope in the van't Hoff plot. However, the slopes of these curves have large uncertainties. Despite the uncertainty in the measurement, some discussion of this interesting behavior is warranted. At high temperature, the alkyl chains of the stationary phase become more fluid like, making the surface of the underlying particle more accessible. It is possible that at the higher temperatures used in this study, 1- and 4-azapyrene are able to

access the underlying particle more easily. In this case, these solutes may be able to adsorb more strongly at the residual silanol sites. Thus, the retention mechanism for these solutes changes over the temperature range investigated. A change in molar enthalpy is not meaningful when two separate processes, in this case a change in retention mechanism, are occurring.

4.4.1.2 Kinetic behavior

Thermodynamics provides information about steady-state behavior for the change between mobile and stationary phases; however it does not fully explain the retention mechanism. By considering a transition state, the pseudo-first order rate constants and activation energies can be calculated with the equations developed in Chapter 1.2.2. These values help to quantify the kinetic aspects of mass transfer between the mobile and stationary phases as a function of solute structure. These data provide information about the retention mechanism that would not be available from thermodynamic data alone.

4.4.1.2.1 Rate constants

Table 4.2 summarizes the rate constants for the PAHs and NPAHs. At 288 K, benz[a]anthracene, 1-aminopyrene, and dibenz[c,h]acridine undergo the fastest rate of mass transfer, followed by pyrene, benz[a]acridine, and dibenz[a,j]acridine, with 1-azapyrene and 4-azapyrene having the slowest rate of transfer. 1-Azapyrene and 4-azapyrene are given only as an indication of their slow rate of transfer; the kinetic values are not reliable based on the uncertainty in the experimental measurement for those solutes. The rate-limiting step for dibenz[c,h]acridine is the transfer from stationary to mobile phase, since the

Table 4.2: Rate constants (k_{ms} and k_{sm}) for PAH and NPAH solutes in methanol. Solutes defined in Table 4.1.

Solute	Rate constant, k_{ms} (s^{-1})		Rate constant, k_{sm} (s^{-1})	
	T = 288 K	T = 313 K	T = 288 K	T = 313 K
P	0.69	220	0.53	120
1AmP	27	--	4.1	--
1AzaP	0.005	0.003	0.003	0.003
4AzaP	0.009	0.01	0.006	0.006
B[a]A	500	--	460	--
B[a]Ac	0.03	0.09	0.02	0.03
D[aj]Ac	0.03	0.96	0.04	0.49
D[ch]Ac	8.1	500	15	180

retention factor ($k = k_{sm}/k_{ms}$) is greater than one. In contrast, the rate-limiting step for all other solutes is the transfer from mobile to stationary phase, since the retention factor is less than one.

The rate constants for the four-ring NPAHs are notably smaller than those for their parent PAHs, with the exception of 1-aminopyrene. 1-Azapyrene and 4-azapyrene have rate constants that are two orders of magnitude smaller than pyrene. In addition, the rate constant for benz[a]acridine is five orders of magnitude smaller than benz[a]anthracene. In this case, the nitrogen in benz[a]acridine can adsorb to silanol groups causing a decrease in the rate constant compared to its parent PAH. This effect was not observed in the thermodynamic data, however, kinetic information provides a more sensitive indication of the retention mechanism.

Table 4.2 demonstrates the effect of temperature on rate constants. The rate constants for most solutes increase significantly, while the rate constants for 1-azapyrene and 4-azapyrene decrease with increasing temperature. Some rate constants are not provided for 1-aminopyrene and benz[a]anthracene at the highest temperature due to overcorrection of the plate height for these narrow peaks. According to Equation 3.9, if the sum of the theoretical A, B, and C terms is larger than the observed plate height, an overcorrection will occur that causes the corrected plate height and the rate constants to be negative and, thus, indeterminate. This is common for very narrow peaks, where the theoretical correction terms overestimate the width of the experimental zone profile. An increase in rate is expected with an increase in temperature due to increased

diffusion coefficients and enhanced fluidity of the stationary phase. An increase in kinetic energy due to increased temperature allows the alkyl chains to become more labile, which in turn allows the solutes to diffuse in and out of the stationary phase more freely.

4.4.1.2.2 Activation energy

Figure 4.4 shows a representative graph of the logarithm of the rate constant from stationary to mobile phase (k_{ms}) versus the inverse temperature. The graph does not contain information for 1-azapyrene and 4-azapyrene, due to uncertainty in the measurement, or for 1-aminopyrene, due to the narrow peak shape. Of those shown, the graph for each solute is roughly linear (R^2 = 0.442 – 0.980) and the slope is negative. A negative slope is indicative of a positive energy barrier for mass transfer.

The activation energy is calculated from the slope of this graph, according to Equation 1.13, and is summarized in Table 4.3. The activation energies are positive for all solutes listed. The activation energy for the transfer from stationary phase to transition state ($\Delta E_{\ddagger s}$) is greater that that from mobile phase to transition state ($\Delta E_{m\ddagger}$). These data indicate that it is easier for the solutes to enter the stationary phase than to exit. With the exception of benz[a]acridine, all solutes seem to have a similar energy barrier, which suggests they encounter a similar barrier at the interface between mobile and stationary phases. In addition, the activation energies are similar to those reported on silica-based materials [12,24].

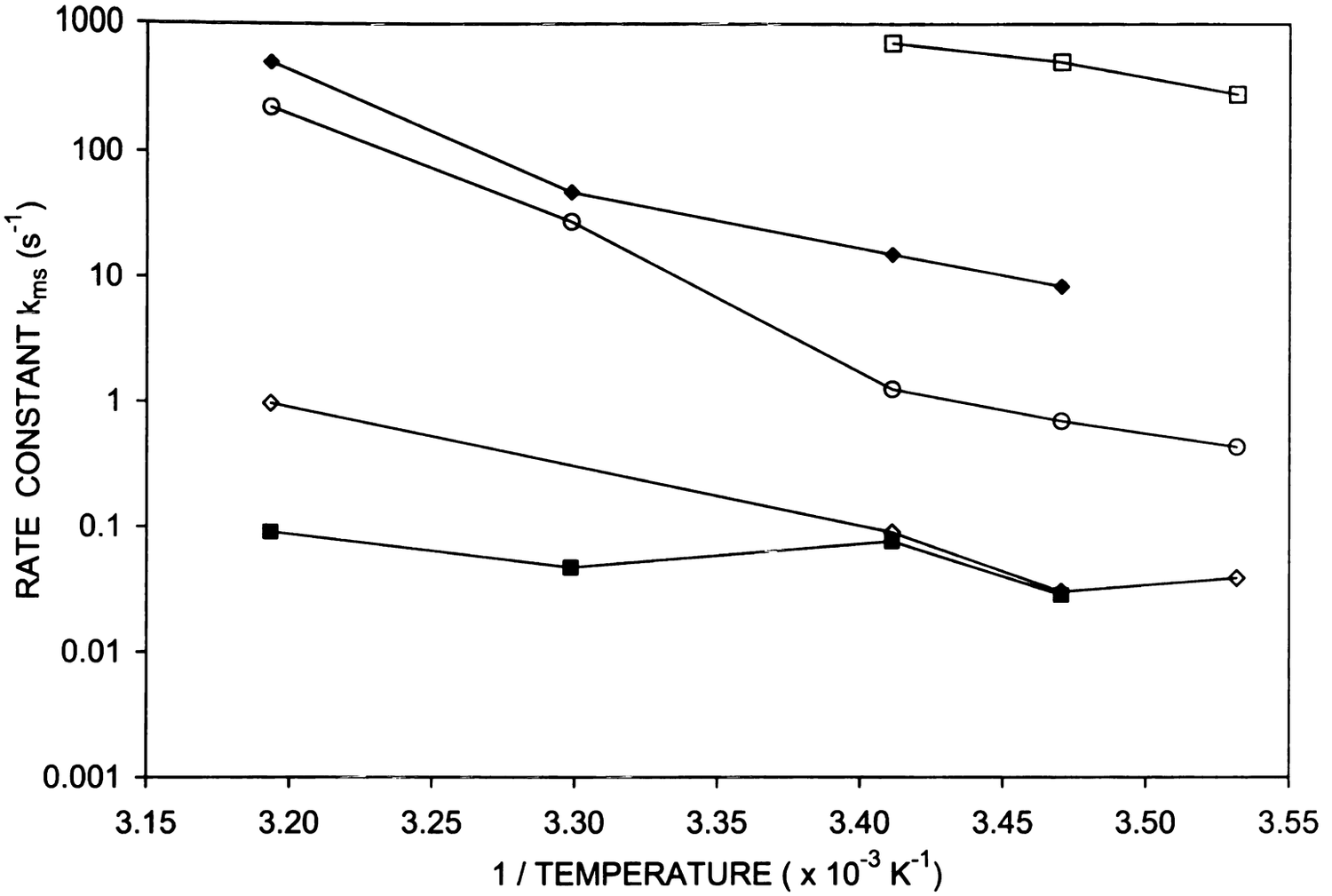

Figure 4.4: Representative graph of rate constant versus inverse temperature for acetonitrile mobile phase. pyrene (○), benz[a]anthracene (□), benz[a]acridine (■), dibenz[a,j]acridine (◆), dibenz[c,h]acridine (◇)

Table 4.3: Activation energy ($\Delta E_{\ddagger m}$ and $\Delta E_{\ddagger s}$) for PAH and NPAH solutes in methanol. Solutes defined in Table 4.1.

Solute	Activation Energy	
	$\Delta E_{\ddagger m}$ (kcal/mol)	$\Delta E_{\ddagger s}$ (kcal/mol)
P	37 ± 4	39 ± 4
B[a]A	30 ± 11	33 ± 10
B[a]Ac	2 ± 3	6 ± 3
D[aj]Ac	17 ± 3	21 ± 4
D[ch]Ac	25 ± 5	29 ± 4

4.4.2 Acetonitrile mobile phase

Figure 4.2 shows a representative set of chromatograms in acetonitrile mobile phase. In acetonitrile, a neutral solute, such as pyrene (Figure 4.2A) has a tailing peak shape. However, a basic solute, such as 4-azapyrene (Figure 4.2B) has a more pronounced tailing peak shape. The peak shapes for benz[a]anthracene and 1-aminopyrene remain symmetric in acetonitrile. The peak shape of pyrene is representative of the peak shape for dibenz[c,h]acridine. The peak shape for 4-azapyrene is representative of the remaining NPAHs.

4.4.2.1 Thermodynamic behavior

4.4.2.1.1 Retention factor

Table 4.4 summarizes the retention factors for the PAHs and NPAHs. When compared to the methanol mobile phase (Table 4.1), almost all solutes demonstrate an increase in retention factor in acetonitrile. Benz[a]anthracene and dibenz[c,h]acridine show a decrease in retention in acetonitrile. Since acetonitrile is less polar than methanol, the retention factor would be expected to decrease if the partition mechanism were dominant. Thus, the observed increase in retention factor suggests that for many solutes, the adsorption mechanism is contributing more greatly to retention in acetonitrile than in methanol. The increase in retention factor going from methanol to acetonitrile is moderate for pyrene (5 %), but is more substantial for the other solutes (50 – 69 %). In addition, retention factors for the NPAHs are very similar to or larger than those for the parent PAHs, also suggesting that the adsorption mechanism is dominant for these solutes in acetonitrile.

Table 4.4: Retention factor (k) and change in molar enthalpy (ΔH) for PAH and NPAH solutes in acetonitrile (2000 psi). Solutes defined in Table 4.1.

Solute	Retention factor, k		Molar Enthalpy ΔH (kcal/mol)
	T = 288 K	T = 313 K	
P	0.82	0.52	-3.5 ± 0.2
1AmP	0.23	0.16	-2.7 ± 0.1
1AzaP	1.33	0.58	(-6.8 ± 3.1)
4AzaP	0.93	0.47	-4.4 ± 0.5
B[a]A	0.78	0.47	-3.7 ± 0.1
B[a]Ac	0.71	0.33	-5.9 ± 0.4
D[aj]Ac	1.56	0.76	-6.0 ± 0.5
D[ch]Ac	1.64	0.91	-4.4 ± 0.2

Table 4.4 demonstrates the effect of temperature on retention factor. Retention factors decrease significantly with increasing temperature. In fact, for the same change in temperature, the change is more significant in acetonitrile than in methanol.

4.4.2.1.2 Molar enthalpy

Figure 4.5 displays a representative graph of the logarithm of the retention factor versus inverse temperature (van't Hoff plot). The graph for each solute in Figure 4.5A is linear (R^2 = 0.978 – 0.999) and the slope is positive. The positive slope indicates a negative change in molar enthalpy, suggesting the transfer from mobile to stationary phase is an enthalpically favorable process. The graph of 1-azapyrene and 4-azapyrene in Figure 4.5B is roughly linear (R^2 = 0.573 and 0.929), however due to the uncertainty in the measurement, the thermodynamic and kinetic information for these solutes is unreliable and is given for illustrative purposes only.

Table 4.4 summarizes the change in molar enthalpy for all solutes. The change in molar enthalpy is least negative for 1-aminopyrene, followed by pyrene, benz[a]anthracene, and dibenz[c,h]acridine. The most negative change in molar enthalpy occurs for benz[a]acridine and dibenz[a,j]acridine. These trends indicate that the change in molar enthalpy does not consistently become more negative with increasing ring number and with less condensed annelation structure, as would be seen in a partition mechanism. The changes in molar enthalpy are more negative in acetonitrile than in methanol for most solutes by 1.0 – 4.3 kcal/mol. This change in molar enthalpy is consistent with adsorption in

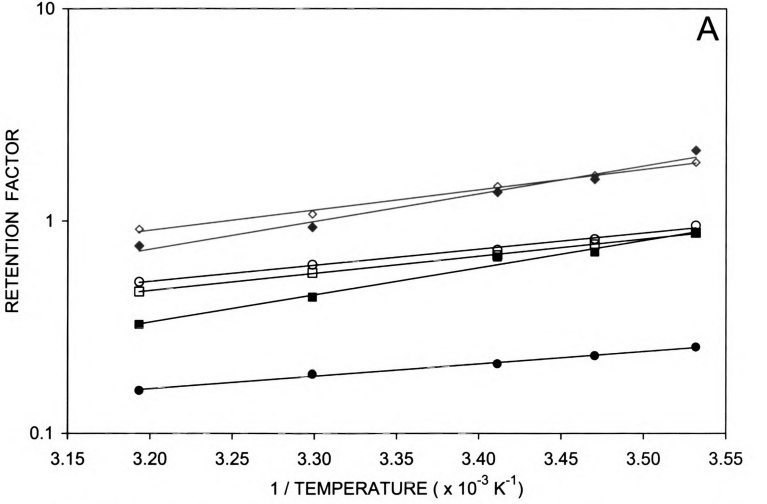

Figure 4.5A: Representative graph of retention factor versus inverse temperature for acetonitrile mobile phase. pyrene (○), 1-aminopyrene (●), benz[a]anthracene (□), benz[a]acridine (■), dibenz[a,j]acridine (◆), dibenz[c,h]acridine (◇)

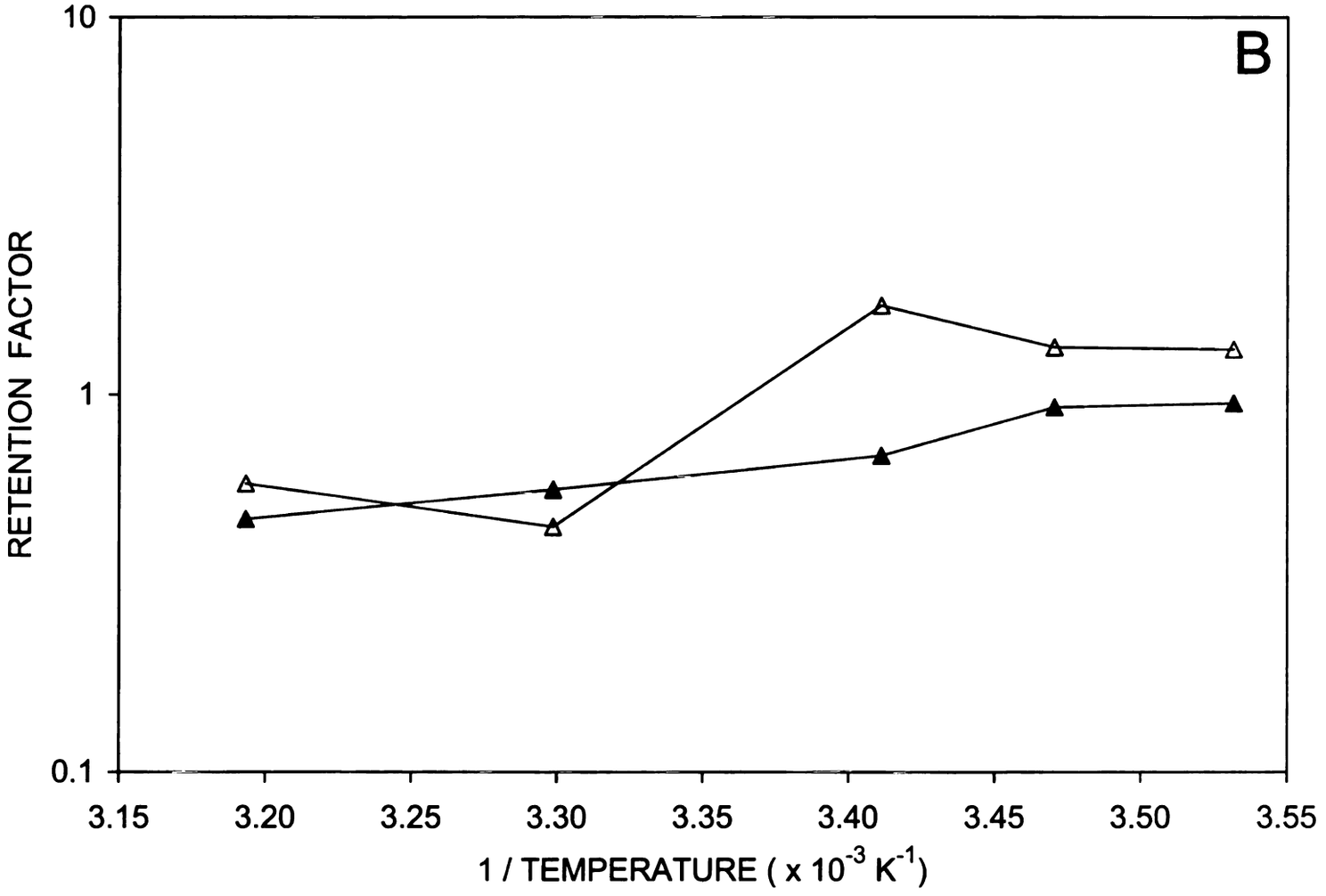

Figure 4.5B: Representative graph of retention factor versus inverse temperature for acetonitrile mobile phase. 1-azapyrene (△), 4-azapyrene (▲)

an aprotic solvent [12]. However, the change in molar enthalpy is comparable in acetonitrile for benz[a]anthracene and dibenz[c,h]acridine (a difference of 0.1 – 0.7 kcal/mol). This suggests that the partition mechanism is still important for these solutes, such that the less polar mobile phase, acetonitrile, competes more effectively than methanol with the nonpolar stationary phase. These solutes are suspected to have less basic character, due to lack of nitrogen (benz[a]anthracene) and sterically-hindered nitrogen placement (dibenz[c,h]acridine), and, hence, less adsorption at residual silanol sites.

The difference in molar enthalpy for acetonitrile compared to methanol is directly a result of the difference in retention factor. That is, the slopes of the van't Hoff plots for the two solvents are comparable to one another. This behavior is unlike that seen on silica-based materials, where the molar entropy contributed more to the difference in retention factor than the molar enthalpy. In this study, the intercept of the van't Hoff plots are very similar for acetonitrile and methanol, which suggests that the entropy term does not change significantly with solvent.

4.4.2.2 Kinetic behavior

4.4.2.2.1 Rate constants

Table 4.5 summarizes the rate constants for the PAHs and NPAHs. In acetonitrile, benz[a]anthracene and 1-aminopyrene undergo the fastest rate of transfer, followed by pyrene, benz[a]acridine, dibenz[a,j]acridine, and dibenz[c,h]acridine, which are three orders of magnitude slower. 1-Azapyrene and 4-azapyrene have the slowest rate of transfer, an order of magnitude slower

Table 4.5: Rate constants (k_{ms} and k_{sm}) for PAH and NPAH solutes in acetonitrile. Solutes defined in Table 4.1.

Solute	Rate constant, k_{ms} (s^{-1})		Rate constant, k_{sm} (s^{-1})	
	T = 288 K	T = 313 K	T = 288 K	T = 313 K
P	0.03	0.16	0.02	0.08
1AmP	1.1	--	0.24	--
1AzaP	0.002	0.005	0.002	0.003
4AzaP	0.003	0.002	0.003	0.002
B[a]A	8.4	4.7	6.2	2.1
B[a]Ac	0.03	0.02	0.02	0.003
D[aj]Ac	0.01	0.02	0.01	0.02
D[ch]Ac	0.03	0.05	0.05	0.04

than the majority of the solutes. 1-Azapyrene and 4-azapyrene are given only as an indication of their slow rate of transfer. As previously stated, the kinetic values for those solutes are not reliable based on the uncertainty in the experimental measurement. The rate constants in acetonitrile are one to four orders of magnitude smaller when compared to those in methanol. The differences in the rate constants result from the increased ability of the NPAHs to interact with available silanols on the hybrid support. The aprotic solvent, acetonitrile, does not interact with the silanol sites as does the protic solvent, methanol. Therefore, the rate constants between the mobile and stationary phases are substantially slower.

Table 4.5 demonstrates the effect of temperature on the rate constants. The rate constants for most solutes increase significantly, while the rate constants for 4-azapyrene, benz[a]anthracene, and benz[a]acridine decrease with increasing temperature. An increase in rate is expected with an increase in temperature due to increased diffusion coefficients and enhanced fluidity of the stationary phase. An increase in kinetic energy as a consequence of increased temperature allows the alkyl chains to become more labile, allowing easier access for the solutes.

4.4.2.2.2 Activation energy

Figure 4.6 shows a representative graph of the logarithm of the rate constant versus the inverse temperature. The graph does not contain information for 1-azapyrene and 4-azapyrene, due to uncertainty in the measurement, or for 1-aminopyrene, due to its narrow peak shape. Of those

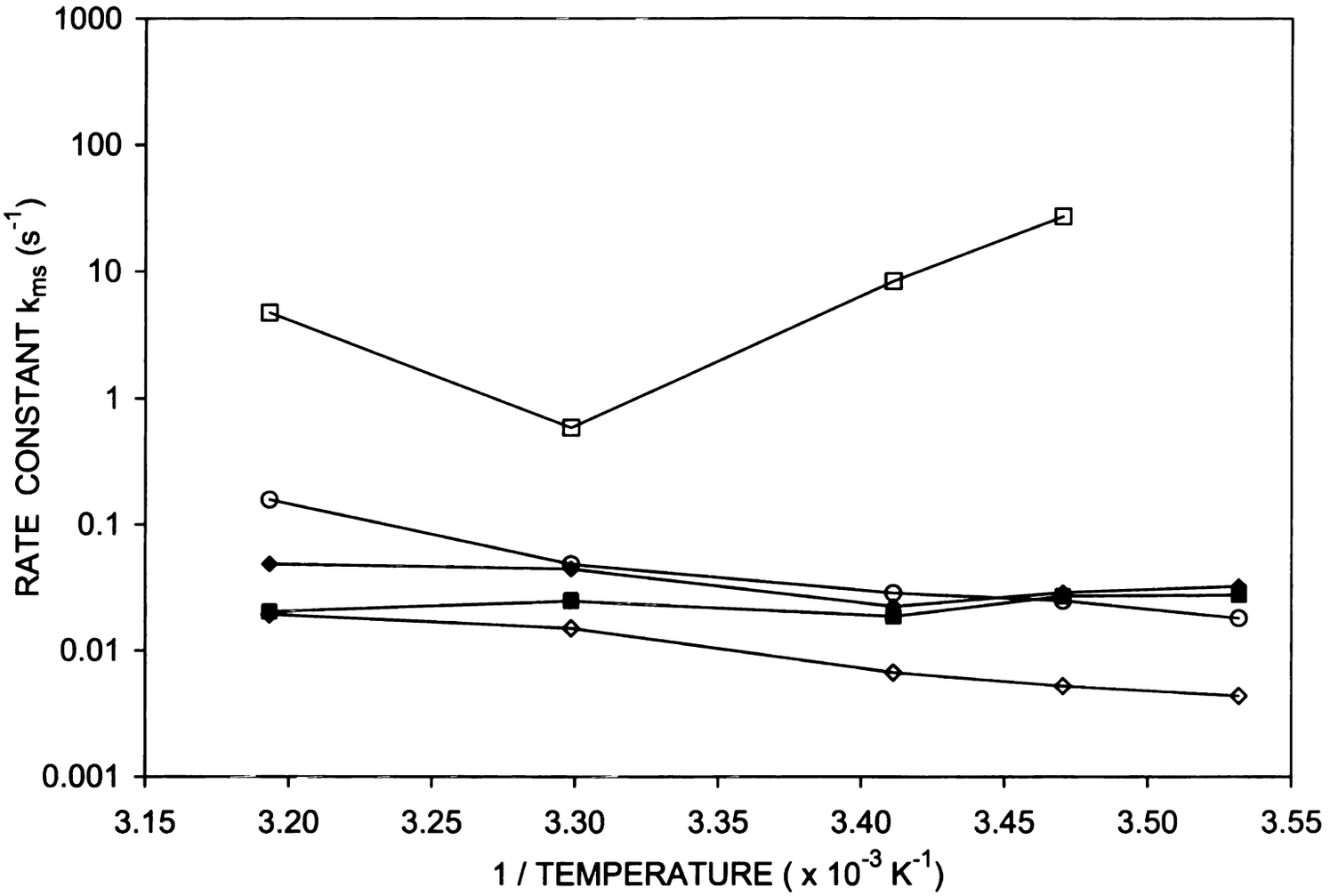

Figure 4.6: Representative graph of rate constant versus inverse temperature for acetonitrile mobile phase. pyrene (○), benz[a]anthracene (□), benz[a]acridine (■), dibenz[a,j]acridine (◆), dibenz[c,h]acridine (◇)

shown, the graph for almost all solutes is roughly linear (R^2 = 0.525 – 0.970) and the slope is negative. A negative slope is indicative of a positive energy barrier for mass transfer. The rate constants for benz[a]anthracene fluctuate with temperature and, therefore, the slope is not linear.

The activation energy is calculated from the slope of this graph, according to Equation 1.13, and is summarized in Table 4.6. The activation energies are positive for pyrene and dibenz[a,j]acridine. The activation energy is negative for the other solutes, however, due to uncertainty in the measurement these values are likely not meaningful. For pyrene and dibenz[a,j]acridine, the activation energy for the transfer from stationary phase to transition state ($\Delta E_{\ddagger s}$) is greater that that from mobile phase to transition state ($\Delta E_{\ddagger m}$). These data indicate that it is easier for the solutes to enter the stationary phase than to exit. This behavior is similar to that seen in methanol.

4.5 Conclusions

In this study, the thermodynamic and kinetic behavior of NPAHs was examined in reversed-phase liquid chromatography. The parent PAHs are separated primarily by the partition mechanism with the octadecyl groups, but some minor interaction with the silanol groups can occur through the aromatic system. In methanol mobile phase, the retention factors for the NPAHs are less than those for the parent PAHs. This is consistent with a partition mechanism, where retention decreases as the polarity of the solute increases. In addition, the trends of retention with ring number and annelation structure are consistent with the partition mechanism. However, the kinetic rate constants indicate that

Table 4.6: Activation energy ($\Delta E_{\ddagger m}$ and $\Delta E_{\ddagger s}$) for PAH and NPAH solutes in acetonitrile. Solutes defined in Table 4.1.

Solute	Activation Energy	
	$\Delta E_{\ddagger m}$ (kcal/mol)	$\Delta E_{\ddagger s}$ (kcal/mol)
P	9 ± 2	12 ± 2
B[a]A	(-17 ± 10)	(-14 ± 10)
B[a]Ac	(-11 ± 2)	(-2 ± 1)
D[aj]Ac	4 ± 1	10 ± 1
D[ch]Ac	(-0.9 ± 2)	3 ± 2

adsorption at silanol sites could play a role, as they are significantly smaller for the NPAHs than for the parent PAHs.

The different thermodynamic and kinetic behavior in the presence of the aprotic solvent acetonitrile provides an interesting picture of the retention process. Methanol is able to hydrogen bond with both the NPAH solutes and the underlying silanols, which causes a reduction in the number of available silanols. Acetonitrile cannot hydrogen bond in this way to shield interactions of the solute with the underlying particle. Thus, the retention factors for the NPAHs are larger than those in methanol. Moreover, the retention factors for the NPAHs are more similar to or larger than those for the PAHs, suggesting the adsorption mechanism is likely dominant for the NPAH solutes. The changes in molar enthalpy for the NPAHs are slightly more negative than for the PAHs and are sufficient to account for the small changes in retention factor. If the change in molar enthalpy was not sufficient to account for the change in retention factor, a change in entropy or the phase ratio would be responsible, according to Equation 1.7, as was the case for silica-based C_{18} [12]. However, for the hybrid support, there does not seem to be a significant change in the molar entropy or phase ratio for acetonitrile. The kinetic behavior also reflects the increased role of adsorption, as the rate constants are one to four orders of magnitude smaller than those in methanol.

The thermodynamic and kinetic behavior of the solutes on this hybrid phase is similar in nature to those built of silica supports [12]. The retention factors in both mobile phases are smaller for the same set of solutes under

similar conditions than on the silica phases. The rate constants in methanol are faster, while those in acetonitrile are slower on the hybrid phase compared to the silica phase. The change in molar enthalpy is less negative for the hybrid phases compared to the silica phases for the same solutes. However, the bonding density of the hybrid phase is more similar to the bonding density of the monomeric phase than the polymeric phase used in previous studies [21,28]. When this monomeric silica phase is considered, the changes in molar enthalpy are more consistent to the hybrid phase in this study. The thermodynamic and kinetic information provide a clearer description of the retention mechanism of NPAHs on hybrid supports in reversed-phase liquid chromatography.

4.6 References

[1] J.W. Dolan, *LCGC North America 23* (**2005**) 470-475.

[2] T.V. Koval'chuk, U. Lewin, V.N. Zaitsev, W. Engewald, *J. Anal. Chem. 54* (**1999**) 115-121.

[3] J.J. Kirkland, J.L. Glajch, R.D. Farlee, *Anal. Chem. 61* (**1989**) 2-11.

[4] N. Sagliano, T.R. Floyd, R.A. Hartwick, J.M. Dibussolo, N.T. Miller, *J. Chromatogr. A 443* (**1988**) 155-172.

[5] J. Layne, *J. Chromatogr. A 957* (**2002**) 149-164.

[6] U.D. Neue, Y.-F. Cheng, Z. Lu, B.A. Alden, P.C. Iraneta, C.H. Phoebe, K. Van Tran, *Chromatographia 54* (**2001**) 169-177.

[7] J.W. Coym, *J. Sep. Sci. 31* (**2008**) 1712-1718.

[8] K.D. Wyndham, J.E. O'Gara, T.H. Walter, K.H. Glose, N.L. Lawrence, B.A. Alden, G.S. Izzo, C.J. Hudalla, P.C. Iraneta, *Anal. Chem. 75* (**2003**) 6781-6788.

[9] J.E. O'Gara, K.D. Wyndham, *J. Liq. Chromatogr. Relat. Technol. 29* (**2006**) 1025-1045.

[10] Y. Liu, N. Grinberg, K.C. Thompson, R.M. Wenslow, U.D. Neue, D. Morrison, T.H. Walter, J.E. O'Gara, K.D. Wyndham, *Anal. Chim. Acta 554* (**2005**) 144-151.

[11] S. Shen, H. Lee, J. McCaffrey, N. Yee, C. Senanayake, N. Grinberg, J. Clark, *J. Liq. Chromatogr. Relat. Technol. 29* (**2006**) 2823-2834.

[12] V.L. McGuffin, S.B. Howerton, X. Li, *J. Chromatogr. A 1073* (**2005**) 63-73.

[13] H. Colin, J.-M. Schmitter, G. Guiochon, *Anal. Chem. 53* (**1981**) 625-631.

[14] B.L. Van Duuren, J.A. Bilbao, C.A. Joseph, *J. Natl. Cancer Inst. 25* (**1960**) 53.

[15] M. Dong, I. Schmeltz, E. Jacobs, D.J. Hoffman, *J. Anal. Toxicol. 2* (**1978**) 21.

[16] E. Sawicki, J.E. Meeker, M.J. Morgan, *Arch. Environ. Health 11* (**1965**) 773.

[17] J.M. Schmitter, H. Colin, J.L. Excoffier, P. Arpino, G. Guiochon, *Anal. Chem. 54* (**1982**) 769-772.

[18] C. Borra, D. Wiesler, M. Novotny, *Anal. Chem. 59* (**1987**) 339-343.

[19] S.G. Wakeham, *Environ. Sci. Technol. 13* (**1979**) 1118.

[20] J.C. Arcos, M.P. Argus, Chemical Introduction of Cancer, Academic Press, New York, **1974**.

[21] S.B. Howerton, V.L. McGuffin, *Anal. Chem. 75* (**2003**) 3539-35448.

[22] V.L. McGuffin, C. Lee, *J. Chromatogr. A 987* (**2003**) 3.

[23] S.B. Howerton, C. Lee, V.L. McGuffin, *Anal. Chim. Acta 478* (**2003**) 99.

[24] S.B. Howerton, V.L. McGuffin, *J. Chromatogr. 1030* (**2004**) 3-12.

[25] C.J. Orendorff, M.W. Ducey Jr., J.E. Pemberton, *J. Phys. Chem. A 106* (**2002**) 6991.

[26] M.W. Ducey Jr., C.J. Orendorff, J.E. Pemberton, L.C. Sander, *Anal. Chem. 74* (**2002**) 5576.

[27] M.W. Ducey Jr., C.J. Orendorff, J.E. Pemberton, L.C. Sander, *Anal. Chem. 74* (**2002**) 5585.

[28] V.L. McGuffin, S.-H. Chen, *J. Chromatogr. A 762* (**1997**) 35-46.

CHAPTER 5

EFFECT OF MOBILE PHASE MODIFIERS ON PEAK SHAPE USING BRIDGED-ETHYLENE HYBRID STATIONARY PHASES

5.1 Introduction

As demonstrated in Chapter 4, nitrogen-containing polycyclic aromatic hydrocarbons (NPAHs) exhibit severely tailing peak shapes under typical reversed-phase liquid chromatographic (RPLC) conditions. This phenomenon is believed to arise from interaction of the solute with two types of sites: one with a high population yet a weak interaction (C_{18}) and another with a low population yet a strong interaction (residual silanols and metals). The weak interaction site is kinetically fast and contributes only to symmetric broadening, while the strong interaction site is kinetically slow, and can lead to asymmetric peak shapes. Many investigators have shown that peak shape can be controlled by reducing the interaction of the solute with such sites [1,2].

A common way to reduce tailing caused by surface sites is the use of mobile phase modifiers. A mobile phase modifier can act to reduce tailing in several ways: 1) it can interact with the solute, reducing the ability to interact with the slow site, 2) it can permanently block the slow site, or 3) it can displace the solute from the slow site. Several types of modifiers have been used to reduce the influence of residual surface silanols in silica-based supports. An acidic modifier, such as an alkylsulfonic acid [3,4], can sometimes improve peak shape, however, for many solutes, an improvement is not seen [4,5]. Basic modifiers, containing a form of amine, have proven more useful for eliminating tailing peak shapes of basic analytes [4,6-14]. A pivotal study by Bij *et al.* focused on

reducing the silanophilic interaction of the solute with surface silanol sites using water and amines as silanol masking agents [7]. This study was the first to demonstrate that silanophilic interaction could be eliminated by blocking surface silanols and by masking the solute itself. A number of different types of amines, including primary, secondary, and tertiary amines [9,13], and amines with various alkyl chain lengths [8,12,13] have been investigated. However in many cases, a simple tertiary amine, such as triethylamine, is sufficient to decrease peak tailing caused by interactions with surface silanol groups [6,10,13]. In addition, the combination of acid and base modifiers is commonly used in chiral chromatography to improve both retention and peak shape [3,14,15], although the mechanism of interaction for the modifiers has only been studied by a relatively small number of authors [16].

In addition to silanol sites, metals in the underlying stationary phase can cause deleterious effects. Metals increase the acidity of nearby silanols, which greatly affects the peak shape [17,18]. In addition, the concentration of the metal in the stationary phase was found to be relevant to both retention and peak asymmetry [19]. Therefore, a large effort has been made toward the removal of metals from stationary phase materials, however, many phases still contain trace amounts of various metals. Thus, a mobile phase modifier, acting as a metal chelating agent, could be used to prevent complexation of the amine solutes with the metals [20,21].

Alternatively, stationary phase production has been altered to allow for phases that limit interaction with metal and silanol sites. For instance, phases

have been developed with a lower number of accessible silanol sites, decreased metal content, and the incorporation of a polar functional group embedded in the C_{18} phase to limit interaction with metal and silanol sites [22-24]. In addition, the organic-inorganic hybrid materials are synthesized to have a lower number of silanol sites than traditional silica [25,26]. Regardless, peak tailing is still observed for these hybrid materials, as seen in Chapter 4. This chapter aims to further evaluate and understand the causes of peak tailing in hybrid stationary phases.

The goals of this research are as follows: (1) to separate a series of NPAHs and their parent polycyclic aromatic hydrocarbons (PAHs) using hybrid packing materials, (2) to investigate the effect of the underlying particle on retention and peak shape, (3) to evaluate the effect of a polar embedded group in the C_{18} chain, and (4) to elucidate the effect of typical modifying agents on the retention and peak shape of the NPAHs.

5.2 Methods

5.2.1 Reagents

As shown in Figure 4.1, two PAHs and six nitrogen-containing NPAHs are chosen to study the effect of nitrogen position, ring number, and annelation structure on retention, broadening, and peak asymmetry. Pyrene, benz[a]anthracene, 1-aminopyrene (Sigma-Aldrich), 1-azapyrene, 4-azapyrene, benz[a]acridine, dibenz[c,h]acridine, and dibenz[a,j]acridine (Institute für PAH Förschung) are obtained as solids and dissolved in high-purity methanol and acetonitrile (Burdick and Jackson Division, Honeywell) to yield standard solutions

with concentrations between 10^{-3} M and 10^{-5} M. A non-retained marker, 4-bromomethyl-7-methoxycoumarin (Sigma), is added to each solution at a concentration of 10^{-3} M. Acetic acid, acetyl acetone (Aldrich), triethylamine (Spectrum), and pyridine (Fisher) are separately added to fresh methanol and acetonitrile mobile phases (Burdick and Jackson Division, Honeywell) at a concentration of 0.2 % (v/v). In the case where two mobile phase modifiers are added, the concentration of each modifier is 0.2 %.

5.2.2 Experimental system

The solutes are separated by capillary liquid chromatography with one on-column detector as illustrated in Figure 2.3. The stationary phases are the hybrid-based materials (XBridge C_{18}, XBridge Shield RP_{18}, and bridged-ethylene hybrid (BEH) support, Waters Corporation) described in Chapter 2.2. The mobile phase consists of methanol or acetonitrile with 0.2 % modifier. The sample is split between the capillary column and a fused-silica capillary (50 μm i.d., Polymicro Technologies), resulting in an injection volume of 10 nL. The temperature was not controlled (ambient), while the pressure was maintained at 2000 psi.

5.2.3 Data analysis

After separation, the zone profile for each solute is extracted from the chromatogram. Each profile is fit by nonlinear regression to a combination of Gaussian (Equation 1.33) and asymmetric double sigmoidal (Equation 3.25) equations using a commercially available program (Peakfit v4.14, SYSTAT Software). This method produces high quality fits (correlation coefficients ranging from 0.999 to 0.956), reduces noise, and allows control of peak

integration limits. The fit is regenerated in Microsoft Excel, from which the statistical moments are calculated. In this work, the peak boundaries are identified at 0.1 % of the maximum peak height, as the error in the calculation of the statistical moments has been proven small at this integration limit [27]. The statistical moments are calculated based on the regenerated fit by

$$M_1 = \frac{\int C(t)\, t\, dt}{\int C(t) dt} \tag{5.1}$$

$$M_n = \frac{\int C(t)(t - M_1)^n dt}{\int C(t) dt} \tag{5.2}$$

where C(t) is the solute concentration as a function of time and n is the order of the moment. Values for M_1, M_2, and M_3 describe the mean retention time, variance, and asymmetry, respectively. To evaluate the retention and peak shape, the retention factor (k), reduced plate height (h), and skew (s) are calculated as

$$k = \frac{(M_1 - t_0)}{t_0} \tag{5.3}$$

$$h = \frac{H}{d_p} = \frac{M_2 L}{M_1^2 d_p} \tag{5.4}$$

$$s = \frac{M_3}{M_2^{3/2}} \tag{5.5}$$

where t_0 is the elution time of a non-retained solute, H is the plate height, and d_p is the particle diameter. Each calculated parameter (k, h, s) represents a

normalized value for a statistical moment (M_1, M_2, M_3, respectively), which quantitatively describes retention and peak shape behavior for the separation.

5.3 Results

5.3.1 Methanol mobile phase

5.3.1.1 Without modifier

Table 5.1 summarizes the retention factor, reduced plate height, and skew for each solute on each stationary phase in pure methanol mobile phase.

5.3.1.1.1 XBridge C_{18}

The retention factors for each neutral PAH are larger than those for the related NPAHs. This behavior is consistent with the partition mechanism where the polarity of the NPAHs is increased relative to the PAHs. This behavior was also observed on silica-based supports [28,29]. In addition, solute structure plays an important role in retention. Retention factor increases with number of rings and decreases with more condensed annelation structure, again consistent with the partition mechanism.

The reduced plate height is a measure of the broadening of the peak. The reduced plate heights for XBridge are near 2 for the majority of solutes, which corresponds to plate heights that are roughly 2 times the particle diameter ($H \approx 10\ \mu m$). That is, for these solutes, the broadening is only caused by typical on-column processes such as multiple paths, diffusion, and fast mass transport. The solutes with larger reduced plate heights are 1- and 4-azapyrene and benz[a]acridine, each with a nitrogen atom placed on the outside of the ring

Table 5.1: Retention factor (k), reduced plate height (h), and skew (s) for methanol mobile phase without modifier. Solutes: pyrene (P), 1-aminopyrene (1AmP), 1-azapyrene (1AzaP), 4-azapyrene (4AzaP), benz[a]anthracene (B[a]A), benz[a]acridine (B[a]Ac), dibenz[a,j]acridine (D[aj]Ac), dibenz[c,h]acridine (D[ch]Ac)

Methanol	XBridge C_{18}			XBridge Shield RP_{18}			BEH		
	k	h	s	k	h	s	k	h	s
P	0.595	2.0	0.00	0.510	16	3.21	0.000	6.3	0.00
1AmP	0.087	2.2	0.25	0.238	7.1	0.00	0.000	6.3	0.00
1AzaP	0.239	67	0.40	0.227	230	0.54	0.056	5.0	0.00
4AzaP	0.283	230	2.09	0.295	590	4.04	0.045	5.6	0.00
B[a]A	0.705	2.0	0.00	0.622	6.4	0.00	0.000	6.3	0.00
B[a]Ac	0.290	130	0.88	0.300	40	0.84	0.024	6.6	0.00
D[aj]Ac	0.572	2.4	0.00	0.709	12	1.06	0.020	4.6	0.00
D[ch]Ac	1.322	2.6	2.01	1.261	8.5	1.90	0.000	6.3	0.00

structure. This behavior suggests that, not only the nitrogen, but also its location in the ring structure, influences the broadening.

The skew describes the asymmetry of a peak, where a positive value indicates a tailing peak and a negative value implies a fronting peak. A larger value for the skew indicates a more asymmetric peak. The skew for several solutes (pyrene, benz[a]anthracene, and dibenz[a,j]acridine) is equal to zero, indicating a symmetric peak shape. The skew is positive for the other solutes, indicating a tailing peak shape. For the most part, solutes with positive skew values have a nitrogen located on the outside edge of the ring structure, leaving the nitrogen accessible to interact with surface silanols or other slow sites. It is important to note that large values for the reduced plate height correspond with large positive values for the skew. However, reduced plate height and skew do not correspond with retention factor. That is, positive skews are observed for solutes with both small (4-azapyrene) and large (dibenz[c,h]acridine) retention. This implies that solute structure rather than solute retention is the important factor controlling broadening and asymmetry.

5.3.1.1.2 XBridge Shield RP_{18}

The retention factors on XBridge Shield are comparable in magnitude to those on XBridge (Table 5.1). Neutral or neutral-like solutes (pyrene, benz[a]anthracene, and dibenz[c,h]acridine) are slightly less retained, while 1-aminopyrene and dibenz[a,j]acridine are slightly more retained than on XBridge. The differences in retention are due to the carbamate group in XBridge Shield. That is, as the polarity of the phase increases (due to the carbamate group),

polar compounds become more retained, consistent with the partition mechanism. However, retention factors for 1- and 4-azapyrene are comparable, suggesting their behavior is more consistent with the adsorption mechanism. In addition, the addition of the carbamate group reduces the number of carbons in the alkyl chain to 15 (as seen in Figure 2.2), which can also cause a difference in retention for solutes governed strictly by the partition mechanism.

Reduced plate heights for XBridge Shield are 60 to 80 % larger than those of XBridge, except for benz[a]acridine which is 70 % smaller. All solutes have reduced plate heights greater than 2, with benz[a]anthracene and 1-aminopyrene having the smallest reduced plate heights.

The skews are larger for most solutes on XBridge Shield compared to those on XBridge. The skew is largest for 4-azapyrene and pyrene, indicating they are the most tailing solutes. The skew is next largest for the acridine compounds, followed by 1-azapyrene. The skew for 1-aminopyrene and benz[a]anthracene are equal to zero, indicating symmetric peak shape.

When the two C_{18} phases are compared, an interesting trend is observed as a function of retention factor. A larger retention factor on one phase corresponds to a smaller reduced plate height and skew. For example, the retention factor for pyrene is larger on XBridge than on XBridge Shield, however the reduced plate height and skew are smaller on XBridge. This behavior is observed for all solutes except for 1-aminopyrene, 4-azapyrene, and dibenz[a,j]acridine, which show the opposite trend.

The addition of the polar embedded group affects the broadening and asymmetry. For the solutes in this study, the polar embedded group does not improve the peak shape, as it is intended. If the slow site is located in the hybrid support, the polar embedded group does not adequately block it. Furthermore, the creation of additional slow sites may occur when the polar embedded group is included in the phase. This will be discussed in more detail in Section 5.4.5.

5.3.1.1.3 Bridged-ethylene hybrid (BEH) particle

Several solutes (pyrene, benz[a]anthracene, 1-aminopyrene, and dibenz[c,h]acridine) are non-retained on the bridged-ethylene hybrid (BEH) support. These solutes are the neutral solutes, the amine, and a solute with a sterically-hindered nitrogen. The other solutes, 1- and 4-azapyrene, benz[a]acridine, and dibenz[a,j]acridine are retained on BEH. These retained solutes have similar nitrogen placement, each having a nitrogen atom located on the outside edge of the ring structure, leaving the nitrogen accessible to interact with surface silanols or other slow sites.

Reduced plate heights on BEH range from 4.6 – 6.3 for both retained and non-retained solutes. In addition, all values for the skew are equal to zero, indicating symmetric peak shapes on the underlying support. It is interesting to note that solutes retained on BEH correspond to the same solutes that exhibit peak tailing on the C_{18} derivatized phases. This suggests that retention on the underlying particle, not asymmetry on the underlying particle, contributes to the asymmetry on the C_{18} derivatized phases. This hypothesis will be discussed in more detail in Section 5.4.

5.3.1.2 Effect of mobile phase modifiers

The effect of each modifier in methanol mobile phase is examined as a function of retention factor, reduced plate height, and skew. Detailed information on the change in each parameter is given in Appendix 5A.1.

Figure 5.1 shows the effect of mobile phase modifier on retention factor. The retention factor does not change substantially with the addition of any modifier for any of the phases. In general, acetic acid causes a decrease in retention, with several negative retention factors. On BEH in methanol mobile phase, the retention factor does not decrease with any mobile phase modifier.

Figure 5.2 shows the effect of mobile phase modifier on reduced plate height. A reduced plate height equal to 2 is shown by a black line on the graphs. None of the mobile phase modifiers cause a universal decrease in the reduced plate height towards the ideal value of h = 2. While triethylamine causes a decrease in plate height for XBridge, an increase is observed for XBridge Shield, and no change is seen for BEH. Acetic acid seems to have little effect on the reduced plate height for all phases, while acetyl acetone causes an increase in plate height for the C_{18} phases but causes no significant change for BEH.

Figure 5.3 shows the effect of mobile phase modifier on skew. Overall, only acetic acid causes a reduction in skew. For many solutes the skew becomes negative, indicating a fronting peak shape. This behavior is also observed on BEH. In some cases, a small decrease in skew is observed, however, a reduction in skew for all solutes does not occur. In addition, acetyl acetone seems to increase the skew for many solutes on the C_{18} phases.

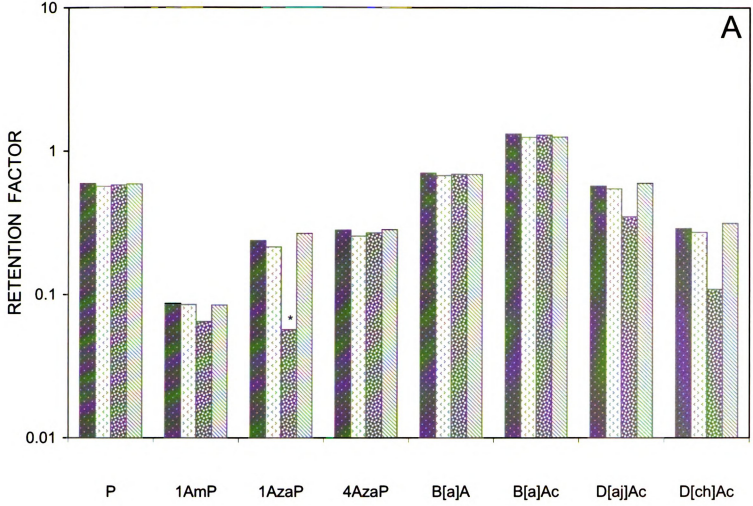

Figure 5.1A: Retention factor for each solute on XBridge C_{18} in methanol as a function of mobile phase modifier. pure methanol (■), triethylamine (▨), acetic acid (▨), acetyl acetone (▨). Solutes defined in Table 5.1. Negative retention factors are indicated by *.

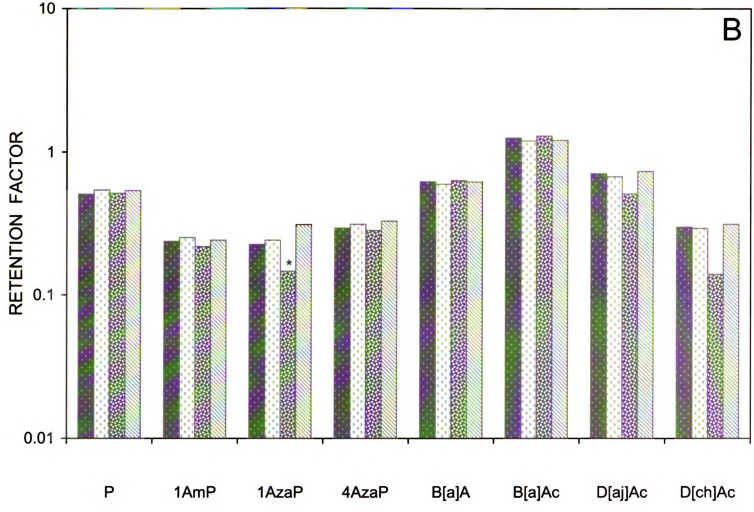

Figure 5.1B: Retention factor for each solute on XBridge Shield RP_{18} in methanol as a function of mobile phase modifier. pure methanol (■), triethylamine (▨), acetic acid (▩), acetyl acetone (▨). Solutes defined in Table 5.1. Negative retention factors are indicated by *.

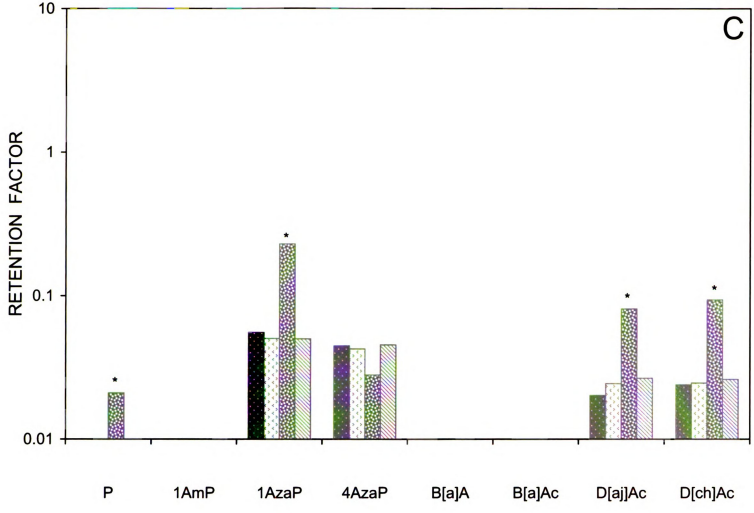

Figure 5.1C: Retention factor for each solute on BEH in methanol as a function of mobile phase modifier. pure methanol (■), triethylamine (▒), acetic acid (▒), acetyl acetone (▒). Solutes defined in Table 5.1. Negative retention factors are indicated by *.

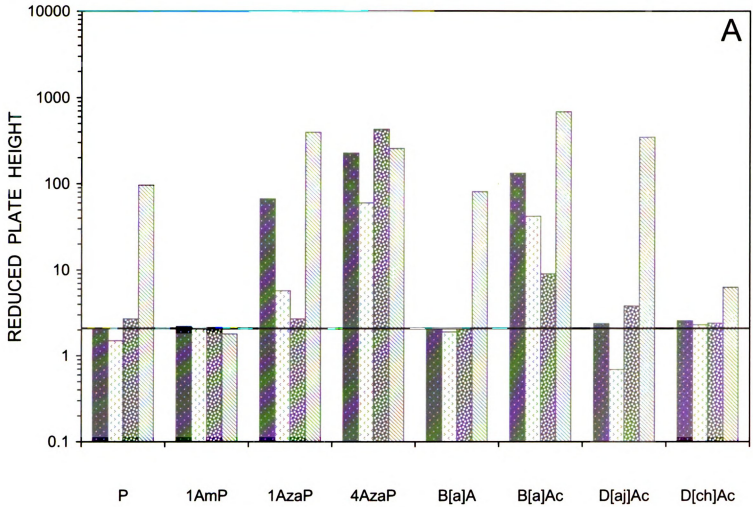

Figure 5.2A: Reduced plate height for each solute on XBridge C_{18} in methanol as a function of mobile phase modifier, pure methanol (■), triethylamine (▒), acetic acid (▒), acetyl acetone (▨). Solutes defined in Table 5.1.

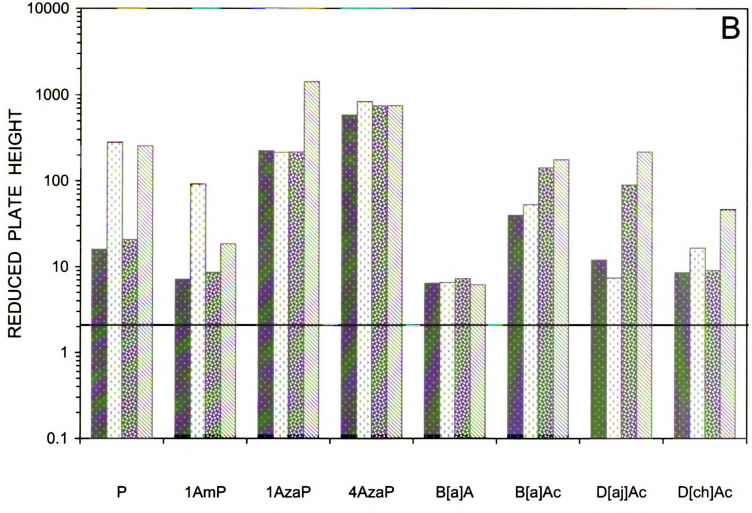

Figure 5.2B: Reduced plate height for each solute on XBridge Shield RP_{18} in methanol as a function of mobile phase modifier. pure methanol (▩), triethylamine (▩), acetic acid (▩), acetyl acetone (▩). Solutes defined in Table 5.1.

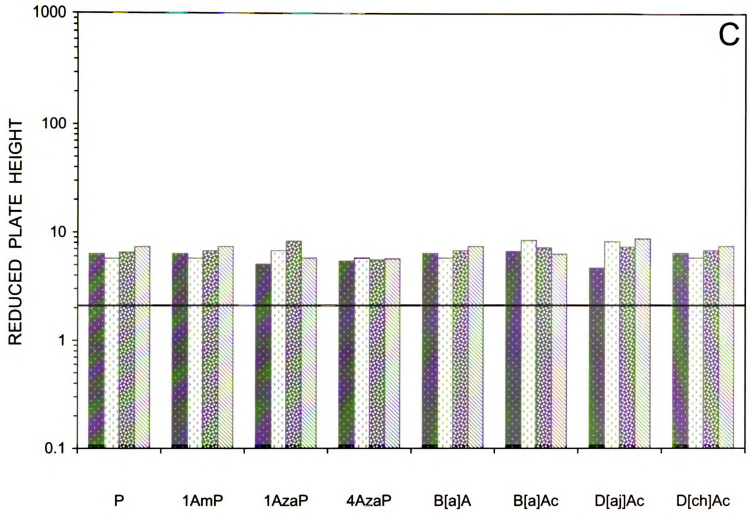

Figure 5.2C: Reduced plate height for each solute on BEH in methanol as a function of mobile phase modifier. pure methanol (■), triethylamine (⁘), acetic acid (▒), acetyl acetone (▨). Solutes defined in Table 5.1.

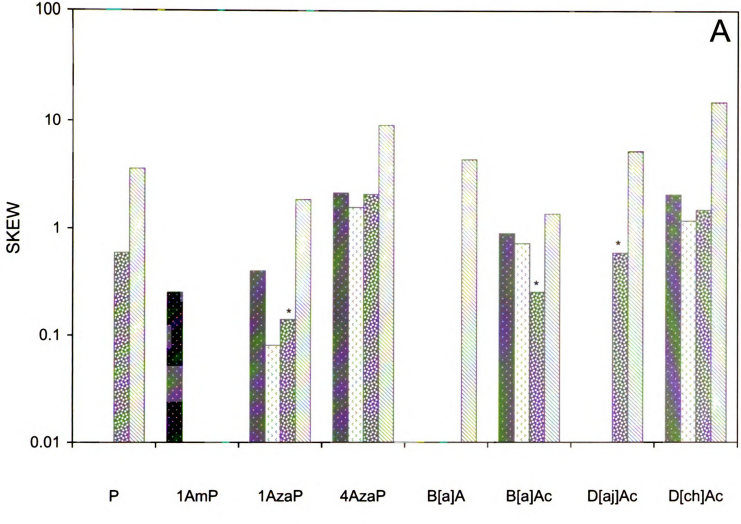

Figure 5.3A: Skew for each solute on XBridge C_{18} in methanol as a function of mobile phase modifier. pure methanol (■), triethylamine (▒), acetic acid (▓), acetyl acetone (▨). Solutes defined in Table 5.1. Negative skews are indicated by *.

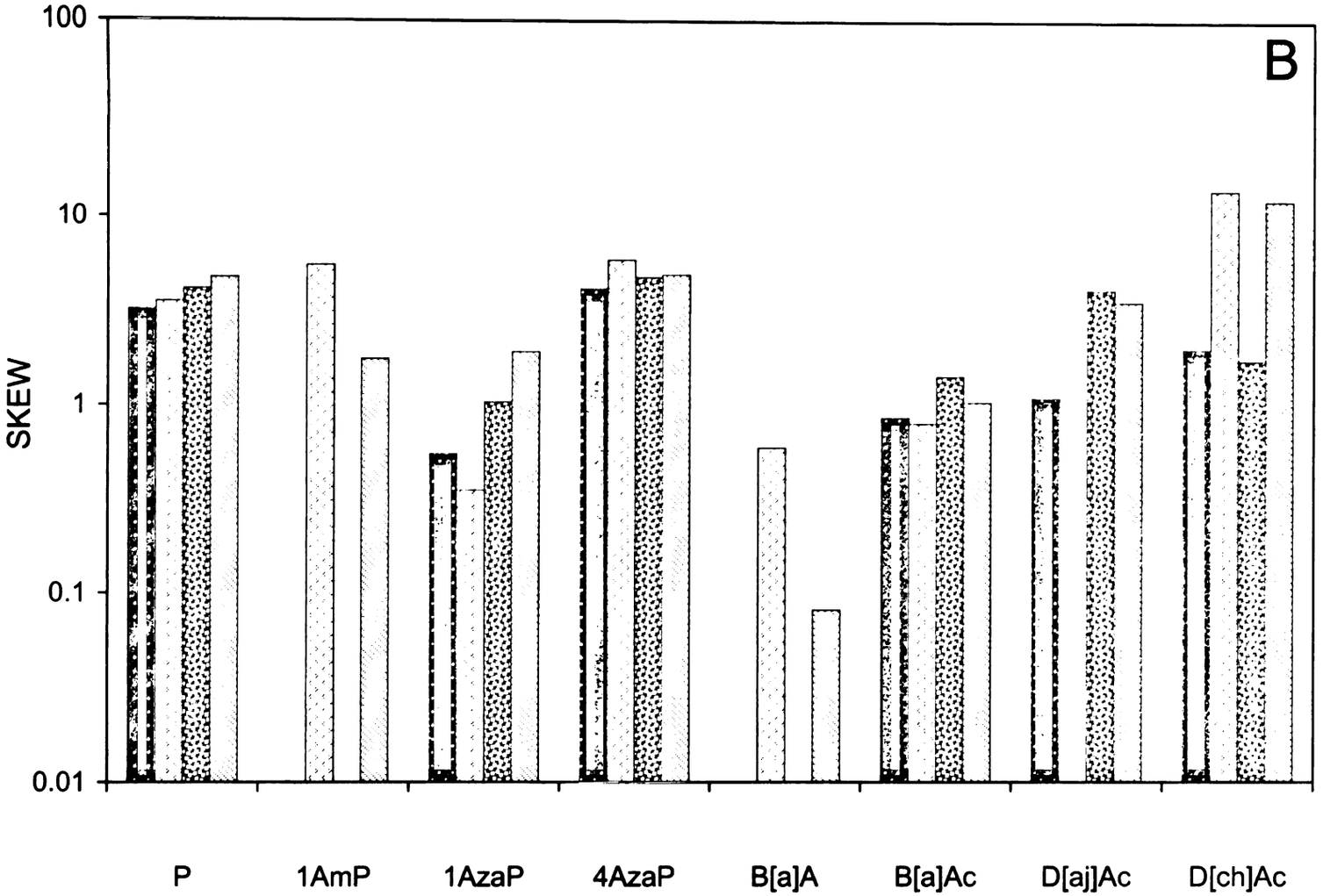

Figure 5.3B: Skew for each solute on XBridge Shield RP_{18} in methanol as a function of mobile phase modifier. pure methanol (▣). triethylamine (▨). acetic acid (▩). acetyl acetone (▨). Solutes defined in Table 5.1.

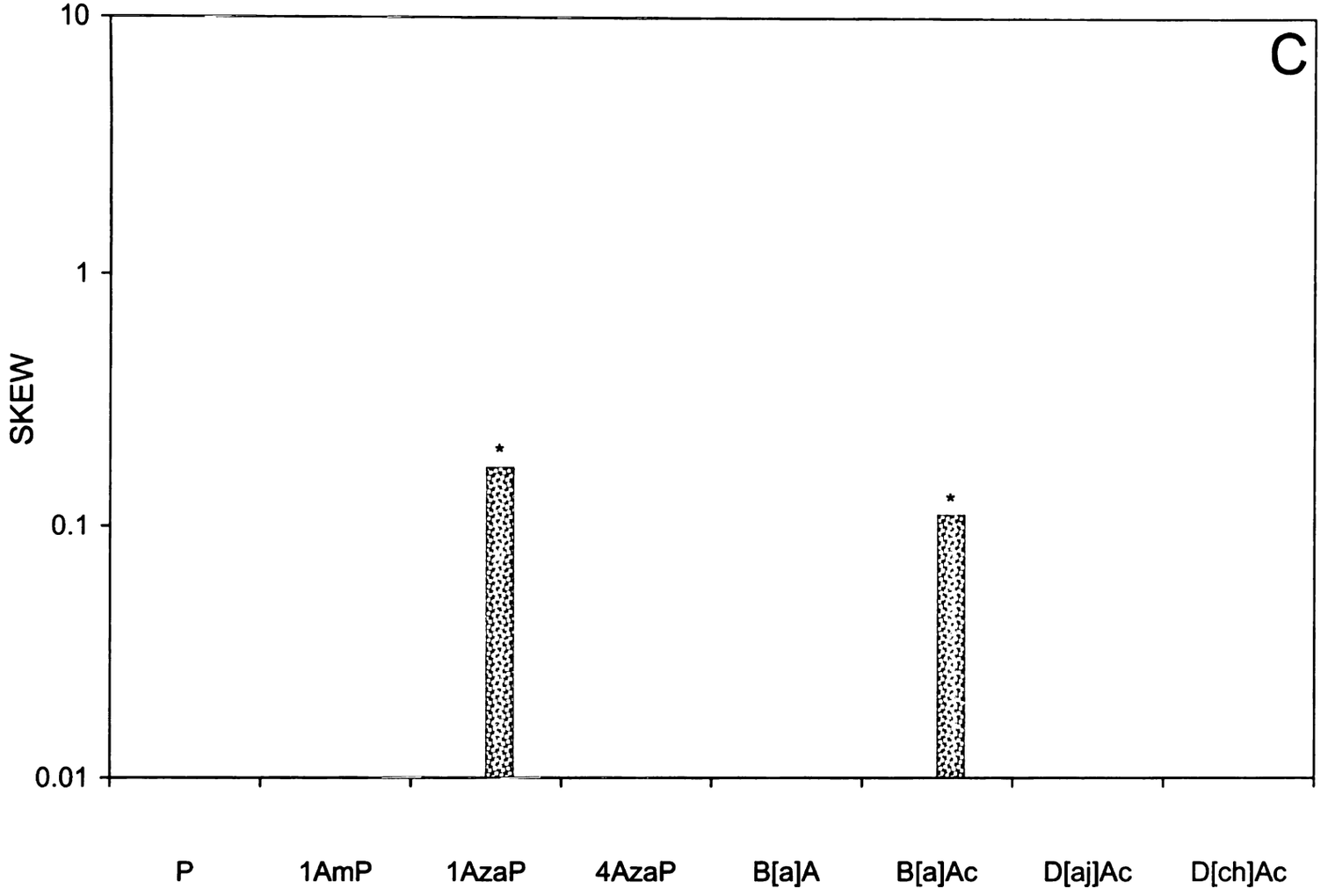

Figure 5.3C: Skew for each solute on BEH in methanol as a function of mobile phase modifier. pure methanol (▪), triethylamine (▪), acetic acid (▪), acetyl acetone (▪). Solutes defined in Table 5.1. Negative skews are indicated by *.

5.3.2 Acetonitrile mobile phase

5.3.2.1 Without modifier

Table 5.2 summarizes the retention factor, reduced plate height, and skew for each solute on each stationary phase in pure acetonitrile mobile phase.

5.3.2.1.1 XBridge C_{18}

The retention factors for most solutes are larger in acetonitrile (Table 5.2) than in methanol mobile phase (Table 5.1), yet are smaller for benz[a]anthracene and dibenz[c,h]acridine. In addition, the retention factors for 1- and 4-azapyrene are larger than that of their parent PAH, pyrene. Since acetonitrile is less polar than methanol, the retention factor is expected to decrease under a partition-dominated mechanism, as observed for benz[a]anthracene. However, the solutes with increased retention are likely dominated by an adsorption mechanism. The increase is small for pyrene (2 %), but larger for the other solutes (38 – 70 %). The increase in retention is consistent with silica supports, however, the increase is less pronounced on the hybrid phases than that reported on the silica phases (320 – 850 %) [29]. In addition, the role of annelation structure is different in acetonitrile mobile phase, with pyrene and benz[a]anthracene having equivalent values for retention factor.

The reduced plate heights are larger in acetonitrile than in methanol, indicating increased broadening. The reduced plate height is largest for 1- and 4-azapyrene, followed by dibenz[a,j]acridine, and pyrene. The first three of these solutes are expected to have larger plate heights than the other solutes due to the accessible nitrogen in the ring structure.

Table 5.2: Retention factor (k), reduced plate height (h), and skew (s) for acetonitrile mobile phase without modifier. Solutes defined in Table 5.1.

Acetonitrile	XBridge C_{18}			XBridge Shield RP_{18}			BEH		
	k	h	s	k	h	s	k	h	s
P	0.608	1200	7.53	0.522	560	11.14	0.016	4.3	0.00
1AmP	0.142	52	3.69	0.276	180	4.74	0.000	7.7	0.00
1AzaP	0.797	6900	4.25	0.581	520	1.29	0.621	160	1.04
4AzaP	0.789	11000	21.09	0.677	4900	9.37	0.334	190	3.76
B[a]A	0.586	250	3.58	0.503	56	2.30	0.000	7.7	0.00
B[a]Ac	0.467	460	3.65	0.476	74	0.44	0.230	11	0.00
D[aj]Ac	0.989	3500	6.87	0.889	280	1.19	0.207	18	0.00
D[ch]Ac	1.096	250	17.67	0.980	14	8.27	0.000	7.7	0.00

The skew is larger for all solutes in acetonitrile than in methanol. Thus, all solutes, both NPAHs and PAHs exhibit more asymmetric peak shapes in acetonitrile. The largest skew occurs for 4-azapyrene and dibenz[c,h]acridine, while the smallest skew occurs for benz[a]anthracene and benz[a]acridine. This is interesting behavior, as dibenz[c,h]acridine has comparable retention to the neutral PAHs in methanol, however is more comparable to the retention of the NPAHs in acetonitrile. On the other hand, benz[a]acridine which has an accessible nitrogen, has similar tailing behavior to its parent PAH, benz[a]anthracene in acetonitrile mobile phase.

5.3.2.1.2 XBridge Shield RP_{18}

The retention factors for all solutes on XBridge Shield follow similar trends to those on XBridge in terms of ring number and annelation (Table 5.2). However, the retention factors for some solutes on XBridge Shield are smaller than those on XBridge.

The reduced plate heights for all solutes are larger in acetonitrile (Table 5.2) than in methanol (Table 5.1). The reduced plate height is largest for 1- and 4-azapyrene, pyrene, and dibenz[a,j]acridine. However, the reduced plate height is smaller for most solutes on XBridge Shield than on XBridge, indicating that less symmetric broadening occurs on the shielded phase. This is evidenced by the value of h for dibenz[c,h]acridine on XBridge Shield (h = 13.5). Dibenz[c,h]acridine is the only solute with such a low value for the reduced plate height, however it indicates that some solutes are not as greatly affected by the symmetric sources of broadening as others.

The skew for most solutes on XBridge Shield is similar to that on XBridge. The skew is largest for pyrene, followed by 4-azapyrene and dibenz[c,h]acridine. However, the skew is smaller on XBridge Shield than on XBridge for all solutes except 1-aminopyrene and pyrene. This behavior suggests that the shielded phase decreases the tailing for most solutes for acetonitrile mobile phase.

When the two C_{18} phases are compared, an interesting trend is observed as a function of retention factor. An increase in retention factor between the two phases causes an increase in both reduced plate height and skew. For example, k for pyrene is larger on XBridge than on XBridge Shield with correspondingly larger values for h and skew. This behavior is observed for all solutes except benz[a]acridine, which shows only a small change in retention factor, but large changes for plate height and skew. The opposite trend was observed for methanol mobile phase, which suggests an inherent difference in the separation behavior for the two mobile phases.

5.3.2.1.3 Bridged-ethylene hybrid (BEH)

The retention factors for the retained solutes are larger in acetonitrile (Table 5.2) than in methanol (Table 5.1). Several of the solutes (1-aminopyrene, benz[a]anthracene, and dibenz[c,h]acridine) are non-retained, while the other solutes are retained to some degree. Pyrene is slightly retained, which is inconsistent with its behavior in methanol. This increase in retention for pyrene in acetonitrile is consistent with the increase in broadening and skew on the C_{18} phases.

Reduced plate heights are larger in acetonitrile than in methanol for BEH. The reduced plate height for the retained acridines are two times the magnitude of those in methanol, while those for the azapyrenes are approximately 35 times those in methanol. This indicates a large increase in broadening on the hybrid support for acetonitrile mobile phase.

Of the retained solutes, only 1- and 4-azapyrene have positive skew, indicating tailing behavior. The solutes that are retained on the BEH material correspond to the same solutes that exhibit severe peak tailing on the C_{18} derivatized phases. This further confirms that retention on the underlying particle, not asymmetry on the underlying particle, contributes to the asymmetry on the C_{18} derivatized phases. The same trend was observed for methanol mobile phase.

Considering the increased retention and broadening in acetonitrile, it is clear than the apparent retention mechanism is different for the two mobile phases. Hybrid supports are greatly affected by the type of mobile phase (i.e. protic vs. aprotic). The hydrogen bonding ability of methanol with surface silanols and the nitrogen-containing solutes could be the main reason for the differences in retention and shape.

5.3.2.2 With mobile phase modifier

The effect of each mobile phase modifier is examined as a function of retention factor, reduced plate height, and skew. Detailed information on the change in each parameter is given in Appendix 5A.1.

Figure 5.4 shows the effect of mobile phase modifier on retention factor. For most solutes, triethylamine and acetic acid modifiers cause a decrease in retention factor for all phases. For acetyl acetone modifier, the retention factor increases for some solutes yet decreases for others. Pyridine causes an increase in retention factor for XBridge and BEH, the only phases where it was examined. The combination of acetic acid and triethylamine as mobile phase modifiers does not cause a change in retention factor for XBridge. However, a significant decrease in retention factor is observed for most solutes on BEH.

Figure 5.5 shows the effect of mobile phase modifier on reduced plate height. Triethylamine causes a decrease for most solutes on most phases, however, there are several exceptions where an increase is observed. Acetic acid does not cause an overall improvement in reduced plate height. The plate height increases for some solutes, yet decreases or remains the same for others on the C_{18} phases. Acetic acid does not cause any noticeable change in plate height for BEH. Acetyl acetone causes an increase in plate height for some solutes and a decrease for others. Pyridine causes an increase in plate height for all solutes on the XBridge and BEH phases, the only two phases examined. The combination of acetic acid and triethylamine modifier causes an overall reduction in plate height on XBridge and BEH.

Figure 5.6 shows the effect of mobile phase modifier on skew. Almost all mobile phase modifiers cause a decrease in skew for acetonitrile. The combination of acetic acid and triethylamine causes the greatest decrease in skew, with some solutes having a skew equal to zero. Triethylamine causes the

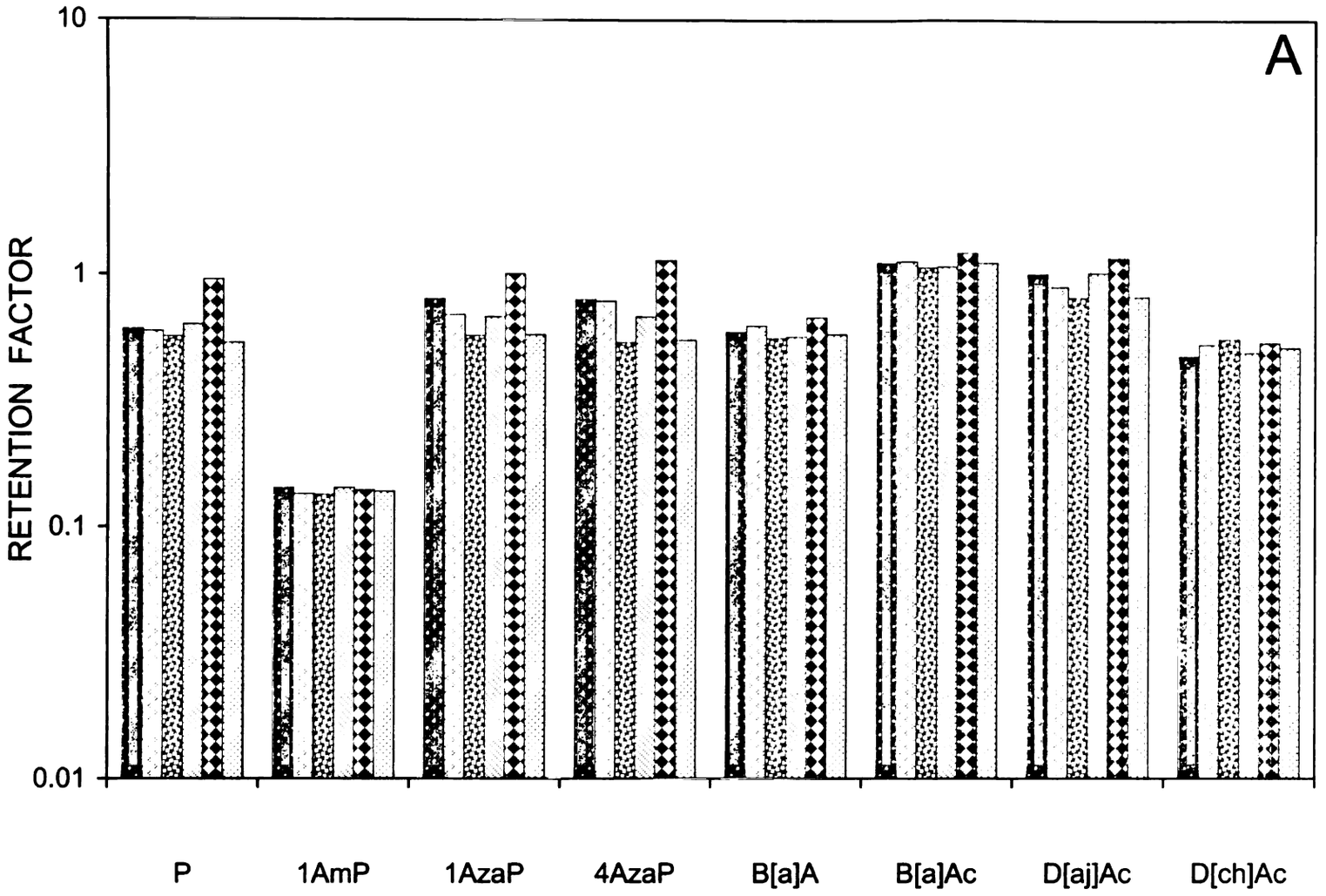

Figure 5.4A: Retention factor for each solute on XBridge C_{18} in acetonitrile as a function of mobile phase modifier. pure acetonitrile (▪), triethylamine (▨), acetic acid (▩), acetyl acetone (▨), pyridine (▪), acetic acid with triethylamine (▨). Solutes defined in Table 5.1.

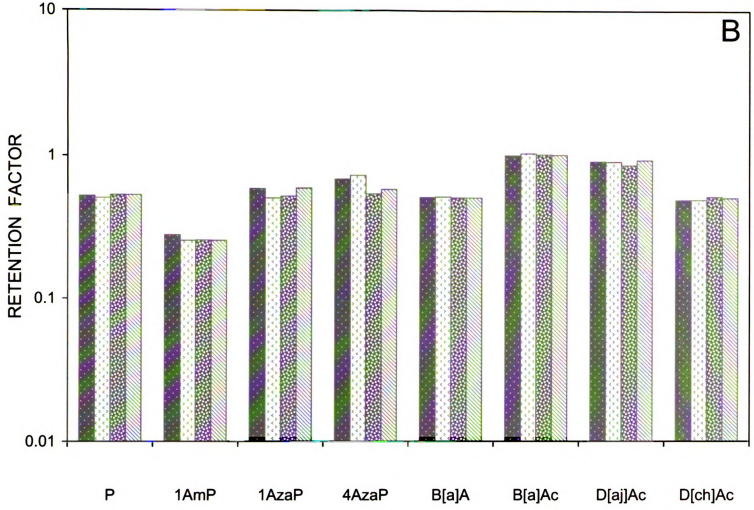

Figure 5.4B: Retention factor for each solute on XBridge Shield RP_{18} in acetonitrile as a function of mobile phase modifier. pure acetonitrile (▩), triethylamine (⁘), acetic acid (▩), acetyl acetone (▨). Solutes defined in Table 5.1.

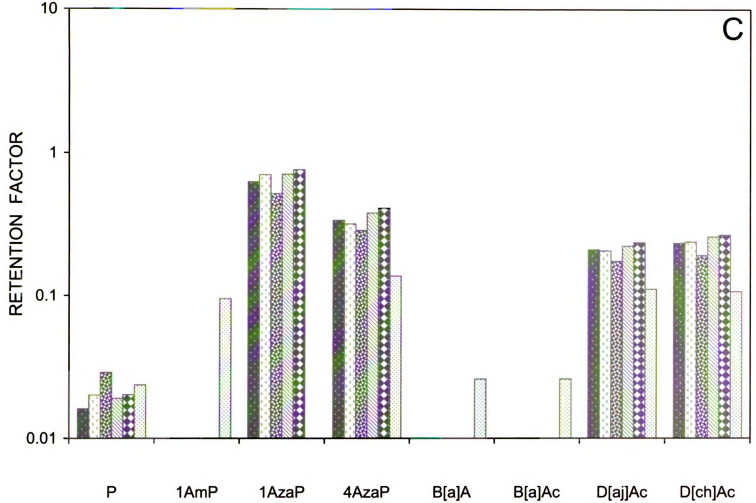

Figure 5.4C: Retention factor for each solute on BEH in acetonitrile as a function of mobile phase modifier. pure acetonitrile (■), triethylamine (▒), acetic acid (▒), acetyl acetone (▒), pyridine (▒), acetic acid with triethylamine (▒). Solutes defined in Table 5.1.

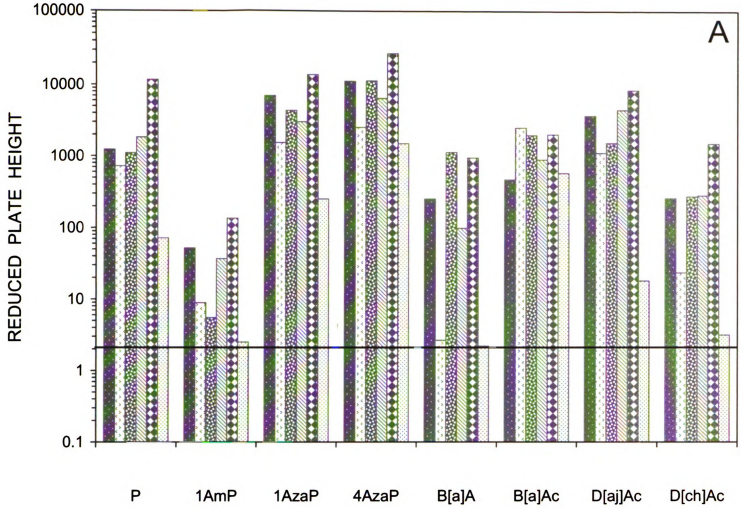

Figure 5.5A: Reduced plate height for each solute on XBridge C_{18} in acetonitrile as a function of mobile phase modifier. pure acetonitrile (■), triethylamine (▒), acetic acid (▒), acetyl acetone (▒), pyridine (▒), acetic acid with triethylamine (▒). Solutes defined in Table 5.1.

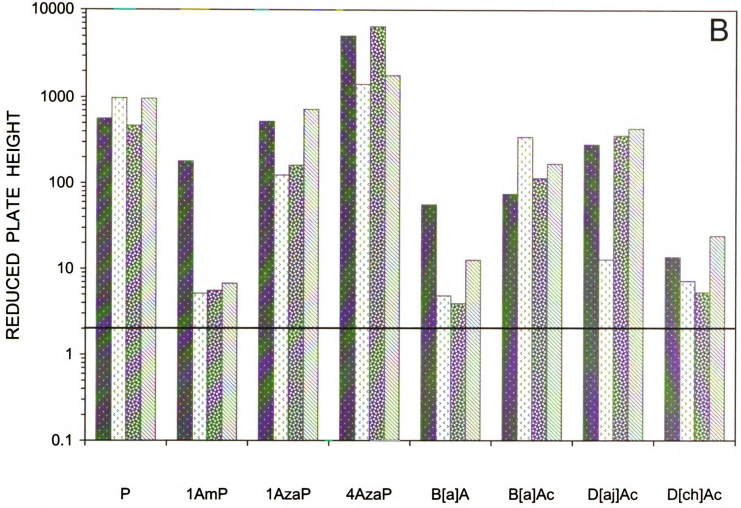

Figure 5.5B: Reduced plate height for each solute on XBridge Shield RP_{18} in acetonitrile as a function of mobile phase modifier. pure acetonitrile (■), triethylamine (▒), acetic acid (▓), acetyl acetone (▨). Solutes defined in Table 5.1.

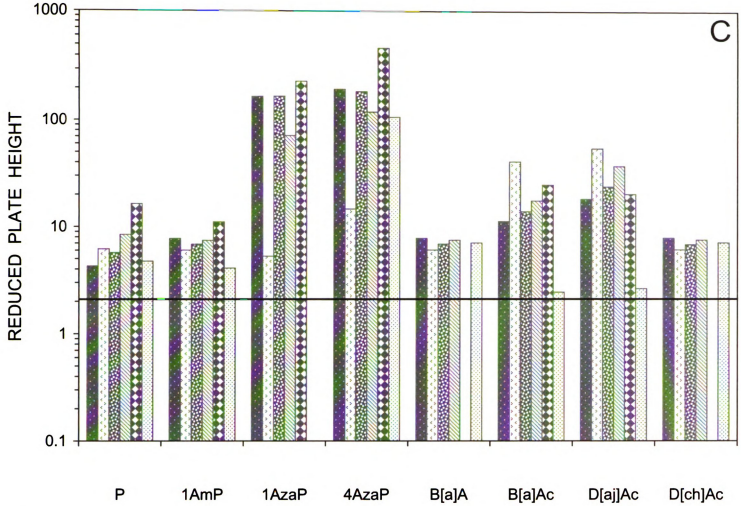

Figure 5.5C: Reduced plate height for each solute on BEH in acetonitrile as a function of mobile phase modifier. pure acetonitrile (■), triethylamine (▒), acetic acid (▒), acetyl acetone (▒), pyridine (▒), acetic acid with triethylamine (▒). Solutes defined in Table 5.1.

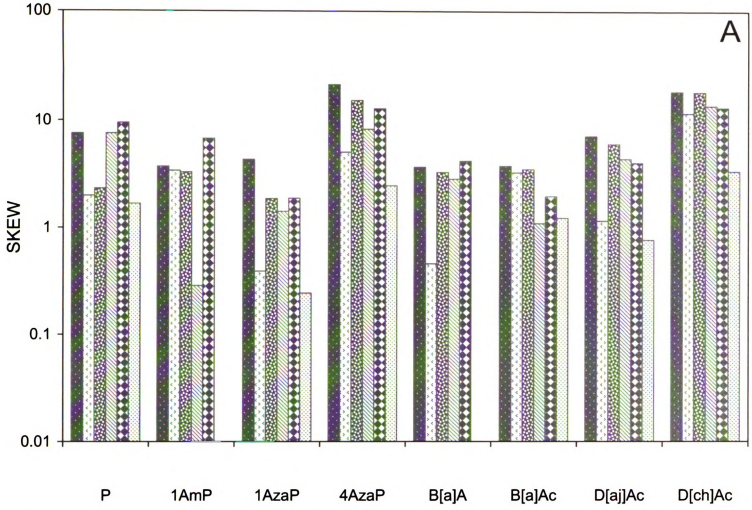

Figure 5.6A: Skew for each solute on XBridge C_{18} in acetonitrile as a function of mobile phase modifier. pure acetonitrile (■), triethylamine (⁘), acetic acid (▩), acetyl acetone (▨), pyridine (▦), acetic acid with triethylamine (▧). Solutes defined in Table 5.1.

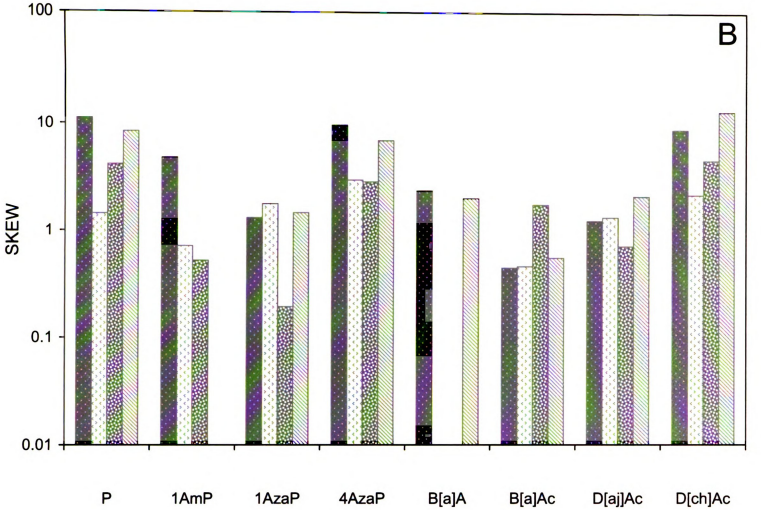

Figure 5.6B: Skew for each solute on XBridge Shield RP_{18} in acetonitrile as a function of mobile phase modifier. pure acetonitrile (■), triethylamine (▒), acetic acid (▓), acetyl acetone (▨). Solutes defined in Table 5.1.

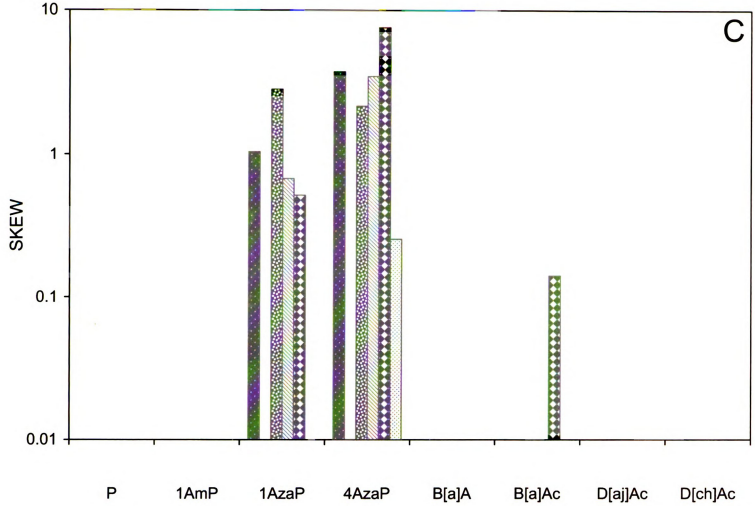

Figure 5.6C: Skew for each solute on BEH in acetonitrile as a function of mobile phase modifier. pure acetonitrile ( ), triethylamine ( ), acetic acid ( ), acetyl acetone ( ), pyridine ( ), acetic acid with triethylamine ( ). Solutes defined in Table 5.1.

next greatest decrease, followed by acetic acid and acetyl acetone. On the other hand, pyridine causes an increase in skew for most solutes. It is important to note that skew decreases for most solutes, however is not completely eliminated. This phenomenon will be discussed further in Section 5.4.

5.4 Discussion

As seen in Section 5.3, interesting behavior is observed as a function of solutes, mobile phase, and stationary phase. In this section, possible explanations for the behavior are discussed and hypotheses concerning the types of sites contributing to the retention and peak shape are examined.

5.4.1 Effect of bridged-ethylene hybrid (BEH) particle

The BEH particle has interesting retention behavior. Only basic solutes are retained in methanol, while almost all solutes are more retained in acetonitrile. Interestingly, almost all solutes have symmetric peak shape on BEH. The symmetric peak shape suggests that the adsorption-desorption step is not rate-limiting. The peak shapes are asymmetric for solutes on the C_{18} phases. Thus, the asymmetry arises after derivatization of the support particle. That is, the kinetically slow step is not adsorption of the solute at silanol sites in the underlying support. This hypothesis will be discussed in more detail in Section 5.4.5.

5.4.2 Effect of polar embedded group

The direct comparison of the two C_{18} derivatized phases provides specific information concerning the polar embedded group. Typically, the polar embedded group improves the peak asymmetry for most, if not all, basic solutes.

Several authors have discussed the reason for this improvement. First, the carbamate polar embedded group could directly interact with surface silanols, decreasing the interaction of those silanols with the solutes. O'Gara *et al.* [23] studied the effect of carbamate surface concentration on tailing behavior using aqueous mobile phases. They determined that peak shape improvement did not result from the direct interaction of the carbamate with silanols. They suggested that, instead, the surface layer contains a higher concentration of the aqueous mobile phase component due to the presence of the polar carbamate group. Thus, the strength of the interaction between a basic solute and residual silanols is reduced. A similar argument was made by Neue *et al.* that, in aqueous mobile phases, the polar embedded group attracts water molecules from the bulk mobile phase to form a tightly bound water layer [24]. The water layer effectively blocks the accessible silanols in the underlying material, yet does not interfere with the C_{18} region, resulting in symmetric peak shapes.

In the present research, however, aqueous mobile phases are not employed, thus eliminating water from playing a role in peak symmetry. Instead, the polar embedded group is free to interact with the solute, the mobile phase, and residual silanols in the support. The difference in peak shape as a function of solute, mobile phase, and stationary phase suggests that each of these variables play a role in the separation process. In methanol mobile phase, the peak tailing worsens for four solutes and remains constant for the others, while in acetonitrile, the peak tailing improves for six of the eight solutes for the phase containing a polar embedded group. In methanol, the solvent can hydrogen

bond to the residual silanols in the support and, in addition, hydrogen bond to the carbamate polar embedded group. In acetonitrile, hydrogen bonding cannot occur between the solvent and the silanols, leaving the silanols free to hydrogen bond with the polar embedded group. The polar embedded group – silanol site interaction masks the silanols, reducing the interaction of solute and silanol, and in turn, decreases peak tailing. However, many of the C_{18} chains would remain unbent (unbound to silanols) so that the carbamate polar group is accessible. This hypothesis explains the greater tailing in acetonitrile than methanol, as the same interactions of the solutes with the carbamate could occur, yet without hydrogen bonding from solvent. For XBridge, the tailing worsens by as much as 15 times for methanol compared to acetonitrile, while for XBridge Shield, the tailing worsens only by as much as 4 times. However, the benefit of the polar embedded group is not as apparent using pure organic mobile phase as it is using aqueous mobile phases.

5.4.3 Effect of mobile phase

The differences in retention behavior and peak shape that occur for methanol (Table 5.1) compared to acetonitrile mobile phase (Table 5.2) are apparent. The difference in peak tailing is due to the difference in the chemical properties of the solvent. In silica-based materials, it has been hypothesized that methanol hydrogen bonds to accessible silanols. Methanol can also hydrogen bond to residual silanols in the hybrid support, as discussed in Chapter 4. For this reason, tailing in methanol is less severe than that in acetonitrile. Relative to a methanol mobile phase, increased tailing is observed for acetonitrile on the

hybrid C_{18} materials used in the current study. Differences in mobile phase properties also manifest themselves on the underlying BEH support, where increased retention occurs in acetonitrile compared to methanol. This behavior suggests that the bulk mobile phase not only plays a role in retention, but also plays a significant role in the peak shape for a given solute.

5.4.4 Effect of mobile phase modifiers

5.4.4.1 Triethylamine

Triethylamine blocks residual silanol sites in silica supports, which reduces or eliminates the interaction of silanols with other amines to decrease the tailing for such solutes [7]. This process occurs because triethylamine acts as a proton acceptor, and can effectively bind to silanols in the underlying support. In this study, peak shape sometimes improves in the presence of triethylamine, but a universal improvement is not seen. On XBridge with methanol mobile phase, an improvement in peak shape is observed. This behavior suggests that many of the slow sites are blocked, however, they are not completely eliminated. However, on XBridge Shield, an increase in plate height and skew is observed. This behavior suggests that the slow sites are not blocked, and perhaps additional slow sites are created. The retention and symmetry of solutes on BEH does not change with addition of triethylamine, which suggests limited interaction of the modifier with the support material. Thus, in XBridge Shield, triethylamine may interact with the carbamate embedded group in the C_{18} chain in such a way to cause an increase in the broadening and asymmetry. The change is not universal, suggesting that solute structure plays a significant role.

On the other hand, triethylamine is beneficial for both C_{18} stationary phases in acetonitrile, where tailing is more pronounced. The reduced plate height and skew decrease on all phases including BEH. In fact, the reduced plate height and skew are comparable to those in pure methanol for XBridge Shield. This reduction is due to the ability of triethylamine to hydrogen bond to silanols. The effect is greater in acetonitrile as no hydrogen bonding of the solvent with residual silanols can occur.

The concentration of triethylamine in each mobile phase is similar to concentrations reported in the literature [7,9,13]. This concentration is chosen because the number of molecules of triethylamine should be sufficient to cover the number of accessible silanols. This point suggests that broadening and asymmetry may come from another set of sites in the stationary phase. Therefore, triethylamine improves peak shape under some conditions, yet does not provide a clear indication as to the type of slow site.

5.4.4.2 Acetic acid

The change in retention and skew associated with acetic acid modifier can be ascribed to the acid dissociation constant for each solute. In acidic media, the NPAHs could become protonated. The protonation could change the mechanism of interaction with the slow site to yield lower retention factors and a change in peak asymmetry. This behavior is also observed on BEH, where many solutes elute before the non-retained marker. When solutes become protonated they are excluded from the pores of the solute and thus elute prior to the non-retained marker. The degree of protonation is indicated by the retention factor. For

example, 1-azapyrene elutes before the non-retained marker and is likely fully protonated. Benz[a]acridine and dibenz[a,j]acridine are more retained than the non-retained marker, yet have decrease retention compared to pure mobile phase and are likely only partially protonated. The neutral solutes, pyrene and benz[a]anthracene, are least affected by the acetic acid because of the lack of nitrogen in the structure. The difference in retention and skew for similar solutes can be explained by their ability to accept a hydrogen atom. For example, 4-azapyrene does not exhibit the same behavior as 1-azapyrene, which suggests that the two isomers have different pK_a values. While information regarding the pK_a for the azapyrenes is not currently available, it is available for isomers of benz[a]acridine. The pK_a of benz[a]acridine is 4.70, while the pK_a of benz[c]acridine is 3.45 in water at 298 K. In addition, the pK_a values explain some of the trends observed in this study. For example, benz[a]acridine contains one fewer ring than dibenz[a,j]acridine, while benz[c]acridine contains one fewer ring that dibenz[c,h]acridine. If the pK_as of the dibenzacridines are similar to their benzacridine counterparts, then dibenz[a,j]acridine would have a higher pK_a value and become neutral at a higher pH value. The difference in protonation of dibenz[a,j]acridine and dibenz[c,h]acridine would explain the retention and asymmetry observed on XBridge.

On XBridge Shield, however, acetic acid only causes a negative retention factor for one solute and none of the solutes exhibit fronting behavior. All NPAHs are less retained when acetic acid is present. However, the increase in skew

indicates an increased interaction with the slow site or the addition of a new slow site. In this case, the protonated solute may be attracted to the carboxyl group of the carbamate due to the positive charge, which causes an increase in the skew for any protonated solute. Therefore, acetic acid is not beneficial for improvement of peak shape for NPAHs in methanol mobile phase.

Retention and skew decrease relative to pure acetonitrile for most solutes on the C_{18} phases when acetic acid is present in the mobile phase. In addition, k and skew on BEH are similar with and without acetic acid modifier, indicating protonation does not occur to the same extent as it did with methanol mobile phase. The difference in protonation in methanol versus acetonitrile is expected as the pK_a for simple amines is known to differ as a function of solvent. The pK_as of both simple and complex amines are larger in acetonitrile than in methanol, indicating a difference in protonation with solvent [30,31]. In this case, acetic acid can hydrogen bond with residual silanols (in XBridge and XBridge Shield) and to both the carboxyl and amine groups of the carbamate (in XBridge Shield) to block both types of sites. When these sites are blocked, the solute cannot interact with the slow site and, thus, tailing decreases. This also explains the slight decrease in retention on both phases. Thus, acetic acid is an adequate mobile phase modifier for an acetonitrile mobile phase, yet does not improve the peak shape to the same extent as triethylamine.

5.4.4.3 Acetyl acetone

Acetyl acetone is chosen for its ability to selectively bind to metals in the support material. If the cause of the tailing is due to solute interaction with

metals, then a decrease in tailing behavior would be observed. However, acetyl acetone is detrimental to the peak shape for the C_{18} phases when using a methanol mobile phase. No change in the retention or peak shape is observed on BEH. In acetonitrile, the peak shape is improved for most solutes on all phases. If metal chelation is occurring with the acetyl acetone, it seems that it is only occurring in acetonitrile mobile phase. In addition, acetyl acetone could hydrogen bond with silanols or with the carbamate embedded group. However, these effects would cause an improvement in tailing, which is not seen in methanol mobile phase. While it is unclear what role acetyl acetone is playing in the separation, this role is solvent dependent. That is, acetyl acetone is detrimental in methanol, but beneficial in acetonitrile.

5.4.4.4 Pyridine

Pyridine is a basic amine with similar chemical structure to the solutes of interest and, for this reason, was chosen as a possible displacing agent. Overall, the tailing behavior worsens with the addition of pyridine for XBridge C_{18} and BEH phases. Clearly, pyridine does not act as a displacing agent for either phase. While the mechanism of interaction is unclear, it is clear that pyridine is not an ideal choice for a mobile phase modifier under the current conditions.

5.4.4.5 Acetic acid and triethylamine

Overall, the combination of triethylamine and acetic acid modifiers is most influential in improving the peak shape. This combination could cause the change in two types of sites simultaneously. Values for retention factor for the solutes are between the retention factors for the two modifiers separately.

However, the values for reduced plate height and skew are dramatically reduced. This observation provides evidence for at least two types of sites that can be modified simultaneously when two distinctly different types of modifiers are added to the mobile phase. While it is unclear exactly how this acid – base combination interacts with the solutes or stationary phases, it is an obvious improvement over each of the other modifiers.

5.4.5 Additional arguments

It is clear that one type of modifier does not completely eliminate the broadening and tailing behavior. These results indicate that a solutes affinity for silanol sites may be the initial source of the problem, however, it alone is not the slow step. Only when the support is derivatized with C_{18} is peak asymmetry observed. Thus, solutes that have an affinity for the silanol sites will be attracted to them, but must migrate through the C_{18} layer to interact. Diffusion through this C_{18} layer is slow compared to the actual adsorption-desorption step. Thus, diffusion dominates the kinetic behavior and is the kinetically slow step. The attraction of the solutes to the residual silanols is greater is acetonitrile. This attraction causes a greater number of solute molecules to migrate through the C_{18}, thus creating a greater degree of peak asymmetry.

The polar embedded group did not improve peak asymmetry. In fact, the polar embedded group may deleteriously effect the diffusion through the C_{18} layer, creating an additional site that solutes must navigate. The addition of mobile phase modifiers somewhat improves the asymmetry for some solutes under some conditions. This slight improvement is due to competition at the

silanol site from the modifier. However, the solutes continue to have affinity for the silanol sites and diffuse through the C_{18}. Since diffusion is the slow step, it continues to dominate the kinetic behavior even when mobile phase modifiers are included.

5.5 Conclusions

The effect of the underlying particle, the polar embedded group, and mobile phase modifiers on retention and peak shape provides interesting results. Basic NPAH solutes are slightly retained in methanol, yet are more retained in acetonitrile on the underlying particle. However, the peak shapes are symmetric, indicating that adsorption and desorption at residual silanols is not a kinetically slow process. The polar embedded group does improve the overall peak shape in acetonitrile mobile phase. However, asymmetry is still observed. Therefore the polar embedded group in the C_{18} phase only partially helps shield the solute from the support material.

Peak tailing in methanol is substantially better than that in acetonitrile. This is due to the hydrogen bonding ability of methanol as discussed in Chapter 4. The additional tailing in acetonitrile can be reduced using mobile phase modifiers, but does not compare to pure methanol mobile phase. The effect of each modifier is both solute and phase dependent. Many of the mobile phase modifiers improve peak shape for several solutes on one or both C_{18} phases, but do not cause an overall improvement. The combination of triethylamine and acetic acid substantially improves the overall peak shape. Triethylamine

provides comparable improvement on the XBridge phase. However, no modifier or pair of modifiers completely removes the tailing from all peaks.

The combination of these results indicates that a solutes affinity for silanol sites may be the initial source of the problem, however, it alone is not the slow step. Only when the support is derivatized with C_{18} is peak asymmetry observed. Thus, solutes can partition into and out of the C_{18} chain and can adsorb and desorb from silanol sites. These steps, taken individually, have relatively rapid mass transfer and adsorption-desorption kinetics. However, when the steps are combined sequentially, as is the case in a chromatographic separation, they are kinetically slow. That is, the solutes that have an affinity for the silanol sites will be attracted to them, but must migrate through the C_{18} layer to interact. Diffusion through this C_{18} layer is slow compared to the actual adsorption-desorption step. Thus, diffusion dominates the kinetic behavior and is the kinetically slow step.

Refe

[1]

[2]

[3]

[4]

[5]

[

References

[1] J. Nawrocki, *Chromatographia 31* (**1991**) 177-192.

[2] J. Nawrocki, *Chromatographia 31* (**1991**) 193-205.

[3] Y.K. Ye, R.W. Stringham, *J. Chromatogr. A 927* (**2001**) 47-52.

[4] R.K. Gilpin, S.S. Yang, G. Werner, *J. Chromatogr. Sci. 26* (**1988**) 388-400.

[5] J.J. Naleway, N.E. Hoffman, *J. Liq. Chromatogr. 4* (**1981**) 1323-1338.

[6] A. Wehrli, J.C. Hildenbrand, H.P. Keller, R. Stampfli, R.W. Frei, *J. Chromatogr. A 149* (**1978**) 199-210.

[7] K.E. Bij, C. Horváth, W.R. Melander, A. Nahum, *J. Chromatogr. 203* (**1981**) 65-84.

[8] R. Gill, S.P. Alexander, A.C. Moffat, *J. Chromatogr. A 247* (**1982**) 39-45.

[9] J.S. Kiel, S.L. Morgan, R.K. Abramson, *J. Chromatogr. A 320* (**1985**) 313-323.

[10] R.W. Roos, C.A. Lau-Cam, *J. Chromatogr. A 370* (**1986**) 403-418.

[11] G. Stoev, D. Uzunov, *J. Liq. Chromatogr. 15* (**1992**) 3097-3114.

[12] A.I. Gasco-Lopez, A. Santos-Montes, R. Izquierdo-Hornillos, *J. Chromatogr. Sci. 35* (**1997**) 525-535.

[13] M. Reta, P.W. Carr, *J. Chromatogr. A 855* (**1999**) 121-127.

[14] Y.K. Ye, R. Stringham, *J. Chromatogr. A 927* (**2001**) 53-60.

[15] X. Li, V.L. McGuffin, *J. Liq. Chromatogr. Relat. Technol. 30* (**2007**) 937-964.

[16] Y.K. Ye, R.W. Stringham, M.J. Wirth, *J. Chromatogr. A 1057* (**2004**) 75-82.

[17] P.C. Sadek, C.J. Koester, L.D. Bowers, *J. Chromatogr. Sci. 25* (**1987**) 489-493.

[18] P.C. Sadek, P.W. Carr, L.D. Bowers, *J. Liq. Chromatogr. 8* (**1985**) 2369-2386.

[19] R.C. Watson, P.N. Shaw, H.J. Ritchie, P. Ross, D.A. Barrett, *J. Liq. Chromatogr. Relat. Technol. 24* (**2001**) 1253-1273.

[20] T. Cecchi, F. Pucciarelli, P. Passamonti, S. Ferraro, *J. Liq. Chromatogr. Relat. Technol. 22* (**1999**) 429-440.

[21] A.E. Martell, Determination and Use of Stability Constants, VCH Publishers, New York, **1992**.

[22] T.L. Ascah, B. Feibush, *J. Chromatogr. 506* (**1990**) 357-369.

[23] J.E. O'Gara, D.P. Walsh, B.A. Alden, P. Casellini, T.H. Walter, *Anal. Chem. 71* (**1999**) 2992-2997.

[24] U.D. Neue, Y.-F. Cheng, Z. Lu, B.A. Alden, P.C. Iraneta, C.H. Phoebe, K. Van Tran, *Chromatographia 54* (**2001**) 169-177.

[25] K.D. Wyndham, T.H. Walter, P.C. Iraneta, U.D. Neue, P.D. McDonald, D. Morrison, M. Baynham, *Waters White Paper 720001159EN* (**2006**) 8 pp.

[26] J.E. O'Gara, K.D. Wyndham, *J. Liq. Chromatogr. Relat. Technol. 29* (**2006**) 1025-1045.

[27] S.B. Howerton, C. Lee, V.L. McGuffin, *Anal. Chim. Acta 478* (**2003**) 99.

[28] S.B. Howerton, V.L. McGuffin, *J. Chromatogr. 1030* (**2004**) 3-12.

[29] V.L. McGuffin, S.B. Howerton, X. Li, *J. Chromatogr. A 1073* (**2005**) 63-73.

[30] R. Carabias-Martinez, E. Rodriguez-Gonzalo, J. Dominguez-Alvarez, E. Miranda-Cruz, *Anal. Chim. Acta 584* (**2007**) 410-418.

[31] M.D. Cantu, S. Hillebrand, E. Carrilho, *J. Chromatogr. A 1068* (**2005**) 99-105.

APPENDIX 5A.1

DETAILED AFFECTS OF THE MOBILE PHASE MODIFIERS

5A.1. Introduction

As discussed in Chapter 5, the addition of mobile phase modifiers affects solute retention and peak shape. This appendix provides a detailed examination of the effect of each mobile phase modifier in methanol and acetonitrile mobile phases.

5A.2. Methanol mobile phase with modifiers

5A.2.1. XBridge C_{18}

Table 5A.1 provides the retention factor, reduced plate height, and skew for solutes on XBridge C_{18}. Compared with pure methanol mobile phase (Table 5.1), triethylamine modifier causes a decrease in retention factor (2 to 10 %), as well as smaller plate heights for each solute (by as much as 92 %). The skew decreases for solutes with asymmetric peak shape, but the asymmetry is not completely removed.

Acetic acid modifier causes a decrease in retention. The most notable decreases occur for 1-azapyrene, benz[a]acridine, and dibenz[a,j]acridine. 1-Azapyrene has a negative retention factor, indicating it has an elution time less than that of the non-retained marker. In a strictly partition-like mechanism, this behavior could indicate that 1-azapyrene becomes charged (via protonation) in the presence of acetic acid. The reduced plate height remains unchanged for most solutes, yet decreases by 95 % for 1-azapyrene and benz[a]acridine. The skew decreases for all solutes that exhibit asymmetric peak shapes.

Table 5A.1: Effect of mobile phase modifier on retention factor (k), reduced plate height (h), and skew (s) for XBridge C_{18} with methanol mobile phase. Solutes defined in Table 5.1.

XBridge C_{18}	Triethylamine			Acetic Acid			Acetyl Acetone		
	k	h	s	k	h	s	k	h	s
P	0.570	1.5	0.00	0.583	2.7	0.59	0.592	96	3.56
1AmP	0.085	2.1	0.00	0.065	2.2	0.00	0.085	1.8	0.00
1AzaP	0.216	5.7	0.08	-0.057	2.7	-0.14	0.268	400	1.82
4AzaP	0.257	60	1.54	0.270	430	2.04	0.285	260	8.87
B[a]A	0.677	1.9	0.00	0.693	2.1	0.00	0.689	81	4.25
B[a]Ac	0.273	42	0.71	0.109	9.0	-0.25	0.316	680	1.33
D[aj]Ac	0.548	0.69	0.00	0.351	3.8	-0.58	0.597	350	5.05
D[ch]Ac	1.252	2.3	1.15	1.295	2.4	1.45	1.258	6.2	14.30

(

o

fo

5A

ske

pha

for

reter

(anth

(2 to

skew

and

asym

effect

PAHs

retentio

Furthermore, the skew is negative for several solutes, 1-azapyrene, benz[a]acridine, and dibenz[a,j]acridine, indicating a fronting peak shape. The fronting shape corresponds with decreased retention and reduced plate height for the same solutes.

Acetyl acetone modifier does not cause a significant change in retention (0.5 to 11 %), with retention increasing for some solutes and decreasing for others. The reduced plate height and asymmetry increase for all solutes, except for 1-aminopyrene, where a decrease in the skew is observed.

5A.2.2. XBridge Shield RP_{18}

Table 5A.2 summarizes the retention factor, reduced plate height, and skew for solutes on XBridge Shield RP_{18}. Relative to pure methanol mobile phase (Table 5.1), triethylamine modifier causes an increase in retention factor for PAHs and NPAHs with condensed annelation structure (pyrenes). The retention factor decreases for NPAHs with extended annelation structure (anthracenes and acridines). The reduced plate height increases for all solutes (2 to 94 %), yet remains unchanged for 1-azapyrene and dibenz[a,j]acridine. The skew increases for most solutes, yet decreases for 1-azapyrene, benz[a]acridine, and dibenz[a,j]acridine. Thus, the majority of peaks are wider and more asymmetric when triethylamine is present in the mobile phase, opposite the effect on XBridge.

Acetic acid modifier causes an increase in retention factor for the neutral PAHs and dibenz[c,h]acridine, while a decrease occurs for all other solutes. The retention factor for 1-azapyrene is negative, as was observed on XBridge. The

Table 5A.2: *Effect of mobile phase modifier on retention factor (k), reduced plate height (h), and skew (s) for XBridge Shield RP*

Table 5A.2: Effect of mobile phase modifier on retention factor (k), reduced plate height (h), and skew (s) for XBridge Shield RP_{18} with methanol mobile phase. Solutes defined in Table 5.1.

XBridge Shield RP_{18}	Triethylamine			Acetic Acid			Acetyl Acetone		
	k	h	s	k	h	s	k	h	s
P	0.542	280	3.54	0.516	21	4.12	0.540	260	4.73
1AmP	0.253	92	5.46	0.219	8.6	0.00	0.243	19	1.74
1AzaP	0.243	220	0.35	-0.147	220	1.02	0.312	1400	1.88
4AzaP	0.314	830	5.73	0.285	750	4.63	0.330	750	4.79
B[a]A	0.598	6.6	0.58	0.635	7.3	0.00	0.620	6.2	0.08
B[a]Ac	0.294	53	0.78	0.140	140	1.38	0.314	180	1.01
D[aj]Ac	0.674	7.4	0.00	0.513	90	3.89	0.735	220	3.37
D[ch]Ac	1.199	17	12.94	1.296	9.0	1.65	1.213	47	11.39

reduc

solute

symm

oppos

XBrid

excep

reduce

5A.2.3

for sol

triethyl

height

change

more t

solutes

dibenz

for all

becom

symm

chang

occurs

reduced plate height increases for all solutes. The skew increases for most solutes, decreases for dibenz[a,j]acridine, yet remains unchanged for the symmetric solutes. The increase in broadening and skew on XBridge Shield is opposite that on XBridge. In contrast, fronting peak shapes do not arise on XBridge Shield.

Acetyl acetone causes an increase in retention factor for all solutes, except benz[a]anthracene and dibenz[c,h]acridine, which remain constant. The reduced plate height and skew increase for all solutes.

5A.2.3. Bridged-ethylene hybrid (BEH) particle

Table 5A.3 tabulates the retention factor, reduced plate height, and skew for solutes on BEH. Compared to pure methanol mobile phase (Table 5.1), triethylamine modifier produces no change in retention factor. The reduced plate height increases (6 to 43 %) for each retained solute. The skew does not change. That is, the majority of the peaks are wider, but not more retained or more tailing when triethylamine is present.

Acetic acid modifier causes a decrease in retention factor for all retained solutes. Several solutes (pyrene, 1-azapyrene, benz[a]acridine, and dibenz[a,j]acridine) exhibit negative retention factors. The reduced plate height for all solutes slightly increases. Two solutes (1-azapyrene and benz[a]acridine) become fronting with negative values for the skew, while all others remain symmetric (skew = 0). Acetyl acetone modifier brings about no significant change in retention factor. An overall increase in the reduced plate height occurs. There is no change in the skew, with all solutes remaining symmetric.

Table 5A.3: Effect of mobile phase modifier on retention factor (k), reduced plate height (h), and skew (s) for BEH support with methanol mobile phase. Solutes defined in Table 5.1.

BEH	Triethylamine			Acetic Acid			Acetyl Acetone		
	k	h	s	k	h	s	k	h	s
P	0.000	5.7	0.00	-0.021	6.5	0.00	0.000	7.3	0.00
1AmP	0.000	5.7	0.00	0.000	6.7	0.00	0.000	7.3	0.00
1AzaP	0.050	6.7	0.00	-0.230	8.2	-0.17	0.050	5.7	0.00
4AzaP	0.043	5.7	0.00	0.028	5.5	0.00	0.046	5.6	0.00
B[a]A	0.000	5.7	0.00	0.000	6.7	0.00	0.000	7.3	0.00
B[a]Ac	0.025	8.3	0.00	-0.094	7.1	-0.11	0.026	6.2	0.00
D[aj]Ac	0.024	8.1	0.00	-0.081	7.2	0.00	0.027	8.6	0.00
D[ch]Ac	0.000	5.7	0.00	0.000	6.7	0.00	0.000	7.3	0.00

5A.3.

5A.3.1

and sk

phase

to 32

benz[a

%) and

larger

shape,

solutes

dibenz

solutes

values

%). wh

%). S

as 96

decrea

small

solutes

5A.3. Acetonitrile mobile phase with modifiers

5A.3.1. XBridge C_{18}

Tables 5A.4 and 5A.5 provide the retention factor, reduced plate height, and skew for solutes on XBridge C_{18}. Compared with pure acetonitrile mobile phase (Table 5.2), triethylamine modifier causes a decrease in retention factor (4 to 32 %) for most solutes. An increase in retention factor is observed for benz[a]acridine. An overall decrease in both the reduced plate height (41 to 99 %) and skew (8 to 91 %) is observed. However, the amount of broadening is still larger than that in pure methanol. Therefore, the triethylamine improves peak shape, but does not completely mask the effect of the kinetically slow site.

Acetic acid modifier causes a decrease in retention factors for most solutes, yet an increase for benz[a]anthracene, benz[a]acridine, and dibenz[c,h]acridine. Similarly, the reduced plate height decreases for most solutes, yet increases for the same three solutes. All solutes have decreased values for skew (1 to 70 %).

Acetyl acetone cause a decrease in retention for most solutes (0.1 to 15 %), while pyrene, benz[a]acridine, and dibenz[a,j]acridine increase slightly (1 to 4 %). Similarly, the reduced plate height decreases for most solutes (by as much as 96 %), yet increases for the same three solutes (17 to 47 %). The skew decreases for all solutes, except for pyrene which remains unchanged.

Two additional modifiers were examined for acetonitrile. Pyridine is a small nitrogen-containing aromatic that has similar chemical structure to the solutes, and may act as a displacing agent at the kinetically slow site. If pyridine

Table 5A.4: *Effect of mobile phase modifier on*

Table 5A.4: Effect of mobile phase modifier on retention factor (k), reduced plate height (h), and skew (s) for XBridge C_{18} with acetonitrile mobile phase. Solutes defined in Table 5.1.

XBridge C_{18}	Triethylamine			Acetic Acid			Acetyl Acetone		
	k	h	s	k	h	s	k	h	s
P	0.567	720	1.98	0.596	1100	2.31	0.632	1800	7.54
1AmP	0.134	8.9	3.37	0.135	5.5	3.25	0.142	37	0.29
1AzaP	0.568	1500	0.39	0.687	4300	1.84	0.675	3000	1.40
4AzaP	0.535	2500	4.96	0.775	11000	15.05	0.673	6300	8.09
B[a]A	0.553	2.6	0.46	0.619	110	3.19	0.560	97	2.77
B[a]Ac	0.546	2400	3.17	0.519	1900	3.39	0.483	860	1.07
D[aj]Ac	0.797	1100	1.13	0.875	1500	5.80	0.996	4200	4.22
D[ch]Ac	1.051	23	11.12	1.107	270	17.51	1.062	270	13.05

Table 5A.5: Effect of mobile phase modifier on retention factor (k), reduced plate height (h), and skew (s) for XBridge C_{18} with acetonitrile mobile phase. Solutes defined in Table 5.1.

XBridge C_{18}	Pyridine			Acetic acid and triethylamine		
	k	h	s	k	h	s
P	0.951	12000	9.45	0.535	71	1.67
1AmP	0.139	130	6.69	0.138	2.5	0.00
1AzaP	0.997	14000	1.85	0.573	250	0.24
4AzaP	1.123	26000	12.56	0.545	1500	2.42
B[a]A	0.666	900	4.06	0.572	2.2	0.00
B[a]Ac	0.528	1900	1.91	0.504	559	1.20
D[aj]Ac	1.140	8000	3.85	0.800	18	0.75
D[ch]Ac	1.202	1400	12.53	1.097	3.1	3.21

f

fo

di

de

pla

rec

rem

5A.

skew

phase

solute

dibenz

acts as a displacing agent, the retention factor should decrease due to the competition. However, the retention factor increases for all solutes (2 to 56 %). The reduced plate height increases for each solute. The skew decreases for all NPAHs, except 1-aminopyrene, and increases for both PAHs. Surprisingly, the addition of pyridine causes a detrimental effect on retention and peak shape.

The combination of acetic acid and triethylamine is commonly used in chiral separations in an effort to improve retention and peak shape, however little is known about the mechanism of interaction. In addition, the combination of amine and acid mimics the behavior of ethylenediaminetetraacetic acid (EDTA), a common metal chelating agent. The addition of this combination may provide further information about the kinetically slow site. The retention factor decreases for all solutes (2 to 31 %), yet increases for benz[a]acridine and dibenz[c,h]acridine (8 and 0.8 %, respectively). The reduced plate height decreases for all solutes, yet increases for benz[a]acridine. The lowest reduced plate heights are obtained using this modifier pair. Several of the solutes have reduced plate heights near 2. The skew decreases for all solutes, and results in removal of all asymmetry (skew = 0) for 1-aminopyrene and benz[a]anthracene.

5A.3.2. XBridge Shield RP_{18}

Table 5A.6 summarizes the retention factor, reduced plate height, and skew for solutes on XBridge Shield RP_{18}. Relative to pure acetonitrile mobile phase (Table 5.2), triethylamine modifier decreases the retention factor for most solutes, while increasing the retention factor for pyrene, benz[a]acridine, and dibenz[c,h]acridine. The reduced plate height is smaller for most solutes, yet an

Table 5A.6: Effect of mobile phase modifier on retention factor (k), reduced plate height (h), and skew (s) for XBridge Shield RP_{18} with acetonitrile mobile phase. Solutes defined in Table 5.1.

XBridge Shield RP_{18}	Triethylamine			Acetic Acid			Acetyl Acetone		
	k	h	s	k	h	s	k	h	s
P	0.530	470	4.13	0.504	970	1.44	0.528	960	8.35
1AmP	0.254	5.5	0.52	0.252	5.1	0.71	0.252	6.7	0.00
1AzaP	0.515	160	0.19	0.500	120	1.74	0.586	710	1.44
4AzaP	0.534	6400	2.79	0.719	1400	2.89	0.573	1760	6.70
B[a]A	0.499	3.9	0.00	0.506	4.8	0.00	0.497	13	1.95
B[a]Ac	0.501	110	1.69	0.478	34	0.45	0.493	170	0.54
D[aj]Ac	0.835	350	0.69	0.883	13	1.28	0.904	430	2.00
D[ch]Ac	0.995	5.3	4.30	1.013	7.1	2.06	0.988	24	12.06

increase occurs for 4-azapyrene, benz[a]acridine, and dibenz[a,j]acridine. The skew decreases for all solutes except benz[a]acridine. Values for h and skew are lower for XBridge Shield than for XBridge, indicating more symmetric and less tailing peak shapes, however, some degree of tailing remains for all solutes except benz[a]anthracene.

Acetic acid modifier causes only small changes (less than 15 %) in the retention factor with some increasing and some decreasing. There are no discernable trends in the data. The reduced plate height decreases drastically for most solutes, yet increases for 4-azapyrene, benz[a]acridine, and dibenz[a,j]acridine. The skew decreases for most solutes, except 1-azapyrene, benz[a]acridine, and dibenz[a,j]acridine, which remain unchanged.

Acetyl acetone causes an increase in retention factor for most solutes, yet a decrease for 1-aminopyrene, 4-azapyrene, and benz[a]anthracene. The reduced plate height increases for most solutes (27 to 56 %), yet decreases for the same three solutes (64 to 96 %). The skew increases for half of the solutes and decreases for the others (1-aminopyrene, pyrene, 4-azapyrene, benz[a]anthracene). Acetyl acetone seems to improve peak shape for several solutes, however is deleterious for others.

5A.3.3. Bridged-ethylene hybrid (BEH) particle

Tables 5A.7 and 5A.8 display the retention factor, reduced plate height, and skew for solutes on BEH. Relative to pure acetonitrile mobile phase (Table 5.2), triethylamine modifier causes a decrease in retention factors for all retained solutes except for pyrene. The reduced plate height decreases for 1- and 4-

Table 5A.7: Effect of mobile phase modifier on retention factor (k), reduced plate height (h), and skew (s) for BEH support with acetonitrile mobile phase. Solutes defined in Table 5.1.

BEH	Triethylamine			Acetic Acid			Acetyl Acetone		
	k	h	s	k	h	s	k	h	s
P	0.029	6.2	0.00	0.020	5.7	0.00	0.019	8.4	0.00
1AmP	0.000	6.0	0.00	0.000	6.8	0.00	0.000	7.4	0.00
1AzaP	0.514	5.2	0.00	0.698	160	2.84	0.702	70	0.67
4AzaP	0.284	15	0.00	0.315	180	2.16	0.375	120	3.49
B[a]A	0.000	6.0	0.00	0.000	6.8	0.00	0.000	7.4	0.00
B[a]Ac	0.189	40	0.00	0.235	14	0.00	0.255	17	0.00
D[aj]Ac	0.172	52	0.00	0.203	23	0.00	0.220	35	0.00
D[ch]Ac	0.000	6.0	0.00	0.000	6.8	0.00	0.000	7.4	0.00

Table 5A.8: Effect of mobile phase modifier on retention factor (k), reduced plate height (h), and skew (s) for BEH support with acetonitrile mobile phase. Solutes defined in Table 5.1.

BEH	Pyridine			Acetic acid and triethylamine		
	k	h	s	k	h	s
P	0.000	16	0.00	0.024	4.7	0.00
1AmP	0.000	11	0.00	0.095	4.1	0.00
1AzaP	0.755	230	0.51	--	--	--
4AzaP	0.405	450	7.56	0.136	100	0.25
B[a]A	--	--	--	0.026	7.0	0.00
B[a]Ac	0.261	24	0.14	0.106	2.4	0.00
D[aj]Ac	0.232	20	0.00	0.110	2.6	0.00
D[ch]Ac	--	--	--	0.026	7.0	0.00

azapyrene, but increases for the other retained solutes. The skew decreases substantially for 1- and 4-azapyrene (skew = 0). That is, the peak shapes for all solutes are symmetric, however, several solutes continue to be retained on BEH (Table 5A.7).

Acetic acid causes an increase in retention factor for pyrene and 1-azapyrene, a decrease for 4-azapyrene, and no change for benz[a]acridine and dibenz[a,j]acridine. The reduced plate heights remain constant or increase. The skew remains constant for the symmetric solutes, increases for 1-azapyrene, and decreases for 4-azapyrene.

Acetyl acetone modifier causes an increase in retention factor for all retained solutes (5 to 16 %). The reduced plate height decreases for 1- and 4-azapyrene, but increases for the other retained solutes. The skew remains unchanged for the symmetric solutes, but decreases for 1- and 4-azapyrene.

Pyridine causes an increase in retention factor for all retained solutes (12 to 25 %), a substantial increase in reduced plate height, and an increase in skew. Thus, the broadening and skew worsen when pyridine is added to the mobile phase.

The acetic acid and triethylamine pair cause a decrease in retention factor for 4-azapyrene, benz[a]acridine and dibenz[a,j]acridine. However, the retention factor increases for 1-aminopyrene, benz[a]anthracene, and dibenz[c,h]acridine, which were not previously retained. The reduced plate height decreases for all solutes except for pyrene. Again, several solutes have reduced plate heights near 2. The skew is also dramatically reduced for 1- and 4-azapyrene.

5A.3.4. Conclusions

This appendix provides a detailed examination of the effect of mobile phase modifiers in methanol and acetonitrile mobile phases. This description supplements the prior discussion held in Chapter 5 concerning the effect of mobile phase modifiers on retention and peak shape.

CHAPTER 6

CONCLUSIONS AND FUTURE DIRECTIONS

6.1 Introduction

Liquid chromatography is used in more than 75 % of all analytical methods, with reversed-phase chromatography (RPLC) leading the way [1,2]. The separation of a series of solutes is governed by the retention mechanism of the phase. For this reason, a deep understanding of the retention mechanism is necessary in order to maximize the beneficial contributions and minimize the detrimental contributions to the separation. Hybrid stationary phases, comprised of both organic and inorganic components, are among the newest advancements in the field of liquid chromatography. Thus, a thorough investigation of these phases is essential to understand their retention behavior. Thermodynamic and kinetic investigations provide insight into the retention mechanism and illustrate solute interaction with the stationary phase at the molecular level. In this dissertation, the effect of the analysis method (Chapter 3), temperature (Chapter 4), and mobile phase composition (Chapter 5) on retention and peak shape were examined.

6.2 Study of theoretical analysis methods

Chapter 3 details the comparison and validation of theoretical methods to extract thermodynamic and kinetic information from liquid chromatographic data. The effect of column length, linear velocity, and solute carbon number are evaluated. Overall, values for the retention factor are similar for each model. Retention factors are constant with distance, decrease with velocity, and

increase with chain length of the solute. However, the values for the kinetic rate constants differ for each model. The statistical moment and EMG models show the largest variation in rate constant as a function of distance. However, the variation decreases substantially when the rate constants are calculated by difference between two detectors. The moment and EMG methods by difference are more reliable than the Thomas model at one detector. As a function of velocity and chain length, the moment and EMG models show the most consistent and reliable trends, as compared with the Thomas method. Problems with the Thomas model could be related to the inherent assumptions of the model, as it assumes that broadening arises due to nonlinear isotherms and slow kinetics, and that all column and extra-column effects are negligible. However, due to the nature of the model, extra-column effects cannot be eliminated using the difference approach. Based on these results, the statistical moment and EMG models yield reasonable values for retention factors and rate constants in an experimental liquid chromatographic system.

While this work validates the use of several methods under experimental conditions, additional information could be obtained using simulation studies. Earlier work in this lab used stochastic simulation to validate different mathematical models for extracting thermodynamic and kinetic information. However, only the partition mechanism was employed. A further understanding could be obtained by examining methods to validate different mathematical methods for the adsorption mechanism, as well as for a mixed-mode partition-adsorption mechanism, as is commonly seen in experimental investigations.

6.3 Study of hybrid stationary phases

Chapters 4 and 5 detail the thermodynamic and kinetic investigation of hybrid stationary phases. The statistical moment model is used for all data analysis. The effect of temperature and mobile phase (Chapter 4) and mobile phase modifiers (Chapter 5) are evaluated.

Temperature effects are typically neglected in liquid chromatographic separations. However, the effect of temperature is substantial for the separation of polycyclic aromatic hydrocarbons (PAHs) and nitrogen-containing polycyclic aromatic hydrocarbons (NPAHs). Detailed thermodynamic and kinetic information is obtained as a function of temperature. The parent PAHs are separated primarily by the partition mechanism with the octadecyl groups, but some minor interaction with the silanol groups can occur through the aromatic system. In methanol mobile phase, the retention factors for the NPAHs are less than those for the parent PAHs, which is consistent with a partition mechanism. In addition, the trends of retention with ring number and annelation structure are consistent with the partition mechanism. The changes in molar enthalpy are very similar for all solutes indicating similarity in their retention mechanism. However, the kinetic rate constants indicate that adsorption at silanol sites could play a role, as they are significantly smaller for the NPAHs than for the parent PAHs.

The different thermodynamic and kinetic behavior in the presence of the aprotic solvent acetonitrile provides an interesting picture of the retention process. Methanol is able to hydrogen bond with both the NPAH solutes and the underlying silanols, which causes a reduction in the number of available silanols.

However, acetonitrile cannot hydrogen bond in this way to shield interactions of the solute with the underlying particle. Therefore, the retention factors for the NPAHs are larger in acetonitrile than those in methanol. In addition, the retention factors for the NPAHs are more similar to those for their parent PAHs, indicating the adsorption mechanism is likely dominant for the NPAH solutes. The changes in molar enthalpy are slightly more negative and are sufficient to account for the small changes in retention factor. In this case, there does not seem to be a significant change in the entropy of the phase when acetonitrile is used. The kinetic behavior also reflects the increased role of adsorption, as the rate constants are one to four orders of magnitude smaller than those in methanol.

The thermodynamic and kinetic behavior of the solutes on this hybrid phase is similar in nature to that on silica supports [3]. The retention factors in both mobile phases are smaller for the same set of solutes under similar conditions than on the silica phases. The rate constants in methanol are faster, while those in acetonitrile are slower on the hybrid phase compared to the silica phase. The change in molar enthalpy is less negative for the hybrid phases compared to the silica phases for the same solutes. However, the bonding density of the hybrid phase is more similar to the bonding density of the monomeric phase used for the separation of fatty acids [4,5]. When this silica phase is considered, the changes in molar enthalpy are more consistent. The thermodynamic and kinetic information provides a clearer description of the retention mechanism of NPAHs on hybrid supports in reversed-phase liquid chromatography.

The addition of mobile phase modifiers is a common and important practice towards the improvement of chromatographic peak shapes. In this work, the mobile phase itself shows remarkable differences in solute retention and peak shape (also shown in Chapter 4). However, mobile phase modifiers change the peak shape in both protic and aprotic solvents. Mobile phase modifiers used for silanol blockage, such as triethylamine and pyridine, and those for metal chelation, such as acetic acid and acetyl acetone, are investigated. The effect of each modifier is both solute and phase dependent. Many of the mobile phase modifiers improve peak shape for several solutes on one or both C_{18} phases, but do not cause an overall improvement to symmetric and asymmetric peak shape. Using the combination of triethylamine and acetic acid provides the best results for overall peak shape improvement. The only other modifier that provides comparable improvement is triethylamine on XBridge. However, no modifier or pair of modifiers completely removed the tailing from all peaks.

The contribution of the underlying support, BEH, and the polar embedded group in XBridge Shield RP_{18} are also investigated. Based on the observed retention factors, the underlying support does not contribute to the retention and peak shape that is observed on the C_{18} phases. The BEH seems to contribute more to the overall retention and asymmetry when acetonitrile is the mobile phase. The additional tailing caused from acetonitrile can be reduced using mobile phase modifiers, but does not compare to using methanol alone. The XBridge Shield material contains a polar embedded group in the C_{18} phase,

which has been known to shield the solute from the support material. However, in these studies, asymmetric peak shapes are observed for several solutes. The combination of these results indicates that a solutes affinity for silanol sites may be the initial source of the problem, however, it alone is not the slow step. Only when the support is derivatized with C_{18} is peak asymmetry observed. Thus, solutes can partition into and out of the C_{18} chain and can adsorb and desorb from silanol sites. These steps, taken individually, have relatively rapid mass transfer and adsorption-desorption kinetics. However, when the steps are combined sequentially, as is the case in a chromatographic separation, they are kinetically slow. That is, the solutes that have an affinity for the silanol sites will be attracted to them, but must migrate through the C_{18} layer to interact. Diffusion through this C_{18} layer is slow compared to the actual adsorption-desorption step. Thus, diffusion dominates the kinetic behavior and is the kinetically slow step.

The interesting behavior of the hybrid phases provides detailed information concerning the retention mechanism in protic and aprotic solvents. However, additional information could be learned from these phases. The hybrid phases are designed to operate well under pH controlled conditions, specifically at high pH. Thus, it would be beneficial to characterize the retention mechanism at several carefully controlled pH values in the acidic, neutral, and basic pH ranges. The retention and peak shape for the NPAHs could be evaluated as a function of pH. In addition, temperature studies would allow for calculation and comparison of the change in molar enthalpy at each pH.

The cause of the severe asymmetry is not yet completely understood for these materials. Several analytical measurements could be made on the support particle to provide a more detailed description of its chemical nature. For example, inductively coupled plasma atomic emission spectrometry could be used to identify the concentration of various metals in the underlying support. Values for Al, Fe, and Na are reported in the 1 – 2 ppm range, however, these and other metals effect the acidity of nearby silanols [6]. Knowing the type and concentration of each metal would permit accurate calculation of the amount of chelating mobile phase modifier needed.

6.4 Conclusions

The characterization of stationary phase retention behavior is an important practice in liquid chromatography. Many parameters can affect the quality of the separation including mobile phase modifiers, temperature, and pressure. In addition, the theoretical method used for characterization is important to the overall quality of the data. Thus, chromatographic parameters and theoretical methods for characterizing retention behavior should be carefully selected for a given separation.

6.5 References

[1] L.R. Snyder, J.J. Kirkland, Introduction to Modern Liquid Chromatography, John Wiley & Sons, New York, NY, **1974**.

[2] High Performance Liquid Chromatography Fundamental Principles & Practice, Blackie Academic & Professional, Glasgow, United Kingdom, **1996**.

[3] V.L. McGuffin, S.B. Howerton, X. Li, *J. Chromatogr. A 1073* (**2005**) 63-73.

[4] V.L. McGuffin, S.-H. Chen, *J. Chromatogr. A 762* (**1997**) 35-46.

[5] S.B. Howerton, V.L. McGuffin, *Anal. Chem. 75* (**2003**) 3539-35448.

[6] J. Nawrocki, *Chromatographia 31* (**1991**) 193-205.

MICHIGAN STATE UNIVERSITY LIBRARIES
3 1293 03062 7750